frontiers | Research Topics

Community series in recent advances in *Drosophila* cellular and humoral innate immunity, volume II

Edited by
Susanna Valanne, Laura Vesala and Dan Hultmark

Published in
Frontiers in Immunology

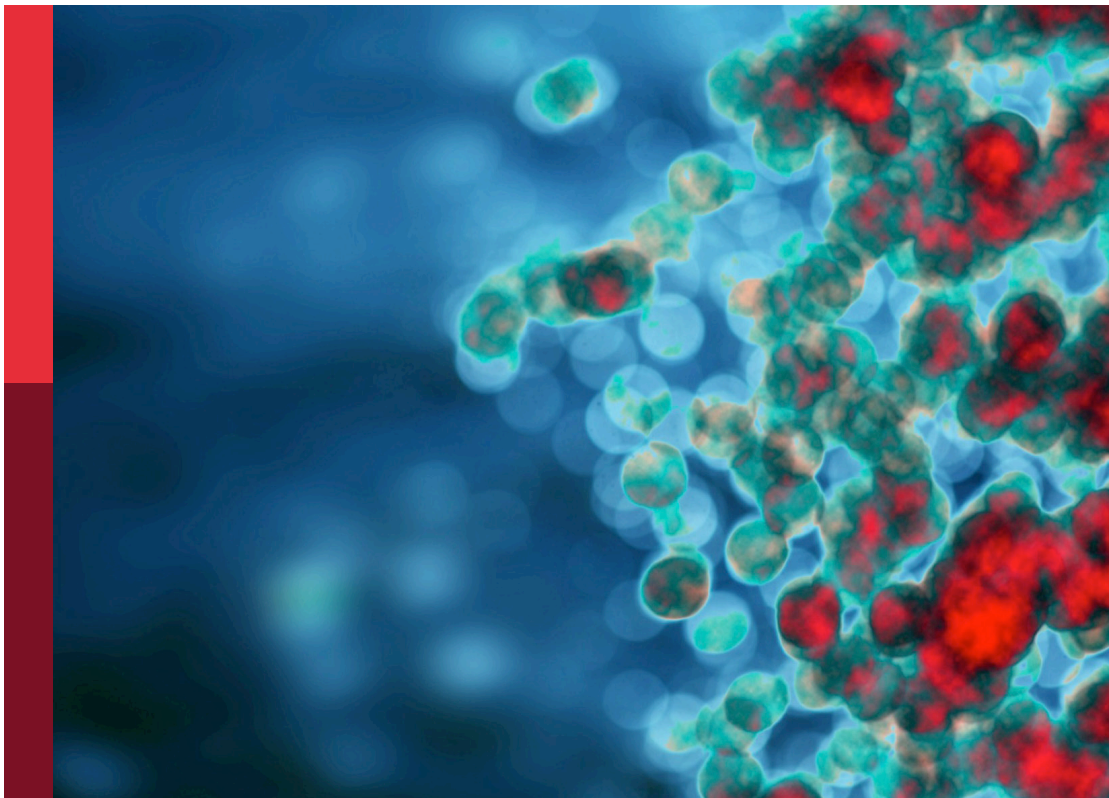

ISSN 1664-8714
ISBN 978-2-8325-5083-0
DOI 10.3389/978-2-8325-5083-0

About Frontiers

Frontiers is more than just an open access publisher of scholarly articles: it is a pioneering approach to the world of academia, radically improving the way scholarly research is managed. The grand vision of Frontiers is a world where all people have an equal opportunity to seek, share and generate knowledge. Frontiers provides immediate and permanent online open access to all its publications, but this alone is not enough to realize our grand goals.

Frontiers journal series

The Frontiers journal series is a multi-tier and interdisciplinary set of open-access, online journals, promising a paradigm shift from the current review, selection and dissemination processes in academic publishing. All Frontiers journals are driven by researchers for researchers; therefore, they constitute a service to the scholarly community. At the same time, the *Frontiers journal series* operates on a revolutionary invention, the tiered publishing system, initially addressing specific communities of scholars, and gradually climbing up to broader public understanding, thus serving the interests of the lay society, too.

Dedication to quality

Each Frontiers article is a landmark of the highest quality, thanks to genuinely collaborative interactions between authors and review editors, who include some of the world's best academicians. Research must be certified by peers before entering a stream of knowledge that may eventually reach the public - and shape society; therefore, Frontiers only applies the most rigorous and unbiased reviews. Frontiers revolutionizes research publishing by freely delivering the most outstanding research, evaluated with no bias from both the academic and social point of view. By applying the most advanced information technologies, Frontiers is catapulting scholarly publishing into a new generation.

What are Frontiers Research Topics?

Frontiers Research Topics are very popular trademarks of the *Frontiers journals series*: they are collections of at least ten articles, all centered on a particular subject. With their unique mix of varied contributions from Original Research to Review Articles, Frontiers Research Topics unify the most influential researchers, the latest key findings and historical advances in a hot research area.

Find out more on how to host your own Frontiers Research Topic or contribute to one as an author by contacting the Frontiers editorial office: frontiersin.org/about/contact

Community series in recent advances in *Drosophila* cellular and humoral innate immunity, volume II

Topic editors

Susanna Valanne — Tampere University, Finland

Laura Vesala — Tampere University, Finland

Dan Hultmark — Umeå University, Sweden

Citation

Valanne, S., Vesala, L., Hultmark, D., eds. (2024). *Community series in recent advances in Drosophila cellular and humoral innate immunity, volume II*. Lausanne: Frontiers Media SA. doi: 10.3389/978-2-8325-5083-0

Table of contents

frontiers | Frontiers in Immunology

TYPE Editorial
PUBLISHED 18 June 2024
DOI 10.3389/fimmu.2024.1416296

OPEN ACCESS

EDITED AND REVIEWED BY
Humberto Lanz-Mendoza,
National Institute of Public Health (Mexico), Mexico

*CORRESPONDENCE
Susanna Valanne
susanna.valanne@tuni.fi

RECEIVED 12 April 2024
ACCEPTED 10 June 2024
PUBLISHED 18 June 2024

CITATION
Vesala L, Hultmark D and Valanne S (2024) Editorial: Community series in recent advances in *Drosophila* cellular and humoral innate immunity: volume II.
Front. Immunol. 15:1416296.
doi: 10.3389/fimmu.2024.1416296

Editorial: Community series in recent advances in *Drosophila* cellular and humoral innate immunity: volume II

Laura Vesala[1], Dan Hultmark[2] and Susanna Valanne[1]*

[1]Faculty of Medicine and Health Technology, Tampere University, Tampere, Finland, [2]Department of Molecular Biology, Umeå University, Umeå, Sweden

KEYWORDS

***Drosophila melanogaster*, innate immunity, cellular immunity, humoral immunity, model for human diseases, metabolism, parasitoid wasp, host-pathogen interaction**

Editorial on the Research Topic

Community series in recent advances in *Drosophila* cellular and humoral innate immunity: volume II

We are happy to present the Community series in Recent advances in *Drosophila* cellular and humoral innate immunity: Volume II, exploring the advances made in the field since our previous Research Topic in 2019–2020. This Research Topic is comprised of original research and review articles by experts in the field.

Intricacies of especially the cell-mediated innate immune responses are currently under active research in *Drosophila melanogaster* and recent studies have increased our understanding of the functions of *Drosophila* blood cells, the hemocytes, in immune responses and beyond (1–3). Particularly the phagocytic plasmatocytes have proven to be much more diverse than previously acknowledged [reviewed in (4)] and new parallels between plasmatocytes and mammalian monocyte/macrophage lineage have been drawn (5).

Here, the work of several contributors sheds light on immune cell diversity and the regulatory mechanisms that govern their function in developmental and immune contexts. Bazzi et al. discovered a role for the zinc finger transcription factor glial cells missing (gcm) in hemocytes as an anti-inflammatory factor. Loss of *gcm* exacerbates Toll-induced hemocyte activation and differentiation of an immune-activated hemocyte, the lamellocyte, possibly via increase in reactive oxygen species (ROS). Furthermore, their data indicate that hemocyte proliferation can be regulated via the activation of nicotinic acetylcholine receptors expressed in hemocytes, rising interesting questions on the role of neurotransmitter signaling in the control of hemocyte homeostasis. Brooks et al. examined the heterogeneity of plasmatocytes in their response to developmental transitions and apoptotic cells. They show that the phosphatidylserine receptor Simu and Ecdysone receptor signaling influence the identity and function of plasmatocyte subpopulations. Their findings provide insights into hemocyte plasticity and the potential for hemocyte reprogramming in response to environmental challenges. Khalili et al. utilized single cell RNA sequencing to study tumor-associated hemocytes (TAHs). Their work nicely illustrates how TAHs have different characteristics

depending on the tumor model and finds similarities to mammalian tumor-associated macrophages. Hemocyte repertoire and functions get even more diverse when other drosophilid species are considered. Cinege et al. studied the multinucleated giant hemocytes in *Drosophila ananassae* and *Zaprionus indianus*. Akin to lamellocytes, these hemocytes encapsulate parasitoid eggs and larvae but resemble human megakaryocytes. Their work gives intriguing insights into the various ways species have adapted to combat pathogenic parasitoids.

Metabolic changes shaping, or dictating, immune cell functions and lineage specification is an active research area especially in vertebrate model systems. Immunometabolism is an increasingly intense field of study also in *Drosophila* (6), see e.g. the recent research by McMullen and coworkers (7). Following on the metabolic processes shaping immune reactions, Darby & Lazzaro review the interactions between innate immunity and insulin-like signaling (IlS) in insects, namely *D. melanogaster* but also *Bombyx mori* and *Anopheles* mosquitos. Insulin signaling and innate immune mechanisms are well conserved from insects to men, and research on the interplay of these processes in insects produces information also applicable to human health. The review concludes that innate immunity and IIS are interconnected, highlighting the energetic demands of an immune response and the role of IlS as a metabolic regulator. Dolezal sums up what is known about metabolic changes occurring in hemocytes during the immune response against parasitoid wasps. A central conundrum is how immune cells balance between generating toxic molecules such as ROS to the extent that kills the parasitoid and, at the same time, protecting the host larva from detrimental effects of ROS. As both generating and eliminating ROS require nicotinamide adenine dinucleotide phosphate ($NADP^+$/NADPH), the cyclic pentose phosphate pathway reducing $NADP^+$ to NADPH has emerged as a central metabolic pathway in immune-activated hemocytes (lamellocytes). Dolezal further discusses the metabolic intricacies of hemocytes responsible for the encapsulation and poses several questions remaining to be answered. Leitão et al. studied the cost of the immune response against the parasitoids and concluded that the cost comes rather from the direct harm caused by the parasitoid than from mounting the immune response itself, including differentiation and proliferation of hemocytes and the melanization response.

The review by Mpamhanga and Kounatidis discusses the rising global impact of fungal infections, particularly in individuals with chronic and immunosuppressive conditions. It emphasizes the need for advanced research and public health interventions considering the WHO's fungal priority list. The authors highlight the utility of *D. melanogaster* as a great model organism in the context of studying host-pathogen interactions and immunopathogenesis of fungal diseases, including studying human fungal pathogens and testing antifungal compounds.

Finally, Aalto et al. took advantage of the conservation and tractability of the immune system of *D. melanogaster* and studied the putative anti-inflammatory function of stilbenoids, antioxidant compounds found in plants (8). They discovered that stilbenoids suppress the inflammatory response via dampening the NF-κB-mediated gene expression and that this effect was dependent on the transient receptor potential ankyrin 1 (TrpA1), similarly to mammals. This study demonstrates the potential of *Drosophila* for detailed analysis of the molecular mode of action of putative therapeutic compounds *in vivo*. Recent research shows the power of *Drosophila* in revealing therapeutic targets for cancer (9, 10), rare genetic disorders (11) and neurodegenerative diseases (12), to name a few. It will be exciting to see the innovative approaches taken in the future on various frontiers in drug discovery.

We would like to thank the authors for their contribution to the Research Topic as well as the reviewers for their insightful comments and suggestions. We have no doubt that there are more discoveries to be made regarding the pathways and patterns of immunity in *Drosophila* and are looking forward to the future work done on the findings published in our topic.

Author contributions

LV: Writing – original draft, Writing – review & editing. DH: Writing – original draft, Writing – review & editing. SV: Writing – original draft, Writing – review & editing.

Funding

The author(s) declare financial support was received for the research, authorship, and/or publication of this article. The Drosophila work in Tampere University was carried out in the Tampere Drosophila Facility, partly funded by Biocenter Finland. DH was supported by the Swedish Research Council.

Conflict of interest

The authors declare that the research was conducted in the absence of any commercial or financial relationships that could be construed as a potential conflict of interest.

Publisher's note

References

1. Stephenson HN, Streeck R, Grüblinger F, Goosmann C, Herzig A. Hemocytes are essential for *Drosophila melanogaster* post-embryonic development, independent of control of the microbiota. *Development*. (2022) 149:dev200286. doi: 10.1242/dev.200286

2. Evans CJ, Liu T, Girard JR, Banerjee U. Injury-induced inflammatory signaling and hematopoiesis in Drosophila. *Proc Natl Acad Sci U.S.A*. (2022) 119:e2119109119. doi: 10.1073/pnas.2119109119

3. Cattenoz PB, Monticelli S, Pavlidaki A, Giangrande A. Toward a consensus in the repertoire of hemocytes identified in Drosophila. *Front Cell Dev Biol*. (2021) 9:643712. doi: 10.3389/fcell.2021.643712

4. Hultmark D, Andó I. Hematopoietic plasticity mapped in *Drosophila* and other insects. *Elife*. (2022) 11:e78906. doi: 10.7554/eLife.78906

5. Yoon S-H, Cho B, Lee D, Kim H, Shim J, Nam J-W. Molecular traces of *Drosophila* hemocytes reveal transcriptomic conservation with vertebrate myeloid cells. *PloS Genet*. (2023) 19:e1011077. doi: 10.1371/journal.pgen.1011077

6. Galenza A, Foley E. Immunometabolism: insights from the *Drosophila* model. *Dev Comp Immunol*. (2019) 94:22–34. doi: 10.1016/j.dci.2019.01.011

7. McMullen E, Strych L, Chodáková L, Krebs A, Dolezal T. JAK/STAT mediated insulin resistance in muscles is essential for effective immune response. *Cell Commun Signal*. (2024) 22:203. doi: 10.1186/s12964–024-01575–0

8. Rivière C, Pawlus AD, Mérillon J-M. Natural stilbenoids: distribution in the plant kingdom and chemotaxonomic interest in Vitaceae. *Nat Prod Rep*. (2012) 29:1317. doi: 10.1039/c2np20049j

9. Sekiya S, Fukuda J, Yamamura R, Ooshio T, Satoh Y, Kosuge S, et al. *Drosophila* screening Identifies dual Inhibition of MEK and AURKB as an effective therapy for pancreatic ductal adenocarcinoma. *Cancer Res*. (2023) 83:2704–15. doi: 10.1158/0008–5472.CAN-22–3762

10. Bangi E, Smibert P, Uzilov AV, Teague AG, Gopinath S, Antipin Y, et al. A *Drosophila* platform identifies a novel, personalized therapy for a patient with adenoid cystic carcinoma. *iScience*. (2021) 24:102212. doi: 10.1016/j.isci.2021.102212

11. Hope KA, Berman AR, Peterson RT, Chow CY. An in *vivo* drug repurposing screen and transcriptional analyses reveals the serotonin pathway and GSK3 as major therapeutic targets for NGLY1 deficiency. *PloS Genet*. (2022) 18:e1010228. doi: 10.1371/journal.pgen.1010228

12. Lo Piccolo L, Umegawachi T, Yeewa R, Potikanond S, Nimlamool W, Prachayasittikul V, et al. A novel *Drosophila*-based drug repurposing platform identified fingolimod as a potential therapeutic for TDP-43 proteinopathy. *Neurotherapeutics*. (2023) 20:1330–46. doi: 10.1007/s13311-023-01406-z

frontiers | Frontiers in Immunology

TYPE Original Research
PUBLISHED 19 September 2023
DOI 10.3389/fimmu.2023.1243797

OPEN ACCESS

EDITED BY
Martin Rottenberg,
Karolinska Institutet (KI), Sweden

REVIEWED BY
Luis Alberto Baena-Lopez,
University of Oxford, United Kingdom
Shanming Ji,
Anhui Agricultural University, China

*CORRESPONDENCE
Ulrich Theopold
uli.theopold@su.se

†These authors have contributed equally to this work

RECEIVED 21 June 2023
ACCEPTED 31 August 2023
PUBLISHED 19 September 2023

CITATION
Khalili D, Mohammed M, Kunc M, Sindlerova M, Ankarklev J and Theopold U (2023) Single-cell sequencing of tumor-associated macrophages in a *Drosophila* model.
Front. Immunol. 14:1243797.
doi: 10.3389/fimmu.2023.1243797

Single-cell sequencing of tumor-associated macrophages in a *Drosophila* model

Dilan Khalili[1†], Mubasher Mohammed[1†], Martin Kunc[1,2†], Martina Sindlerova[1], Johan Ankarklev[1] and Ulrich Theopold[1*]

[1]The Wenner-Gren Institute, Department of Molecular Biosciences, Stockholm University, Stockholm, Sweden, [2]Department of Clinical Medicine, Aarhus University, Aarhus, Denmark

Introduction: Tumor-associated macrophages may act to either limit or promote tumor growth, yet the molecular basis for either path is poorly characterized.

Methods: We use a larval *Drosophila* model that expresses a dominant-active version of the Ras-oncogene (Ras^{V12}) to study dysplastic growth during early tumor progression. We performed single-cell RNA-sequencing of macrophage-like hemocytes to characterize these cells in tumor- compared to wild-type larvae. Hemocytes included manually extracted tumor-associated- and circulating cells.

Results and discussion: We identified five distinct hemocyte clusters. In addition to Ras^{V12} larvae, we included a tumor model where the activation of effector caspases was inhibited, mimicking an apoptosis-resistant setting. Circulating hemocytes from both tumor models differ qualitatively from control wild-type cells—they display an enrichment for genes involved in cell division, which was confirmed using proliferation assays. Split analysis of the tumor models further reveals that proliferation is strongest in the caspase-deficient setting. Similarly, depending on the tumor model, hemocytes that attach to tumors activate different sets of immune effectors—antimicrobial peptides dominate the response against the tumor alone, while caspase inhibition induces a shift toward members of proteolytic cascades. Finally, we provide evidence for transcript transfer between hemocytes and possibly other tissues. Taken together, our data support the usefulness of *Drosophila* to study the response against tumors at the organismic level.

KEYWORDS

***Drosophila melanogaster*, macrophages, tumor model, hemocyte, single-cell transcriptomics, ScRNA-seq**

1 Introduction

When cellular homeostasis is impaired, affected cells may limit the damage by inducing either cellular arrest or cell death. Best characterized in this context is the tumor suppressor p53, which—depending on the amount of DNA damage or other forms of cellular stress—induces cellular senescence, apoptosis, or alternative forms of cell death (1–3). Collectively or individually, these responses will prevent malfunction at the tissue/organ and organismic levels. Notably, this may also prevent the transition from benign to more aggressive forms of tumor growth by eliminating or silencing damaged cells locally in the tumor microenvironment (TME) and at an early stage of tumorigenesis (1). Cell cycle arrest is usually expected to prevent this transition on its own, while apoptosis involves the clearance of apoptotic bodies by phagocytic neighboring cells or professional phagocytes such as macrophages, which migrate into the TME (2, 3).

While apoptosis thus acts as a tumor suppressor mechanism, tumor cells have been found to evade cell death, and in several tumors with poor prognosis, high levels of apoptosis are detected (4). This raises the question of whether apoptosis, both when occurring naturally or as part of anti-cancer treatments, is fully beneficial (4).

Tumor progression depends on factors that act both locally in the tumor microenvironment and on the communication with tissues in trans, which modulate physiological and immune responses towards tumors. Key actors in the TME are tumor-associated macrophages (TAMs), which may affect tumor progression both positively or negatively. *In vitro* activated macrophages have been roughly classified as either classically activated (M1-type macrophages) or alternative (M2 macrophages (5)). M1 macrophages are pro-inflammatory and are involved in anti-viral, anti-bacterial, and anti-tumor responses, whereas M2 macrophages are anti-inflammatory, contribute to anti-helminth and tissue repair responses, and are considered pro-tumoral (6, 7). Additional *in vitro* and *in vivo* data led to further subdivision, in particular of M2 macrophages, and show that their activation state is only partially reflected by the M1/M2 classification (6, 8).

Facilitating the communication within the tumor microenvironment, which includes tumor cells, non-tumor stroma, and TAMs, extracellular vesicles (EVs) have gained increasing attention in recent years (4). EVs include (a) tumor-derived apoptotic fragments, (b) microparticles, which are shed from the cell surface, and (c) exosomes, which are released through the fusion of multivesicular bodies with the cell surface (9). EVs may have tumor and metastasis-promoting capacity both within the TME (4) and systemically. Apoptotic bodies contain nuclear fragments (including DNA and primary transcripts), while the content of microparticles and exosomes is derived from the cytosol and therefore contains mature RNAs. Potential intermediaries of EV-mediated communication include proteins, lipids, and different types of RNA, including long non-coding RNAs (lncRNAs) (9, 10).

Despite lacking adaptive immunity in a mammalian sense, insects possess a highly effective innate immune system. This comprises both humoral and cellular elements. Humoral components are secreted into the hemolymph—the insect equivalent of blood—primarily from the fat body, which fulfills functions of both the mammalian fat body and liver. In *Drosophila melanogaster*, one of the major models for insect immunity, the cellular branch comprises three classes of cells collectively called hemocytes (11) (1): plasmatocytes, which are functionally equivalent to both mammalian macrophages and white blood cells; (2) crystal cells, which contain prophenoloxidases, the precursors for key enzymes involved in antimicrobial and wound responses; and (3) lamellocytes, which are absent in naive animals but produced in response to wounding and invasion by large intruders such as parasitoid eggs. Recent hemocyte transcriptome profiling at the single-cell level revealed a much higher diversity, in particular among plasmatocytes (11–14).

The interplay between fly tumors and hemocytes was first studied in a pioneering work by Pastor Pareja et al. (15), where it was shown that upon recognition of damage to the basement membrane, hemocytes are recruited to tumor tissue with tumor-limiting effects. Conversely, when in subsequent work tumors were induced in a background expressing a dominant-active version of the Ras oncogene (Ras^{V12}), tumor-associated hemocytes (TAHs) were instead involved in a positive feedback loop that involved JNK signaling and promoted tumor growth (16, 17). Thus, similar to what is found in mammals, the effects of TAHs appear to be in many cases tissue- and tumor stage dependent. In a previous work, we found that expression of dominant active Ras^{V12} in larval *Drosophila* salivary glands (SGs) induced ductal hypertrophy (18) similar to what is observed in ductal tumors in humans. In SGs, this led to (1) the loss of cellular integrity, (2) nuclear disintegration and caspase activation, (3) loss of the SG lumen and of secretory activity, (4) damage to the basement membrane, (5) induction of fibrotic lesions including activation of the flies' coagulation system, and (6) recruitment of TAHs (18–20). Despite the presence of hallmarks of apoptosis and activation of JNK signaling, SG cells were not eliminated (18, 20), although SG cell fragments were released into the hemolymph (18). Surprisingly, forced expression of the antimicrobial peptide Drosomycin (Drs) across whole SGs reverted the majority of tumor-associated phenotypes through negative regulation of JNK signaling (19, 20).

Here, to identify genes that are differentially expressed in hemocytes from tumor larvae, we profiled the transcriptome of circulating single-cell hemocytes from wild-type and tumor larvae and from TAHs, which were extracted manually from tumorous salivary glands (Figure 1A). In contrast, there are too few hemocytes to allow profiling of TAHs attached to wild-type SGs. Since we had previously observed strong activation of caspases in Ras^{V12}-expressing SGs (20), and in light of the bi-edged nature of caspase activation and apoptosis in cancer (see above), we included larvae where effector caspases were inhibited by the expression of the specific inhibitor p35.

2 Materials and methods

2.1 Fly strains and sample preparation

w^{1118}, $Beadex^{MS1096}$-*Gal4* (referred here as *Bx*: 8860/Bl), $Beadex^{MS1096}$-*Gal4; EaterDsRed,* w^{1118}, w^{1118};*p35* (5072/Bl), w^{1118};

10.3389/fimmu.2023.1243797

UAS-Ras^{V12}(4847/Bl), *w*^{1118}*;p35;UAS-Ras*^{V12}*,;Arc1*^{esm18}*;* (37530/Bl), and B*x;Arc1*^{esm18}*;,;Arc1*^{esm18}*;Ras*^{V12} flies were used in the experiments. Flies were cultured in a 25°C, 12-h dark/light cycle room. Female virgins were collected for 5 days and crossed with respective males on day 7. Progeny larvae were kept as described in (20). Approximately 20–30 salivary gland pairs were fixed in 4% paraformaldehyde (PFA) for 20 min. Samples for extracellular staining were washed 3 × 10 min with 1× phosphate-buffered saline (PBS).

2.2 Immunohistochemistry

Antibodies against P1 (Plasmatocytes, 1:50), L1 (Lamellocytes, 1:50), and C4 (Crystal cells, 1:50) were incubated for 1 h at room temperature in PBS and subsequently washed 3 × 10 min in PBS. For intracellular proteins, the samples were incubated overnight at 4°C in anti-pJNK (1:250), anti-Idgf3 (1:50), or anti-CC3 (1:400) diluted in PBST (1% TritonX-100) and subsequently washed 3 ×

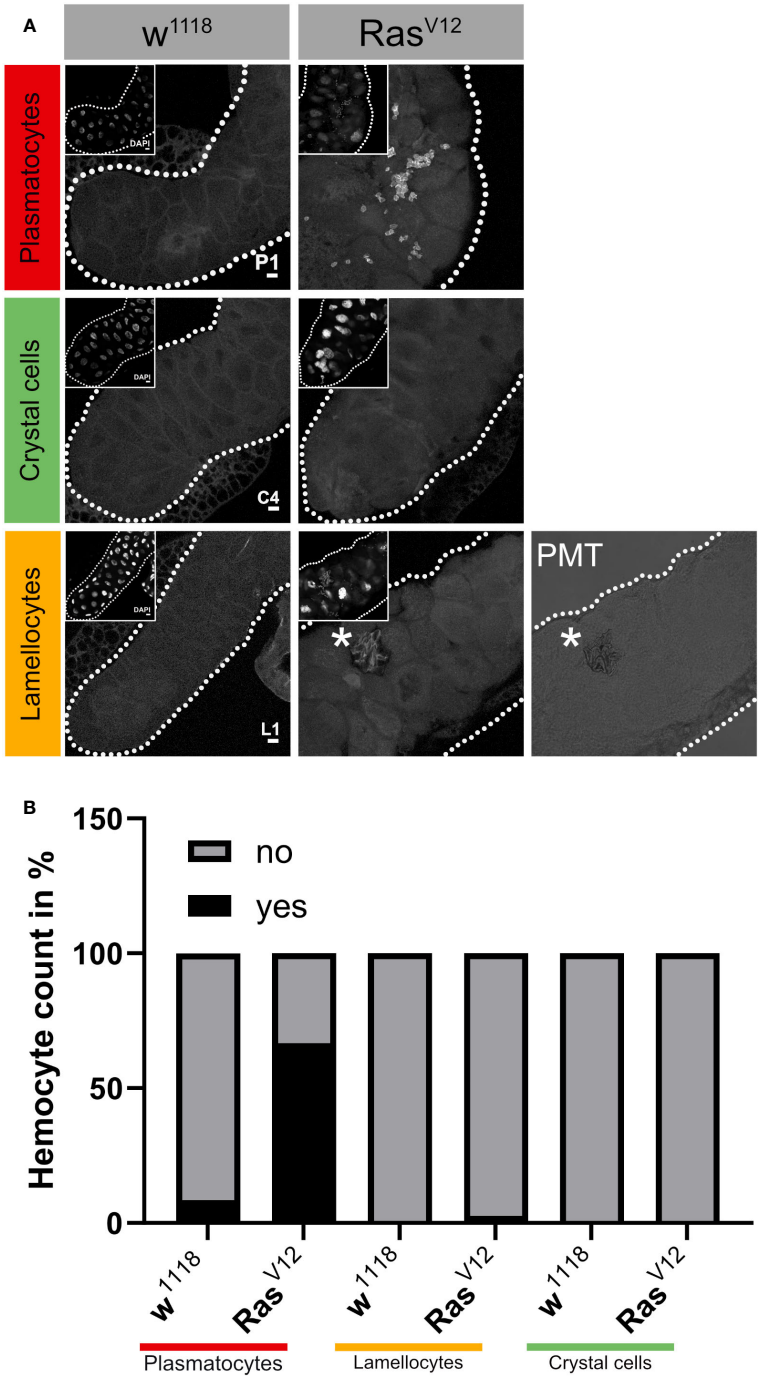

FIGURE 1
Classification of tumor-associated hemocytes. **(A)** Tumor-associated hemocytes were labeled using plasmatocyte (P1), crystal cell (C4), and lamellocytes (L1)-specific antibodies. **(B)** The frequency of the three hemocyte classes is shown in the lower part for wild type and Ras^{V12}-SGs. *, marks the cropped area of the figure.

10 min in PBS. The samples were incubated with secondary antibody anti-mouse-546 (1:500, Thermo Fisher #A11030), anti-mouse-488 (1:250, Thermo Fisher #A11001), anti-rabbit-568 (1:500, Thermo Fisher #A21063), and anti-rabbit-488 (1:500, Thermo Fisher #A11008), or 4',6-Diamidino-2-phenylindole dihydrochloride (DAPI) (1:500, Sigma-Aldrich D9542) for 1 h at room temperature and washed 3 × 10 min with PBS before mounting in Fluoromount-G (Thermo Fisher, 00-4958-02).

2.3 Proliferation assay

Drosophila larvae at 120 h after egg deposition (AED) were bled into 10 µL of PBS, and the sample was incubated for 5 min at room temperature. The sample was fixed in 4% PFA for 20 min and washed 3 × 5 min with PBS. The sample was stained with antibody against pH3 (phosphorylated histone 3, 1:800, Sigma-Aldrich 06-570) and H2 (Hemese, 1:5 kindly provided by Istvan Ando, Szeged) overnight in 4°C. After incubation, the sample was washed 3 × 5 min with PBS and stained with secondary antibodies anti-rabbit-568 (1:500, Thermo Fisher A-21069), anti-mouse-488 (1:250, Thermo Fisher A-11001), and DAPI (1:500, Sigma-Aldrich D9542) for 2 h in room temperature. Subsequently, the sample was washed 3 × 5 min with PBS and mounted in Fluoromount-G (Thermo Fisher, 00-4958-02). A total of 15 samples per genotype were prepared and photographed using a tile scan at a confocal microscope Zeiss LSM780 (Zeiss, Germany), and the count of cells was evaluated in ImageJ (version 1.53t). Statistics and graph plotting were performed in Prism software (GraphPad Software, 9.3.0, USA).

2.4 Image acquisition and analysis

Whole salivary glands were photographed using a Zeiss Axioscope II (Zeiss, Germany) microscope, and images were exported as.tiff files. The intensity was measured using ImageJ (version 1.53t), and representative pictures were obtained from a confocal Zeiss LSM780 (Zeiss, Germany) microscope. Statistics was performed in Prism software (GraphPad Software, 9.3.0, USA).

2.5 Micro-manipulation of attached hemocytes

A total of 10 pairs of salivary glands per genotype were dissected into individual droplets of 200 µL PBS. A fluorescent microscope Leica DMi8 (Leica, Germany) was used to locate the attached hemocytes at the surface of the salivary gland. The hemocytes were collected using a micromanipulator TransferMan NK2 (Eppendorf, Germany) with ø 7 µm collection capillary and separated by a piezo-vibrator PiezoXpert (Eppendorf, Germany). Single-cell state hemocytes were individually transferred to 2.3 µL of lysis buffer (21), and each sample library was prepared as described below.

2.6 cDNA synthesis and library preparation for attached hemocytes

cDNA libraries of single attached hemocytes were generated using a modified version of the Smart-seq2 protocol (21). In short, cDNA synthesis was performed using universal primers, and PCR amplification was carried out over 24 cycles. cDNA products were subsequently purified using CA beads (Sigma; catalog no. 81260) for size selection using 8.8% polyethylene glycol 6000 (PEG 6000) to exclude primer dimers and nonspecific amplicons with sizes <150 bp. Combinatorial indexing via tagmentation was carried out in 96-well plates using 200 pg (measured in a Qubit fluorometer) of amplified cDNA, for a final volume of 10 mL/well. cDNA fragmentation using Tn5 transposase was carried out for 20 min on ice using the Illumina Nextra XT DNA sample preparation kit. Ligation and amplification of adaptors were carried out over 15 cycles in a final volume of 25 mL/well. Primer indices were used in the reaction from Illumina (Nextera index primers i7 and i5, catalog no. FC-131-1001). Tagmented and barcoded amplicons were then purified using CA beads for size selection. Quality control and fragment size distribution of the cDNA libraries were performed on a Bioanalyzer with the Agilent high-sensitivity DNA chip (catalog no. 5067-4626). Concentrations of each sample of cDNA libraries were measured on a PicoGreen 96-well plate NucleoScan fluorometer using a high-sensitivity double-stranded DNA (dsDNA) (HS assay kit; catalog no. Q32851). To perform library dilutions, the average fragment sizes of all cDNA libraries were measured for a final concentration of 2 nM in each sample. Finally, cDNA libraries were pooled and sequenced using Illumina NextSeq with 75-bp paired-end reads.

2.7 Cell sorting and cDNA library preparation for circulating hemocytes

A total of 10 larvae per genotype were bled into 500 µL of PBS, and the cells were sorted. The sorting was performed with a MoFlo Astrios EQ (Beckman Coulter, USA) cell sorter using a 488- and 532-nm laser for excitation, 100 µm nozzle, sheath pressure of 25 psi, and 0.1 µm sterile-filtered 1× PBS as sheath fluid. Flow sorting data was interpreted and displayed using the associated software, Summit v 6.3.1.

To test the precision of the adjustments made to center the drop in each well, a colorimetric test mimicking the sort was done based on (22). A 1.5 mg/µL solution of horseradish peroxidase (HRP) (catalog no. 31490, Thermo Fisher Scientific) with one drop of flow check beads (Beckman Coulter, USA) was sorted into each well of an Eppendorf 384-well plate (Cat no 34028, Thermo Fisher Scientific). A color change after sorting indicated that the drop hit the sort buffer and that the precision was adequate.

Single hemocytes were sorted directly into a 384-well plate containing 2.3 µL of lysis buffer (Eppendorf twin.tecTM PCR plates) using a CyClone™ robotic arm and at highly stringent single-cell sort settings (single mode, 0.5 drop envelope), and cDNA libraries were generated by the Eukaryotic Single Cell Genomics Facility at

SciLifeLab, Stockholm using a slightly modified version of Smart-seq2 as previously described (21), but where we used 20 cycles for cDNA amplification. The plate and sample holder were always kept at 4°C during the sort. After the sort, the plates were immediately spun down and put on dry ice.

2.8 Single-cell RNA sequencing

Single-cell libraries were sequenced at the National Genomics Infrastructure, SciLifeLab Stockholm, using the HiSeq2500 platform (Illumina) for 56 bp single-end sequencing. We sequenced a total of 384 single cells from the circulating hemocytes (negative controls, n=2, per plate) and 79 from attached hemocytes.

2.9 Mapping, annotation, and filtering of low-quality cells

A reference genome *D. melanogaster* (Dm6 v r6.37) was indexed, raw fastq files were used in mapping to the genome using STAR v 2.7.2 (23), and gene expression was measured using featureCounts v 2.0.0 (24), using default settings. The expression matrix was filtered to obtain high-quality cells using the following criteria: cells with >5% mitochondrial transcripts (stressed/dead/dying cells), <200 genes (low-quality cells), and those expressing more than 4,000 features (genes) (potential doublets or triplets) were removed in each replicate, and the remaining cells were subjected to subsequent computational analysis. A total of 380 and 61 single cells have passed the computational filtering from the circulating and the attached hemocyte, respectively, and are used for the data integration.

2.10 Normalization, dimensionality reduction, and clustering

The main computational analysis of read-count matrices was performed using the Seurat package (v 4.0.3) (25) in R (v 4.1.0). The complete R workflow can be assessed and reproduced in the R markdown (see code availability section). We used the default processing pipeline, https://satijalab.org/seurat/v3.2/pbmc3k_tutorial.html. First, count matrices and metadata were loaded. A mitochondrial gene count above 10% was filtered. Quality filtering was performed, and cells with a minimum of 200 genes expressed were kept for further processing. Subsequently, reads were normalized for sequencing depth using the "NormalizeData" function in the Seurat toolkit, selecting the top 2,000 variable genes. Thereafter, dimensionality reduction was performed using Principal component analysis (PCA) computing the first 50 Principal components (PCs). The first 10 PCs from the analysis were then subjected to shared-nearest-neighbor (SNN) inspired graph-based clustering via the "FindNeighbors" and "FindClusters" functions. For modularity optimization, the Louvain algorithm was used, and clustering was performed at a resolution of 0.4 for clustering granularity, resulting in five clusters. After clustering, a UMAP dimensionality reduction was performed using the first 10 dimensions of the PCA.

2.11 Differential gene expression analysis

Differential gene expression analysis (DGEA) of genes in identified clusters was performed using the function "FindAllMarkers" from the Seurat package (v. 4.0.3). Following the default option of the method, differentially expressed genes for each cluster were identified using a non-parametric Wilcoxon rank sum test. Differentially expressed genes in a cluster were defined by setting initial thresholds above a logarithmic fold-change of 0.5 and being present in at least 25% of the cells belonging to the same cluster. Representative marker genes with an adjusted *p*-value below 0.05 for each cluster were further selected. *p*-Values were adjusted using a Bonferroni correction including all genes in the dataset. To find representative marker genes with elevated expression in comparison to the remaining clusters, only positive log fold-changes were considered. For individual analyses such as gene enrichment analysis (see "Gene set enrichment analysis (gsea)"), threshold values for differential gene expressions were modified and will be described in detail in the respective sections of the *Material and methods* and *Results*. To identify DEGs between specific clusters of interest, the "FindMarkers" function in Seurat was used, and the identities were set to the respective clusters of interest. The same thresholds as stated above were used to define DEGs.

2.12 Biological pathways and GSEA

To track tests for top functional class enrichment among the global clusters, we used "ClusterProfiler" package v 3.16 (26) tool to conclude the enriched ontology terms as previously mentioned specifying the database "Org.Dm.db" to calculate the top 5 biological pathway enrichment. The gene set enrichment analysis (GSEA) was performed on top differentially expressed genes over the identified clusters in regard to gene expression profiles "Log2FC" as input in cluster profiler v 3.18.1 and ggupset package v 0.3.1 with a p-value cutoff of 0.05, minGSSsize of 3, maxGSSize of 800, and scoreType of "pos" to estimate for biological process ontology across clusters.

2.13 Computational summary

The read alignment and gene count matrix generation were performed as previously described in *Material and methods* (Section 2.9) (27). The single-cell gene count matrix cells with fewer than 250 UMIs, more than 10,000 UMIs, reads mapping to more than 7,000 genes, or more than 10% of read counts mapping to ribosomal genes were excluded. Each single-cell transcriptome was mapped to its original time window from which it was extracted by using the RT barcode. We performed standard processing of the data split by experiments as recommended by Seurat v4 documentation including NormalizeData, FindVariableFeatures (with the method set

to "vst"), ScaleData, RunPCA, RunUMAP (with dims set to 1:50 and n.components to 2), FindNeighbors (with reduction set to UMAP and dims set to 1:2), and FindClusters. This version uses the first 10 principal components, along with pN of 0.2 and pK of 0.005. This version uses the first 10 principal components, along with pN of 0.2and pK of 0.005 for dimensionality reduction, clustering, and identification of cluster-specific marker genes. The standard Seurat processing pipeline, as described in the previous section, was performed on each non-overlapping inferred age window separately. We found that the default Seurat clustering resolution parameter did not capture the dynamics of the presence of different cell types. For each batch, we clustered the data with a variety of resolutions (from 0.1 to 1.5 in increments of 0.3) and then computed the Silhouette score for finding the best resolution for clustering, we found that 0.4 resolution provides the best Silhouette score for each single-cell fitting in cluster community, as increasing the resolution resulted in lower number of cells per clusters and insignificant results when performing differentially expressed genes text. Finally, we integrated and clustered the data, and from these clusters, we used Seurat's FindMarkers to iteratively loop through all clusters and identify marker genes.

2.14 RNA velocity and lineage interference

To interpret the global transcriptional progression of hemocytes and their cell fate decision, we established the cell continuum of cell differentiation and data layers of unspliced and spliced mRNA for the entire data generated with Velocyto CLI (v.0.17.17) according to the CLI usage guide (Velocyto run-smartseq2). The output loom files were combined using "loompy." The merged loom file was imported into the scVelo package (v1.0.6) (28, 29). The unspliced and spliced mRNA counts of cells from clusters C0–C4 were extracted. We used the "merged.utilis" function in the scVelo pipeline, where cells with low pre-mRNA counts were removed as part of the filtering. In short, the gene-specific velocities are obtained by fitting a ratio between unspliced and spliced mRNA abundances and then computing how the observed abundances change from those observed in a steady state. The ratio of "spliced," "unspliced," and "ambiguous" transcripts were calculated, and data were pre-processed using functions for detection of minimum count number, filtering, and normalization using "scv.pp.filter_and_normalise" and followed by "scv.pp.moments" function. The gene-specific velocities were then calculated using "scv.tl.velocity" with mode set to "deterministic" and "scv.tl.velocity_graph" function to generate velocity graph and visualization using "scv.pl.velocity_graph" function. In addition, we used the "scv.tl.recover_latent_time" function to infer a shared latent time from splicing dynamics and plotted the genes along the time axis.

2.15 Data availability

The raw processed data generated for this study have been deposited on Zenodo repository under accession number 7997643 and can be accessed via https://zenodo.org/deposit/7997643 and interactively on https://mubasher-mohammed.shinyapps.io/Sc-drosophila/. The custom code scripts used to analyze data for this study are available at https://github.com/ANKARKLEVLAB/Single-cell-P.f-gametocyte.

3 Results

3.1 Single-cell profiling of tumor-associated hemocytes reveals transcriptional heterogeneity

We initially characterized the population of TAHs that attach to Ras^{V12} salivary glands (SGs) and found that they consist mainly of plasmatocytes and the occasional lamellocyte (Figures 1A, B). To identify genes that are differentially regulated in hemocytes (DEGs) from tumor larvae, we profiled the transcriptome of single circulating hemocytes from wild-type and tumor larvae and from TAHs, which were extracted manually from tumorous SGs. Additionally, to characterize the contribution of effector caspases to tumor progression, we analyzed larvae in which the effector caspase inhibitor p35 was co-expressed with Ras^{V12}: p35;Ras. We had previously shown that similar to Drosomycin (Drs), the expression of p35 in Ras-SGs restores the spherical nuclear shape that is disturbed upon sole Ras expression, although SGs from both combinations show the same size increase as Ras^{V12} larvae (20) and (Figures 2A–D, quantified in Figure 2E). In contrast to Drs (20), co-expression of p35 still led to hemocyte recruitment (Figures 2A'–D' quantified in Figure 2F). This allowed us to compare TAHs both between wild-type and tumor larvae and in settings with and without active caspases downstream of JNK signaling. TAHs and circulating hemocytes were selected for expression of the plasmatocyte-specific marker Eater (Figure 3A, see *Material and Methods*).

Collectively, hemocyte transcriptomes displayed additional plasmatocyte markers indicating successful purification of these macrophage-related cells (Figures 3B–H). Plasmatocyte markers include Nimrod C1 (NimC1), serpent (srp), Hemolectin (Hml), and spätzle (spz), several of which have been used as pan-plasmatocyte markers and more recently as markers for specific plasmatocyte subpopulations (30). As expected, the crystal cells and lamellocytes markers lozenge (lz) and Atilla, respectively; were not detected (Figures 3C, D). Crystal cell prophenoloxidase 1 (PPO1) was detected in a few cells (Figure 3H) (see also below).

Clustering analysis revealed true variation between the single cell transcriptomes for the identified five clusters (at $p<0.05$ and a difference in expression >2 if not stated otherwise; Figures 4A–C, middle panel), three of which included tumor cells (clusters C0, C2, and C3 (Figures 4C, D). Cluster C2 overlaps largely with TAHs (Figure 4A). Gene Ontology analysis for biological processes of upregulated genes in the clusters highlighted several gene sets that overlapped between clusters but also some cluster-specific sets (Figure 4E). The latter category included genes involved in cell motility (cluster C1), translation (C0), protein folding (C4), and immune response genes for cluster 2 (attached cells) and several

10.3389/fimmu.2023.1243797

categories specific for cell division (C3, circulating cells from both tumor models). Taken together, despite the technically limited number of cells compared to other studies (30), we identified subpopulations of plasmatocytes whose signatures differed significantly depending on genotype (tumor versus wild type) and cell status (attached versus circulating).

3.2 The expression of signature genes for the different clusters differs between tumor models

To obtain more detailed insight into the gene categories that specified the clusters, we identified the genes whose expression significantly specified the clusters (Supplementary Tables S1-S5). In parallel, we compared expression strengths between genotypes focusing on the three populations that comprised cells from the tumor models (clusters 0, 2, and 3 in Figures 4D, 5A–C). For attached hemocytes (C2), the list of the most strongly expressed genes varied between the two tumor models (Figure 5A). To follow this up, we scanned cluster 2-specific genes for gene set enrichment and identified two enriched categories (1): pupal adhesion and (2) immune response (Supplementary Figures S1A, B). Pupal adhesion was due to the presence of genes that code for salivary gland secretions (Supplementary Figure S1B). Since these genes are hardly expressed outside salivary glands (FlyAtlas (31)), we interpret their presence in hemocytes as being passenger transcripts (32), i.e., transcripts that have been taken up by TAHs by way of cellular fragments released from the glands. Alternatively, SG transcripts may have been co-purified together with TAHs during extraction. This latter explanation implies that expression of p35 partially prevented the release of SG fragments from Ras^{V12} SGs in line with its anti-apoptotic function. The second category (immune genes) contains genes that are most strongly (although not mutually exclusively) expressed in either tumor model (Supplementary Figure S1A). Taken together, we show that hemocytes in both tumor models differ qualitatively from hemocytes in control larvae and that inhibition of effector caspases in tumors reveals additional quantitative differences.

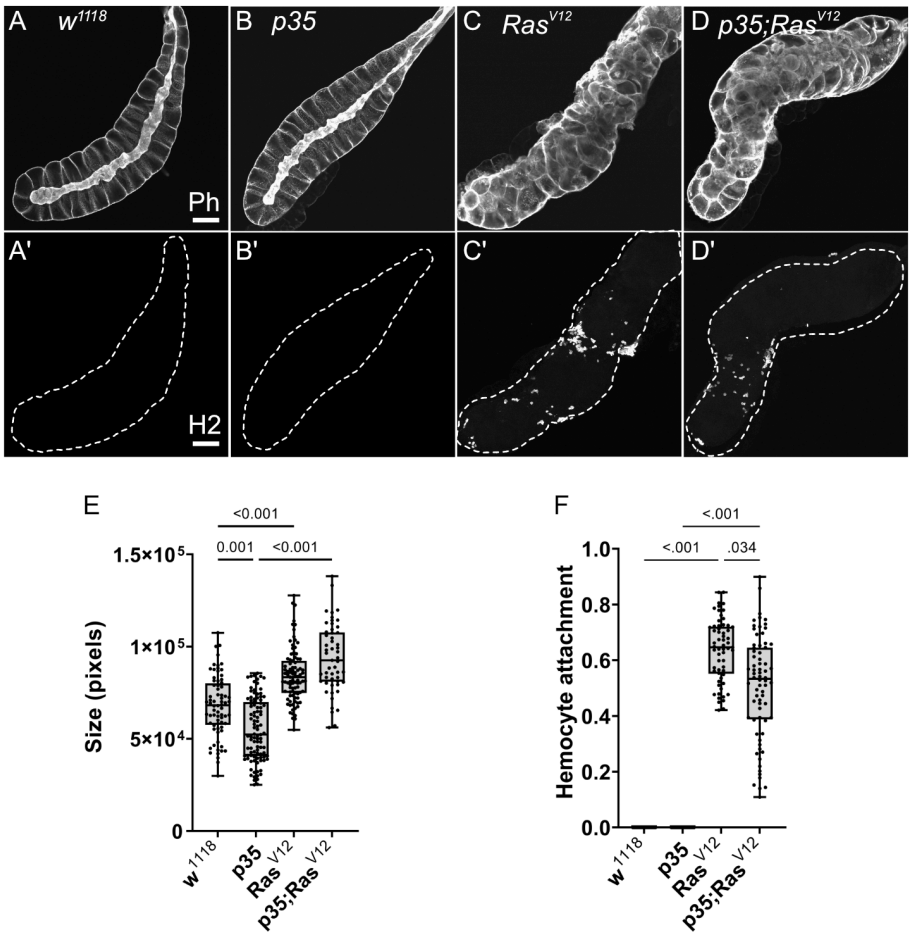

FIGURE 2
Characterization of SGs from the used genotypes. **(A–D)** SGs from wild type (w^{1118}), p35 expressing larvae, Ras^{V12} larvae, and p35;Ras^{V12} larvae were stained with phalloidin and a plasmatocyte-specific antibody (Hemese, H2, **(A'–D')**. SG size for the different genotypes was quantified shown in **(E)** and hemocyte attachment in **(F)**. Whisker length min to max, bar represents median. p-value quantified with ANOVA.

3.3 The response towards tumors differs between the two models

Generally, TAHs in the Ras model show strong expression of AMPs including Dpt(Diptericin)A and B, Att(Attacin)C, and Cec (Cecropin)C. In contrast, p35;Ras^{V12} TAHs show higher levels of all three phenoloxidases PPO1–3 (Supplementary Figure S1A). This is in line with the previously identified function of the TGF-like protein dawdle (*daw*), which promotes AMP activation (33) and, indeed, *daw* clusters with AMP expression in our hands (Supplementary Figure S1A). A second TGF member (*dpp*) with immune-regulatory function (33) is less expressed in tumors compared to wild-type hemocytes. Similarly, the M1 marker iNOS is more strongly expressed in p35;Ras^{V12} TAHs, while the M2 marker Arginase (Arg) peaks in Ras TAHs.

For both clusters 0 and 3 (Figures 5B, C), the same set of genes was more strongly induced in circulating tumor compared with circulating wild-type hemocytes, although the majority showed stronger expression when effector caspases were repressed (p35;Ras^{V12}) compared to the tumor-only (Ras) model. Gene set enrichment analysis fully confirmed the enrichment for genes involved in cell division (Figure 4E) in cluster 3 (circulating cells from both tumor models) but failed to deliver significant returns for the category "Biological process" for cluster 0. In line, the quantification of hemocyte proliferation fully confirmed an increase in cell divisions in both tumor models including the additional increase in the p35;Ras^{V12} model (Figure 5D). This may contribute more to the differentiation of TAHs rather than circulating cells, which show similar counts (18).

Finally, when searching for pathways compatible with expression in the five clusters using the Reactome database

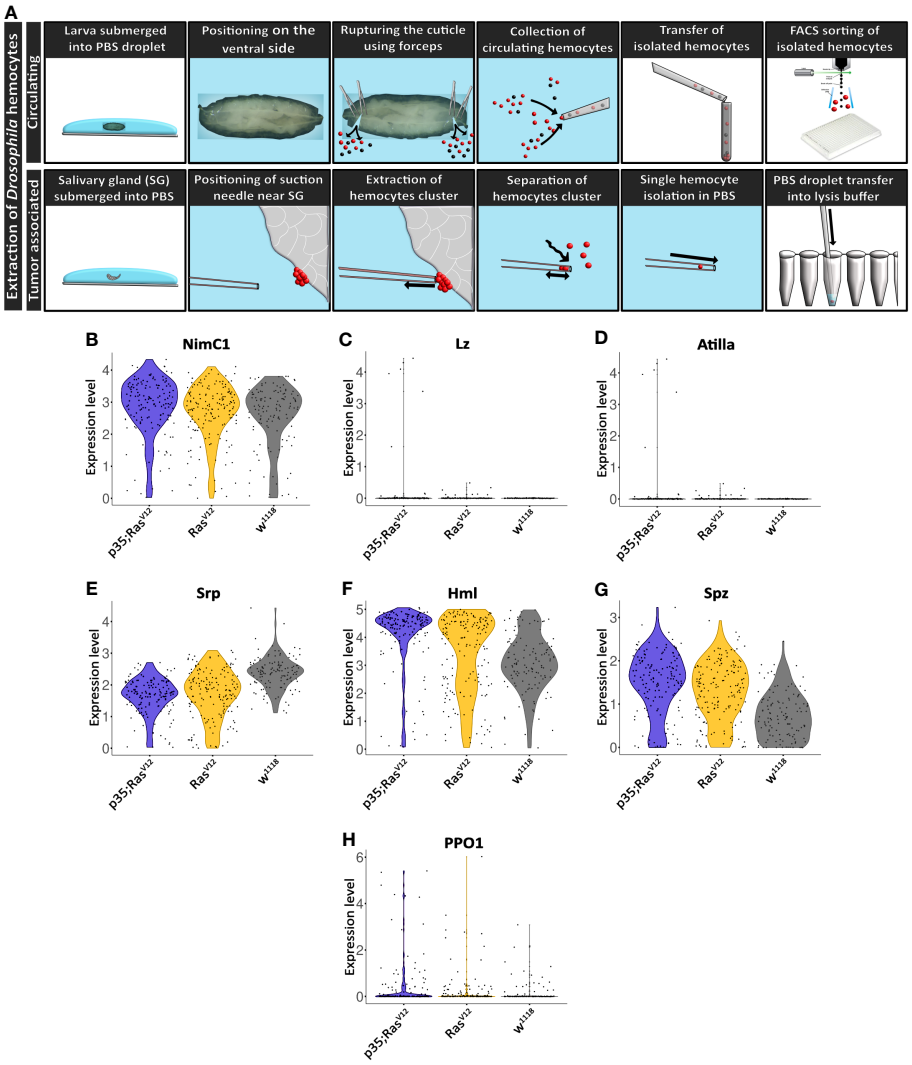

FIGURE 3
Extraction and initial characterization of circulating hemocytes and TAHs from wild-type and tumor larvae. **(A)** Upper panel: circulating hemocytes were extracted from larvae and individualized using cells sorting. Lower panel: TAHs were extracted from salivary glands using capillary suction, individualized and processed for single-cell RNA sequencing. See text for further details. **(B–H)** Classification of single hemocytes confirms their plasmatocyte identity and the absence of lamellocytes (Atilla) or crystal cell (Lozenge) markers.

10.3389/fimmu.2023.1243797

(https://reactome.org), an enrichment for genes involved in neutrophil degranulation was found for cluster 0 (Supplementary Figure S1C), which, when using a split analysis, also indicated that this pathway was more strongly expressed in p35;Ras^{V12} hemocytes. Pseudotime analysis using RNA velocity (Figures 6A–D) indicated that TAHs and circulating hemocytes from both tumor models follow distinct pathways, although due to the restricted number of TAHs, a rarer intermediate population may have been missed.

3.4 Transcript transfer between hemocytes and other tissues

Recently, we and others have characterized the activation of crystal cells and the subsequent release of leaderless PPO2 into the extracellular environment via cell rupture (34, 35). Functionally, crystal cell activation bears similarities to pyroptotic cell death in mammals, including its dependence on caspase activity, which can be inhibited by p35 (36). While our findings explained how PPO2 was released into the hemolymph, the mechanism for secretion of PPO1, which also lacks a signal peptide, remained obscure. Since we found that PPO2 was enriched in TAHs (Figure 7A, Supplementary S1A), we wondered which secretion mechanism led to their spread to other plasmatocytes. In line with crystal cell rupture and similar to passenger transcripts from SGs, the mRNA encoding PPO2 was detected in plasmatocytes both as a mature (spliced) form and as a non-spliced (nuclear) immature mRNA (Figures 7C, D). This indicates that phagocytic hemocytes had access to both the nuclear and the cytosolic fraction of ruptured crystal cells. In contrast, PPO1 transcripts were only detected in their mature form (Figure 7B). We conclude that PPO2 transcripts in TAHs originate either from pyroptotic crystal cells or TAHs, which have acquired crystal cell characteristics, while PPO1 mRNA originates from live crystal cells. Taken together, this explains why both PPO1 and PPO2 had been located on *Ras* SGs (19) despite the apparent absence of crystal cells (Figure 1).

In addition to PPO1, two transcripts (CG 13962, and the transcription factor Relish) were detected only in their mature form, indicating a possible origin outside TAHs.

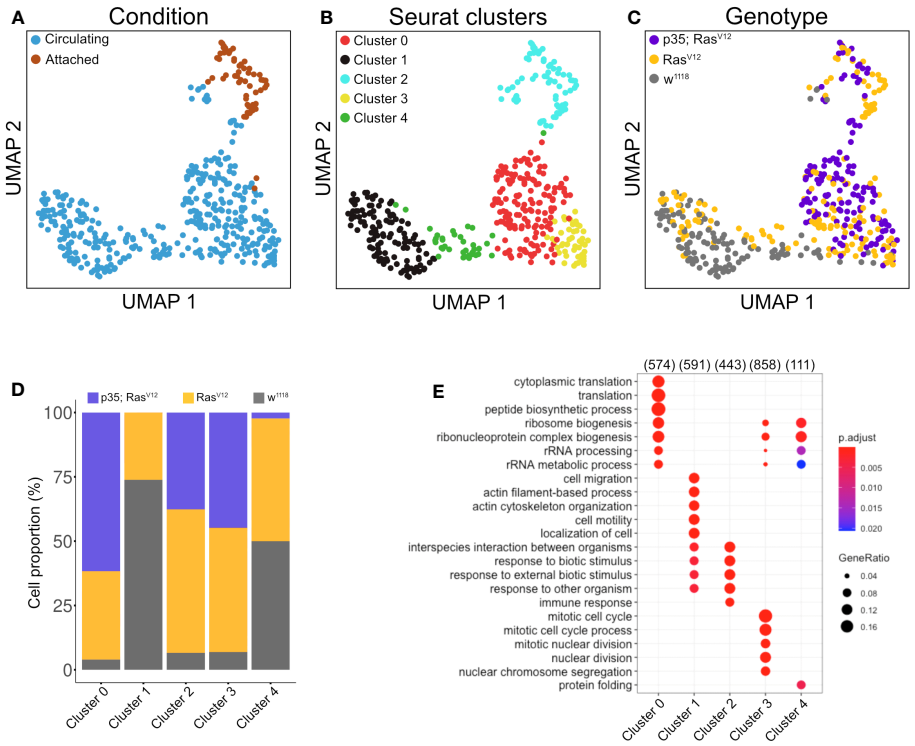

FIGURE 4
Clustering analysis of hemocytes. Circulating single cells (Genotype: w^{1118}, Ras^{V12} and p35;Ras^{V12}) were processed using Smart-seq2. For manually extracted TAHs (Genotype: Ras^{V12}, p35;Ras^{V12}), libraries were generated according to the Smart-seq2 protocol. **(A)** UMAP projection of single-cell transcriptome integrated datasets overlaid with batch labels. **(B)** Louvain clustering analysis based on the first 10 PCs shows the biological variation of the data and cell communities' assignments. **(C)** UMAP projection overlaid with single-cell-specific genotypes. The global transcriptome similarities and differences were assessed based on k-nearest neighbors (kNN) force-directed graph with a true signal variation of the single-cell transcriptome on the integrated datasets. **(D)** Relative frequency of w^{1118}, Ras^{V12}, and p35Ras^{V12} hemocytes within the five identified clusters. **(E)** Gene set enrichment analysis (GSEA) (biological processes) of upregulated genes in a minimum of 25% of the cells in each cell community with a cutoff of 0.25 log fold-change threshold, comparing different cell communities (clusters) and highlighting the various biological processes' heterogeneity. Color scale indicating the corrected p-values, where blue is less significant and red is highly significant. Black circular dots indicate the gene ratio in comparison to the universal background gene list. Numbers in brackets indicate the gene numbers overlapping the ontology terms for a specific cluster.

10.3389/fimmu.2023.1243797

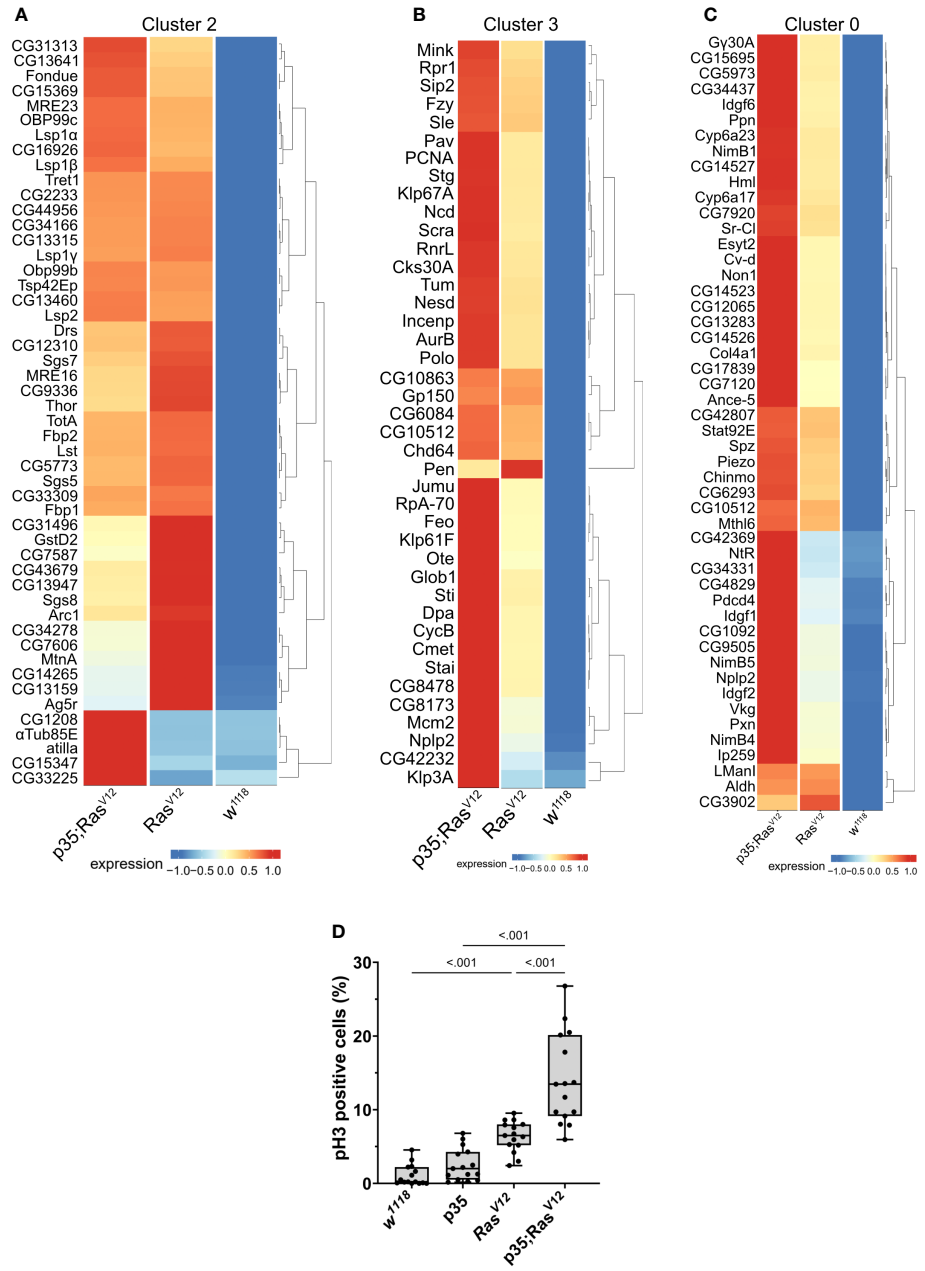

FIGURE 5
Contribution of the three genotypes to clusters 2 **(A)**, 3 **(B)**, and 0 **(C)**. Expression intensity was analyzed for the most significantly enriched genes in the respective clusters using the visualization tool created for this project (see: https://mubasher-mohammed.shinyapps.io/Sc-drosophila/). **(D)** The enrichment of genes involved in cell division in cluster 3 (see also Figure 4E) was functionally confirmed using anti-phospho Histone 3 labeling to detect proliferating cells. Whisker length min to max, bar represents median. p-value quantified with ANOVA.

4 Discussion

To our best knowledge, we provide the first transcript profile of TAHs—the invertebrate equivalent of mammalian tumor-associated macrophages (TAMs). Relying on a molecularly induced early stage of tumor progression that affects the salivary glands (18, 20), we find that TAHs display some features of mammalian M2-like macrophages, which have been implicated in regenerative processes. These include the presence of members of the chitinase-like proteins (IDGFs in *Drosophila*), which are among the most abundant proteins in activated macrophages and are used as markers for M2 macrophages (37) (Supplementary Figure S1C). Notably, TAHs show a clear signature of immune activation, which includes several antimicrobial peptides and members of clotting systems including IDGF3, Fondue, and phenoloxidases (Supplementary Figure S1A). Although both effector branches are activated in the TAHs from both tumor models, there are differences (Supplementary Figure S1A): AMPs appear to dominate the TAH response in Ras-SGs, whereas clotting factors are more strongly expressed in p35;Ras^{V12} SGs. AMP induction

10.3389/fimmu.2023.1243797

may be in line with the presence of SG (passenger) transcripts in the Ras-alone model (Figure 8, right part) and may serve to degrade tumor fragments during efferocytosis including cytosolic and nuclear parts. In contrast, inhibition of caspases appears to activate immune reactions that are more akin to the formation of mammalian granulomas (Figure 8, left part). Bifurcation in hemocyte differentiation is reminiscent of the division of labor between *Drosophila* hemocytes shown previously, which depends on two members of the TGF family (the BMP-like member Dpp and the Activin-like member Dawdle (33)). In line with Dpp's role in suppressing antimicrobial responses, we find that two receptors for BMP-like TGFs (thickveins; tkv and saxophone; sax) are strongly expressed in p35:Ras^{V12} hemocytes but not in Ras or control hemocytes (Supplementary Figure S2). While the difference in responses between Ras larvae and larvae that co-express the caspase inhibitor p35 may be explained by a lack of apoptosis downstream of caspases, we prefer alternative explanations that include non-apoptotic form of cell death or non-apoptotic functions of caspases (38, 39). Taken together, our results identify targets for modifier screens that address the contribution of TAH-DEGs to tumor development using both classical and molecularly induced tumor mutants.

Additionally, our work points toward a potential communication network that links TAHs, SG tumors, and non-tumor tissues (Figure 8). This likely includes efferocytosis of apoptotic bodies derived from hyperplastic SGs (18), leading to an extended presence of SG transcripts (passenger transcripts) in TAHs before their degradation. While most of the DEGs in TAHs are genuine TAH transcripts, we find exceptions. These include two prophenoloxidases (35), which are known to be exclusively expressed in crystal cells (40) and not in the plasmatocytes that we sequenced and the NF-kappaB-like factor Relish. While the mechanism for this cell's non-autonomous presence of transcripts in TAHs is unknown, we hypothesize that exosomes may be likely candidates (Figure 8, dashed arrows). Alternatively, plasmatocytes may transdifferentiate and express transcripts that are more specific for crystal cells and lamellocytes (41, 42) (Figure 8, solid arrows). Supporting an exosome origin, two long non-coding RNAs (CR

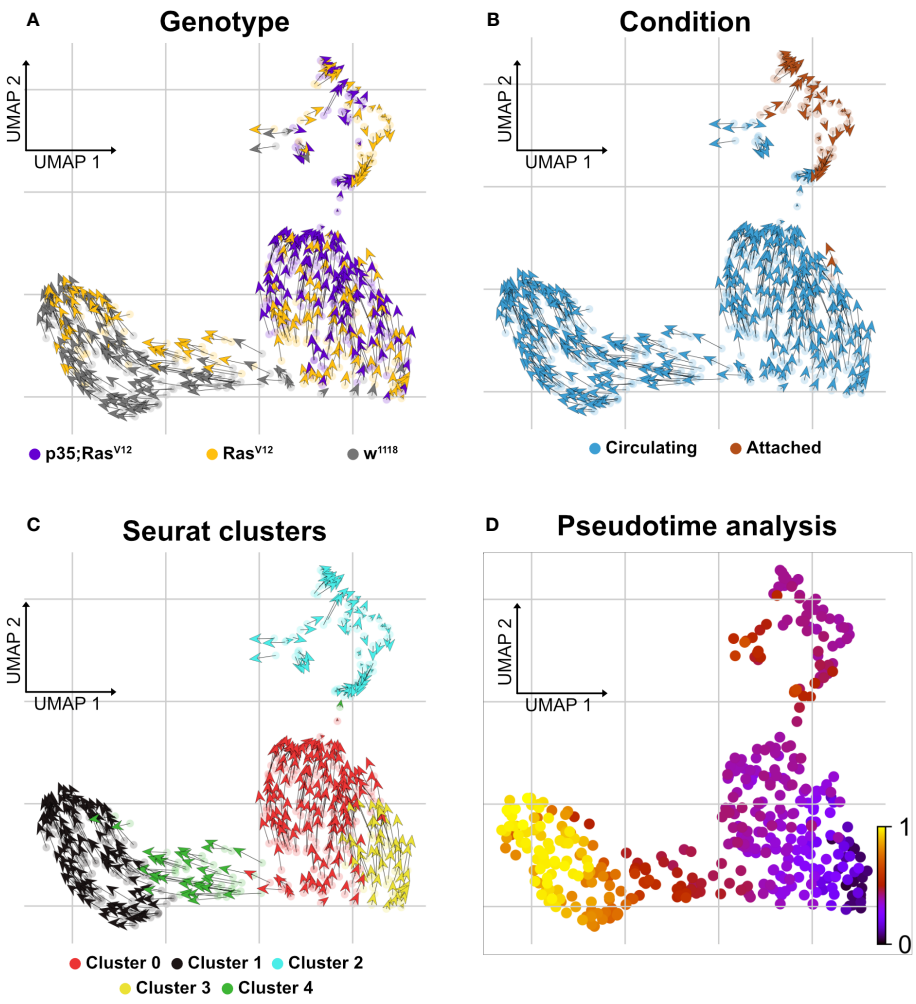

FIGURE 6
Delineating splicing kinetics through generalizing RNA velocity to cell population clusters. **(A)** Projecting velocities across the wild type, Ras^{V12}, and p35;Ras^{V12} hemocytes. **(B)** Across conditions (attached and circulating). **(C)** Identified Seurat clusters. **(D)** Pseudotime inference of integrated datasets shows the root cells composed mainly of cluster 3 cells (mixture of p35;Ras^{V12} and Ras^{V12} larvae) and trajectory depicting pseudotime units assignment with terminal state composed mainly of cluster 1 (wild type and Ras^{V12} larvae).

10.3389/fimmu.2023.1243797

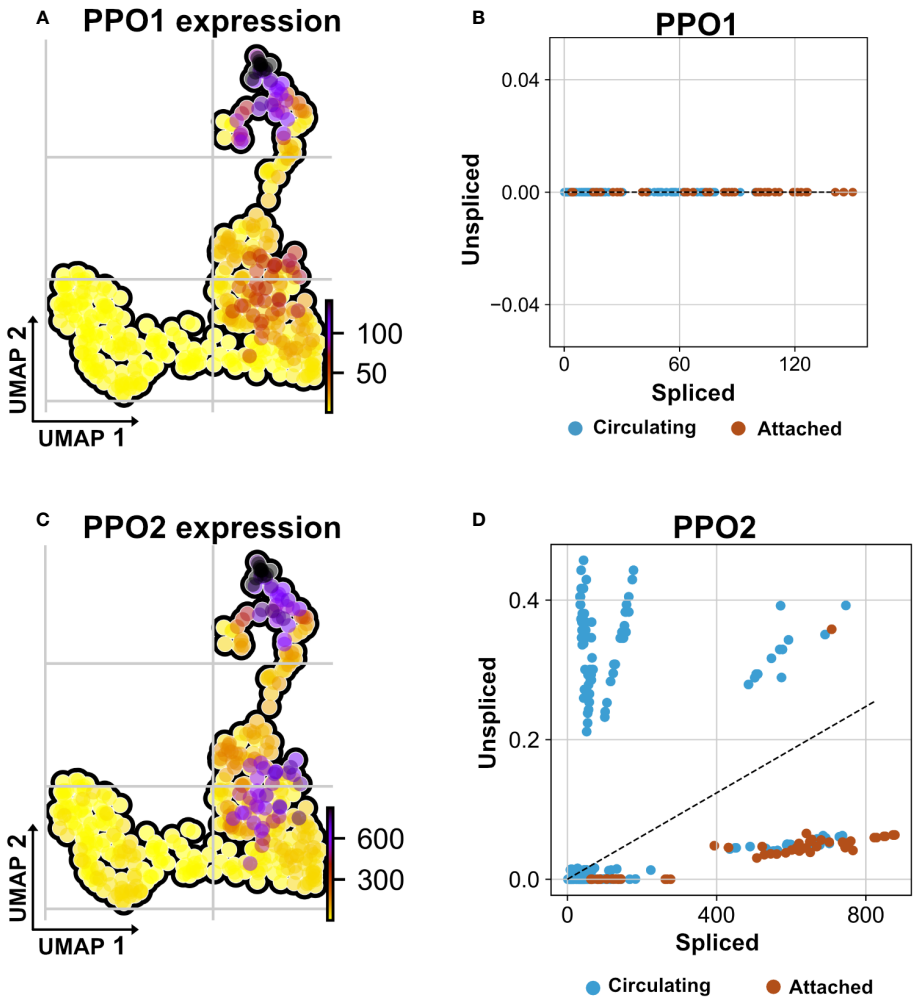

FIGURE 7
Non-autonomous distribution of crystal cell derived prophenoloxidase transcripts. **(A)** UMAP visualizes transcripts analysis showing the strongest presence of mature (spliced) mRNA of crystal cell-derived prophenoloxidase 1 (PPO1) across attached hemocyte TAHs condition corresponding to Ras^{V12} larvae. **(B)** Scatter plot shows the absence of immature transcripts (unspliced) reads across conditions (attached and circulating). **(C)** UMAP visualizes transcripts depicting cell-derived prophenoloxidase 2 (PPO2) in attached hemocyte TAHs condition. **(D)** Scatter plot indicates the exclusive presence of mature and immature (spliced vs. unspliced) PPO2 transcripts in plasmatocytes (higher ratio of unspliced across circulating condition), in contrast to PPO2, which is released from crystal cells through cell rupture and subsequently taken up by plasmatocytes most likely through phagocytosis.

34335 and R 40469) that we found in TAHs have been identified among the 10 most abundant non-ribosomal RNAs in exosomes released from *Drosophila* cell lines (43). Additionally, in the same study, *Arc1* was shown to be among the most abundant mRNAs in exosomes from one of the two cell lines used (43). Notably, in the flies' nervous system, Arc1 is involved in the formation of capsid-like vesicles, which also contain Arc1 transcripts that are recruited through the binding of Arc1 protein to the 3′ end of the *Arc1* transcript (44). Both Arc1 and its human equivalent derive from retroviral Gag proteins (44–46) and mediate neuronal plasticity. A function for *Drosophila* Arc1 in immunity has so far not been suggested, although it is expressed in non-neural tissues (FlyAtlas (31)) and we find it is enriched in TAHs (Figure 5A, Supplementary Figure S3A). When combined with our Ras model, Arc mutants alleviate some of the Ras-associated phenotypes: SG size, pJNK activity, and expression of Idgf3 in SGs are reduced in *Arc1;Ras* larvae. Notably, we recently showed that Idgf3 is involved in several tumor phenotypes in the *Ras* model (47). A similar trend is observed for caspase activity (Supplementary Figures S3B–E). It should be noted though that a reduction for the first three phenotypes was also observed in *Arc1* SGs, although with lower significance (Supplementary Figures S3B–D). To more specifically study transcript transfer from TAHs to SGs, we chose the transcription factor Relish, whose transcript we only detected in its spliced form (see above). Indicating TAH-SG transfer of the transcript, Relish protein is detected in *Ras*- but not in wild-type SGs. This is inhibited in *Arc1* mutants, although hemocytes still attach (Supplementary Figures S3F, G). Further supporting a function for hemocytes, we had previously failed to detect differences in Rel expression between wild-type and Ras SGs at 96 h when hemocytes had not attached (20). Future work using tissue-specific knockdowns will identify the tissue of origin for *Rel* transcripts. Of note, similar to tumor-associated

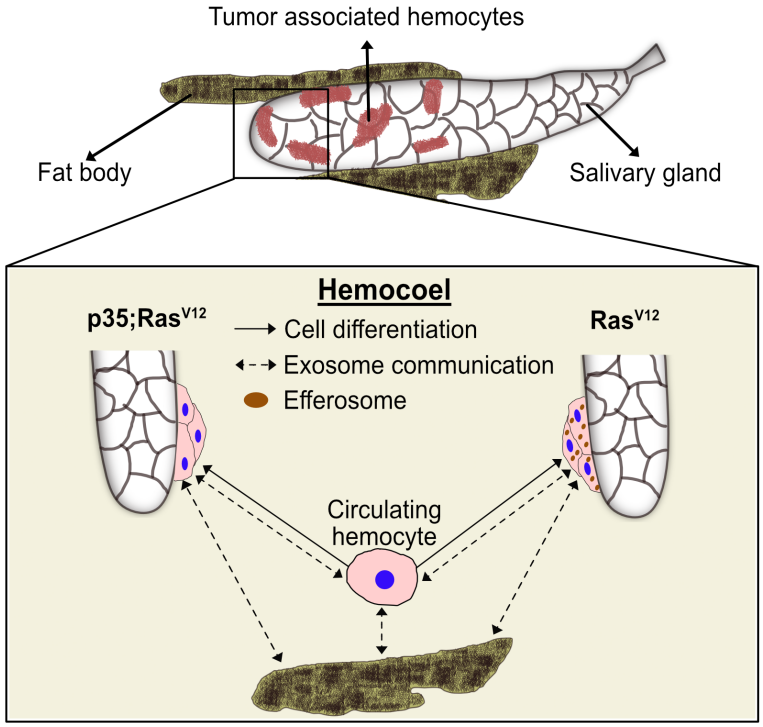

FIGURE 8
A proposed model for the differentiation and distribution of hemocyte transcriptomes. Hemocyte reactions towards SG dysplasia are schematically depicted for the Ras^{V12} model (right part) and after inhibition of effector caspases by p35 (left part). Communication via exosomes (dashed arrows) and transdifferentiation (solid arrows) are indicated. Efferosomes are present in Ras^{V12} model as result of efferocytosis of apoptotic bodies from hyperplastic salivary gland. See text for further details.

macrophages, extracellular vesicles have been shown to display both pro- and anti-tumor potential. Taken together, our findings on macrophage-like cells from an invertebrate provide targets that may turn out useful to steer tumor therapy even in humans (2).

Data availability statement

The datasets presented in this study can be found in online repository Gene Expression Omnibus (GEO) with accession numbers GSE242774, GSM7770352, and GSM7770353.

Ethics statement

The manuscript presents research on animals that do not require ethical approval for their study.

Author contributions

UT conceived the study. JA and UT supervised the study. DK experimental design, investigation, methodology, and visualization. MK and MS performed immunohistochemistry analyses and *Drosophila* genetics. MK performed proliferation assays. JA and DK performed sorting and scSeq. MM performed mapping and computational analyses of the data. MM, DK, MS, and MK generated figures. JA supervised the computational analysis. UT and MM wrote the manuscript. All authors read and reviewed the manuscript. All authors contributed to the article and approved the submitted version.

Funding

This work was supported by grants from the Swedish Cancer Foundation (CAN 2015-546 to UT), the Wenner-Gren Foundation (UPD2020-0094 and UPD2021-0095 to MK), the Swedish Research Council (VR 2016-04077 and VR 2021-04841 to UT), the Carl-Tryggers Foundation (CTS 21:1263 to UT), the Swedish Research Council (VR 2021-05057 to JA), and the Swedish Society for Medical Research (SSMF) to JA.

Acknowledgments

We thank the Microbial Single Cell Genomics and the Eukaryotic Single Cell Genomics facilities at Science for Life Laboratory (SciLifeLab), Sweden, for cell sorting and smart-seq2 library preparations, respectively, and the National Genomics Infrastructure, SciLifeLab for sequencing. The computations were performed using resources provided by SNIC through Uppsala Multidisciplinary Center for Advanced Computational Science (UPPMAX). We also thank Jiwon Shim (Hanyang University, Korea) and the reviewers for useful comments on the manuscript.

Conflict of interest

The authors declare that the research was conducted in the absence of any commercial or financial relationships that could be construed as a potential conflict of interest.

Publisher's note

All claims expressed in this article are solely those of the authors and do not necessarily represent those of their affiliated organizations, or those of the publisher, the editors and the reviewers. Any product that may be evaluated in this article, or claim that may be made by its manufacturer, is not guaranteed or endorsed by the publisher.

Supplementary material

The Supplementary Material for this article can be found online at: https://www.frontiersin.org/articles/10.3389/fimmu.2023.1243797/full#supplementary-material

References

1. Dhokia V, Moss JAY, Macip S, Fox JL. At the crossroads of life and death: The proteins that influence cell fate decisions. *Cancers.* (2022) 14(11):2745. doi: 10.3390/cancers14112745

2. Gregory CD, Paterson M. An apoptosis-driven "onco-regenerative niche": roles of tumour-associated macrophages and extracellular vesicles. *Philos Trans R Soc Lond B Biol Sci* (2018) 373(1737):20170003. doi: 10.1098/rstb.2017.0003

3. Lees A, Sessler T, McDade S. Dying to survive-the p53 paradox. *Cancers.* (2021) 13(13):3257. doi: 10.3390/cancers13133257

4. Morana O, Wood W, Gregory CD. The apoptosis paradox in cancer. *Int J Mol Sci* (2022) 23(3):1328. doi: 10.3390/ijms23031328

5. Viola A, Munari F, Sánchez-Rodríguez R, Scolaro T, Castegna A. The metabolic signature of macrophage responses. *Front Immunol* (2019) 10:1462. doi: 10.3389/fimmu.2019.01462

6. Cassetta L, Pollard JW. Tumor-associated macrophages. *Curr Biol CB* (2020) 30 (6):R246–8. doi: 10.1016/j.cub.2020.01.031

7. Kelly B, O'Neill LAJ. Metabolic reprogramming in macrophages and dendritic cells in innate immunity. *Cell Res* (2015) 25(7):771–84. doi: 10.1038/cr.2015.68

8. Kolliniati O, Ieronymaki E, Vergadi E, Tsatsanis C. Metabolic regulation of macrophage activation. *J Innate Immun* (2022) 14(1):51–68. doi: 10.1159/000516780

9. Soltész B, Buglyó G, Németh N, Szilágyi M, Pös O, Szemes T, et al. The role of exosomes in cancer progression. *Int J Mol Sci* (2021) 23(1):8. doi: 10.3390/ijms23010008

10. Zhang WL, Liu Y, Jiang J, Tang YJ, Tang YL, Liang XH. Extracellular vesicle long non-coding RNA-mediated crosstalk in the tumor microenvironment: Tiny molecules, huge roles. *Cancer Sci* (2020) 111(8):2726–35. doi: 10.1111/cas.14494

11. Bilder D, Ong K, Hsi TC, Adiga K, Kim J. Tumour-host interactions through the lens of Drosophila. *Nat Rev Cancer.* (2021) 21(11):687–700. doi: 10.1038/s41568-021-00387-5

12. Cho B, Yoon SH, Lee D, Koranteng F, Tattikota SG, Cha N, et al. Single-cell transcriptome maps of myeloid blood cell lineages in Drosophila. *Nat Commun* (2020) 11(1):4483. doi: 10.1038/s41467-020-18135-y

13. Fu Y, Huang X, Zhang P, van de Leemput J, Han Z. Single-cell RNA sequencing identifies novel cell types in Drosophila blood. *J Genet Genomics Yi Chuan Xue Bao.* (2020) 47(4):175–86. doi: 10.1016/j.jgg.2020.02.004

14. Leitão AB, Arunkumar R, Day JP, Geldman EM, Morin-Poulard I, Crozatier M, et al. Constitutive activation of cellular immunity underlies the evolution of resistance to infection in Drosophila. *eLife.* (2020) 9:e59095. doi: 10.7554/eLife.59095

15. Pastor-Pareja JC, Wu M, Xu T. An innate immune response of blood cells to tumors and tissue damage in Drosophila. *Dis Model Mech* (2008) 1(2–3):144–54. doi: 10.1242/dmm.000950

16. Fogarty CE, Diwanji N, Lindblad JL, Tare M, Amcheslavsky A, Makhijani K, et al. Extracellular reactive oxygen species drive apoptosis-induced proliferation via drosophila macrophages. *Curr Biol CB.* (2016) 26(5):575–84. doi: 10.1016/j.cub.2015.12.064

17. Fogarty CE, Bergmann A. Killers creating new life: caspases drive apoptosis-induced proliferation in tissue repair and disease. *Cell Death Differ* (2017) 24(8):1390–400. doi: 10.1038/cdd.2017.47

18. Hauling T, Krautz R, Markus R, Volkenhoff A, Kucerova L, Theopold U. A Drosophila immune response against Ras-induced overgrowth. *Biol Open* (2014) 3 (4):250–60. doi: 10.1242/bio.20146494

19. Khalili D, Kalcher C, Baumgartner S, Theopold U. Anti-fibrotic activity of an antimicrobial peptide in a drosophila model. *J Innate Immun* (2021) 13(6):376–90. doi: 10.1159/000516104

20. Krautz R, Khalili D, Theopold U. Tissue-autonomous immune response regulates stress signaling during hypertrophy. *eLife.* (2020) 9:e64919. doi: 10.7554/eLife.64919

21. Picelli S, Faridani OR, Björklund AK, Winberg G, Sagasser S, Sandberg R. Full-length RNA-seq from single cells using Smart-seq2. *Nat Protoc* (2014) 9(1):171–81. doi: 10.1038/nprot.2014.006

22. Rodrigues OR, Monard S. A rapid method to verify single-cell deposition setup for cell sorters. *Cytom Part J Int Soc Anal Cytol.* (2016) 89(6):594–600. doi: 10.1002/cyto.a.22865

23. Dobin A, Davis CA, Schlesinger F, Drenkow J, Zaleski C, Jha S, et al. STAR: ultrafast universal RNA-seq aligner. *Bioinforma Oxf Engl* (2013) 29(1):15–21. doi: 10.1093/bioinformatics/bts635

24. Anders S, Pyl PT, Huber W. HTSeq—a Python framework to work with high-throughput sequencing data. *Bioinformatics.* (2015) 31(2):166–9. doi: 10.1093/bioinformatics/btu638

25. Hao Y, Hao S, Andersen-Nissen E, Mauck WM, Zheng S, Butler A, et al. Integrated analysis of multimodal single-cell data. *Cell.* (2021) 184(13):3573–87. doi: 10.1016/j.cell.2021.04.048

26. Wu T, Hu E, Xu S, Chen M, Guo P, Dai Z, et al. clusterProfiler 4.0: A universal enrichment tool for interpreting omics data. *Innovation.* (2021) 2(3):100141. doi: 10.1016/j.xinn.2021.100141

27. Mohammed M, Dziedziech A, Sekar V, Ernest M, Alves E Silva TL, Balan B, et al. Single-cell transcriptomics to define plasmodium falciparum stage transition in the mosquito midgut. *Microbiol Spectr.* (2023) 11(2):e0367122. doi: 10.1128/spectrum.03671-22

28. Bergen V, Lange M, Peidli S, Wolf FA, Theis FJ. Generalizing RNA velocity to transient cell states through dynamical modeling. *Nat Biotechnol* (2020) 38(12):1408–14. doi: 10.1038/s41587-020-0591-3

29. Svensson V, Natarajan KN, Ly LH, Miragaia RJ, Labalette C, Macaulay IC, et al. Power analysis of single-cell RNA-sequencing experiments. *Nat Methods* (2017) 14 (4):381–7. doi: 10.1038/nmeth.4220

30. Tattikota SG, Cho B, Liu Y, Hu Y, Barrera V, Steinbaugh MJ, et al. A single-cell survey of Drosophila blood. *eLife.* (2020) 9:18:e548. doi: 10.7554/eLife.54818

31. Leader DP, Krause SA, Pandit A, Davies SA, Dow JAT. FlyAtlas 2: a new version of the Drosophila melanogaster expression atlas with RNA-Seq, miRNA-Seq and sex-specific data. *Nucleic Acids Res* (2018) 46(D1):D809–15. doi: 10.1093/nar/gkx976

32. Lantz C, Radmanesh B, Liu E, Thorp EB, Lin J. Single-cell RNA sequencing uncovers heterogenous transcriptional signatures in macrophages during efferocytosis. *Sci Rep* (2020) 10(1):14333. doi: 10.1038/s41598-020-70353-y

33. Clark RI, Tan SWS, Péan CB, Roostalu U, Vivancos V, Bronda K, et al. MEF2 is an in *vivo* immune-metabolic switch. *Cell.* (2013) 155(2):435–47. doi: 10.1016/j.cell.2013.09.007

34. Myers AL, Harris CM, Choe KM, Brennan CA. Inflammatory production of reactive oxygen species by Drosophila hemocytes activates cellular immune defenses. *Biochem Biophys Res Commun* (2018) 505(3):726–32. doi: 10.1016/j.bbrc.2018.09.126

35. Schmid MR, Dziedziech A, Arefin B, Kienzle T, Wang Z, Akhter M, et al. Insect hemolymph coagulation: Kinetics of classically and non-classically secreted clotting factors. *Insect Biochem Mol Biol* (2019) 109:63–71. doi: 10.1016/j.ibmb.2019.04.007

36. Dziedziech A, Theopold U. Proto-pyroptosis: An ancestral origin for mammalian inflammatory cell death mechanism in drosophila melanogaster. *J Mol Biol* (2022) 434(4):167333. doi: 10.1126/sciadv.aay6354

37. Kang Q, Li L, Pang Y, Zhu W, Meng L. An update on Ym1 and its immunoregulatory role in diseases. *Front Immunol* (2022) 13:891220. doi: 10.3389/fimmu.2022.891220

38. Xu DC, Wang L, Yamada KM, Baena-Lopez LA. Non-apoptotic activation of Drosophila caspase-2/9 modulates JNK signaling, the tumor microenvironment, and growth of wound-like tumors. *Cell Rep* (2022) 39(3):110718. doi: 10.1038/nprot.2014.006

39. Shin M, Cha N, Koranteng F, Cho B, Shim J. Subpopulation of macrophage-like plasmatocytes attenuates systemic growth via JAK/STAT in the drosophila fat body. *Front Immunol* (2020) 89. doi: 10.1002/cyto.a.22865

40. Dudzic JP, Kondo S, Ueda R, Bergman CM, Lemaitre B. Drosophila innate immunity: regional and functional specialization of prophenoloxidases. *BMC Biol* (2015) 13:81. doi: 10.1093/bioinformatics/bts635

41. Anderl I, Vesala L, Ihalainen TO, Vanha-Aho LM, Andó I, Rämet M, et al. Transdifferentiation and Proliferation in Two Distinct Hemocyte Lineages in Drosophila melanogaster Larvae after Wasp Infection. *PLoS Pathog* (2016) 12(7): e1005746. doi: 10.1093/bioinformatics/btu638

42. Leitão AB, Sucena É. Drosophila sessile hemocyte clusters are true hematopoietic tissues that regulate larval blood cell differentiation. *eLife*. (2015) 4:e06166. doi: 10.1016/j.cell.2021.04.048

43. Lefebvre FA, Benoit Bouvrette LP, Perras L, Blanchet-Cohen A, Garnier D, Rak J, et al. Comparative transcriptomic analysis of human and Drosophila extracellular vesicles. *Sci Rep* (2016) 6:27680. doi: 10.1038/srep27680

44. Ashley J, Cordy B, Lucia D, Fradkin LG, Budnik V, Thomson T. Retrovirus-like gag protein arc1 binds RNA and traffics across synaptic boutons. *Cell* (2018) 172(1–2):262–274.e11. doi: 10.1038/s41587-020-0591-3

45. Cottee MA, Letham SC, Young GR, Stoye JP, Taylor IA. Structure of Drosophila melanogaster ARC1 reveals a repurposed molecule with characteristics of retroviral Gag. *Sci Adv* (2020) 6(1):eaay6354. doi: 10.1038/nmeth.4220

46. Pastuzyn ED, Day CE, Kearns RB, Kyrke-Smith M, Taibi AV, McCormick J, et al. The neuronal gene arc encodes a repurposed retrotransposon gag protein that mediates intercellular RNA transfer. *Cell*. (2018) 173(1):275. doi: 10.3389/fimmu.2020.00063

47. Khalili D, Kunc M, Herbrich S, Müller AM, Theopold U. Chitinase-like proteins promoting tumorigenesis through disruption of cell polarity via enlarged endosomal vesicles. *Front Oncol* (2023) 13:1170122. doi: 10.3389/fonc.2023.1170122

frontiers | Frontiers in Immunology

TYPE Original Research
PUBLISHED 22 September 2023
DOI 10.3389/fimmu.2023.1253805

OPEN ACCESS

EDITED BY
Laura Vesala,
Tampere University, Finland

REVIEWED BY
Ulrich Theopold,
Stockholm University, Sweden
Ilias Kounatidis,
The Open University, United Kingdom

*CORRESPONDENCE
Annika Meinander
annika.meinander@abo.fi

†PRESENT ADDRESS
Fanny Lindholm,
Institute of Biomedicine, University of Turku, Turku, Finland

RECEIVED 06 July 2023
ACCEPTED 04 September 2023
PUBLISHED 22 September 2023

CITATION
Aalto AL, Saadabadi A, Lindholm F, Kietz C, Himmelroos E, Marimuthu P, Salo-Ahen OMH, Eklund P and Meinander A (2023) Stilbenoid compounds inhibit NF-κB-mediated inflammatory responses in the *Drosophila* intestine. *Front. Immunol.* 14:1253805. doi: 10.3389/fimmu.2023.1253805

Stilbenoid compounds inhibit NF-κB-mediated inflammatory responses in the *Drosophila* intestine

Anna L. Aalto[1,2], Atefeh Saadabadi[3,4,5], Fanny Lindholm[1†], Christa Kietz[1], Emmy Himmelroos[1], Parthiban Marimuthu[3,4], Outi M. H. Salo-Ahen[3,4], Patrik Eklund[5] and Annika Meinander[1,2*]

[1]Cell Biology, Faculty of Science and Engineering, Åbo Akademi University, Turku, Finland, [2]InFLAMES Research Flagship Center, Åbo Akademi University, Turku, Finland, [3]Pharmaceutical Sciences Laboratory, Pharmacy, Åbo Akademi University, Turku, Finland, [4]Structural Bioinformatics Laboratory, Biochemistry, Åbo Akademi University, Turku, Finland, [5]Laboratory of Molecular Science and Engineering, Faculty of Science and Engineering, Åbo Akademi University, Turku, Finland

Introduction: Stilbenoid compounds have been described to have anti-inflammatory properties in animal models *in vivo*, and have been shown to inhibit Ca2+-influx through the transient receptor potential ankyrin 1 (TrpA1).

Methods: To study how stilbenoid compounds affect inflammatory signaling *in vivo*, we have utilized the fruit fly, *Drosophila melanogaster*, as a model system. To induce intestinal inflammation in the fly, we have fed flies with the intestinal irritant dextran sodium sulphate (DSS).

Results: We found that DSS induces severe changes in the bacteriome of the *Drosophila* intestine, and that this dysbiosis causes activation of the NF-κB transcription factor Relish. We have taken advantage of the DSS-model to study the anti-inflammatory properties of the stilbenoid compounds pinosylvin (PS) and pinosylvin monomethyl ether (PSMME). With the help of *in vivo* approaches, we have identified PS and PSMME to be transient receptor ankyrin 1 (TrpA1)-dependent antagonists of NF-κB-mediated intestinal immune responses in *Drosophila*. We have also computationally predicted the putative antagonist binding sites of these compounds at *Drosophila* TrpA1.

Discussion: Taken together, we show that the stilbenoids PS and PSMME have anti-inflammatory properties *in vivo* in the intestine and can be used to alleviate chemically induced intestinal inflammation in *Drosophila*.

KEYWORDS

Drosophila, DSS, inflammation, intestine, NF-κB, stilbenoid, TRPA1

Introduction

Stilbenoids are hydroxylated derivatives of polyphenolic compounds characterized by a 1,2-diphenylethylnucleus and are present in berries, fruits and grape vine, but also in knots, bark, roots and stumps of conifer trees, such as spruce and pine (1–3). Stilbenoids exhibit antioxidant properties, which protect plants from harmful exogenous stimuli such as excessive heat, UV-light, insect attacks and infections caused by microorganisms (4–6). Some stilbenoid compounds, such as resveratrol (3,4′,5-trihydroxystilbene), pinosylvin (3,5-dihydroxystilbene, PS) and pinosylvin monomethyl ether (3-hydroxy-5-methoxystilbene, PSMME) have been described to have anti-inflammatory properties in animal models *in vivo* (7, 8). In mammalian cells, resveratrol, PS and PSMME have been shown to inhibit Ca^{2+}-influx through the transient receptor potential ankyrin 1 (TrpA1) ion channel in response to a potent TrpA1 activator allyl isothiocyanate (AITC) (8, 9).

The ligand-gated, transmembrane (TM) bound TrpA1 receptor is a sensory protein that can be activated by environmental stimuli such as noxious cold and mechanical stimuli, as well as by endogenous irritant and pungent compounds. TrpA1 serves as an attractive target for analgesic and anti-inflammatory drugs, as it is triggered during inflammation, oxidative stress and tissue damage and is considered a key player in acute and chronic pain sensation (10). In flies, TrpA1 is expressed in sensory neurons as well as in the epithelial wall of the intestine (11–14). The receptor has been shown to be involved in oxidative stress-induced intestinal stem cell proliferation and in the clearance of food-borne pathogens in flies (14, 15).

When intestinal homeostasis is disturbed, a local inflammation arises to promote healing and recovery. The *Drosophila* intestinal inflammatory response is induced by epithelial cells that recognise and respond to pathogen-associated molecular patterns (PAMPs). These PAMPs are derived from foreign bacteria or induced by pathological changes of the resident microbiome causing dysbiosis. Recognition of harmful bacteria leads to activation of several inflammation-promoting signalling pathways, including the *Drosophila* nuclear factor κB (NF-κB) pathways. The Immune deficiency (Imd)/Relish pathway is activated upon recognition of bacteria by peptidoglycan recognition proteins (PGRPs) and culminates in the transcriptional activation of the NF-κB transcription factor Relish. In the intestinal epithelial cells of the fly, this is the major NF-κB pathway (16–19). Relish activation leads to the transcription of hundreds of genes, including antimicrobial peptides (AMPs) that upon secretion contribute to intestinal immune responses by fending off intruding pathogens (20–22). Due to the advanced innate immune system of *Drosophila*, as well as several structural and functional similarities between the fly and the mammalian intestine, the fruit fly has emerged as an ethical, inexpensive and fast model to study intestinal inflammatory disease (23).

In this study, we induced intestinal inflammation with the intestinal irritant dextran sodium sulphate (DSS), and analysed the anti-inflammatory properties of stilbenoid compounds *in vivo* in *Drosophila*. We found that while the inflammation caused by DSS is dependent on the commensal microbiome, the elevated immune activation induced by Relish target gene expression can be alleviated by inhibition of the TrpA1 channel by stilbenoid-treatment.

Results

Molecular modelling of PS and PSMME interactions with *Drosophila* TrpA1

PS and PSMME have been shown to inhibit Ca^{2+}-influx through the TrpA1 ion channel in response to TrpA1 activators in mammalian cells (8, 9). The mammalian TrpA1 binding sites have been identified and predicted for two known TrpA1 antagonists, A-967079 and HC-030031, based on phylogenetic, mutational and modelling studies (24). In this study, we have used *Drosophila* as a model to study the effects of stilbenoid compounds on inflammatory responses. To be able to investigate if stilbenes can interact with the *Drosophila* TrpA1 (dTrpA1) channel, we used molecular modelling to computationally predict the antagonist binding sites at the receptor. In the absence of an experimentally defined structure of the dTrpA1 channel, we built a comparative homology model of dTrpA1 based on the experimental human TrpA1 (hTrpA1) structure. The dTrpA1 model with the best Discrete Optimized Protein Energy (DOPE) score (-317763.96875) and the root-mean-square deviation (RMSD) of 0.764 Å from the template was utilized for molecular modelling studies (Figure 1A). The two TrpA1 antagonists A-967079 and HC-030031 were used as reference compounds and were modelled into their respective binding sites described in the literature using molecular docking (Figure 1A, zoom in). The A-967079 binding site has been described to locate within the channel pore between TM5, TM6 and pore helix 1 (PH1) from one subunit and TM6 from the adjacent chain (25). The residues forming this particular binding pocket in hTrpA1 are S873, T874, F877, F909 and M912 (25–27). The respective residues in dTrpA1 are V431, L432, F435, F468 and M471. The HC-030031 binding pocket is situated between the TM4-TM5 linker, preTM1 and TRP-like domains close to the membrane (28). The residues forming the HC-030031 pocket in hTrpA1 are W711, N855, Q979, H983, A971 and in dTrpA1 W268, Q413, Q538, H542 and A530.

To investigate possible binding modes and sites of stilbenes at dTrpA1, PS and PSMME were docked into both known antagonist binding sites. Based on the docking results, both PS and PSMME are predicted to form a hydrogen bond with S501 (of the adjacent TM6) and π-π interactions with F468 (of PH1) in the A-967079 binding site, while A-967079 itself is predicted to engage in hydrogen bonding with L428 backbone oxygen (in TM5) and π-π interactions with F468 (Figure 1A, upper panel). In the HC-030031 binding pocket, PS and PSMME are predicted to form a hydrogen bond with Q538 (of the TRP-like domain) and π-π interactions with W268 (of the preTM1 domain), while HC-030031 itself is predicted to form hydrogen bonds with Q265 (of the preTM1) and D412 (of TM4-TM5 linker) (Figure 1A, lower panel).

In addition to assessing the initial docking scores and favorable ligand-protein interactions to evaluate the predicted binding poses, we employed the Molecular Mechanics-Generalized Born Surface Area (MM-GBSA) method to estimate the free energy of binding (binding affinity) of the docked ligands. Moreover, the best docking poses of A-967079 and HC-030031 in their respective dTrpA1 binding sites and PS (as the representative of the stilbene compounds) in both the known binding pockets of the dTrpA1

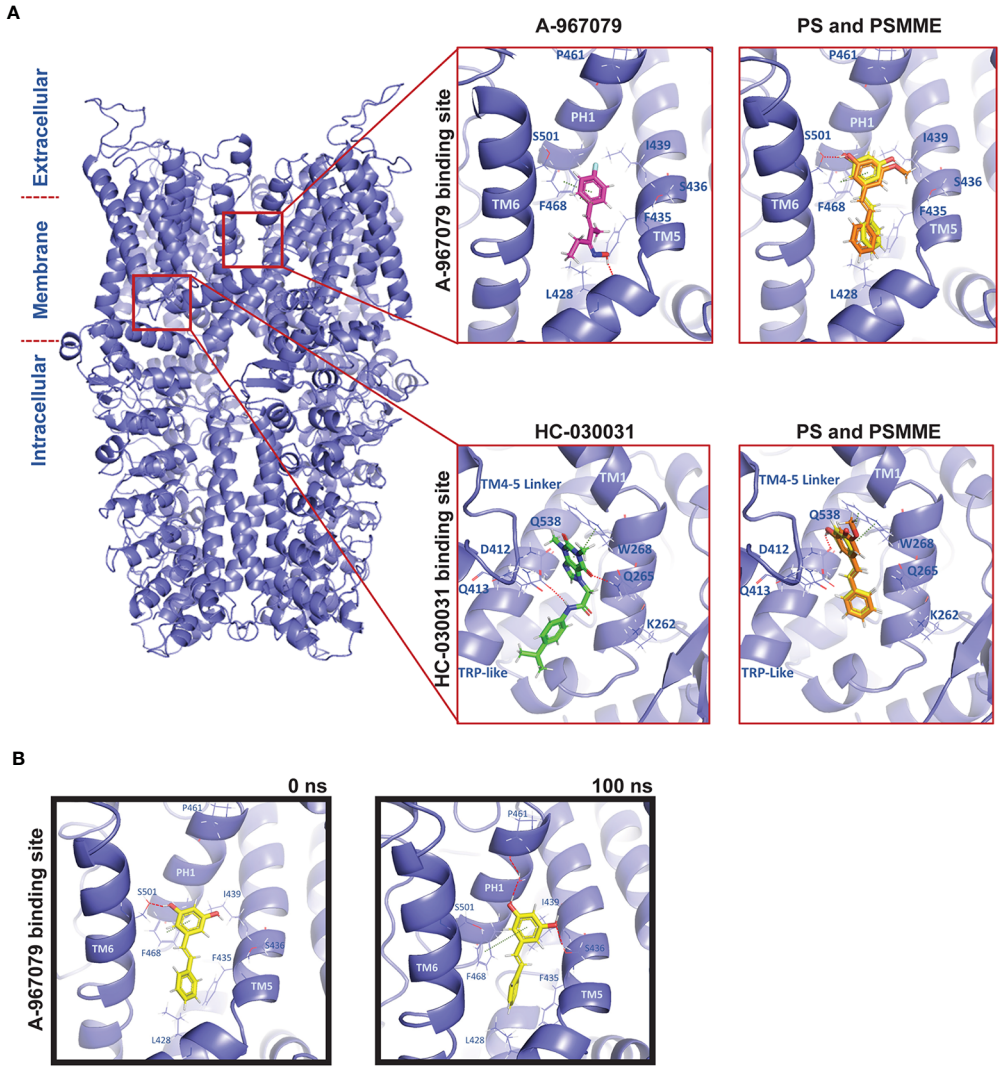

FIGURE 1
Molecular modelling of PS and PSMME interactions with *Drosophila* TrpA1. **(A)** A comparative homology model of *Drosophila* TrpA1 (blue) based on the experimental human TrpA1 structure (PDB ID: 6V9V). Zoom in: Docking studies of PS (yellow), PSMME (orange) and A-967079 (magenta) or HC-030031 (green) in the A-967079 (top panel) or HC-030031 (lower panel) binding pocket of *Drosophila* TrpA1 (blue). **(B)** PS (yellow) in the A-967079 binding pocket of *Drosophila* TrpA1 (blue), before (left) and after (right) a 100ns MD simulation. The oxygen, nitrogen and hydrogen atoms are displayed in red, blue, and white color, respectively. Interaction color code (dashed lines): H-bond – red; π-π – dark green. Key interacting residues are shown in blue sticks and labelled.

model were subjected to molecular dynamics (MD) simulation to evaluate the stability of the predicted ligand-dTrpA1 complexes. After the MD simulation, the MM-GBSA binding affinities were recalculated to see if the simulation had improved or worsened the estimated binding affinity of the ligands. Whereas the MM-GBSA binding free energy of HC-030031 was significantly better after the 100-ns simulation (from -44.39 to -74.42 kcal/mol) at its corresponding binding site, it remained the same for A-967079 (-28 kcal/mol), suggesting a less favorable binding for A-967079 at its binding site. The MM-GBSA binding free energies of PS were also improved during the MD simulation (from -35.30 kcal/mol and -31.73 kcal/mol to -45.62 kcal/mol and -54.89 kcal/mol at the A-967079 and HC-030031 binding sites, respectively). PSMME (non-simulated) had very similar binding free energy values to those of PS (non-simulated) at both binding sites.

The predicted HC-030031-TrpA1 complex remained relatively stable during the simulations and HC-030031 engaged in water-mediated hydrogen bonding interactions with Q261 and L264 (of preTM1) (data not shown). However, the small reference ligand A-967079 was not stable in its predicted binding pose at the binding site during the simulation. It changed its position and orientation, and thus, also the interactions with the protein, e.g., the hydrogen bond with L428 (TM5) was exchanged to hydrogen bonds with S501 (of the adjacent TM6), L464 (of PH1) and S436 (of TM5) (data not shown). Although PS binding at the A-967079 site was relatively stable during the whole simulation *via* π-π interactions with F468

(of PH1), its hydrogen bond swapped from S501 (of the adjacent TM6) (in Figure 1B, left) to S436 (of TM5) and it could form an extra hydrogen bond through a water molecule with P461 (of PH1) (in Figure 1B, right). At the HC-030031 binding site, PS moved deeper into the cavity from its initial docking site, losing the initial interactions while forming a new water-mediated hydrogen bond with D412 (of the TM4-TM5 linker). This suggests that PS is too small for this site and that the A-967079 binding site is the preferred site for PS. Taken together, both PS and PSMME can bind to *Drosophila* TrpA1, according to the *in silico* studies.

DSS-treatment causes microbial dysbiosis in *Drosophila* larvae and induces activation of Relish-mediated inflammatory gene expression

To study the effect of stilbenoid compounds *in vivo*, we wanted to induce activation of the NF-κB-mediated inflammatory Imd/Relish pathway in the *Drosophila* intestine, without direct interference of the signaling mediators of the pathway, or by bacterial infection. In both murine and *Drosophila* models, oral administration with DSS has been used to chemically induce intestinal inflammation (29–31). DSS has been shown to disrupt the epithelia barrier and the intestinal homeostasis, inducing intestinal inflammation (31–35).

To assess the NF-κB-mediated inflammatory response induced by DSS in *Drosophila*, we fed foraging 3rd instar larvae with fly food supplemented with DSS, whereafter, we used qPCR-based analysis to detect Relish-specific AMP target genes. We noticed that 5% w/v of 40 kDa DSS induced an increased gene expression of the NF-κB Relish target gene *diptericin* compared to control fed flies (Figure 2A), also in the absence of pathogenic infection. As Relish is involved in protecting the epithelial borders in the intestine from local insults, and thus maintains tissue homeostasis *in situ* also during non-pathogenic inflammation-inducing conditions (22, 36, 37), we wanted to specifically investigate if the local immune response in the gut is activated in response to DSS. As expected, we were able to detect local activation of the immune response in the *Drosophila* intestine by performing X-Gal staining on the dissected gut of *diptericin-lacZ* reporter flies fed with DSS (Figure 2B).

In addition, we analyzed if DSS treatment affects the intestinal microbiome in the fly. For this purpose, we performed 16S rRNA sequencing on control and DSS-fed larvae. The *Drosophila* gut harbors relatively few bacterial species, usually belonging to the families *Enterococcaceae* and *Lactobacillaceae* from the phylum *Bacillota*, and to the families *Acetobacteraceae* and *Enterobacteriaceae* from the phylum *Pseudomonadota* (38–40). We found the bacterial composition to be changed in DSS-treated larvae compared to control larvae (Figure 2C). The treatment with DSS leads to a decrease in the proportion of *Bacillota* to *Pseudomonadota* (Figure 2C, Supplementary Figure S1 and Table S1), which is a marker for microbial instability and is associated with chronic inflammatory diseases also in humans (41, 42). Concomitantly, the Simpson index indicates a higher dominance and lower biodiversity in DSS treated larvae compared to control treated. Further supporting this notion, both the total number of observed families (Sobs) and the Shannon-wiener H index decreases in DSS treated larvae, indicating a decline in biodiversity (Figure 2C).

To assess if the fly commensal microbiome, alas dysbiotic, affects Relish activation upon DSS treatment, we reared flies under axenic conditions before treating them with DSS. Interestingly, DSS did not induce Relish activation in germ-free flies compared to their conventionally reared counterparts (Figure 2D). Similarly, the inducibility of *diptericin* is impaired in flies lacking the pattern-recognizing receptor (PRR) PGRP-LC (Figure 2E). This indicates that DSS-induced *diptericin* expression is not driven by disruption of the epithelial barrier, but rather mediated by receptor activation in response to a dysbiotic microbiome. In addition, this suggests that DSS-induced Relish target gene expression is mediated *via* activation of the Imd/Relish pathway. Finally, to assess if the DSS-induced expression of AMPs is indeed mediated by the NF-κB Relish, we used loss-of-function (LOF) mutants of Relish and confirmed that the inducibility of *diptericin* expression was Relish-dependent (Figure 2E). Taken together, DSS-treatment induces activation of Relish in flies and can be used to induce a modest inflammation in *Drosophila*.

Stilbenoid compounds reduce inflammatory gene expression

Taking advantage of the model of DSS-induced dysbiosis and inflammation, we wanted to investigate the anti-inflammatory properties of stilbenoid compounds in flies. To relate our modelling studies of stilbenes and the reference TrpA1 antagonists with the experimental data, we first determined the anti-inflammatory properties of the reference compounds A-967079 and HC-030031 in DSS-treated flies. We fed the DSS-treated flies with A-967079 and HC-030031, and both TrpA1-inhibiting drugs alleviated DSS-induced inflammation 24 hours post DSS-treatment (Figure 3A), suggesting that the stilbenoid compounds may also exert their anti-inflammatory properties by inhibiting the TrpA1 ion channel also in *Drosophila*.

Before assessing the anti-inflammatory properties of the stilbenoids, we first fed flies with the stilbenoids to investigate if the treatment alone activates NF-κB in *Drosophila*. We analyzed four different stilbenoid compounds, the compounds modelled together with *Drosophila* TrpA1 pinosylvin (PS) and pinosylvin monomethyl ether (PSMME), as well as the stilbenoid glucosides isorhapontin (4,5'-dihydroxy-3-methoxy-3'-glucopyranosylstilbene) and astringin (3,4,3',5'-tetrahydroxystilbene 3'-glucoside). When used at a concentration of 100 μM, none of the tested stilbenoids induced inflammation after 24 hours of feeding. On the contrary, treatment with 100 μM PS, PSMME and isorhapontin reduced basal Relish target gene expression (Figure 3B). Astringin, on the other hand, did not seem to influence basal Relish activity (Figure 3B). Similar results were obtained when using a higher, 500 μM concentration of PSMME, isorhapontin and astringin (Figure 3B). However, a higher concentration of PS resulted in an adverse spontaneous increase of Relish target gene expression (Figure 3B).

10.3389/fimmu.2023.1253805

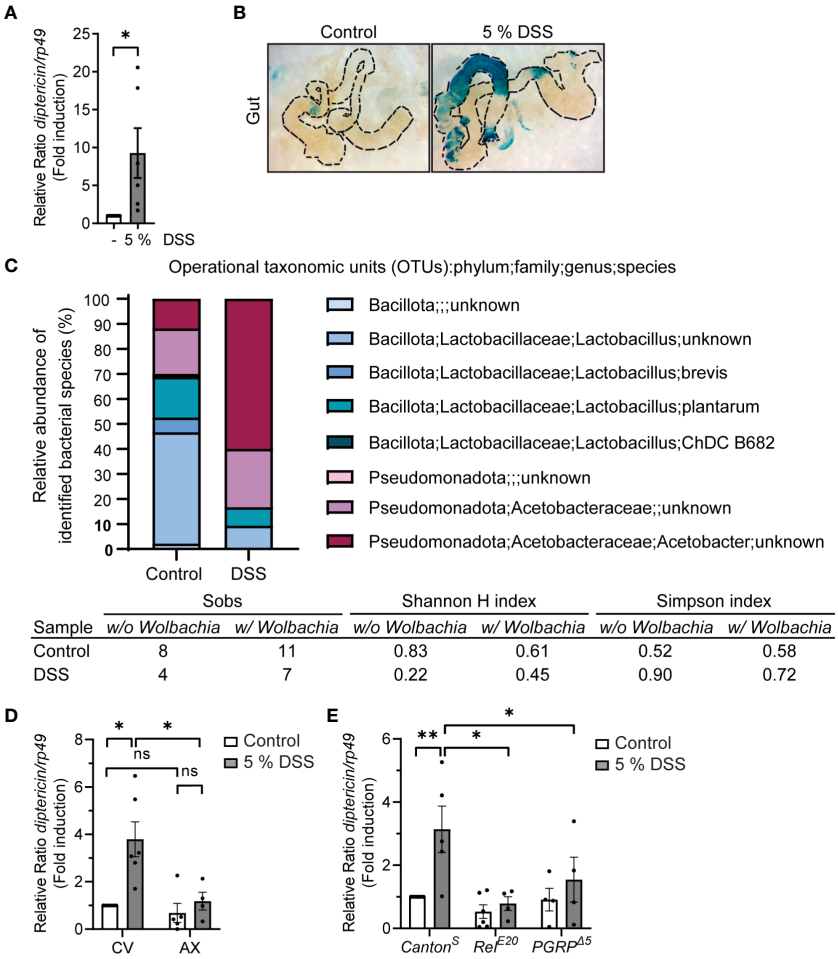

	Sobs		Shannon H index		Simpson index	
Sample	*w/o Wolbachia*	*w/ Wolbachia*	*w/o Wolbachia*	*w/ Wolbachia*	*w/o Wolbachia*	*w/ Wolbachia*
Control	8	11	0.83	0.61	0.52	0.58
DSS	4	7	0.22	0.45	0.90	0.72

FIGURE 2
DSS-feeding induces local inflammation and causes microbial dysbiosis. **(A)** 3rd instar larvae of wild-type *Canton*^{S} were fed with indicated concentrations of DSS for 3 h, with 1 h recovery. Relish activation was studied by analyzing the expression of *diptericin* with qPCR (shown as ΔΔCt). Error bars indicate SEM from 6 independent experimental repeats. **(B)** Dissected larval guts from *diptericin-lacZ* stained for β-galactosidase activity after 3 hours with indicated concentrations of DSS feeding. The images are representatives of 3 independent experimental repeats. **(C)** Bacterial 16S rRNA metagenomics analysis of the 1V-3V region in *Canton*^{S} control and DSS fed flies with 10% of DSS for 3 hours. Colors indicate identified operational taxonomic units (OTUs). The intestinal bacterial diversity of control and DSS treated wild-type *Canton*^{S} larvae with and without *Wolbachia* was analysed by calculating the Simpson index, the Shannon-wiener H index, and the total number of observed families (Sobs). **(D)** 3rd instar larvae of conventionally (CV) or axenically reared (AX) wild-type *Canton*^{S} flies were fed with 5% DSS for 3 h with 1 h recovery. Relish activation was studied by analyzing the expression of *diptericin* with qPCR (shown as ΔΔCt). Error bars indicate SEM from 4 independent experimental repeats. **(E)** 3rd instar larvae of wild-type *Canton*^{S}, LOF *Rel*^{E20} flies and *PGRP*^{Δ5}-receptor mutant flies were fed with 5% DSS for 3 h with 1 h recovery. Relish activation was studied by analyzing the expression of *diptericin* with qPCR (shown as ΔΔCt). Error bars indicate SEM from more than 4 independent experimental repeats. Statistical significance was calculated using Student's t-test **(A)** or one-way ANOVA **(D, E)** on non-normalized -ΔCt-values, ns nonsignificant, * $p < 0.05$, ** $p < 0.01$.

To assess the anti-inflammatory effect of stilbenes, we fed larvae with DSS for 3 hours, after which they were allowed to feed on control food or food supplemented with stilbenoids for 24 hours. While DSS-treated flies still expressed *diptericin* 24 hours post DSS-treatment in control conditions, PS and PSMME, were able to alleviate the DSS-induced inflammation (Figure 3C). However, isorhapontin had no alleviating effect on DSS-induced inflammation and astringin seemed to have an opposite effect (Figure 3D). As both isorhapontin and astringin were unable to reduce DSS-induced inflammation the compounds were excluded from further experiments.

Stilbenoid compounds depend on TrpA1 for their anti-inflammatory activity

To assess if the anti-inflammatory effect of PS and PSMME is indeed mediated *via* the TrpA1 channel *in vivo*, we investigated the ability of the stilbenoids to alleviate inflammation in TrpA1 LOF *TrpA1*^{1}-mutant flies. We first ensured that the larvae of TrpA1 LOF flies responded to DSS-treatment by inducing expression of *diptericin* similarly as wildtype flies (Supplementary Figure S2). At the same time this indicates that the DSS-induced Relish activation is TrpA1-independent. When we next treated the DSS-

10.3389/fimmu.2023.1253805

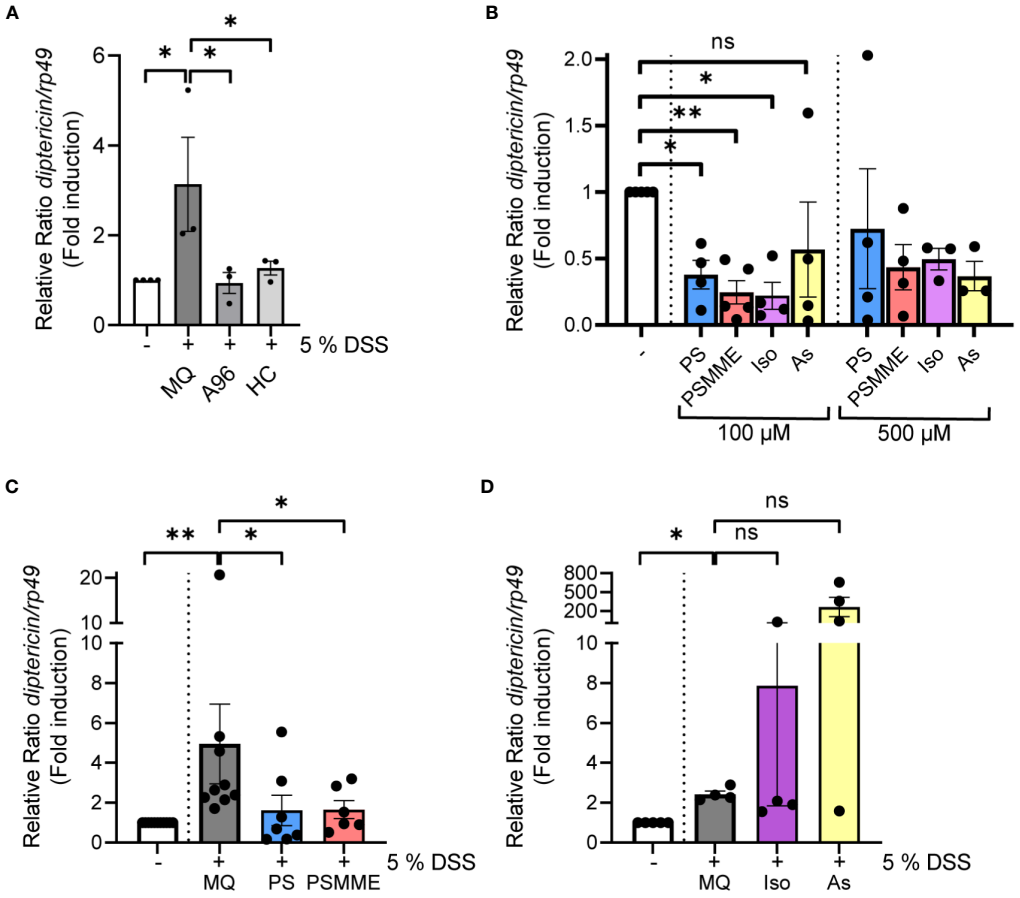

FIGURE 3
The anti-inflammatory properties of stilbenoid-compounds. **(A)** 3rd instar larvae of wild-type *Canton*^{S} were fed with 200 µM of TrpA1 antagonists A-967079 and HC-030031 or MQ for 24 hours after 3 hours DSS feeding. Relish activation was studied by analyzing the expression of *diptericin* with qPCR (shown as ΔΔCt). Error bars indicate SEM from 3 independent experimental repeats. **(B)** 3rd instar larvae of wild-type *Canton*^{S} were fed with indicated concentrations of stilbenoids PS, PSMME, isorhapontin and astringin for 24 hours. Relish activation was studied by analyzing the expression of *diptericin* with qPCR (shown as ΔΔCt). Error bars indicate SEM from more than 3 independent experimental repeats. **(C, D)** 3rd instar larvae of wild-type *Canton*^{S} were fed with 100 µM of stilbenoids PS **(C)**, PSMME **(C)**, isorhapontin **(D)** and astringin **(D)** or MQ for 24 hours after 3 hours DSS feeding. Relish activation was studied by analyzing the expression of *diptericin* with qPCR (shown as ΔΔCt). Error bars indicate SEM from more than 3 independent experimental repeats. Statistical significance was calculated using one-way ANOVA on non-normalized -ΔCt-values, ns nonsignificant, * $p < 0.05$, ** $p < 0.01$.

fed *TrpA1*-mutant larvae with stilbenoid compounds, PS and PSMME lost their anti-inflammatory properties observed in control larvae (Figure 4A). Finally, the DSS-induced *diptericin* expression could not be alleviated by feeding TrpA1 LOF flies with the known antagonists of mammalian TrpA1, A-967079 and HC-030031 (Figure 4B), hence, strengthening the functional role of TrpA1 in the immune response during DSS-induced intestinal inflammation (Figure 4C).

Discussion

When intestinal cellular and microbiome homeostasis is disturbed, as in inflammatory bowels disease (IBD) patients, activation of the transcription factor NF-κB in the epithelium is markedly induced, further promoting intestinal inflammation (43, 44). In this study, we demonstrate that feeding *Drosophila* larvae with DSS leads to an intestinal inflammatory response mediated *via* the NF-κB transcription factor Relish. Interestingly, our results indicate that DSS-induced Relish activation is not prompted by the damage in the epithelial barrier, but instead through activation of inflammatory receptors as a response to the emerging microbial instability. Therefore, the DSS-induced inflammatory response caused by a microbial dysbiosis of commensal bacteria is modest in comparison to immune responses caused by pathogenic infections. While the activation of Relish seems to be TrpA1-independent, feeding flies with DSS has been shown to increase ROS levels (34), which in turn, is suggested to activate the TrpA1 ion channels expressed in the epithelial cells along the *Drosophila* midgut (13, 14). Interestingly, TrpA1 is upregulated in IBD patients

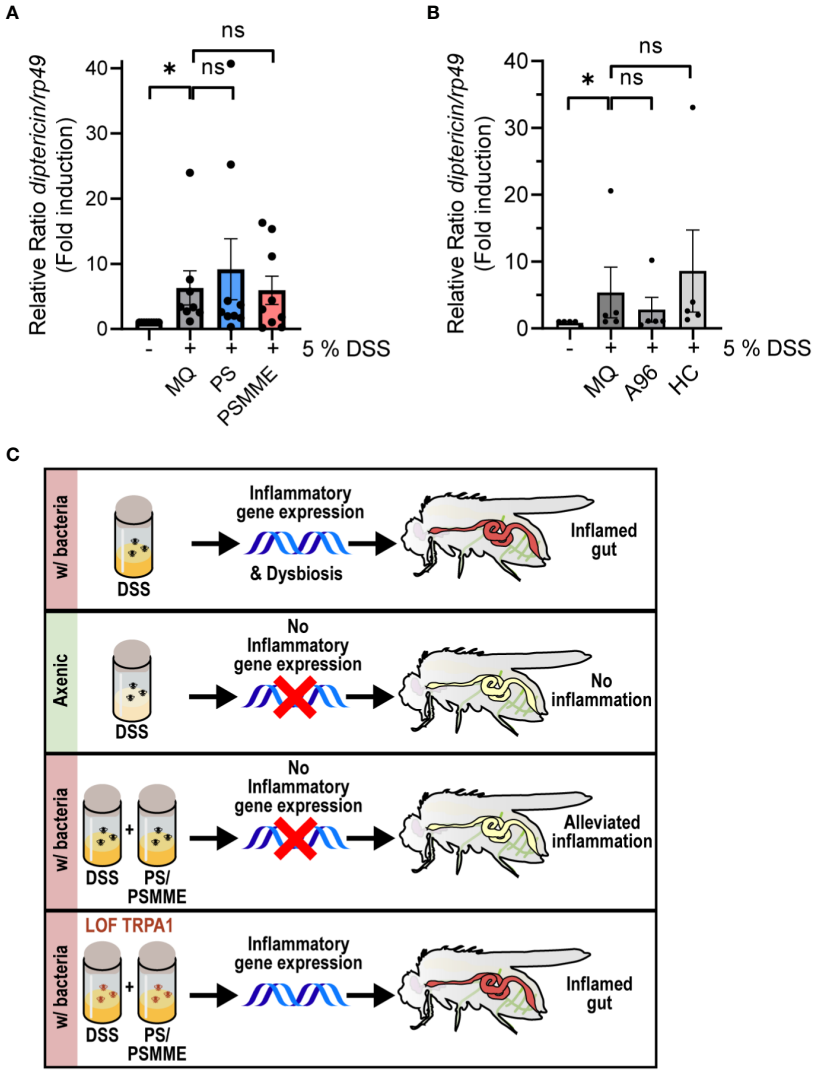

FIGURE 4
TrpA1-dependency of the stilbenoid compound anti-inflammatory activity. 3rd instar larvae of LOF mutant *TrpA1*^{1} were fed with 100 µM of stilbenoids PS and PSMME **(A)** or 200 µM of TrpA1 antagonists A-967079 and HC-030031 **(B)** or MQ for 24 hours after 3 hours DSS feeding. Relish activation was studied by analyzing the expression of *diptericin* with qPCR. Error bars indicate SEM from more than 5 independent experimental repeats (shown as ΔΔCt). Statistical significance was calculated using one-way ANOVA on non-normalized -ΔCt-values, ns nonsignificant, * $p < 0.05$. **(C)** Schematic summary of results showing that inhibition of the TrpA1 channel by stilbenoid-treatment reduces inflammation induced by Relish target gene expression.

and its activation is required to alleviate the expression of several proinflammatory neuropeptides, cytokines and chemokines (45). Here, we show that although TrpA1 is not required for DSS-induced Relish activation, there is a crosstalk between TrpA1 and Relish, as the DSS-induced Relish activation can be modulated pharmacologically with stilbenoid compounds PS and PSMME that target TrpA1.

In this study, we computationally modelled the putative binding interactions of PS and PSMME at *Drosophila* TrpA1. We specifically focused on investigating the binding sites reported for known human TrpA1-antagonists A-967079 and HC-030031. Previous studies have stated that the predicted A-967079 binding site in mammalian TrpA1 consists of different residues than the corresponding pocket in the *Drosophila* TrpA1, thus rendering *Drosophila* TrpA1 insensitive to A-967079 (24, 46, 47). The docking study and the MD analysis of the putative binding poses of the stilbenes showed that PS can form favorable polar and hydrophobic interactions with the target at both studied sites. While PS showed comparable predicted affinities to both antagonist binding sites, its size and interactions suggest that it may favor the A-967079 binding pocket. A-967079 however, did not find a stable binding site at *Drosophila* TrpA1, consistent with the previous observation that *Drosophila* TrpA1 is insensitive to A-967079. However, when analyzing *in vivo*, A-967079 did have anti-inflammatory properties, indicating that A-967079 may bind to TrpA1 sufficiently *in vivo*. While the stilbenoids resveratrol, PS and

PSMME have been previously shown to have anti-inflammatory properties *in vivo* (7, 8, 48), isorhapontin and astringin have not been studied *in vivo* before. We were not able to detect any significant anti-inflammatory effects with neither of these compounds. However, isorhapontin and astringin are both hydrophilic glucosides that may not diffuse through the lipophilic cell membrane to the lipid-surrounded binding site at TrpA1, and would hence need to be metabolized to function properly (49).

Besides their direct interaction with the TrpA1-receptor, stilbenoid compounds also exhibit antimicrobial effects (50, 51), making them potential modulators of the bacteria composition in the intestinal lumen. This could explain why during basal conditions, some of the stilbenoid compounds were able to alleviate basal NF-κB activation. As the microbial dysbiosis caused by DSS seems to be the main reason for Relish activation, the antimicrobial activities of stilbenoids may alleviate the bacterial burden on the intestinal epithelia, which may contribute to the anti-inflammatory effect of PS and PSMME. To further address this, an analysis of the microbial structure in response to stilbenoid treatments would be informative and would elucidate the antimicrobial effects of stilbenoids during intestinal inflammation. In conclusion, both our molecular modelling and our experimental data indicate favorable interactions of the stilbenoid compounds with the *Drosophila* TrpA1, suggesting crosstalk between TrpA1 and NF-κB signaling in maintenance of intestinal immune homeostasis.

Materials and methods

Fly husbandry and strains

Drosophila melanogaster were maintained at 25°C with a 12 h light–dark cycle on Nutri-fly BF (Dutscher Scientific, Essex, UK). $Canton^{S}$ wildtype flies and *diptericin-lacZ* reporter line and balancer lines fly lines were kindly provided by Prof. Pascal Meier and Dr. François Leulier (52, 53). The *Drosophila* fly lines $TrpA1^{1}$ (#36342), $PGRP\text{-}LC^{\Delta 5}$ (#36323), $w{:}Rel^{E20}$ (stock #9457) were obtained from the Bloomington stock center.

DSS treatment of *Drosophila* larvae

Early *Drosophila* 3rd instar larvae were fed 40 kDa DSS (TdB Consultancy AB, Uppsala, Sweden) mixed in the fly food. 40 kDa DSS has been shown to induce the most severe colitis in mammalian model organism (54). For feeding with DSS 3-10 larvae were placed in 2 ml collection tubes with food (1-2 ml) containing DSS and sealed with pieces of *Drosophila* plugs (Genesee Scientific, California, USA). For qPCR experiments, more than 3 larvae were fed for 3 h with indicated DSS concentrations (1%, 5% or 10% w/v) and allowed to recover for at least 1 h before freezing. As DSS has been shown to compromise qPCR results by interfering with the activity of reverse transcriptase during cDNA synthesis and the polymerase during qPCR (55), we decided to use a one-hour recovery post DSS-treatment in all qPCR-experiments. For sequencing of the 16S rRNA gene larvae were fed with 10% w/v DSS for 3 h in room temperature with a 2 h recovery.

Stilbenoid compounds

PS and PSMME were isolated from a mixture of Norway spruce and Scot pine knotwood using a batch reactor. In the first step of isolation, the wood materials were boiled in ethanol for about two hours. After cooling, the ethanol solution was filtrated and then condensed by distillation (56). Further, the ethanol extract was dissolved in Toluene and stirred in a dark place at room temperature to remove the polymers that could interfere with the purification process. After two days, it was filtrated, and the solid residue was returned to the flask. This procedure was repeated two more times. The final filtrate was evaporated with a rotary evaporator at 40℃. The extract was subjected to a normal phase column chromatography (Silica gel 60, 0.040–0.063 mm, Merck, Darmstadt, Germany) and eluted with petroleum ether (peth) and ethyl acetate (EtOAc) as a solvent system. PSMME was separated in a proportion of 80:20 (peth/EtOAc). The remaining obtained fractions contained PS, resin acids and hydroxymatairesinol (HMR) were subjected to the second normal phase column and eluted with 100% chloroform (CHCl3). The procedure continued by using a gradient of CHCl3/MeOH (98:2) and the fractions were collected based on TLC (Silica gel 60 F254, Merck, Darmstadt, Germany) profile. All the organic solvents in analytical grade (99.9%) were purchased from Sigma-Aldrich (St. Louis, MO, USA). The purity of the fractions containing PSMME and PS was analyzed by GC-MS after silylation (Supplementary Figure S3, S4). The purity was determined to be >95% (Supplementary Figure S5, S6). The silylation reagents hexamethyldisiloxane (HMDS) and trimethylchlorosilane (TMSCl) were purchased from Sigma-Aldrich (St. Louis, MO, USA) and pyridine was obtained from VWR (Fontenay-sous-Bois, France). The GC-MS instrument was Agilent 5975C TAD series GC/MSD system (Stevens Creek, Santa Clara, CA, USA). The stilbenoid glucosides (astringin and isorhapontin) were extracted from fresh inner bark of Norway spruce by acetone and further purified by column chromatography over 95% and analyzed by GC-MS and NMR described in detail in our previously reported method (57).

Stilbenoid and TrpA1 antagonist treatment of *Drosophila* larvae

Similarly as with DSS feeding, 3-10 larvae were fed 24 h with indicated concentrations (100 μM or 500 μM) of stilbenoid compounds PS, PSMME, isorhapontin and astringin, or 200 μM

of TrpA1 antagonists A-967079 (Sigma-Aldrich) and HC-030031 (Sigma-Aldrich) mixed in 1-2 ml fly food. For experiments with DSS treatment, larvae were moved from DSS-containing food to new tubes with stilbene/antagonist-containing food.

Quantitative real-time-PCR

Drosophila larvae were homogenized using QIAshredder (QIAGEN) and total RNA was extracted with RNeasy Mini Kit (QIAGEN) and cDNA was synthesized with SensiFast cDNA synthesis kit (Bioline, London, UK) according to the manufacturers' protocols. qPCR was performed using SensiFast SYBR Hi-ROX qPCR kit (Bioline). *rp49* was used as a housekeeping gene for ΔΔCt calculations. The following gene-specific primers were used to amplify cDNA: *diptericin* (5'-ACCGCAGTA CCCACTCAATC-3', 5'-ACTTTCCAGCTCGGTTCTGA-3'), *rp49* (5'-GACGCTTCAAGGGACAGTATCTG-3', 5'-AAACGCGGT TCTGCATGAG-3').

X-gal staining of *Drosophila* larvae

3rd instar fly larvae were dissected in PBS and fixed for 15 minutes with PBS containing 0.4% glutaraldehyde (Sigma-Aldrich) and 1 mM $MgCl_2$ (Sigma-Aldrich). The samples were washed with PBS and incubated with a freshly prepared staining solution containing 5 mg/ml X-gal (5-Bromo-4-chloro-3-indolyl-β-D-galactopyranoside), 5 mM potassium ferrocyanide trihydrate (Sigma-Aldrich), 5 mM potassium ferrocyanide crystalline (Sigma-Aldrich) and 2 mM $MgCl_2$ in PBS at 37°C. After washing with PBS, the samples were mounted using Mowiol (Sigma) and imaged with brightfield microscopy (Leica, Wetzlar, Germany).

Sequencing of the 16S rRNA gene

Genomic DNA was isolated from 40 3rd instar larvae using a modified protocol for the QIAamp DNA mini kit (QIAGEN) (58). Larvae were surface sterilized by vortexing them twice in 2% active hypochlorite and sterile H_2O. The efficiency of the washes was confirmed by 16S PCR of water from the last wash step. Larvae were homogenized in lysis buffer containing 20 mM Tris, pH 8.0, 2 mM EDTA, 1.2% Triton X-100 and 20 mg/ml lysozyme and incubated 90 min at 37°C. 200 µl AL buffer (QIAamp DNA mini kit) with 20 µl proteinase K were added and the lysate was incubated 90 min at 56°C. Subsequent extraction was performed according to manufacturer's protocol. Amplification and Illumina MiSeq sequencing of the V1-V3 region of the 16S rRNA gene, as well as selection of operational taxonomic units (OTUs) and taxonomy assignment of OTUs was done using Eurofins Genomics InView Microbiome Profiling 3.0 service. The data is deposited at NCBI, BioProject ID: PRJNA1005106. The proportion of *Wolbachia* species have been omitted from the bar graph in Figure 2C for easier comparison of bacterial species residing in the gut lumen. However, Wolbachia is included in Figure 2C, Supplementary Figure S1 and Supplementary Table S1.

Computational protein modelling

The fruit fly (*Drosophila melanogaster*) TrpA1 (dTrpA1) sequence was obtained from the UniProt knowledgebase (UniProtKB - Q7Z020). A Basic Local Alignment Search Tool (BLAST) (59) search for the sequence was run to find a suitable template in the Protein Data Bank (PDB) (60) for comparative modelling of its three-dimensional (3D) structure. Among protein structures with similar E-values (0.0) and Sequence Identity (35.81%), the human TrpA1 crystal structure (PDB ID: 6V9V) (61) was selected due to the highest resolution (2.60 Å) and the greatest sequence coverage (residues 1 – 1119). The 3D structure model of dTrpA1 was generated using Modeller (v. 9.24) (62). The modelling alignment was created with Clustal Omega (63) and manually curated. Out of the 20 generated alternative models, the one with the best Discrete Optimized Protein Energy (DOPE) score (64) was selected. The model was further evaluated by superimposition on the template structure using PyMOL (The PyMOL Molecular Graphics System, Version 4.6, Schrödinger, LLC) and the stereochemical quality of the model was verified with MolProbity (65).

Computational docking studies

The structures of natural stilbenes and the reference compounds were prepared using the LigPrep module of Maestro (Release 2020-2: Schrödinger, LLC, New York, NY, 2020) software and the Protein Preparation Wizard of Maestro (66) was used to minimize the dTrpA1 model using the OPLS3e force field (67) and the RMSD of 0.3 Å for heavy atoms as the convergence criteria. Two docking sites were defined based on the previously reported TrpA1 antagonist binding pockets (28) using the Receptor Grid Generation tool of Maestro: (i) A-967079 binding pocket around the amino acids V431, L432, F435, F468 and M471; and (ii) HC-030031 binding site around W268, Q413, Q538, H542 and A530. The stilbene compounds were docked at these alternative sites with the GLIDE docking tool (68–70) of Maestro, using the extra precision (XP) mode with flexible ligand sampling. A maximum of five poses per ligand were ranked based on the Glide XP docking score (XP Gscore) value. To allow for more accurate evaluation of the predicted docking poses, binding free energy calculations with the Prime/MM-GBSA module of Maestro (71) were carried out for the best-docked pose (according to the XP Gscore and the observed binding interactions) of each compound using the VSGB 2.0 solvation model (72) and the OPLS3e force field (67) and allowing the residues within 5 Å from the ligand to move.

Molecular dynamics simulation analysis

The simulation systems (consisting of the membrane embedded dTrpA1 and the receptor-bound ligand in explicit solvent) were created

with the System Builder tool of the Desmond module (Schrödinger Release 2020-2: Desmond Molecular Dynamics System, D. E. Shaw Research, New York, NY, USA, 2020. Maestro-Desmond Interoperability Tools, Schrödinger, New York, NY, USA, 2020) (73) using TIP3P water (74) as the solvent model and POPC (1-palmitoyl-2-oleoyl-sn-glycero-3-phosphocholine) as the membrane model. The systems were neutralized by adding Na^+ counter ions. After the system relaxation, the production simulations were run for 100 ns at constant temperature (300 K) and pressure (1.01325 bar) according to our previously reported simulation protocol (75).

Statistical analysis

Results from qPCR were analyzed by ordinary one-way ANOVA and two-tailed Student's t-test on the non-normalized -ΔCt values, the graphs depict relative fold induction of the target gene compared to a normalized sample (ΔΔCt). Statistical analyses were performed using GraphPad Prism version 9.5.0 for Windows (GraphPad Software, San Diego, California, USA). In figures, ns stands for $p > 0.05$, * $p < 0.05$, ** $p < 0.01$, *** $p < 0.001$, **** $p < 0.0001$. Error bars in figures specify SEM from the indicated number of independent experimental repeats with more than 3 larvae per treatment. Experiments were performed indicated number of times ($n \geq 3$) and statistics were calculated for each individual experiment. For analysis of 16S rRNA sequencing data, Shannon-wiener H index was calculated according to $H = -\Sigma pi*\ln(pi)$ and Simpson index was calculated according to $D = \Sigma ni(ni-1)/N(N-1)$. In addition, the total number of observed families (Sobs) was calculated.

Data availability statement

The data presented in the study are deposited in the NCBI repository, accession number PRJNA1005106, https://www.ncbi.nlm.nih.gov/sra/PRJNA1005106.

Ethics statement

The studies involving transgenic flies and genetically modified material were reviewed and approved by the Finnish Board for Gene Technology (Reg. Nr. 007/S/2021).

Author contributions

AA: Conceptualization, Formal Analysis, Funding acquisition, Investigation, Methodology, Writing – original draft, Writing – review & editing. AS: Investigation, Writing – original draft. FL: Investigation, Writing – review & editing. CK: Investigation, Writing – review & editing. EH: Investigation, Writing – review & editing. PM: Methodology, Supervision, Writing – review & editing. OS: Conceptualization, Supervision, Writing – review & editing. PE: Conceptualization, Supervision, Writing – original draft, Writing – review & editing. AM: Conceptualization, Funding acquisition, Methodology, Project administration, Resources, Supervision, Writing – original draft, Writing – review & editing.

Funding

The research was supported by The Academy of Finland Project (#321850), the InFLAMES Flagship Programme of the Academy of Finland (#337531), the Academy of Finland strategic research profiling area Solutions for Health at Åbo Akademi University (#336355), the Sigrid Jusélius Foundation, the Tor, Joe, and Pentti Borg Memorial Fund, Victoriastiftelsen, Swedish Cultural Foundation, the Orion Research Foundation sr, and the Juhani Aho Foundation for Medical Research, the H2020 HPC-Europa3 research visit programme (#730897).

Conflict of interest

The authors declare that the research was conducted in the absence of any commercial or financial relationships that could be construed as a potential conflict of interest.

Publisher's note

Supplementary material

The Supplementary Material for this article can be found online at: https://www.frontiersin.org/articles/10.3389/fimmu.2023.1253805/full#supplementary-material

SUPPLEMENTARY FIGURE 1
Bacterial 16S rRNA metagenomics analysis of the 1V-3V region, including and excluding Wolbachia.

SUPPLEMENTARY FIGURE 2
Comparison of *Diptericin* expression in wildtype *Canton*^{S} and TRPA1 LOF flies in response to DSS treatment.

References

1. Rivière C, Pawlus AD, Mérillon JM. Natural stilbenoids: Distribution in the plant kingdom and chemotaxonomic interest in Vitaceae. *Natural Product Rep* (2012) 29:1317–33. doi: 10.1039/c2np20049j

2. Routa J, Brännström H, Anttila P, Mäkinen M, Jänis J, Asikainen A. Wood extractives of Finnish pine, spruce and birch-availability and optimal sources of compounds A literature review. *Natural Resour bioeconomy studie* (2017) 73:55.

3. Akinwumi BC, Bordun KAM, Anderson HD. Biological activities of stilbenoids. *Int J Mol Sci* (2018) 19(3):792. doi: 10.3390/ijms19030792

4. Fauconneau B, Waffo-Teguo P, Huguet F, Barrier L, Decendit A, Merillon JM. Comparative study of radical scavenger and antioxidant properties of phenolic compounds from Vitis vinifera cell cultures using *in vitro* tests. *Life Sci Pergamon* (1997) 61(21):2103–10. doi: 10.1016/S0024-3205(97)00883-7

5. Chong J, Poutaraud A, Hugueney P. Metabolism and roles of stilbenes in plants. *Plant Science. Elsevier* (2009) 177(3):143–55. doi: 10.1016/J.PLANTSCI.2009.05.012

6. Quideau S, Deffieux D, Douat-Casassus C, Pouységu L. Plant polyphenols: Chemical properties, biological activities, and synthesis. *Angewandte Chemie - Int Edition* (2011) pp:586–621. doi: 10.1002/anie.201000044

7. Laavola M, Nieminen R, Leppänen T, Eckerman C, Holmbom B, Moilanen E. Pinosylvin and monomethylpinosylvin, constituents of an extract from the knot of Pinus sylvestris, reduce inflammatory gene expression and inflammatory responses *in vivo*. *J Agric Food Chem* (2015) 63(13):3445–53. doi: 10.1021/jf504606m

8. Moilanen LJ, Hämäläinen M, Lehtimäki L, Nieminen RM, Muraki K, Moilanen E. Pinosylvin inhibits TRPA1-induced calcium influx *in vitro* and TRPA1-mediated acute paw inflammation *in vivo*. *Basic Clin Pharmacol Toxicol* (2016) 118(3):238–42. doi: 10.1111/bcpt.12485

9. Yu L, Wang S, Kogure Y, Yamamoto S, Noguchi K, Dai Y. Modulation of TRP channels by resveratrol and other stilbenoids. *Mol Pain* (2013) 9:3. doi: 10.1186/1744-8069-9-3

10. Souza Monteiro de Araujo D, Nassini R, Geppetti P, De Logu F. TRPA1 as a therapeutic target for nociceptive pain. *Expert Opin Ther Targets* (2020) 24(10):997–1008. doi: 10.1080/14728222.2020.1815191

11. Hamada FN, Rosenzweig M, Kang K, Pulver SR, Ghezzi A, Jegla TJ, et al. An internal thermal sensor controlling temperature preference in Drosophila. *Nature* (2008) 454:7201. doi: 10.1038/nature07001

12. Kang K, Pulver SR, Panzano VC, Chang EC, Griffith LC, Theobald DL, et al. Analysis of Drosophila TRPA1 reveals an ancient origin for human chemical nociception. *Nature* (2010) 464(7288):597–600. doi: 10.1038/nature08848

13. Buchon N, Osman D, David FPA, Yu Fang H, Boquete JP, Deplancke B, et al. Morphological and molecular characterization of adult midgut compartmentalization in Drosophila. *Cell Rep Elsevier* (2013) 3(5):1725–38. doi: 10.1016/j.celrep.2013.04.001

14. Jo Du E, Jung Ahn T, Kwon I, Hye Lee J, Park JH, Hwa Park S, et al. TrpA1 regulates defecation of food-borne pathogens under the control of the duox pathway. *PLoS Genet* (2016) 12(1):e1005773. doi: 10.1371/journal.pgen.1005773

15. Xu C, Luo J, He L, Montell C, Perrimon N. Oxidative stress induces stem cell proliferation *via* TRPA1/RyR-mediated Ca2+signaling in the Drosophila midgut. *eLife* (2017) 6:e22441. doi: 10.7554/eLife.22441

16. Silverman N, Zhou R, Stöven S, Pandey N, Hultmark D, Maniatis T. A Drosophila IκB kinase complex required for Relish cleavage and antibacterial immunity. *Genes Dev* (2000) 14(19):2461–71. doi: 10.1101/gad.817800

17. Stöven S, Silverman N, Junell A, Hedengren-Olcott M, Erturk D, Engström Y, et al. Caspase-mediated processing of the Drosophila NF-κB factor Relish. *Proc Natl Acad Sci United States America.* (2003) 100(10):5991–6. doi: 10.1073/pnas.1035902100

18. Ertürk-Hasdemir D, Broemer M, Leulier F, Lane WS, Paquette N, Hwang D, et al. Two roles for the Drosophila IKK complex in the activation of Relish and the induction of antimicrobial peptide genes. *Proc Natl Acad Sci United States America.* (2009) 106(24):9779–84. doi: 10.1073/pnas.0812022106

19. Vaz F, Kounatidis I, Alo Covas G, Parton RM, Harkiolaki M, Davis I, et al. Accessibility to peptidoglycan is important for the recognition of Gram-positive bacteria in Drosophila. *CellReports* (2019) 27:2480–2492.e6. doi: 10.1016/j.celrep.2019.04.103

20. Ferrandon D, Imler JL, Hetru C, Hoffmann JA. The Drosophila systemic immune response: Sensing and signalling during bacterial and fungal infections. *Nat Rev Immunol* (2007) 7:862–74. doi: 10.1038/nri2194

21. Lemaitre B, Hoffmann J. The host defense of Drosophila melanogaster. *Annu Rev Immunol* (2007) 25(1):697–743. doi: 10.1146/annurev.immunol.25.022106.141615

22. Charroux B, Royet J. Drosophila immune response: From systemic antimicrobial peptide production in fat body cells to local defense in the intestinal tract. *Fly. Taylor Francis Inc.* (2010) 4(1):40–7. doi: 10.4161/fly.4.1.10810

23. Apidianakis Y, Rahme LG. Drosophila melanogaster as a model for human intestinal infection and pathology. *Dis Models mechanisms. Company Biologists Ltd* (2011) 4(1):21–30. doi: 10.1242/dmm.003970

24. Ton HT, Phan TX, Abramyan AM, Shi L, Ahern GP. Identification of a putative binding site critical for general anesthetic activation of TRPA1. *Proc Natl Acad Sci United States America.* (2017) 114(14):3762–7. doi: 10.1073/pnas.1618144114

25. Paulsen CE, Armache JP, Gao Y, Cheng Y, Julius D. Structure of the TRPA1 ion channel suggests regulatory mechanisms. *Nature* (2015) 520:7548. doi: 10.1038/nature14367

26. Klement G, Eisele L, Malinowsky D, Nolting A, Svensson M, Terp G, et al. Characterization of a ligand binding site in the human transient receptor potential ankyrin 1 pore. *Biophys J* (2013) 104(4):798–806. doi: 10.1016/J.BPJ.2013.01.008

27. Banzawa N, Saito S, Imagawa T, Kashio M, Takahashi K, Tominaga M, et al. Molecular basis determining inhibition/activation of nociceptive receptor TRPA1 protein. *J Biol Chem* (2014) 289(46):31927–39. doi: 10.1074/JBC.M114.586891

28. Gupta R, Saito S, Mori Y, Itoh SG, Okumura H, Tominaga M. Structural basis of TRPA1 inhibition by HC-030031 utilizing species-specific differences. *Sci Rep* (2016) 6:37460. doi: 10.1038/SREP37460

29. Perše M, Cerar A. Dextran sodium sulphate colitis mouse model: Traps and tricks. *J Biomedicine Biotechnol* (2012) 2012:718617. doi: 10.1155/2012/718617

30. Kiesler P, Fuss IJ, Strober W. Experimental models of inflammatory bowel diseases. *Cell Mol Gastroenterol Hepatology. Elsevier* (2015) 1(2):154–70. doi: 10.1016/J.JCMGH.2015.01.006

31. Eichele DD, Kharbanda KK. Dextran sodium sulfate colitis murine model: An indispensable tool for advancing our understanding of inflammatory bowel diseases pathogenesis. *World J Gastroenterol* (2017) 23:6016–29. doi: 10.3748/wjg.v23.i33.6016

32. Okayasu I, Hatakeyama S, Yamada M, Ohkusa T, Inagaki Y, Nakaya R. A novel method in the induction of reliable experimental acute and chronic ulcerative colitis in mice. *GASTROENTEROLOGY* (1990) 98:694–702. doi: 10.1016/0016-5085(90)90290-H

33. Amcheslavsky A, Jiang J, Ip YT. Tissue damage-induced intestinal stem cell division in Drosophila. *Cell Stem Cell* (2009) 4(1):49–61. doi: 10.1016/j.stem.2008.10.016

34. Wu SC, Liao CW, Pan RL, Juang JL. Infection-induced intestinal oxidative stress triggers organ-to-organ immunological communication in Drosophila. *Cell Host Microbe* (2012) 11(4):410–7. doi: 10.1016/j.chom.2012.03.004

35. Howard AM, Lafever KS, Fenix AM, Scurrah CR, Lau KS, Burnette DT, et al. DSS-induced damage to basement membranes is repaired by matrix replacement and crosslinking. *J Cell Science* (2019) 132(7):cs226860. doi: 1242/JCS.226860

36. Tzou P, Ohresser S, Ferrandon D, Capovilla M, Reichhart JM, Lemaitre B, et al. Tissue-specific inducible expression of antimicrobial peptide genes in Drosophila surface epithelia. *Immunity. Cell Press* (2000) 13(5):737–48. doi: 10.1016/S1074-7613(00)00072-8

37. Davis MM, Engström Y. Immune response in the barrier epithelia: Lessons from the fruit fly Drosophila melanogaster. *J Innate Immun* (2012) 4:273–83. doi: 10.1159/000332947

38. Cox CR, Gilmore MS. Native Microbial Colonization of Drosophila melanogaster and Its Use as a Model of Enterococcus faecalis Pathogenesis. *Infection Immun* (2007) 75(4):1565. doi: 10.1128/IAI.01496-06

39. Qin J, Li R, Raes J, Arumugam M, Burgdorf KS, Manichanh C, et al. A human gut microbial gene catalogue established by metagenomic sequencing. *Nature* (2010) 464:7285. doi: 10.1038/nature08821

40. Wong CNA, Ng P, Douglas AE. Low-diversity bacterial community in the gut of the fruitfly Drosophila melanogaster. *Environ Microbiol* (2011) 13(7):1889–900. doi: 10.1111/j.1462-2920.2011.02511.x

41. Matsuoka K, Kanai T. The gut microbiota and inflammatory bowel disease. *Semin Immunopathol* (2015) 37:47–55. doi: 10.1007/s00281-014-0454-4

42. Shin NR, Whon TW, Bae JW. Proteobacteria: Microbial signature of dysbiosis in gut microbiota. *Trends Biotechnol* (2015) 33:496–503. doi: 10.1016/j.tibtech.2015.06.011

43. Schreiber S, Nikolaus S, Hampe J. Activation of nuclear factor kappa B inflammatory bowel disease. *Gut. Gut* (1998) 42(4):477–84. doi: 10.1136/GUT.42.4.477

44. Atreya I, Atreya R, Neurath MF. NF-κB in inflammatory bowel disease. *J Internal Med* (2008) 263(6):591–6. doi: 10.1111/J.1365-2796.2008.01953.X

45. Kun J, Szitter I, Kemény Á, Perkecz A, Kereskai L, Pohóczky K, et al. Upregulation of the transient receptor potential ankyrin 1 ion channel in the inflamed human and mouse colon and its protective roles. *PloS One* (2014) 9(9):e108164. doi: 10.1371/journal.pone.0108164

46. Xiao B, Dubin AE, Bursulaya B, Viswanath V, Jegla TJ, Patapoutian A. Identification of transmembrane domain 5 as a critical molecular determinant of menthol sensitivity in mammalian TRPA1 channels. *J Neurosci* (2008) 28(39):9640–51. doi: 10.1523/JNEUROSCI.2772-08.2008

47. Ton HT, Smith J, Phan TX, Brown M, Ahern GP. Pungent and non-pungent general anesthetics interact with TRPA1 *via* distinct binding pocket in the pore domain region. *Biophys J* (2016) 110(3):283a–4a. doi: 10.1016/j.bpj.2015.11.1536

48. Poulsen MM, Fjeldborg K, Ornstrup MJ, Kjær TN, Nøhr MK, Pedersen SB. Resveratrol and inflammation: Challenges in translating pre-clinical findings to improved patient outcomes. *Biochim Biophys Acta (BBA) - Mol Basis Dis* (2015) 1852(6):1124–36. doi: 10.1016/J.BBADIS.2014.12.024

49. Henry-Vitrac C, Desmoulière A, Girard D, Mérillon JM, Krisa S. Transport, deglycosylation, and metabolism of trans-piceid by small intestinal epithelial cells. *Eur J Nutr* (2006) 45:7. doi: 10.1007/S00394-006-0609-8

50. Välimaa AL, Honkalampi-Hämäläinen U, Pietarinen S, Willför S, Holmbom B, von Wright A. Antimicrobial and cytotoxic knotwood extracts and related pure compounds and their effects on food-associated microorganisms. *Int J Food Microbiol* (2007) 115(2):235–43. doi: 10.1016/j.ijfoodmicro.2006.10.031

51. Plumed-Ferrer C, Väkeväinen K, Komulainen H, Rautiainen M, Smeds A, Raitanen JE, et al. The antimicrobial effects of wood-associated polyphenols on food pathogens and spoilage organisms. *Int J Food Microbiol* (2013) 164(1):99–107. doi: 10.1016/j.ijfoodmicro.2013.04.001

52. Lemaitre B, Nicolas E, Michaut L, Reichhart JM, Hoffmann JA. The dorsoventral regulatory gene cassette spatzle/Toll/Cactus controls the potent antifungal response in Drosophila adults. *Cell* (1996) 86(6):973–83. doi: 10.1016/S0092-8674(00)80172-5

53. Leulier F, Rodriguez A, Khush RS, Abrams JM, Lemaitre B. The Drosophila caspase Dredd is required to resist Gram-negative bacterial infection. *EMBO Rep* (2000) 1(4):353–8. doi: 10.1093/embo-reports/kvd073

54. Kitajima S, Takuma S, Morimoto M. Histological analysis of murine colitis induced by dextran sulfate sodium of different molecular weights. *Exp Anim* (2000) 49 (1):9–15. doi: 10.1538/expanim.49.9

55. Viennois E, Chen F, Laroui H, Baker MT, Merlin D. Dextran sodium sulfate inhibits the activities of both polymerase and reverse transcriptase: lithium chloride purification, a rapid and efficient technique to purify RNA. *BMC Res Notes* (2013) 6:360. doi: 10.1186/1756-0500-6-360

56. Pärhi S, Puska M, Kalapudas A, Korte H, Hukka P. Method for the production of a phenolic substance from wood. *U.S. Patent No 7,153,982, US Patent and Trademark Office* (2006).

57. Saadabadi A, Ahmed A, Smeds AI, Eklund PC. High recovery of stilbene glucosides by acetone extraction of fresh inner bark of Norway spruce. *Holzforschung* (2021) 75(11):1012–1018. doi: 10.1515/hf-2020-0263

58. Simhadri RK, Fast EM, Guo R, Schultz MJ, Vaisman N, Ortiz L, et al. The gut commensal microbiome of Drosophila melanogaster is modified by the endosymbiont Wolbachia. *mSphere* (2017) 2(5):e00287–17. doi: 10.1128/msphere.00287-17

59. Altschul SF, Gish W, Miller W, Myers EW, Lipman DJ. Basic local alignment search tool. *J Mol Biol J Mol Biol* (1990) 215(3):403–10. doi: 10.1016/S0022-2836(05) 80360-2

60. Berman HM, Westbrook J, Feng Z, Gilliland G, Bhat TN, Weissig H, et al. The protein data bank. *Nucleic Acids Res Oxford Acad* (2000) 28(1):235–42. doi: 10.1093/NAR/28.1.235

61. Zhao J, Lin King JV, Paulsen CE, Cheng Y, Julius D. Irritant-evoked activation and calcium modulation of the TRPA1 receptor. *Nature* (2020) 585:7823. doi: 10.1038/s41586-020-2480-9

62. Webb B, Sali A. Comparative protein structure modeling using MODELLER. *Curr Protoc Bioinf* (2016) 54:5.6.1–5.6.37. doi: 10.1002/CPBI.3

63. Sievers F, Wilm A, Dineen D, Gibson TJ, Karplus K, Li W, et al. Fast, scalable generation of high-quality protein multiple sequence alignments using Clustal Omega. *Mol Syst Biol* (2011) 7:539. doi: 10.1038/msb.2011.75

64. Shen M, Sali A. Statistical potential for assessment and prediction of protein structures. *Protein Sci* (2006) 15(11):2507–24. doi: 10.1110/ps.062416606

65. Chen VB, Arendall WB, Headd JJ, Keedy DA, Immormino RM, Kapral GJ, et al. MolProbity: all-atom structure validation for macromolecular crystallography. *Int Union Crystallogr* (2009) 66(1):12–21. doi: 10.1107/S0907444909042073

66. Madhavi Sastry G, Adzhigirey M, Day T, Annabhimoju R, Sherman W. Protein and ligand preparation: Parameters, protocols, and influence on virtual screening enrichments. *J Computer-Aided Mol Design* (2013) 27(3):221–34. doi: 10.1007/S10822-013-9644-8/TABLES/9

67. Roos K, Wu C, Damm W, Reboul M, Stevenson JM, Lu C, et al. OPLS3e: extending force field coverage for drug-like small molecules. *J Chem Theory Comput* (2019) 15(3):1863–74. doi: 10.1021/ACS.JCTC.8B01026

68. Friesner RA, Banks JL, Murphy RB, Halgren TA, Klicic JJ, Mainz DT, et al. Glide: A new approach for rapid, accurate docking and scoring. 1. Method and assessment of docking accuracy. *J Medicinal Chem* (2004) 47(7):1739–49. doi: 10.1021/jm0306430

69. Halgren TA, Murphy RB, Friesner RA, Beard HS, Frye LL, Pollard WT, et al. Glide: A new approach for rapid, accurate docking and scoring. 2. Enrichment factors in database screening. *J Medicinal Chem* (2004) 47(7):1750–9. doi: 10.1021/jm030644s

70. Friesner RA, Murphy RB, Repasky MP, Frye LL, Greenwood JR, Halgren TA, et al. Extra precision glide: Docking and scoring incorporating a model of hydrophobic enclosure for protein-ligand complexes. *J Medicinal Chem* (2006) 49(21):6177–96. doi: 10.1021/jm051256o

71. Jacobson MP, Pincus DL, Rapp CS, Day TJF, Honig B, Shaw DE, et al. A hierarchical approach to all-atom protein loop prediction. *Proteins: Structure Function Bioinf* (2004) 55(2):351–67. doi: 10.1002/PROT.10613

72. Li J, Abel R, Zhu K, Cao Y, Zhao S, Friesner RA. The VSGB 2.0 model: A next generation energy model for high resolution protein structure modeling. *Proteins: Structure Function Bioinf* (2011) 79(10):2794–812. doi: 10.1002/PROT.23106

73. Bowers KJ, Chow E, Xu H, Dror RO, Eastwood MP, Gregersen BA, et al. Scalable algorithms for molecular dynamics simulations on commodity clusters, in: *Proceedings of the 2006 ACM/IEEE Conference on Supercomputing*, Association for Computing Machinery. New York (2006) SC '06. doi: 10.1145/1188455.1188544

74. Jorgensen WL, Chandrasekhar J, Madura JD, Impey RW, Klein ML. Comparison of simple potential functions for simulating liquid water. *J Chem Phys* (1998) 79(2):926. doi: 10.1063/1.445869

75. Moussaoui O, Bhadane R, Sghyar R, El Hadrami EI, Amrani S, Tama AB, et al. Novel amino acid derivatives of quinolines as potential antibacterial and fluorophore agents. *Scientia Pharm* (2020) 88(4):1–22. doi: 10.3390/scipharm88040057

frontiers | Frontiers in Immunology

TYPE Review
PUBLISHED 17 October 2023
DOI 10.3389/fimmu.2023.1276357

OPEN ACCESS

EDITED BY
Susanna Valanne,
Tampere University, Finland

REVIEWED BY
Adam Bajgar,
University of South Bohemia in České Budějovice, Czechia
Edan Foley,
University of Alberta, Canada

*CORRESPONDENCE
Andrea M. Darby
amd439@cornell.edu

RECEIVED 11 August 2023
ACCEPTED 03 October 2023
PUBLISHED 17 October 2023

CITATION
Darby AM and Lazzaro BP (2023) Interactions between innate immunity and insulin signaling affect resistance to infection in insects.
Front. Immunol. 14:1276357.
doi: 10.3389/fimmu.2023.1276357

Interactions between innate immunity and insulin signaling affect resistance to infection in insects

Andrea M. Darby[1,2]* and Brian P. Lazzaro[1,2]

[1]Department of Entomology, Cornell University, Ithaca, NY, United States, [2]Cornell Institute of Host-Microbe Interactions and Disease, Cornell University, Ithaca, NY, United States

An active immune response is energetically demanding and requires reallocation of nutrients to support resistance to and tolerance of infection. Insulin signaling is a critical global regulator of metabolism and whole-body homeostasis in response to nutrient availability and energetic needs, including those required for mobilization of energy in support of the immune system. In this review, we share findings that demonstrate interactions between innate immune activity and insulin signaling primarily in the insect model *Drosophila melanogaster* as well as other insects like *Bombyx mori* and *Anopheles* mosquitos. These studies indicate that insulin signaling and innate immune activation have reciprocal effects on each other, but that those effects vary depending on the type of pathogen, route of infection, and nutritional status of the host. Future research will be required to further understand the detailed mechanisms by which innate immunity and insulin signaling activity impact each other.

KEYWORDS

innate immunity, insulin signaling, metabolism, immunometabolism, humoral immunity, *Drosophila*, mosquito, *Bombyx*

Introduction

Innate immunity and insulin/insulin-like signaling (IIS) are both integral for homeostasis and anti-pathogen defense in insects. An immune response is critical for protecting an organism from invading pathogens that pirate resources and reproduce within the host (1, 2). The IIS pathway functions as a nutrient-sensing pathway that regulates cell and tissue growth, as well as whole-organism metabolism (3, 4). Innate immunity and IIS activity have been thought of as independent processes, but developments over the past decade have demonstrated them to be connected in mobilizing energy stores required for an effective immune response (5). In this review, we will discuss what we know of the physiological consequences and genetic mechanisms underlying interactions between insulin and immune pathways in insects, emphasizing primary examples from *Drosophila melanogaster* and integrating data from other insect models.

The innate immune system and IIS pathway are highly conserved across insect orders. Comparative genomics has revealed considerable conservation of orthologs in immune genes across almost all insects whose genomes have been sequenced (6). Similarly, insulin like-peptides (ILPs) that share structural and functional homology to mammalian insulin, have also been identified in major insect orders including Orthoptera, Diptera, Hymenoptera, Coleoptera, and Hemiptera (7–11). Concurrently, the development of genetic technologies from RNAi to CRISPR/Cas9 has enabled us to begin to understand how these pathways operate and how they impact each other across diverse insects (12–17), paving the way for future studies of how these systems interact to maintain organismal homeostasis in the presence and absence of infection.

Effect of infection on metabolism and energetic stores

Mounting an immune response is an energetically costly process, requiring systemic physiological shifts in metabolism and energetic stores (16, 18–21). A broad range of pathogenic infections, from bacterial, viral, parasitic, or fungal, can lead to decreases in energetic stores like glycogen and triglycerides (12, 22–26). In insects, the fat body is a multifunctional tissue that can secrete antimicrobial peptides in response to immune stimulus and is also a site for the storage and breakdown of carbohydrates and lipids (27). Energetic stores like glycogen can be critical for supplying energy to activate the immune response. Glycogen is the polymeric form of glucose, and can be broken down in tissues like the fat body to be released into the hemolymph as free glucose by the enzyme glycogen phosphorylase (glyp) (28). *D. melanogaster* exhibit decreased glycogen levels and increased circulating glucose levels after infection with *Streptococcus pneumoniae*, with increased gene expression of *glyp* stimulated by the extracellular release of adenosine (25, 29). Phagocytic immune cells uptake the circulating glucose during the acute phase of *S. pneumoniae* infection, enabling phagocytosis. *D. melanogaster* deficient for the adenosine receptor or *glyp* exhibit lower levels of glycogen and higher mortality after *S. pneumoniae* infection (25, 29).

A metabolomics study on larvae of the silkworm *Bombyx mori* infected with the entomophathogenic fungi *Beauveria bassiana* found major shifts in hemolymph levels of metabolites like lipids, carbohydrates, and amino acids after infection (30). Fungal infection also caused higher levels of glucose and an associated reduction in trehalose (30). Trehalose is a disaccharide comprised of two glucose molecules that can be readily liberated into free glucose by the enzyme trehalase. Trehalose is the primary sugar found in insect hemolymph and is used for energetic needs like flight and metabolic homeostasis (28, 31). Although Xu et al. (30) did not measure trehalase activity, Praveena et al. (32) found that trehalase activity progressively diminishes in the hemolymph of *B. mori* larvae over five days of *B. beauveria* infection while they remain consistent in uninfected controls. These authors hypothesize that trehalase activity reduces over the course of the infection because the early hydrolysis of trehalose to glucose consumes the substrate pool available for conversion. The data suggest that during a fungal infection, trehalose may be converted to glucose to allocate energy to fighting the infection.

The breakdown of glycogen and trehalose provides free glucose for immune cell function (29). However, the role of triglyceride breakdown during infection is less well established. It has been recently demonstrated that *D. melanogaster* larvae exhibit reduced triglyceride stores during an active immune response, and shift from lipid storage to synthesizing phosphatidylcholine (PC) and phosphatidylethanolamine (PE) (16), which are two of the major phospholipids that comprise secretory vesicles and cell and organelle membranes (33). Active humoral immune responses drive high levels of AMP gene expression (e.g., 34), which could put a heavy burden for the endoplasmic reticulum (ER) to synthesize and secrete the encoded effectors into circulation. This shift to PE and PC synthesis during chronic immune activation has been hypothesized to support the secretion of immune effectors during the immune response.

Cellular stresses, including those imposed by immune reactions, stimulate the unfolded protein response (UPR) to allow the endoplasmic reticulum (ER) to regulate proper folding and secretion of proteins (35, 36). One marker of UPR in the ER is the upregulation of the transcription factor X-box binding protein 1 (XBP1), which positively regulates phospholipid synthesis and enzymes that increase the size of the ER (37). Both infection (34, 38) and chronic immune activation in the fat body (16) have been demonstrated to increase gene expression of *XBP1*. This elevated expression of ER-stress response genes is also associated with increased expansion of the ER lumen in infected mated females (38) and in uninfected larvae with an overactive immune response (16). These results suggest that the innate immune response induces ER stress, which increases phospholipid synthesis to support secretion of immune effectors. The infection-induced reduction of triglyceride stores observed across several *D. melanogaster* studies (12, 19, 23, 39) could arise from a need to mobilize energetic stores to support ER homeostasis by way of upregulating phospholipid synthesis.

Sustained long-term infections can result in energetic wasting. In a healthy animal, insulin signaling regulates glucose homeostasis (40, 41). Phosphorylation of the IIS protein Akt leads to uptake of extracellular glucose (42) and promotes glycogen and triglyceride synthesis (43) by positively regulating the genes *glycogen synthase* and *acetyl coenzyme-A* (Figure 1; 44–46). Dionne et al. (12) demonstrated that *Drosophila melanogaster* infected with the bacterium *Mycobacterium marinum* exhibit impaired IIS activity over several days of infection. Reduction in phosphorylation of Akt leads to reduced expression of *glycogen synthase* and *acetyl coenzyme-A*. Consequently, flies infected with *M. marinum* become hyperglycemic and progressively lose glycogen and triglyceride stores until they ultimately die from the infection.

In examples such as this (12, 23) it can be difficult to determine whether the metabolic change reflects a manipulation of the host by the parasite for the parasite's own nutritional benefit, or whether the wasting reflects a collateral cost of sustained immune reactions. In the case of bacteria in the genus *Mycobacterium*, the bacteria primarily depend on lipids like cholesterol as their source of

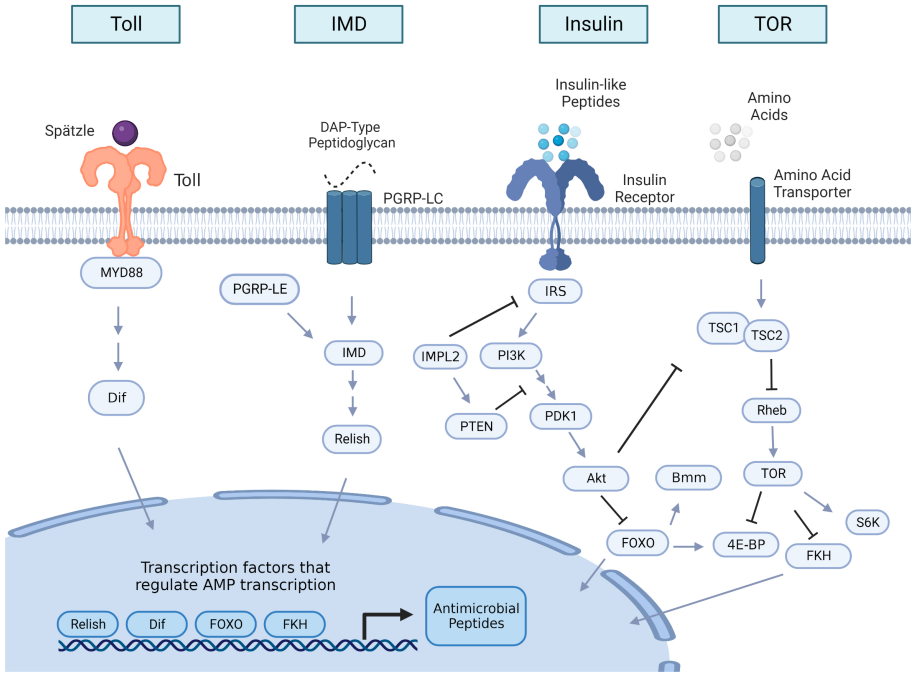

FIGURE 1
Insulin and innate immune pathway signaling overview in insects. The Toll and the immune deficiency (IMD) pathways are the two major innate immune signaling pathways that are induced upon bacterial or fungal infection, leading to the production of antimicrobial peptides (AMPs). The Toll receptor is activated by the cleaved form of the cytokine Spätzle, which is processed in a proteolytic cascade after the detection of Gram-positive bacteria or fungi. Once Toll is active, it initiates an intracellular cascade that leads to activation of the nuclear factor κB (NF-κB) transcription factor Dif. When activated, Dif translocate to the nucleus to initiate AMP transcription. IMD signaling is initiated by peptidoglycan recognition protein LC (PGRP-LC) or peptidoglycan recognition protein LE (PGRP-LE) binding DAP-type peptidoglycan shed by Gram-negative bacteria and some Gram-positive bacteria. This binding triggers a cascade that activates the NF-κB transcription factor Relish to translocate to the nucleus to transcribe AMPs. Insulin signaling activity begins with the production of insulin-like peptides (ILPs), which are predominantly secreted from insulin-producing cells and from other tissue sources like the fat body or muscle. An intracellular cascade occurs after ILPS bind to the insulin receptor, activating the protein Akt. Once Akt is active, it impacts multiple downstream processes within the cell, including inhibition of nuclear translocation of the forkhead family transcription factor, Forkhead box-O (FOXO), which can regulate transcription of AMPs, and the lipase brummer (bmm). Akt activation also stimulates the target of rapamycin (TOR) pathway by TSC1/TSC2 suppression. TOR is also activated by amino acid sensing. Downstream targets of TOR activation include repression of the forkhead box family member forkhead (FKH), which also regulates AMP transcription, activation of the protein kinase S6K, which is critical for growth processes, and the inhibition of translational regulator 4E-BP (eukaryotic initiation factor 4 binding protein). Arrows in the figure denote positive interactions and bars denote negative interactions. Double arrows indicate that additional steps in the pathway are not illustrated. IRS, insulin receptor substrate; IMPL2, ecdysone-inducible gene L2; PI3K; phosphatidylinositol 3-kinase; PTEN, phosphatidylinositol 3,4,5-trisphosphate 3-phosphatase; PDK1 (phosphoinositide-dependent protein kinase); TSC, tuberous sclerosis tumor suppressor Rheb, Ras homolog enriched in brain; S6K, ribosomal S6 kinase.

carbon (47, 48) and a large portion of the genome for this genus is devoted to lipid metabolism (49). It is possible that wasting phenotypes observed in this infection could be a result of pathogen nutrient acquisition. This can be distinguished with appropriately designed experiments. For example, one human study investigated metabolic shifts induced by infection with *Mycobacterium tuberculosis* (Mtb), the causative agent of tuberculosis (TB). These authors measured metabolic shifts in blood samples from patients that were healthy, patients infected with Mtb and given short-term antibiotic treatment, and Mtb-infected patients without treatment (50). They found that Mtb infection, regardless of treatment, significantly shifted metabolic profiles compared to healthy patients, and they observed no significant differences in metabolites between TB patients treated with antibiotics or not, despite reduced pathogen load in patients given antibiotics (50). These authors suggest that their observation that antibiotic treatment does not impact infection-induced metabolic shifts implies that the host consumes metabolites during an active immune response. This study does not rule out the possibility that virulence factors produced by the pathogen could continue to impact host metabolism even after pathogen loads are reduced by antibiotic treatment. However, it can serve as an example of how to begin to study whether metabolic consequences of infection are due to host energetic reallocation or pathogen nutrient acquisition.

Effects of dietary sugar on immune outcome

Both the immune system and insulin signaling are heavily influenced by dietary nutrition (51–55), thus any variation in the composition of diet can influence an organism's ability to resist infection and regulate global metabolism. When *Drosophila melanogaster* are reared on high glucose (0.57 M), they experience reduced resistance to a systemic infection by the

bacterial pathogen *Providencia rettgeri* (56). Similarly, those reared on high sucrose (1 M) experience increased mortality following infection by the pathogen *Pseudomonas aeruginosa* (52). High sucrose diets also impair immunological melanization in larval hemolymph (52) and reduce phagocytosis of fungal spores by *D. melanogaster* larvae (53).

IIS activity might mediate the higher post-infection mortality observed in flies fed high-sugar diets. Musselman et al. (52) found through an RNA-seq analysis that uninfected larvae with knockdown of the insulin receptor (InR) in the fat body exhibit elevated expression of AMPs while larvae with constitutive activation of InR in the fat body exhibit reduced AMP expression. Knockdown of InR in the adult fat body increases survivorship of systemic *P. aerugionsa* infection in flies fed a high-sugar (0.7 M) diet (52). These data suggest that reduction in insulin signaling could increase infection survival on high-sugar diets, potentially due to elevated expression of immune effectors. In that study, however, they did not specifically measure AMP expression during an infection in flies with InR knockdown so it remains to be determined whether InR knockdown promotes survival of infection by elevating AMP expression.

These systemic infections performed by Unckless et al. (56) and Musselman et al. (52) were performed on *Drosophila* reared on high dietary sugar throughout larval development. High-sugar diets cause developmental delays, lipidemia, hyperglycemia, and reduced body size in both larvae and adults (51, 52). Thus, the consequences of a high-sugar diet on adult defense could be due to dietary effects on larval development that may affect immune capacity in the adult stage. For example, *D. melanogaster* larvae fed high yeast diets exhibit increased expression of antimicrobials as adults (57). *Drosophila* larvae fed low-protein diets have lower counts of phagocytic immune cells (58) and are more susceptible to systemic *Pseudomonas entomophila* infection in the adult stage (59). Mosquito larvae fed low protein diets were more susceptible to *Plasmodium falciparum* (60) and Sindbis virus infections (61). Infection in the *D. melanogaster* larval stage can also affect adult fitness, including reduced lifespan (62) and smaller body size (63). Future research should distinguish between the immediate metabolic effects and developmental effects of sugar overnutrition. One strategy for doing this is to rear juveniles on the same rearing medium then transfer adults to varied experimental diets after development is complete. This approach could be directly compared to cohorts of insects that are reared on varied diets high in dietary sugar to determine the relative contributions of developmental history and immediate metabolic dysregulation on immune function.

Some studies suggest a potentially protective effect of dietary sugar during enteric infection. For example, *D. melanogaster* fed high-glucose diets (0.55 M) exhibit increased survival after an enteric *Vibrio cholerae* infection (64). Feeding sugar to the mosquito *Aedes aegypti* also increases expression of antiviral genes in the intestinal tract and protects mosquitos from oral arbovirus infections (65). High-sugar diets have been demonstrated to elevate reactive oxygen species levels (66) and increase expression of antimicrobial peptides (67) in the midgut of *D. melanogaster*. These data suggest high-sugar diets may alter gut immunity, potentially as a consequence of dysregulation of the endogenous microbiota (68), which would not occur in the hemocoel during a systemic infection. These data draw attention to important differences in the consequences of dietary sugar that may depend on whether the infection is acquired systemically or orally.

The dependency of infection-related phenotypes on dietary nutrition raises an important concern for comparisons across studies performed by different research groups. There is very little standardization of diets used for rearing *D. melanogaster* in infection studies (69, 70). For example, the diet used for the enteric infection referenced in (64) was a holidic (chemically-defined) diet, which is known to delay development relative to sugar-yeast based diets that are standard in *D. melanogaster* studies (71, 72), and the definition of "high" sugar varied nearly 2-fold between Musselman et al. (52) and Unckless et al. (56). Potentially, differences in dietary composition between studies could affect metabolism and infection phenotypes even when diet is not itself an explicit focus of the experiment.

Consequences of innate immune activation on insulin signaling

Transcriptomic studies of infected insects often show differential expression of genes in gene ontology (GO) categories related to carbohydrate and lipid metabolism (34, 73–75). The IIS pathway is a critical regulator of carbohydrate and lipid metabolism (4, 76, 77). Thus, infection-induced shifts in carbohydrate and lipid metabolism could be mediated by alterations in IIS activity driven by the immune system.

The Toll signaling pathway (Figure 1) is one of two major innate immune signaling pathways in insects (78). Toll signaling is homologous to Toll-like signaling in vertebrates (79) and leads to activation of the NF-κB transcription factor Dif. Gram-positive bacterial and fungal pathogens primarily activate Toll signaling (80, 81). Activation of Toll in the *D. melanogaster* fat body either through genetic manipulation or infection suppresses insulin signaling as measured by reduced phosphorylation of Akt (19, 39, 82). Since the insulin pathway is critical for regulating growth and lipid metabolism (76, 77), inhibition of IIS activity by Toll activation during development results in reduced body size and depletion of triglyceride stores (19, 82).

Suzawa et al. (82) showed that infection of *D. melanogaster* larvae with the Gram-positive bacterium *Enterococcus faecalis* reduces production of insulin-like peptide 6 (dILP6), which is an ILP secreted from the fat body that regulates larval growth (83, 84). Overexpression of *Dif* in the larval fat body also reduces dILP6 mRNA transcripts, and the infection-induced reduction in dILP6 and growth inhibition can be rescued by RNAi knockdown of *Dif* (82). Roth et al. (39) further found that activation of Toll in the larval fat body inhibits PDK1 from phosphorylating Akt at residue T342, resulting in growth inhibition and reduced triglyceride storage (39). Body size and triglyceride storage were rescued by forced phosphorylation of Akt site T342 in the fat body of larvae with constitutively activated Toll (39). These results clearly place

alteration of dILP6-production and larval insulin signaling downstream of the Toll signaling pathway. However, further experiments are required to test whether Dif directly regulates dILP6 expression or whether insulin signaling is secondarily regulated by proteins whose expression is directly controlled by Dif.

The immune deficiency (IMD) pathway (Figure 1) is the second main arm of the insect innate immune system (73). IMD signaling is responsive to DAP-type peptidoglycan shed by Gram-negative bacteria as well as some *Bacillus* species (81) and activates the NF-κB transcription factor Relish to induce transcription of antimicrobial peptides and other immune response genes (Figure 1; 81, 85). There is mixed evidence of IMD activity impacting insulin signaling and mobilization of energetic stores in *D. melanogaster*. DiAngelo et al. (19) found that constitutive activation of Relish in the fat body did not significantly impact Akt phosphorylation or triglyceride content (19). Although infection with the Gram-negative bacterium *Escherichia coli* reduced Akt phosphorylation, the suppression was lost when Toll pathway mutants were infected with *E. coli*, indicating that the attenuation of IIS was due to cross activation of the Toll pathway and not due to IMD signaling (19). In contrast, Davoodi et al. (86) found that constitutive activation of the IMD protein in the fat body significantly reduces phosphorylation of Akt and S6K throughout the body. S6K is a serine kinase downstream of Akt (Figure 1) that is critical for regulating larval growth (87). IMD activation in the fat body also reduced total triglyceride and trehalose levels in 3rd-instar larvae (86). Those larvae weighed less, had delayed development, and had reduced adult eclosion rates. These phenotypes are similar to those of insulin-signaling mutants and flies that overexpress Toll in the fat body (19, 88). One major difference between these two studies is the fly genotypes used to constitutively activate the IMD signaling pathway. Davoodi et al. (86) overexpressed the IMD protein where DiAngelo et al. (19) forced constitutive expression of the transcription factor Relish. The IMD molecule is an adaptor protein that acts upstream of Relish (Figure 1; 81), and, when activated, it triggers an intracellular signaling cascade that results in Relish activation (89). Potentially, there may be branching of the IMD pathway such that targets downstream of the IMD protein that disrupts insulin signaling and alter metabolic stores may not be regulated by Relish.

Davoodi et al. (86), also performed a transcriptomic analysis on larval fat body with constitutive IMD protein activation and identified modified expression of genes that regulate metabolic processes. Genes involved in the negative regulation of IIS were upregulated, including *impl2* and downstream targets of IIS like *4E-BP* (86). Lipid synthesis and gluconeogenesis genes were conversely downregulated in larvae with constitutive expression of the IMD pathway (86). These transcriptional data suggest that the IMD pathway, like Toll signaling, can influence metabolism.

Toll and IMD signaling are both critical for systemic immunity, however, the IMD pathway is primarily responsible for regulating gut immunity, including in response to endogenous microbiota (90). Impaired IMD signaling in the gut has been demonstrated to affect insulin signaling activity and metabolic stores. Kamareddine et al. (91) found a significant depletion of lipids in the fat body and an accumulation of lipid droplets in the anterior region of the midguts of several IMD mutants of *D. melanogaster* (*Dredd, key, RelE20, PGRP-LC and PGRP-LE*) in the absence of a systemic infection. Despite having depleted lipids in the fat body, whole-body triglyceride content and glucose levels were higher in the IMD mutants. These mutants also exhibited lower levels of *Ilp3* transcripts and reduced phosphorylated Akt in the intestine (91). Davoodi et al. (86) similarly observed that uninfected *imd* mutants have higher whole-body triglyceride levels and reduced expression of *Ilp2, Ilp3*, and *Ilp5*, although only in males. These results demonstrate that IMD signaling plays a critical role in regulating metabolic homeostasis even in the absence of systemic infection, potentially through actions in the gut or on the endogenous gut microbiota.

The insect digestive tract is a complex organ composed of multiple cell types that vary in function including immune defense, absorption of nutrients, and lipid metabolism (92). Enteroendocrine (EE) cells in the midgut epithelium produce hormones, regulate stem cell activity, and express insulin-like peptides (93). Kamareddine et al. (91) found that *Relish* knockdown in EE cells reduced *Ilp3* transcripts in the gut, increased EE lipid content, and reduced phosphorylation of Akt, while *Relish* knockdown in the fat body yielded no effect on Akt phosphorylation, triglyceride levels, or glucose content (91). Previous studies have demonstrated a role for commensal *D. melanogaster* gut microbiota like *Acetobactor pomorum* in regulating host metabolism, particularly via the microbial metabolic byproduct acetate (94, 95). Provision of acetate to germ-free flies increases nuclear localization of Relish and restores Akt phosphorylation (91). Germ-free wildtype flies have reduced IMD activity and exhibit metabolic phenotypes similar to those of flies with IMD knockdown in EE cells (91). Reciprocally, IIS activity and metabolic homeostasis are restored by overexpression of *Relish* in the EE cells of germ-free flies (91).

These data corroborate findings from an earlier microarray study that demonstrate microbiota-induced expression of host gene expression is *Relish*-dependent (96). Particularly, that study found that conventionally-reared flies exhibit upregulation of 285 genes in the gut relative to flies reared germ-free, and that GO categories for metabolic genes were enriched. When those authors then compared the transcriptomes of germ-free and conventionally reared Relish mutants, they found that expression of 151 of those 285 genes upregulated in response to microbiota was altered, including the insulin signaling genes *PI3K, InR*, and *thor* (96). Several other studies similarly demonstrate microbiota-Relish-dependent regulation of host gene expression in the gut. For example, oral infection with *Erwinia carotovora* also causes shifts in midgut gene expression that are *Relish*-dependent, including both immune and metabolic gene regulators (90). *Relish* mutants do not exhibit expression of microbiota-regulated genes observed in wildtype flies, regardless of whether they are germ-free or associated with microbiota (97). These data suggest a model whereby the host IMD pathway regulates the gut microbiota to maintain metabolic homeostasis, including through altered production of IIS activity by microbiota-derived metabolites such as acetate. However, the mechanistic details of signal integration under this model are unclear, and future experiments should study how downstream

effectors of the IMD pathway interact with components of IIS to shape global metabolic regulation.

Since the IIS pathway is a critical global regulator of metabolism (76), it is also vital for regulating communication among tissues, and there are several studies that demonstrate innate immune activation also stimulating inter-organ communication in response to infection in *Drosophila* (98–100; see 101 for a review on inter-organ communication during an immune response). For example, glutamate derived from the muscle stimulates reallocation of lipids from the fat body to improve survivorship during oral infection with *Pseudomonas entomophila* (100). While not often directly investigated, there is evidence to suggest tissue communication during an immune response occurs in part by altered IIS activity. One study found that both systemic infection and overexpression of Toll and IMD in the fat body increased triglyceride and lipid droplet size in the midgut (99). This increase in lipid accumulation in the midgut was also associated with increased midgut gene expression of negative IIS regulators like *Impl2* and *thor* (99), which suggests that Toll and IMD activation in the fat body can suppress IIS activity in the midgut in response to innate immune activity in the fat body. In this study, lipid accumulation in the midgut was critical for surviving systemic *Photorhabdus luminsecens* infection (99). It is an exciting avenue of research to consider the extent to which innate immune activity and IIS activity may communicate across tissues to drive organism-level responses and increase survivorship during infection.

Effects of insulin signaling on innate immunity

Several studies in *D. melanogaster* have characterized the effect that suppressing IIS activity has on infection outcome. The insulin receptor substrate *chico* is important for mediating the downstream cascade of IIS activity after insulin-like peptides bind to the insulin receptor (Figure 1, 76, 88). *Chico* mutants experienced increased survival of systemic infection by *Pseudomonas aeruginosa* and *Enterococcus faecalis* compared to wildtype flies (102). This higher rate of survivorship post-infection was not associated with increased levels of infection-induced gene expression of the AMP-encoding genes *Diptericin*, *Attacin*, and *Drosomycin*, although *chico* mutants do exhibit increased expression of *thor* in response to infection (102). Thor is an inhibitor of 5'-cap-dependent mRNA translation (103) and can prioritize translation of AMPs during an infection (104). Systemic infection with several different bacteria induces higher expression of *thor* (34, 104, 105) and *thor* mutants are highly susceptible to bacterial and fungal infection (104–106). Potentially, suppression of insulin signaling could be indirectly protective against infection due to downstream effects on cap-independent translation of proteins like AMPs.

A subsequent study conducted by McCormack et al. (107) found that *chico* mutants sustained lower pathogen loads after systemic infection with *E. coli* and *Photorhabdus luminescens*, although survivorship proportion was similar to wildtype flies. The effects on immune system activity were mixed, with reduced infection-induced transcription of the AMP genes *Diptericin*, *Cecropin A1*, and *Drosomycin*, and even reduced phagocytic capacity (107). However, the *chico* mutants exhibited increased phenoloxidase activity and melanization compared to wildtype. Melanization is important for insect wound healing and to clear pathogens at an injury site (108) and has been demonstrated to increase survivorship after bacterial and fungal infections (109). Potentially, increased phenoloxidase activity could also contribute to the increased survivorship of *E. faecalis* infection observed by Libert et al. (102) since melanization is also important for surviving *E. faecalis* infection (109). Similarly, higher phenoloxidase and melanization activity has been suggested to increase survivorship after *P. luminescens* infection (110, 111). However, melanization activity is not critical for surviving *E. coli* infection (112), thus improved phenoloxidase activity alone does not fully explain improved survivorship for *chico* mutants after *E. coli* infections observed by Libert et al. (102).

A more recent study assaying the effect of disrupted IIS activity on infection survival in *D. melanogaster* further demonstrated pathogen-specific infection outcomes. Davoodi et al. (86) delivered systemic and oral infections with five different bacterial pathogens (*Vibrio cholerae, Enterococcus faecalis, Pseudomonas sneebia, Providencia rettgeri*, and a virulent strain of *Serratia marcescens*) to triple mutants of *insulin-like peptides 2, 3*, and *5*. *P. sneebia* systemic infections resulted in 100% mortality for both wildtype and ILP mutants, while systemic infection for all other bacteria tested resulted in higher proportion of death in *ilp2,3,5* mutants. Pathogen loads were higher for *ilp2,3,5* mutants only after systemic infection with *P. rettgeri* and *E. faecalis*. In contrast, *ilp2,3,5* mutants showed higher survival of oral infection with *P. sneebia, V. cholerae* and *S. marcescens*, although only *V. cholerae* loads were reduced in *ilp2,3,5* mutants (86). When IIS activity is increased due to mutation in the IIS pathway antagonist *impl2*, flies suffered higher mortality and increased pathogen load than wildtype after oral *V. cholerae* infection (86). Collectively, these data suggest that functional IIS activity increases susceptibility to oral infections. *D. melanogaster* with oral infection of *V. cholerae* exhibit reduced activation of the IIS pathway (95), which further suggest that reduction in IIS activity could be a protective mechanism against enteric *V. cholerae* infections.

The combination of results across all studies demonstrates that the effects of IIS signaling on immunity varies with the specific pathogen and route of infection in *D. melanogaster*. Future experiments using tissue-specific approaches to manipulate IIS could elucidate how specific organs contribute to the interaction between IIS and immunity. Additionally, conditional genetic manipulations could be deployed to differentiate immediate immunological effects of altered insulin signaling from pleiotropic consequences of developmental effects due to constitutively altered IIS.

There is also evidence that IIS affects immunity in mosquitoes. For example, several studies demonstrate that *Plasmodium* infection results in IIS activation and host immune suppression in *Anopheles stephensi* mosquitoes (e.g., 113, 114). *P. falciparum* infection induces the transcription of *insulin-like peptide 1, 3, 4*, and *5* in *A. stephensi* (10, 114). Artificial feeding of insulin-like peptide 3 (ILP3) and insulin-like peptide 4 (ILP4) to *A. stephensi*

results in reduced expression of NF-kB-dependent genes in the midgut, including those encoding the antimicrobial peptides Gambicin, Cecropin, and Defensin (113, 115) and encapsulation-related proteins APL1, TEP1, LRIM1 (115). Similarly, feeding ILP4 or human insulin to *A. stephensi* at levels expected to be present in a bloodmeal (170 pM) induces IIS pathway activation and increases prevalence *Plasmodium falciparum* (113, 115, 116), where prevalence is defined as the proportion of mosquitos within the experimental population that become infected with *Plasmodium*. Reciprocally, inhibition of IIS activity with the PI3K inhibitor LY294002 or morpholinos that target *ILP3* and *ILP4* reduces the prevalence of *P. falciparum* infection and increases the expression level of immune effector genes in the mosquito midgut (113, 114). Together, these results demonstrate that insulin produced endogenously or obtained from a bloodmeal can suppress mosquito immune activity and could benefit infecting *Plasmodium*.

In a reciprocal experiment, Hauck et al. (117) demonstrated that overexpression of a negative regulator of Akt, phosphatase and tensin homolog (PTEN, Figure 1), in the *A. stephensi* midgut can reduce prevalence of *Plasmodium* infection. The proportion of PTEN-overexpressing mosquitos that became infected with *P. falciparum* was significantly lower than in wildtype controls and the transgenic mosquitoes developed fewer oocysts (117). Despite reduced prevalence of *Plasmodium* in the midgut, there was no effect on infection-induced expression of the AMP gene *Defensin* or in genes responsible for controlling *P. falciparum*, including *NOS, TEP1, APL1, LRIM1* (117). PTEN overexpression enhanced expression of genes that promote autophagy, which is associated with midgut integrity and improves infection resistance, and midguts that overexpressed PTEN were less permeable than midguts that overexpress Akt (117). Thus, enhanced midgut integrity may provide another mechanism for reduced prevalence of *Plasmodium* in IIS-suppressed mosquitoes.

Nevertheless, an independent set of studies suggested an opposite phenomenon. Corby-Harris et al. (13) generated transgenic *A. stephensi* lines that drive constitutive activation of Akt under the control of the midgut carboxypeptidase promoter to assay the effects that midgut Akt activation has on *Plasmodium* development. In contrast to the previously cited studies, they found that activation of Akt significantly reduced prevalence of oocysts in the midgut and the proportion of mosquitos infected with *P. falciparum* (13), with Akt overexpression impacting mitochondrial function and the production of nitric oxide species (NOS) (13, 118). NOS has been associated with killing *Plasmodium berghei* and *Plasmodium falciparum* (119–121). Suppression of NOS in mosquitos that overexpress Akt increases their susceptibility to *P. falciparum* infection, demonstrating that the Akt-induced suppression of *Plasmodium* prevalence is mediated at least in part by elevated NOS levels (122). Overexpression of Akt in the midgut also results in abnormal mitochondria morphology and significantly reduced number of mitochondria in the midgut (122), with mitochondrial dysfunction evident in reduced activity of Mitochondrial Complexes I, II-II, and V. Additionally, Akt-overexpression in the fat body of mosquitos systemically infected with *E. coli* or *Bacillus subtilis* led to higher induction of antimicrobial peptides and higher survivorship of infection (118). These findings suggest that activation of IIS pathway in the fat body and midgut can induce an immune response to limit *Plasmodium falciparum* development and control bacterial infections.

These inconsistency between studies showing that insulin suppresses the immune response and increases *P. falciparum* prevalence (113, 115–117) versus those showing that overexpression of Akt increases immunity and suppresses *Plasmodium* establishment (13, 118) may result from differences in IIS activity or expression pattern. Surachetpong et al. (116) demonstrated that feeding human insulin to *A. stephensi* increased ROS production and NOS synthesis but that the elevated NOS synthesis was not associated with reduced *P. falciparum* prevalence (116). Potentially, transgenic mosquitos that overexpress Akt in the midgut or fat body may synthesize higher levels of NOS and ROS than is produced in wildtype mosquitos fed insulin. This could be tested in future studies. Additionally, insulin may have other immune-suppressive effects on mosquito physiology independent of Akt activation. More refined experimentation, including tissue-specific transcriptomic contrasts between mosquitoes fed on insulin compared to those overexpressing Akt could help elucidate the cause of the differences between the studies.

Interestingly, insulin treatment of vertebrate macrophages similarly suppresses inflammation and innate immunity regulated by NF-κB transcription factors (123–126). For example, mouse macrophages primed with insulin prior to immune challenge with lipopolysaccharide (LPS) exhibited attenuated activity of Toll-like Receptor 4, significantly reduced nuclear localization of NF-κB, and reduced gene expression of Tumor Necrosis Factor alpha (TNFα) (126). When insulin-primed cells were treated with a PI3K inhibitor, insulin-mediated suppression of immune activity was alleviated (126). These data further suggest that insulin-mediated suppression of NF-κB activity is evolutionary conserved between vertebrates and invertebrates.

TOR regulation of immune activity

Target of Rapamycin (TOR) is a nutrient sensing pathway that is jointly regulated by IIS activity and the abundance of free amino acids (Figure 1; 76, 127, 128). The Tsc1/Tsc2 complex negatively regulates TOR, and is inhibited by Akt (76). Thus, Akt phosphorylation activates the TOR complex to induce downstream cellular processes that promote growth (76). Inhibition of TOR can potentiate immunity in both mosquitos and Drosophila (129–131). For example, inhibition of *A. stephensi* TOR with rapamycin increased expression of genes like those encoding the NF-kB transcription factor *Rel2*, antimicrobial peptides *Attacin* and *Cecropin*, the complement-like protein thioester-containing protein 1 (TEP1), and the CLIP domain serine protease SPCLIP1 (130). TOR inhibition also reduced infection prevalence of *Plasmodium berghei* in *A. stephensi* (130). Similarly, suppressing TOR using rapamycin treatment in *D. melanogaster* increased expression of the antimicrobial peptides *Diptericin* and *Metchnikowin* (129), and also improved survival of systemic infection against the Gram-negative bacterium *Pseudomonas aeruginosa* (132).

Suppression of TOR through genetic manipulation has similar effects on immune function as rapamycin treatment (129, 132). For example, both uninfected *TOR* mutants and ubiquitous overexpression of the negative TOR regulator *Tsc1/Tsc2* increased *Diptericin* and *Metchnikowin* expression in *D. melanogaster* under conditions of high protein availability (129). RagA is a GTPase that positively stimulates TOR activity (133), and flies that expressed a dominant negative form of RagA (which suppresses TOR activity) exhibited increased survivorship after *P. aeruginosa* infection (132). Rheb is a GTP-binding protein that positively regulates TOR activity (134, 135). Overexpression of Rheb reduced expression of the AMP genes *Diptericin* and *Metchnikowin* (129). Interestingly, genetic suppression of TOR by overexpression of *Tsc1/Tsc2* increased susceptibility to systemic infection with the human pathogen *Burkholderia cepacia*, with flies exhibiting higher mortality and pathogen burden (136). TOR associates with two complexes, TOR complex 1 (TORC1) which is responsive to rapamycin and Tsc1/Tsc2 activity, and the less-studied TOR complex 2 (TORC2), which does not interact with Tsc1/Tsc2 or rapamycin treatment (137). When TORC2 is genetically suppressed via mutations lacking TORC2-specific components SIN1 and Rictor, flies exhibit increased survivorship and lower pathogen loads after *B. cepacia* (136). It is not clear to what extent TORC2 activity effects survivorship of other pathogens or its effects on immune capacity such as AMP expression.

TOR activity has also been recently demonstrated to play a role in *D. melanogaster* survival after oral infection. Deshpande et al. (131) discovered that active TOR signaling is necessary to survive an enteric infection with the entomopathogenic bacteria *Pseudomonas entomophila*. Oral infection with *P. entomophila* increases TOR activity and elevates expression of lipid synthesis genes like *fatty acid synthase 1* and *Lipin*. Suppression of TOR via rapamycin treatment decreases infection survivorship without affecting bacterial load or AMP gene transcription (131). The higher mortality post-infection observed in flies with suppressed TOR activity was associated with significant depletion of lipid stores, specifically in the fat body and anterior region of the gut. This reduction in lipid after infection is associated with decrease in expression of lipid synthesis genes and an excessive loss in lipid stores (131), and suggests that TOR can regulate lipid homeostasis for tolerance of enteric infection.

Interactions between FOXO and active immune response

Forkhead box proteins are a family of transcription factors whose activity is suppressed by IIS (Figure 1) (138, 139). The forkhead box-O (FOXO) protein in particular is involved in various physiological functions including apoptosis, stress responses and metabolic homeostasis (140–142), which are conserved from invertebrates to vertebrates (139, 143–146). Activated Akt phosphorylates FOXO, preventing FOXO from localizing to the nucleus to drive transcription of target genes including those that mobilize metabolic stores (76). FOXO is responsive to varied stress stimuli including starvation, diapause, hypoxia, and infection (12, 147–151) and regulates processes like lipolysis and autophagy in response to these stressors (149, 152).

Even in the absence of infection, starvation induces FOXO-dependent expression of antimicrobial peptides in the gut, trachea, fat body, and epidermis of *D. melanogaster* that is independent of Toll and IMD signaling (153). Similarly, the transcription factor Forkhead (FKH) drives AMP transcription in *Drosophila* in the absence of infection as a function of inhibited TOR signaling, again independent of Toll and IMD signaling (129). Starving larvae of the silkworm *Bombyx mori* larvae also exhibit decreased Akt phosphorylation and elevated expression of the AMP genes *CecropinB6*, *Attacin1* and *Defensin B* (154). AMP gene promoters in varied insects frequently contain binding sites for forkhead-family transcription factors (153–156). These may allow infection-independent FKH/FOXO-regulated expression of these genes, and there may also be synergism between forkhead family and NF-kB family transcription factors. Future study should emphasize the extent to which forkhead-family transcription factors synergize with canonical immune signaling during an active infection.

Inhibition of FOXO results in increased nutrient storage and activation of FOXO results in nutrient mobilization and release. As could then be expected, *D. melanogaster* mutants for FOXO experience reduced loss of glycogen and a partial rescue of metabolic wasting compared to wildtype flies during a systemic *Mycobacterium marinum* infection (12). FOXO-deficient flies have increased survival of infection with *M. marinum* despite having pathogen load similar to that of wildtype flies, which suggests that the progressive loss of nutrient stores associated with activated FOXO increases mortality.

FOXO additionally has also been implicated in contributing to IMD-mediated effects on lipid metabolism in the absence of infection. Molaei et al. (149) found Relish mutants to have lower whole-body levels of triglyceride. Knockdown of Relish in the fat body had no effect on triglyceride content under normal rearing conditions, but when knockdown flies were fasted, they exhibited a significant reduction in triglyceride levels that was not seen in starved, wildtype flies (149). This drastic reduction in triglyceride levels in a Relish knockdown background was also associated with elevated expression of the lipase gene *brummer* (*bmm*). These authors determined that the depletion of lipids in starved Relish-deficient flies was due to FOXO-dependent regulation of *bmm*.

FOXO activates transcription of the lipase *bmm* (Figure 1) to positively regulate lipolysis (157, 158). Reducing FOXO activity in Relish mutants restores wildtype levels of fasting-dependent *bmm* gene expression and triglyceride storage in the fat body (149). In flies that are starved or fully fed, Relish can bind to the Bmm locus (149). Relish has been suggested to modify histone acetylation during starvation conditions demonstrated by enrichment of histone 3 lysine 9 acetylation (H3K9ac) in *relish* mutants at the site where Relish binds the Bmm locus (149) Together, these data suggest that Relish may antagonize FOXO-dependent regulation of lipolysis to prevent rapid loss of lipids during starvation. Future experiments could elucidate whether Relish-FOXO antagonism mediates the shifts in lipid metabolism observed during infection (12, 23, 131).

FOXO also plays tissue-specific roles during oral infections. During oral infection of *D. melanogaster* with *Serratia marcescens*,

FOXO becomes activated and localized to the nucleus in gut epithelial cells, where it contributes to infection-induced expression of antimicrobial peptides (155). Even in the absence of infection, overexpression of FOXO in *D. melanogaster* intestines increases transcript levels of antimicrobial peptide genes *Attacin*, *Drosomycin*, *Diptericin*, and *Defensin* in gut cells (155). FOXO mutants experience reduced survivorship and higher bacteria load in response to oral infection with *S. marcescens* compared to wildtype, presumably as a consequence of the impaired AMP expression (155).

Recent evidence in *B. mori* demonstrates a role for FOXO in controlling infection by the orally-acquired baculovirus *Bombyx mori* nuclear polyhedrosis virus (BmNPV). *B. mori* cell lines infected with BmNPV exhibit increased phosphorylation of Akt (159, 160) and reduced FOXO gene expression (17). Phosphoenolpyruvate carboxykinase (PEPCK) is a downstream target of FOXO that is known for its role in regulating gluconeogenesis (161), and more recently for its antiviral role in *B. mori* (17, 162). *B. mori* cells overexpressing PEPCK exhibited a reduction in replication of BmNPV and elevated expression of the autophagy-related protein ATG8 (162). PGRP2-2 negatively regulates PTEN, which is itself a negative regulator of IIS (160). Thus PGRP2-2 is a positive regulator of IIS, and consequently a negative regulator of FOXO and PEPCK. *PGRP2-2* knockdown and *FOXO* overexpression reduce replication of BmNPV in a *B. mori* cell line (160) and increase expression of *PEPCK* and autophagy-related genes like *ATG6*, *ATG7*, and *ATG8* (17). Pharmaceutical inhibition of Akt phosphorylation in *B. mori* cells using a PI3K inhibitor also suppresses viral replication (160). These results suggest that FOXO plays a critical role in this antiviral immune response, and viruses like BmNPV can impact expression of its host IIS to evade the immune response.

Evidence from *D. melanogaster* also suggests FOXO mediates anti-viral immunity. Constitutive activation of FOXO can reduce the viral load of the Cricket Paralysis virus in *D. melanogaster* S2 cells (148). FOXO mutants are also more susceptible to RNA virus infections (148). FOXO regulates stress responses like autophagy and apoptosis that can be critical for combatting viral infection, providing a potential mechanism for FOXO-mediated resistance to viruses. The anti-viral effects of FOXO have thus far been predominantly evaluated in cell culture. Future experiments may determine whether FOXO is involved in tissue-specific antiviral responses and how those may impact host survivorship *in vivo*.

Future directions and considerations in experimental design

In this review, we have discussed examples of known interactions between innate immune and IIS pathways in the model insect *D. melanogaster* as well as in insects of economic and public health relevance like *B. mori* and *A. stephensi*. Figure 2 summarizes known interactions between Toll and IMD and IIS/TOR and questions to consider for further investigation. Supplementary Table 1 contains a list of published experiments in *D. melanogaster, A. stephensi*, and *B. mori* that have evaluated how

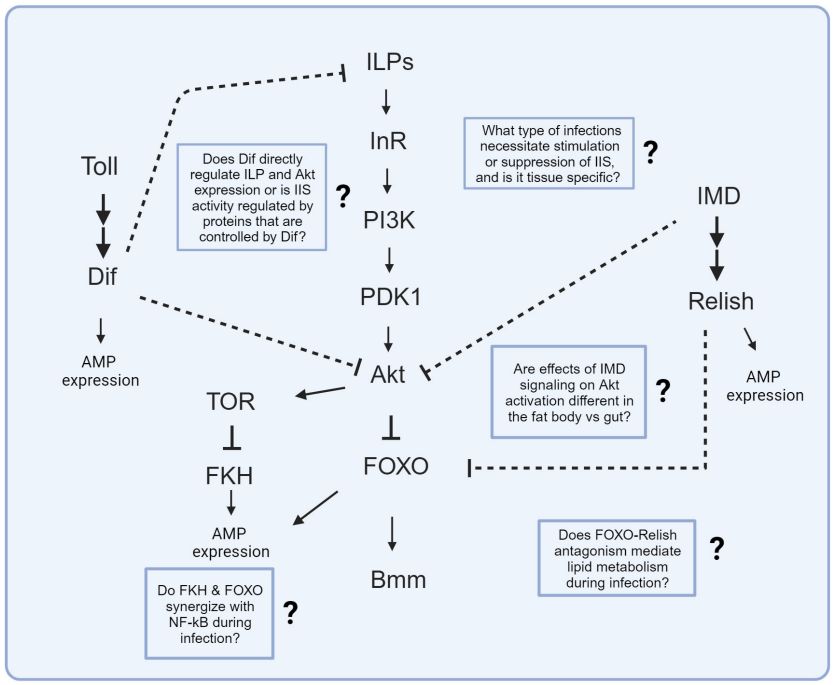

FIGURE 2
Known signaling interactions between innate immune and IIS/TOR pathways. Arrows depict known activation while bars represent known suppression in molecular interactions. Dashed bars represent known suppression between innate immune and IIS pathways, but the specific molecular interaction is unknown. Text boxes with question marks indicate outstanding questions regarding these signaling interactions that could be the study of future research.

different pathogens and routes of infection (i.e., oral vs. systemic) impact IIS/TOR activity and immunological phenotypes. Supplementary Table 2 summarizes several published studies in *D. melanogaster* that tested how manipulating the expression of innate immune genes affects IIS activity and IIS-dependent metabolism. The literature reviewed demonstrates a key role of insulin signaling in responding to oral, parasitic, viral, and systemic infections (12, 17, 19, 39, 115, 155). It also reveals critical differences between tissues, pathogens, life stages, and routes of infection in how insulin-immunity interactions play out. Different adaptive strategies of IIS regulation could be deployed by the host depending on the type of pathogenic infection. IIS and TOR upregulation could promote tolerance of pathogens that stimulate wasting of nutrient stores. For example, Akt and TOR are activated by oral infection with *P. entomophila*, which promotes lipid synthesis and alleviates infection-induced wasting to increase survivorship (131). But for infections that may not pose a threat of host wasting, suppression of IIS and promotion of FOXO-dependent signaling to regulate lipid metabolism and transcription of immune effectors may be more advantageous. Akt activation is inhibited after oral infection with *S. marcescens*, which activates FOXO to potentially help upregulate transcription of AMPs that may act as a defense at the gut epithelium (155). Potentially, FOXO-dependent regulation of AMPs in the gut epithelial barrier may enable a localized response that is more efficient than dumping antimicrobials into the gut lumen, where they would be at lower effective concentrations and could cause dysbiosis of the resident microbiota. Additionally, pathogens and parasites may manipulate their host metabolism to gain nutritional resources or may cause host metabolic changes as a consequence of nutrient consumption. Future experiments are necessary to explore to what extent infection-induced shifts to IIS activity serve as an adapted host response to infection versus as a mechanism for pathogens to exploit host physiology for their own gains.

Studies that make use of genetic manipulation have been critical in advancing our understanding of how IIS and innate immune activity interact. While infection studies in *D. melanogaster* IIS mutants have shown varying effects on infection outcome (86, 102, 107), overexpression experiments driving Toll and IMD signaling in the *D. melanogaster* fat body demonstrate an antagonistic response of innate immune signaling on IIS activation (16, 19, 39, 82, 86). Future experiments using tissue-specific or conditionally inducible knockdowns and overexpressions (e.g. 163) will further reveal how IIS affects immune function, including disentangling direct antagonisms from pleiotropic developmental effects and distinguishing tissue autonomy from interorgan communication. Additionally, experiments coupling pharmacological intervention and genetic manipulation of IIS could help elucidate the contributions of TOR- and IIS- mediated effects on immunity. IIS, metabolism, and innate immunity are interrelated in a feedback network, and carefully conceived experiments will be required to disentangle the mechanisms that connect them.

Genetic manipulation of insulin signaling in mosquitos has revealed that activation of IIS can increase production of immune effectors, leading to reduced prevalence of *Plasmodium* infection (117, 118, 122). Overexpression of negative regulators of IIS similarly contributes to reduced *Plasmodium* infectivity (117). It is thus possible that either upregulation or downregulation of IIS could create unfavorable environments for parasite development, increasing the potential for control of disease transmission via genetic manipulation of the mosquito vector. However, direct feeding of insulin to mosquitoes promotes *Plasmodium falciparum* infection success, and the parasite can induce expression of ILPs to suppress the mosquito immune response. The discrepancy between direct feeding of insulin versus genetic manipulation of IIS activity in mosquitos remains to be understood and brings an appropriate note of caution in interpreting individual experiments. Despite these nuances in experimental design, studies that demonstrate how feeding insulin or treating mosquitos with pharmaceutical inhibitors alter metabolic and immune function in mosquitos can inform novel strategies to target for vector pest management.

Common themes of interaction between IIS and immunity have emerged from the body of work described throughout this review. Infection may stimulate or suppress IIS activity to initiate nutrient mobilization in support of an immune response or to preserve metabolic stores. Potentially, we could expect an adapted metabolic response to support varying metabolic needs that could arise when a host is challenged with diverse types of pathogens. Understanding how IIS activity and the innate immune system interact within insects is an exciting avenue of research with compelling foundation but clearly much left to learn.

Author contributions

AMD: Conceptualization, Investigation, Project administration, Visualization, Writing – original draft, Writing – review & editing. BPL: Investigation, Resources, Supervision, Writing – review & editing.

Funding

The author(s) declare financial support was received for the research, authorship, and/or publication of this article. This work was supported by NIH grant AI141385. AMD is supported by fellowships from the Ford Foundation and the State University of New York (SUNY) system.

Acknowledgments

We are thankful to members of the Lazzaro lab for advice and comments on the manuscript, including Katie Gordon and Scott Keith. Additional thanks to Tory Hendry, Angela Poole, Sri Lakshmi Sravani Devarakonda, Taylar Mouton, and Dorian Jackson for additional comment and feedback on the manuscript. The main figures were created with BioRender.com.

Conflict of interest

The authors declare that the research was conducted in the absence of any commercial or financial relationships that could be construed as a potential conflict of interest.

Publisher's note

All claims expressed in this article are solely those of the authors and do not necessarily represent those of their affiliated organizations, or those of the publisher, the editors and the reviewers. Any product that may be evaluated in this article, or claim that may be made by its manufacturer, is not guaranteed or endorsed by the publisher.

Supplementary material

The Supplementary Material for this article can be found online at: https://www.frontiersin.org/articles/10.3389/fimmu.2023.1276357/full#supplementary-material

References

1. Danilova N. The evolution of immune mechanisms. *J Exp Zool Part B: Mol Dev Evol* (2006) 306B:496–520. doi: 10.1002/jez.b.21102
2. Wang X, Zhang Y, Zhang R, Zhang J. The diversity of pattern recognition receptors (PRRs) involved with insect defense against pathogens. *Curr Opin Insect Sci* (2019) 33:105–10. doi: 10.1016/j.cois.2019.05.004
3. Badisco L, Van Wielendaele P, Vanden Broeck J. Eat to reproduce: a key role for the insulin signaling pathway in adult insects. *Front Physiol* (2013) 4:202. doi: 10.3389/fphys.2013.00202
4. Nässel DR, Liu Y, Luo J. Insulin/IGF signaling and its regulation in *Drosophila*. *Gen Comp Endocrinol* (2015) 221:255–66. doi: 10.1016/j.ygcen.2014.11.021
5. Hotamisligil GS. Inflammation, metaflammation and immunometabolic disorders. *Nature* (2017) 542:177–85. doi: 10.1038/nature21363
6. Viljakainen L. Evolutionary genetics of insect innate immunity. *Brief Funct Genomics* (2015) 14:407–12. doi: 10.1093/bfgp/elv002
7. Lagueux M, Lwoff L, Meister M, Goltzene F, Hoffmann JA. cDNAs from neurosecretory cells of brains of *Locusta migratoria* (Insecta, Orthoptera) encoding a novel member of the superfamily of insulins. *Eur J Biochem* (1990) 187:249–54. doi: 10.1111/j.1432-1033.1990.tb15302.x
8. Ishizaki H. Molecular characterization of the brain secretory peptides, prothoracicotropic hormone (PTTH) and bombyxin, of the silkmoth *Bombyx mori*. *Proc Jpn Acad Ser B Phys Biol Sci* (2004) 80:195–203. doi: 10.2183/pjab.80.195
9. Wu Q, Brown MR. Signaling and function of insulin-like peptides in insects. *Annu Rev Entomol* (2006) 51:1–24. doi: 10.1146/annurev.ento.51.110104.151011
10. Marquez AG, Pietri JE, Smithers HM, Nuss A, Antonova Y, Drexler AL, et al. Insulin-like peptides in the mosquito *Anopheles stephensi*: Identification and expression in response to diet and infection with Plasmodium falciparum. *Gen Comp Endocrinol* (2011) 173:303–12. doi: 10.1016/j.ygcen.2011.06.005
11. Ihle KE, Baker NA, Amdam GV. Insulin-like peptide response to nutritional input in honey bee workers. *J Insect Physiol* (2014) 69:49–55. doi: 10.1016/j.jinsphys.2014.05.026
12. Dionne MS, Pham LN, Shirasu-Hiza M, Schneider DS. Akt and foxo dysregulation contribute to infection-induced wasting in. *Drosophila Curr Biol* (2006) 16:1977–85. doi: 10.1016/j.cub.2006.08.052
13. Corby-Harris V, Drexler A, Jong LW, Antonova Y, Pakpour N, Ziegler R, et al. Activation of Akt signaling reduces the prevalence and intensity of malaria parasite infection and lifespan in *Anopheles stephensi* mosquitoes. *PloS Pathog* (2010) 6:e1001003. doi: 10.1371/journal.ppat.1001003
14. Sun D, Guo Z, Liu Y, Zhang Y. Progress and prospects of CRISPR/Cas systems in insects and other arthropods. *Front Physiol* (2017) 8:608. doi: 10.3389/fphys.2017.00608
15. Christiaens O, Niu J, Nji Tizi Taning C. RNAi in insects: A revolution in fundamental research and pest control applications. *Insects* (2020) 11:415. doi: 10.3390/insects11070415
16. Martínez BA, Hoyle RG, Yeudall S, Granade ME, Harris TE, Castle JD, et al. Innate immune signaling in *Drosophila* shifts anabolic lipid metabolism from triglyceride storage to phospholipid synthesis to support immune function. *PloS Genet* (2020) 16:e1009192. doi: 10.1371/journal.pgen.1009192
17. Kang X, Wang Y, Liang W, Tang X, Zhang Y, Wang L, et al. *Bombyx mori* nucleopolyhedrovirus downregulates transcription factor BmFoxO to elevate virus infection. *Dev Comp Immunol* (2021) 116:103904. doi: 10.1016/j.dci.2020.103904
18. Sheldon BC, Verhulst S. Ecological immunology: costly parasite defences and trade-offs in evolutionary ecology. *Trends Ecol Evol* (1996) 11:317–21. doi: 10.1016/0169-5347(96)10039-2
19. DiAngelo JR, Bland ML, Bambina S, Cherry S, Birnbaum MJ. The immune response attenuates growth and nutrient storage in *Drosophila* by reducing insulin signaling. *Proc Natl Acad Sci* (2009) 106:20853–8. doi: 10.1073/pnas.0906749106
20. Adamo SA, Bartlett A, Le J, Spencer N, Sullivan K. Illness-induced anorexia may reduce trade-offs between digestion and immune function. *Anim Behav* (2010) 79:3–10. doi: 10.1016/j.anbehav.2009.10.012
21. Povey S, Cotter SC, Simpson SJ, Wilson K. Dynamics of macronutrient self-medication and illness-induced anorexia in virally infected insects. *J Anim Ecol* (2014) 83:245–55. doi: 10.1111/1365-2656.12127
22. Schilder RJ, Marden JH. Metabolic syndrome and obesity in an insect. *Proc Natl Acad Sci* (2006) 103:18805–9. doi: 10.1073/pnas.0603156103
23. Chambers MC, Song KH, Schneider DS. *Listeria monocytogenes* infection causes metabolic shifts in *Drosophila melanogaster*. *PloS One* (2012) 7:e50679. doi: 10.1371/journal.pone.0050679
24. Yang H, Hultmark D. *Drosophila* muscles regulate the immune response against wasp infection via carbohydrate metabolism. *Sci Rep* (2017) 7:15713. doi: 10.1038/s41598-017-15940-2
25. Bajgar A, Dolezal T. Extracellular adenosine modulates host-pathogen interactions through regulation of systemic metabolism during immune response in. *Drosophila PloS Pathog* (2018) 14:e1007022. doi: 10.1371/journal.ppat.1007022
26. Vincent CM, Simoes da Silva CJ, Wadhawan A, Dionne MS. Origins of metabolic pathology in *Francisella*-infected *Drosophila*. *Front Immunol* (2020) 11:1419. doi: 10.3389/fimmu.2020.01419
27. Li S, Yu X, Feng Q. Fat body biology in the last decade. *Annu Rev Entomol* (2019) 64:315–33. doi: 10.1146/annurev-ento-011118-112007
28. Arrese EL, Soulages JL. Insect fat body: Energy, metabolism, and regulation. *Annu Rev Entomol* (2010) 55:207–25. doi: 10.1146/annurev-ento-112408-085356
29. Krejčová G, Danielová A, Nedbalová P, Kazek M, Strych L, Chawla G, et al. *Drosophila* macrophages switch to aerobic glycolysis to mount effective antibacterial defense. *eLife* (2019) 14(4):e1007022. doi: 10.7554/eLife.50414
30. Xu Y-J, Luo F, Gao Q, Shang Y, Wang C. Metabolomics reveals insect metabolic responses associated with fungal infection. *Anal Bioanal Chem* (2015) 407:4815–21. doi: 10.1007/s00216-015-8648-8
31. Thompson SN. Trehalose – The insect 'blood' sugar. *Adv Insect Physiol* (2003) 31:205–85. doi: 10.1016/S0065-2806(03)31004-5
32. Praveena M, Savithri G. Analysis of digestive enzymes in different breeds of *Bombyx mori* in response to Beauveria bassiana infection. *Int J Entomol Res* (2021) 6:3:129–34.
33. Strahl T, Thorner J. Synthesis and function of membrane phosphoinositides in budding yeast, *Saccharomyces cerevisiae*. *Biochim Biophys Acta (BBA) Mol Cell Biol Lipids* (2007) 1771:353–404. doi: 10.1016/j.bbalip.2007.01.015
34. Troha K, Im JH, Revah J, Lazzaro BP, Buchon N. Comparative transcriptomics reveals CrebA as a novel regulator of infection tolerance in *D. melanogaster*. *PloS Pathog* (2018) 14:e1006847. doi: 10.1371/journal.ppat.1006847
35. Rutkowski DT, Kaufman RJ. A trip to the ER: coping with stress. *Trends Cell Biol* (2004) 14:20–8. doi: 10.1016/j.tcb.2003.11.001
36. Sriburi R, Jackowski S, Mori K, Brewer JW. XBP1 : a link between the unfolded protein response, lipid biosynthesis, and biogenesis of the endoplasmic reticulum. *J Cell Biol* (2004) 167:35–41. doi: 10.1083/jcb.200406136
37. Grootjans J, Kaser A, Kaufman RJ, Blumberg RS. The unfolded protein response in immunity and inflammation. *Nat Rev Immunol* (2016) 16:469–84. doi: 10.1038/nri.2016.62
38. Gupta V, Frank AM, Matolka N, Lazzaro BP. Inherent constraints on a polyfunctional tissue lead to a reproduction-immunity tradeoff. *BMC Biol* (2022) 20:127. doi: 10.1186/s12915-022-01328-w
39. Roth SW, Bitterman MD, Birnbaum MJ, Bland ML. Innate immune signaling in *Drosophila* blocks insulin signaling by uncoupling PI(3,4,5)P 3 production and Akt activation. *Cell Rep* (2018) 22:2550–6. doi: 10.1016/j.celrep.2018.02.033

40. Kwak S-J, Hong S-H, Bajracharya R, Yang S-Y, Lee K-S, Yu K. *Drosophila* adiponectin receptor in insulin producing cells regulates glucose and lipid metabolism by controlling insulin secretion. *PloS One* (2013) 8:e68641. doi: 10.1371/journal.pone.0068641

41. Ugrankar R, Theodoropoulos P, Akdemir F, Henne WM, Graff JM. Circulating glucose levels inversely correlate with *Drosophila* larval feeding through insulin signaling and SLC5A11. *Commun Biol* (2018) 1:1–15. doi: 10.1038/s42003-018-0109-4

42. Huang X, Liu G, Guo J, Su Z. The PI3K/AKT pathway in obesity and type 2 diabetes. *Int J Biol Sci* (2018) 14:1483–96. doi: 10.7150/ijbs.27173

43. DiAngelo JR, Birnbaum MJ. Regulation of fat cell mass by insulin in *Drosophila melanogaster*. *Mol Cell Biol* (2009) 29:6341–52. doi: 10.1128/MCB.00675-09

44. Cross DAE, Alessi DR, Cohen P, Andjelkovich M, Hemmings BA. Inhibition of glycogen synthase kinase-3 by insulin mediated by protein kinase B. *Nature* (1995) 378:785–9. doi: 10.1038/378785a0

45. Xu C, Kim N-G, Gumbiner BM. Regulation of protein stability by GSK3 mediated phosphorylation. *Cell Cycle* (2009) 8:4032–9. doi: 10.4161/cc.8.24.10111

46. Armstrong AR, Drummond-Barbosa D. Insulin signaling acts in adult adipocytes via GSK-3β and independently of FOXO to control *Drosophila* female germline stem cell numbers. *Dev Biol* (2018) 440:31–9. doi: 10.1016/j.ydbio.2018.04.028

47. Wipperman MF, Sampson NS, Thomas ST. Pathogen roid rage: Cholesterol utilization by *Mycobacterium tuberculosis*. *Crit Rev Biochem Mol Biol* (2014) 49:269–93. doi: 10.3109/10409238.2014.895700

48. Ghith A, Bruning JB, Bell SG. The oxidation of cholesterol derivatives by the CYP124 and CYP142 enzymes from Mycobacterium marinum. *J Steroid Biochem Mol Biol* (2023) 231:106317. doi: 10.1016/j.jsbmb.2023.106317

49. Singh G, Singh G, Jadeja D, Kaur J. Lipid hydrolizing enzymes in virulence: Mycobacterium tuberculosis as a model system. *Crit Rev Microbiol* (2010) 36:259–69. doi: 10.3109/1040841X.2010.482923

50. Ding Y, Raterink R-J, Marín-Juez R, Veneman WJ, Egbers K, van den Eeden S, et al. Tuberculosis causes highly conserved metabolic changes in human patients, mycobacteria-infected mice and zebrafish larvae. *Sci Rep* (2020) 10:11635. doi: 10.1038/s41598-020-68443-y

51. Musselman LP, Fink JL, Narzinski K, Ramachandran PV, Hathiramani SS, Cagan RL, et al. A high-sugar diet produces obesity and insulin resistance in wild-type Drosophila. *DMM Dis Models Mech* (2011) 4(6):842–9. doi: 10.1242/dmm.007948

52. Musselman LP, Fink JL, Grant AR, Gatto JA, Tuthill BF, Baranski TJ. A complex relationship between immunity and metabolism in *Drosophila* diet-induced insulin resistance. *Mol Cell Biol* (2017) 38(2). doi: 10.1128/mcb.00259-17

53. Yu S, Zhang G, Jin LH. A high-sugar diet affects cellular and humoral immune responses in *Drosophila*. *Exp Cell Res* (2018) 368:215–24. doi: 10.1016/j.yexcr.2018.04.032

54. Ponton F, Morimoto J, Robinson K, Kumar SS, Cotter SC, Wilson K, et al. Macronutrients modulate survival to infection and immunity in *Drosophila*. *J Anim Ecol* (2020) 89:460–70. doi: 10.1111/1365-2656.13126

55. Regan JC, Froy H, Froy H, Walling CA, Moatt JP, Nussey DH. Dietary restriction and insulin-like signalling pathways as adaptive plasticity: A synthesis and re-evaluation. *Funct Ecol* (2020) 34:107–28. doi: 10.1111/1365-2435.13418

56. Unckless RL, Rottschaefer SM, Lazzaro BP. The complex contributions of genetics and nutrition to immunity in *Drosophila melanogaster*. *PloS Genet* (2015) 11:1005030. doi: 10.1371/journal.pgen.1005030

57. Fellous S, Lazzaro BP. Larval food quality affects adult (but not larval) immune gene expression independent of effects on general condition. *Mol Ecol* (2010) 19:1462–8. doi: 10.1111/j.1365-294X.2010.04567.x

58. Bakopoulos D, Beadle LF, Esposito KM, Mirth CK, Warr CG, Johnson TK. Insulin-like signalling influences the coordination of larval hemocyte number with body Size in *Drosophila melanogaster*. *G3 Genes|Genomes|Genetics* (2020) 10:2213–20. doi: 10.1534/g3.120.401313

59. Savola E, Montgomery C, Waldron FM, Monteith KM, Vale P, Walling C. Testing evolutionary explanations for the lifespan benefit of dietary restriction in fruit flies (*Drosophila melanogaster*). *Evolution* (2021) 75:450–63. doi: 10.1111/evo.14146

60. Linenberg I, Christophides GK, Gendrin M. Larval diet affects mosquito development and permissiveness to *Plasmodium* infection. *Sci Rep* (2016) 6:38230. doi: 10.1038/srep38230

61. Muturi EJ, Kim C-H, Alto BW, Berenbaum MR, Schuler MA. Larval environmental stress alters *Aedes aEgypti* competence for Sindbis virus. *Trop Med Int Health* (2011) 16:955–64. doi: 10.1111/j.1365-3156.2011.02796.x

62. Duneau DF, Lazzaro BP. Persistence of an extracellular systemic infection across metamorphosis in a holometabolous insect. *Biol Lett* (2018) 14:20170771. doi: 10.1098/rsbl.2017.0771

63. Futerman PH, Layen SJ, Kotzen ML, Franzen C, Kraaijeveld AR, Godfray HCJ. Fitness effects and transmission routes of a microsporidian parasite infecting *Drosophila* and its parasitoids. *Parasitology* (2006) 132:479–92. doi: 10.1017/S0031182005009339

64. Galenza A, Hutchinson J, Campbell SD, Hazes B, Foley E. Glucose modulates *Drosophila* longevity and immunity independent of the microbiota. *Biol Open* (2016) 5:165–73. doi: 10.1242/bio.015016

65. Almire F, Terhzaz S, Terry S, McFarlane M, Gestuveo RJ, Szemiel AM, et al. Sugar feeding protects against arboviral infection by enhancing gut immunity in the mosquito vector *Aedes aEgypti*. *PloS Pathog* (2021) 17:e1009870. doi: 10.1371/journal.ppat.1009870

66. Zhang X, Jin Q, Jin LH. High sugar diet disrupts gut homeostasis though JNK and STAT pathways in *Drosophila*. *Biochem Biophys Res Commun* (2017) 487:910–6. doi: 10.1016/j.bbrc.2017.04.156

67. Bonfini A, Dobson AJ, Duneau D, Revah J, Liu X, Houtz P, et al. Multiscale analysis reveals that diet-dependent midgut plasticity emerges from alterations in both stem cell niche coupling and enterocyte size. *eLife* (2021) 10:e64125. doi: 10.7554/eLife.64125

68. Vandehoef C, Molaei M, Karpac J. Dietary adaptation of microbiota in *Drosophila* requires NF-κB-dependent control of the translational regulator 4E-BP. *Cell Rep* (2020) 31:107736. doi: 10.1016/j.celrep.2020.107736

69. Lüersen K, Röder T, Rimbach G. Drosophila melanogaster in nutrition research - The importance of standardizing experimental diets. *Genes Nutr* (2019) 14(3). doi: 10.1186/s12263-019-0627-9

70. Lesperance DNA, Broderick NA. Meta-analysis of diets used in drosophila microbiome research and introduction of the drosophila dietary composition calculator (DDCC). *G3 Genes|Genomes|Genetics* (2020) 10:2207–11. doi: 10.1534/g3.120.401235

71. Piper MD, Blanc E, Leitão-Gonçalves R, Yang M, He X, Linford NJ, et al. A holidic medium for Drosophila melanogaster. *Nat Methods* (2014) 11:100–5. doi: 10.1038/nmeth.2731

72. Piper MD. Using artificial diets to understand the nutritional physiology of Drosophila melanogaster. *Curr Opin Insect Sci* (2017) 23:104–11. doi: 10.1016/j.cois.2017.07.014

73. De Gregorio E. The Toll and Imd pathways are the major regulators of the immune response in. *Drosophila EMBO J* (2002) 21:2568–79. doi: 10.1093/emboj/21.11.2568

74. Li G, Qian H, Luo X, Xu P, Yang J, Liu M, et al. Transcriptomic analysis of resistant and susceptible *Bombyx mori* strains following BmNPV infection provides insights into the antiviral mechanisms. *Int J Genomics* (2016) 2016:e2086346. doi: 10.1155/2016/2086346

75. Caragata EP, Pais FS, Baton LA, Silva JBL, Sorgine MHF, Moreira LA. The transcriptome of the mosquito *Aedes fluviatilis* (Diptera: Culicidae), and transcriptional changes associated with its native *Wolbachia* infection. *BMC Genomics* (2017) 18:6. doi: 10.1186/s12864-016-3441-4

76. Grewal SS. Insulin/TOR signaling in growth and homeostasis: A view from the fly world. *Int J Biochem Cell Biol* (2009) 41:1006–10. doi: 10.1016/j.biocel.2008.10.010

77. Chatterjee N, Perrimon N. What fuels the fly: Energy metabolism in *Drosophila* and its application to the study of obesity and diabetes. *Sci Adv* (2021) 7:eabg4336. doi: 10.1126/sciadv.abg4336

78. Imler J-L, Zheng L. Biology of Toll receptors: lessons from insects and mammals. *J Leukocyte Biol* (2004) 75:18–26. doi: 10.1189/jlb.0403160

79. Medzhitov R. Toll-like receptors and innate immunity | Nature Reviews Immunology. *Nat Rev Immunol* (2001) 1(2):135–45. doi: 10.1038/35100529

80. Khush RS, Leulier F, Lemaitre B. *Drosophila* immunity: two paths to NF-κB. *Trends Immunol* (2001) 22:260–4. doi: 10.1016/S1471-4906(01)01887-7

81. Buchon N, Silverman N, Cherry S. Immunity in *Drosophila melanogaster* — from microbial recognition to whole-organism physiology. *Nat Rev Immunol* (2014) 14:796–810. doi: 10.1038/nri3763

82. Suzawa M, Muhammad NM, Joseph BS, Bland ML. The Toll signaling pathway targets the insulin-like peptide Dilp6 to inhibit growth in *Drosophila*. *Cell Rep* (2019) 28:1439–1446.e5. doi: 10.1016/j.celrep.2019.07.015

83. Okamoto N, Yamanaka N, Yagi Y, Nishida Y, Kataoka H, O'Connor MB, et al. A fat body-derived IGF-like peptide regulates postfeeding growth in Drosophila. *Dev Cell* (2009) 17:885–91. doi: 10.1016/j.devcel.2009.10.008

84. Slaidina M, Delanoue R, Gronke S, Partridge L, Léopold P. A *Drosophila* insulin-like peptide promotes growth during nonfeeding states. *Dev Cell* (2009) 17:874–84. doi: 10.1016/j.devcel.2009.10.009

85. Keehnen NLP, Rolff J, Theopold U, Wheat CW. Chapter one - insect antimicrobial defences: A brief history, recent findings, biases, and a way forward in evolutionary studies. In: Ligoxygakis P, editor. *Advances in Insect Physiology Insect Immunity*. Cambridge, Massachusetts: Academic Press (2017). p. 1–33. doi: 10.1016/bs.aiip.2017.02.003

86. Davoodi S, Galenza A, Panteluk A, Deshpande R, Ferguson M, Grewal S, et al. The immune deficiency pathway regulates metabolic homeostasis in Drosophila. *J Immunol* (2019) 202:2747–59. doi: 10.4049/jimmunol.1801632

87. Miron M, Lasko P, Sonenberg N. Signaling from Akt to FRAP/TOR targets both 4E-BP and S6K in *Drosophila melanogaster*. *Mol Cell Biol* (2003) 23:9117–26. doi: 10.1128/MCB.23.24.9117-9126.2003

88. Böhni R, Riesgo-Escovar J, Oldham S, Brogiolo W, Stocker H, Andruss BF, et al. Autonomous control of cell and organ Size by CHICO, a Drosophila homolog of vertebrate IRS1–4. *Cell* (1999) 97:865–75. doi: 10.1016/S0092-8674(00)80799-0

89. Paquette N, Broemer M, Aggarwal K, Chen L, Husson M, Ertürk-Hasdemir D, et al. Caspase mediated cleavage, IAP binding and ubiquitination: Linking three mechanisms crucial for *Drosophila* NF-κB signaling. *Mol Cell* (2010) 37:172. doi: 10.1016/j.molcel.2009.12.036

90. Buchon N, Broderick NA, Poidevin M, Pradervand S, Lemaitre B. Drosophila intestinal response to bacterial infection: activation of host defense and stem cell proliferation. *Cell Host Microbe* (2009) 5:200–11. doi: 10.1016/j.chom.2009.01.003

91. Kamareddine L, Robins WP, Berkey CD, Mekalanos JJ, Watnick PI. The *Drosophila* immune deficiency pathway modulates enteroendocrine function and host metabolism. *Cell Metab* (2018) 28(3):449–62.e5. doi: 10.1016/j.cmet.2018.05.026

92. Miguel-Aliaga I, Jasper H, Lemaitre B. Anatomy and physiology of the digestive tract of drosophila melanogaster. *Genetics* (2018) 210:357–96. doi: 10.1534/genetics.118.300224

93. Amcheslavsky A, Song W, Li Q, Nie Y, Bragatto I, Ferrandon D, et al. Enteroendocrine cells support intestinal stem cell-mediated homeostasis in. *Drosophila Cell Rep* (2014) 9:32–9. doi: 10.1016/j.celrep.2014.08.052

94. Shin SC, Kim SH, You H, Kim B, Kim AC, Lee KA, et al. *Drosophila* microbiome modulates host developmental and metabolic homeostasis via insulin signaling. *Science* (2011) 334:670–4. doi: 10.1126/science.1212782

95. Hang S, Purdy AE, Robins WP, Wang Z, Mandal M, Chang S, et al. The acetate switch of an intestinal pathogen disrupts host insulin signaling and lipid metabolism. *Cell Host Microbe* (2014) 16:592–604. doi: 10.1016/j.chom.2014.10.006

96. Broderick NA, Buchon N, Lemaitre B. Microbiota-induced changes in drosophila melanogaster host gene expression and gut morphology. *mBio* (2014) 5 (3). doi: 10.1128/mBio.01117-14

97. Combe BE, Defaye A, Bozonnet N, Puthier D, Royet J, Leulier F. *Drosophila* microbiota modulates host metabolic gene expression via IMD/NF-κB signaling. *PloS One* (2014) 9(7):e104120. doi: 10.1371/journal.pone.0094729

98. Thomson TC, Schneemann A, Johnson J. Oocyte destruction is activated during viral infection. *genesis* (2012) 50:453–65. doi: 10.1002/dvg.22004

99. Harsh S, Heryanto C, Eleftherianos I. Intestinal lipid droplets as novel mediators of host–pathogen interaction in Drosophila. *Biol Open* (2019) 8:bio039040. doi: 10.1242/bio.039040

100. Zhao X, Karpac J. Glutamate metabolism directs energetic trade-offs to shape host-pathogen susceptibility in *Drosophila*. *Cell Metab* (2021) 33:2428–2444.e8. doi: 10.1016/j.cmet.2021.10.003

101. Yu S, Luo F, Xu Y, Zhang Y, Jin LH. *Drosophila* innate immunity involves multiple signaling pathways and coordinated communication between different tissues. *Front Immunol* (2022) 13:2022.905370. doi: 10.3389/fimmu.2022.905370

102. Libert S, Chao Y, Zwiener J, Pletcher SD. Realized immune response is enhanced in long-lived puc and chico mutants but is unaffected by dietary restriction. *Mol Immunol* (2008) 5(3):810–7. doi: 10.1016/j.molimm.2007.06.353

103. Bai H, Post S, Kang P, Tatar M. *Drosophila* longevity assurance conferred by reduced insulin receptor substrate Chico partially requires d4eBP. *PloS One* (2015) 10: e0134415. doi: 10.1371/journal.pone.0134415

104. Vasudevan D, Clark NK, Sam J, Cotham VC, Ueberheide B, Marr MT, et al. The GCN2-ATF4 signaling pathway activates 4E-BP to bias mRNA translation and boost antimicrobial peptide synthesis in response to bacterial infection. *Cell Rep* (2017) 21:2039–47. doi: 10.1016/j.celrep.2017.10.096

105. Bernal A, Kimbrell DA. *Drosophila* Thor participates in host immune defense and connects a translational regulator with innate immunity. *Proc Natl Acad Sci U.S.A.* (2000) 97:6019–24. doi: 10.1073/pnas.100391597

106. Levitin A, Marcil A, Tettweiler G, Laforest MJ, Oberholzer U, Alarco AM, et al. *Drosophila melanogaster* thor and response to *Candida albicans* infection. *Eukaryotic Cell* (2007) 6:658–63. doi: 10.1128/EC.00346-06

107. McCormack S, Yadav S, Shokal U, Kenney E, Cooper D, Eleftherianos I. The insulin receptor substrate Chico regulates antibacterial immune function in *Drosophila*. *Immun Ageing* (2016) 13(15). doi: 10.1186/s12979-016-0072-1

108. Tang H. Regulation and function of the melanization reaction in Drosophila. *Fly* (2009) 3:105–11. doi: 10.4161/fly.3.1.7747

109. Binggeli O, Neyen C, Poidevin M, Lemaitre B. Prophenoloxidase activation is required for survival to microbial infections in. *Drosophila PloS Pathog* (2014) 10: e1004067. doi: 10.1371/journal.ppat.1004067

110. Shokal U, Eleftherianos I. Thioester-containing protein-4 regulates the *Drosophila* immune signaling and function against the pathogen *Photorhabdus*. *J Innate Immun* (2016) 9:83–93. doi: 10.1159/000450610

111. Shokal U, Kopydlowski H, Eleftherianos I. The distinct function of Tep2 and Tep6 in the immune defense of *Drosophila melanogaster* against the pathogen *Photorhabdus*. *Virulence* (2017) 8:1668–82. doi: 10.1080/21505594.2017.1330240

112. Ayres JS, Schneider DS. A signaling protease required for melanization in *Drosophila* affects resistance and tolerance of infections. *PloS Biol* (2008) 6:e305. doi: 10.1371/journal.pbio.0060305

113. Pakpour N, Corby-Harris V, Green GP, Smithers HM, Cheung KW, Riehle MA, et al. Ingested human insulin inhibits the mosquito NF-κB-dependent immune response to Plasmodium falciparum. *Infect Immun* (2012) 80:2141–9. doi: 10.1128/IAI.00024-12

114. Pietri JE, Pietri EJ, Potts R, Riehle MA, Luckhart S. *Plasmodium falciparum* suppresses the host immune response by inducing the synthesis of insulin-like peptides (ILPs) in the mosquito *Anopheles stephensi*. *Dev Comp Immunol* (2015) 53:134–44. doi: 10.1016/j.dci.2015.06.012

115. Pietri JE, Pakpour N, Napoli E, Song G, Pietri E, Potts R, et al. Two insulin-like peptides differentially regulate malaria parasite infection in the mosquito through effects on intermediary metabolism. *Biochem J* (2016) 473:3487–503. doi: 10.1042/BCJ20160271

116. Surachetpong W, Pakpour N, Cheung KW, Luckhart S. Reactive oxygen species-dependent cell signaling regulates the mosquito immune response to *Plasmodium falciparum*. *Antioxid Redox Signaling* (2011) 14:943–55. doi: 10.1089/ars.2010.3401

117. Hauck ES, Antonova-Koch Y, Drexler A, Pietri J, Pakpour N, Liu D, et al. Overexpression of phosphatase and tensin homolog improves fitness and decreases *Plasmodium falciparum* development in Anopheles stephensi. *Microbes Infect* (2013) 15:775–87. doi: 10.1016/j.micinf.2013.05.006

118. Hun LV, Cheung KW, Brooks E, Zudekoff R, Luckhart S, Riehle MA. Increased insulin signaling in the *Anopheles stephensi* fat body regulates metabolism and enhances the host response to both bacterial challenge and *Plasmodium falciparum* infection. *Insect Biochem Mol Biol* (2021) 139:103669. doi: 10.1016/j.ibmb.2021.103669

119. Kumar S, Christophides GK, Cantera R, Charles B, Han YS, Meister S, et al. The role of reactive oxygen species on *Plasmodium* melanotic encapsulation in Anopheles Gambiae. *Proc Natl Acad Sci* (2003) 100:14139–44. doi: 10.1073/pnas.2036262100

120. Peterson TML, Luckhart S. A mosquito 2-Cys peroxiredoxin protects against nitrosative and oxidative stresses associated with malaria parasite infection. *Free Radic Biol Med* (2006) 40:1067–82. doi: 10.1016/j.freeradbiomed.2005.10.059

121. Molina-Cruz A, DeJong RJ, Charles B, Gupta L, Kumar S, Jaramillo-Gutierrez G, et al. Reactive oxygen species modulate *Anopheles Gambiae* immunity against bacteria and. *Plasmodium*. *J Biol Chem* (2008) 283:3217–23. doi: 10.1074/jbc.M705873200

122. Luckhart S, Giulivi C, Drexler AL, Antonova-Koch Y, Sakaguchi D, Napoli E, et al. Sustained activation of Akt elicits mitochondrial dysfunction to block *Plasmodium falciparum* infection in the mosquito host. *PloS Pathog* (2013) 9:e1003180. doi: 10.1371/journal.ppat.1003180

123. Aljada A, Ghanim H, Saadeh R, Dandona P. Insulin inhibits NFκB and MCP-1 expression in human aortic endothelial cells. *J Clin Endocrinol Metab* (2001) 86:450–3. doi: 10.1210/jcem.86.1.7278

124. Dandona P, Aljada A, Mohanty P, Ghanim H, Hamouda W, Assian E, et al. Insulin inhibits intranuclear nuclear factor κB and stimulates IκB in mononuclear cells in obese subjects: evidence for an anti-inflammatory effect? *J Clin Endocrinol Metab* (2001) 86:3257–65. doi: 10.1210/jcem.86.7.7623

125. Ghanim H, Mohanty P, Deopurkar R, Sia CL, Korzeniewski K, Abuaysheh S, et al. Acute modulation of toll-like receptors by insulin. *Diabetes Care* (2008) 31:1827–31. doi: 10.2337/dc08-0561

126. Pal S, Nath P, Das D, Hajra S, Maitra S. Cross-talk between insulin signalling and LPS responses in mouse macrophages. *Mol Cell Endocrinol* (2018) 476:57–69. doi: 10.1016/j.mce.2018.04.009

127. Oldham S, Montagne J, Radimerski T, Thomas G, Hafen E. Genetic and biochemical characterization of dTOR, the *Drosophila* homolog of the target of rapamycin. *Genes Dev* (2000) 14:2689–94. doi: 10.1101/gad.845700

128. Parisi F, Riccardo S, Daniel M, Saqcena M, Kundu N, Pession A, et al. *Drosophila* insulin and target of rapamycin (TOR) pathways regulate GSK3 beta activity to control Myc stability and determine Myc expression in *vivo*. *BMC Biol* (2011) 9:65. doi: 10.1186/1741-7007-9-65

129. Varma D, Bülow MH, Pesch Y-Y, Loch G, Hoch M. Forkhead, a new cross regulator of metabolism and innate immunity downstream of TOR in *Drosophila*. *J Insect Physiol* (2014) 69:80–8. doi: 10.1016/j.jinsphys.2014.04.006

130. Feng Y, Chen L, Gao L, Dong L, Wen H, Song X, et al. Rapamycin inhibits pathogen transmission in mosquitoes by promoting immune activation. *PloS Pathog* (2021) 17:e1009353. doi: 10.1371/journal.ppat.1009353

131. Deshpande R, Lee B, Qiao Y, Grewal SS. TOR signalling is required for host lipid metabolic remodelling and survival following enteric infection in. *Drosophila Dis Models Mech* (2022) 15:dmm049551. doi: 10.1242/dmm.049551

132. Lee J-E, Rayyan M, Liao A, Edery I, Pletcher SD. Acute dietary restriction acts via TOR, PP2A, and Myc signaling to boost innate immunity in *Drosophila*. *Cell Rep* (2017) 20:479–90. doi: 10.1016/j.celrep.2017.06.052

133. Kim E, Goraksha-Hicks P, Li L, Neufeld TP, Guan K-L. Regulation of TORC1 by Rag GTPases in nutrient response. *Nat Cell Biol* (2008) 10:935–45. doi: 10.1038/ncb1753

134. Yamagata K, Sanders LK, Kaufmann WE, Yee W, Barnes CA, Nathans D, et al. rheb, a growth factor- and synaptic activity-regulated gene, encodes a novel Ras-related protein. *J Biol Chem* (1994) 269:16333–9. doi: 10.1016/S0021-9258(17)34012-7

135. Saucedo LJ, Gao X, Chiarelli DA, Li L, Pan D, Edgar BA. Rheb promotes cell growth as a component of the insulin/TOR signalling network. *Nat Cell Biol* (2003) 5:566–71. doi: 10.1038/ncb996

136. Allen VW, O'Connor RM, Ulgherait M, Zhou CG, Stone EF, Hill VM, et al. period-regulated feeding behavior and TOR signaling modulate survival of infection. *Curr Biol: CB* (2016) 26:184–94. doi: 10.1016/j.cub.2015.11.051

137. Loewith R, Jacinto E, Wullschleger S, Lorberg A, Crespo JL, Bonenfant D, et al. Two TOR complexes, only one of which is rapamycin sensitive, have distinct roles in cell growth control. *Mol Cell* (2002) 10:457–68. doi: 10.1016/s1097-2765(02)00636-6

138. Cantley LC. The phosphoinositide 3-kinase pathway. *Science* (2002) 296:1655–7. doi: 10.1126/science.296.5573.1655

139. Accili D, Arden KC. FoxOs at the crossroads of cellular metabolism, differentiation, and transformation. *Cell* (2004) 117:421–6. doi: 10.1016/S0092-8674(04)00452-0

140. Gross DN, van den Heuvel APJ, Birnbaum MJ. The role of FoxO in the regulation of metabolism. *Oncogene* (2008) 27:2320–36. doi: 10.1038/onc.2008.25

141. Teleman AA, Hietakangas V, Sayadian AC, Cohen SM. Nutritional control of protein biosynthetic capacity by insulin via Myc in *Drosophila*. *Cell Metab* (2008) 7:21–32. doi: 10.1016/j.cmet.2007.11.010

142. Eijkelenboom A, Burgering BMT. FOXOs: signalling integrators for homeostasis maintenance. *Nat Rev Mol Cell Biol* (2013) 14:83–97. doi: 10.1038/nrm3507

143. Wang B, Moya N, Niessen S, Hoover H, Mihaylova MM, Shaw RJ, et al. A hormone-dependent module regulating energy balance. *Cell* (2011) 145:596–606. doi: 10.1016/j.cell.2011.04.013

144. Webb AE, Brunet A. FOXO transcription factors: key regulators of cellular quality control. *Trends Biochem Sci* (2014) 39:159–69. doi: 10.1016/j.tibs.2014.02.003

145. Tsuchiya K, Ogawa Y. Forkhead box class O family member proteins: The biology and pathophysiological roles in diabetes. *J Diabetes Investig* (2017) 8:726–34. doi: 10.1111/jdi.12651

146. Gui T, Burgering BMT. FOXOs: masters of the equilibrium. *FEBS J* (2021) 289(24):7918 –39. doi: 10.1111/febs.16221

147. Kramer JM, Davidge JT, Lockyer JM, Staveley BE. Expressionof *Drosophila* FOXO regulates growth and can phenocopy starvation. *BMC Dev Biol* (2003) 3:5. doi: 10.1186/1471-213X-3-5

148. Spellberg MJ, Marr MT. FOXO regulates RNA interference in *Drosophila* and protects from RNA virus infection. *Proc Natl Acad Sci* (2015) 112:14587–92. doi: 10.1073/pnas.1517124112

149. Molaei M, Vandehoef C, Karpac J. NF-κB shapes metabolic adaptation by attenuating Foxo-mediated lipolysis in. *Drosophila Dev Cell* (2019) 49:802–810.e6. doi: 10.1016/j.devcel.2019.04.009

150. Barretto EC, Polan DM, Beevor-Potts AN, Lee B, Grewal SS. Tolerance to hypoxia is promoted by FOXO regulation of the innate immunity transcription factor NF-κB/Relish in *Drosophila*. *Genetics* (2020) 215:1013–25. doi: 10.1534/genetics.120.303219

151. Li Y-N, Ren X-B, Liu Z-C, Ye B, Zhao Z-J, Fan Q, et al. Insulin-like peptide and FoxO mediate the trehalose catabolism enhancement during the diapause termination period in the Chinese Oak Silkworm (A*ntheraea pernyi*). *Insects* (2021) 12:784. doi: 10.3390/insects12090784

152. Demontis F, Perrimon N. FOXO/4E-BP signaling in *Drosophila* muscles regulates organism-wide proteostasis during aging. *Cell* (2010) 143:813–25. doi: 10.1016/j.cell.2010.10.007

153. Becker T, Loch G, Beyer M, Zinke I, Aschenbrenner AC, Carrera P, et al. FOXO-dependent regulation of innate immune homeostasis. *Nature* (2010) 463:369–73. doi: 10.1038/nature08698

154. Zhang J, Yang W, Xu J, Yang W, Li Q, Zhong Y, et al. Regulation of antimicrobial peptide genes via insulin-like signaling pathway in the silkworm Bombyx mori. *Insect Biochem Mol Biol* (2018) 103:12–21. doi: 10.1016/j.ibmb.2018.10.002

155. Fink C, Hoffmann J, Knop M, Li Y, Isermann K, Roeder T. Intestinal FoxO signaling is required to survive oral infection in. *Drosophila Mucosal Immunol* (2016) 9:927–36. doi: 10.1038/mi.2015.112

156. Zhong X, Chowdhury M, Li C-F, Yu X-Q. Transcription factor forkhead regulates expression of antimicrobial peptides in the tobacco hornworm, *Manduca sexta*. *Sci Rep* (2017) 7(2688). doi: 10.1038/s41598-017-02830-w

157. Kang P, Chang K, Liu Y, Bouska M, Birnbaum A, Karashchuk G, et al. *Drosophila* Kruppel homolog 1 represses lipolysis through interaction with dFOXO. *Sci Rep* (2017) 7:16369. doi: 10.1038/s41598-017-16638-1

158. Yoshinari Y, Kosakamoto H, Kamiyama T, Hoshino R, Matsuoka R, Kondo S, et al. The sugar-responsive enteroendocrine neuropeptide F regulates lipid metabolism through glucagon-like and insulin-like hormones in Drosophila melanogaster. *Nat Commun* (2021) 12:4818. doi: 10.1038/s41467-021-25146-w

159. Jin S, Cheng T, Guo Y, Lin P, Zhao P, Liu C, et al. *Bombyx mori* epidermal growth factor receptor is required for nucleopolyhedrovirus replication. *Insect Mol Biol* (2018) 27:464–77. doi: 10.1111/imb.12386

160. Jiang L, Liu W, Guo H, Dang Y, Cheng T, Yang W, et al. Distinct functions of *Bombyx mori* peptidoglycan recognition protein 2 in immune responses to bacteria and viruses. *Front Immunol* (2019) 11:776. doi: 10.3389/fimmu.2019.00776

161. Méndez-Lucas A, Duarte JAG, Sunny NE, Satapati S, He T, Fu X, et al. PEPCK-M expression in mouse liver potentiates, not replaces, PEPCK-C mediated gluconeogenesis. *J Hepatol* (2013) 59:105–13. doi: 10.1016/j.jhep.2013.02.020

162. Guo H, Xu G, Wang B, Xia F, Sun Q, Wang Y, et al. Phosphoenolpyruvate carboxykinase is involved in antiviral immunity against *Bombyx mori* nucleopolyhedrovirus. *Dev Comp Immunol* (2019) 92:193–8. doi: 10.1016/j.dci.2018.11.015

163. McClure CD, Hassan A, Aughey GN, Butt K, Estacio-Gómez A, Duggal A, et al. An auxin-inducible, GAL4-compatible, gene expression system for Drosophila. *eLife* (2022) 11:e67598. doi: 10.7554/eLife.67598

frontiers | Frontiers in Immunology

TYPE Brief Research Report
PUBLISHED 15 November 2023
DOI 10.3389/fimmu.2023.1293766

OPEN ACCESS

EDITED BY
Laura Vesala,
Tampere University, Finland

REVIEWED BY
Ilias Kounatidis,
The Open University, United Kingdom
Holly Stephenson,
University of Plymouth, United Kingdom

*CORRESPONDENCE
Angela Giangrande
angela@igbmc.fr
Pierre B. Cattenoz
cattenoz@igbmc.fr

RECEIVED 13 September 2023
ACCEPTED 26 October 2023
PUBLISHED 15 November 2023

CITATION
Bazzi W, Monticelli S, Delaporte C, Riet C, Giangrande A and Cattenoz PB (2023) Gcm counteracts Toll-induced inflammation and impacts hemocyte number through cholinergic signaling. *Front. Immunol.* 14:1293766. doi: 10.3389/fimmu.2023.1293766

Gcm counteracts Toll-induced inflammation and impacts hemocyte number through cholinergic signaling

Wael Bazzi[1,2,3,4], Sara Monticelli[1,2,3,4], Claude Delaporte[1,2,3,4], Céline Riet[1,2,3,4], Angela Giangrande[1,2,3,4]* and Pierre B. Cattenoz[1,2,3,4]*

[1]Université de Strasbourg, IGBMC UMR 7104- UMR-S 1258, Illkirch, France, [2]CNRS, UMR 7104, Illkirch, France, [3]Inserm, UMR-S 1258, Illkirch, France, [4]IGBMC, Institut de Génétique et de Biologie Moléculaire et Cellulaire, Illkirch, France

Hemocytes, the myeloid-like immune cells of *Drosophila*, fulfill a variety of functions that are not completely understood, ranging from phagocytosis to transduction of inflammatory signals. We here show that downregulating the hemocyte-specific Glial cell deficient/Glial cell missing (Glide/Gcm) transcription factor enhances the inflammatory response to the constitutive activation of the Toll pathway. This correlates with lower levels of glutathione S-transferase, suggesting an implication of Glide/Gcm in reactive oxygen species (ROS) signaling and calling for a widespread anti-inflammatory potential of Glide/Gcm. In addition, our data reveal the expression of acetylcholine receptors in hemocytes and that Toll activation affects their expressions, disclosing a novel aspect of the inflammatory response mediated by neurotransmitters. Finally, we provide evidence for acetylcholine receptor nicotinic acetylcholine receptor alpha 6 (nAchRalpha6) regulating hemocyte proliferation in a cell autonomous fashion and for non-cell autonomous cholinergic signaling regulating the number of hemocytes. Altogether, this study provides new insights on the molecular pathways involved in the inflammatory response.

KEYWORDS

hemocytes, toll, Glide/Gcm, nAchRalpha6, inflammation, *Drosophila*

Introduction

Inflammation is the first response of the organism to pathogenic cues and tissue damages. It allows the removal of the infectious agent and induces the healing process. Prolonged or chronic activation of the inflammatory response is highly detrimental for the organism and constitutes a major aggravating factor in the etiology of many diseases ranging from cancers to neurodegenerative disorders (1–3). Thus, the coordination of the

inflammatory response requires robust regulatory mechanisms to prevent its adverse effects.

The inflammatory response is well conserved across evolution, and the *Drosophila* model has been instrumental for the identification of the molecular mechanisms underlying innate immunity (4). Two major signaling pathways transducing the inflammatory response are the Toll and the Janus kinase/signal transducer and activator of transcription (Jak/Stat) pathways. Microbial particles activate the Toll receptor, which promotes the degradation of the nuclear factor-kappa B (NF-κB) inhibitor Cactus (i.e., Inhibitor-kappa B (IκB) in mammals), hence allowing the nuclear translocation of the NF-κB transcription factors Dorsal (Dl) and Dorsal-related immunity factor (Dif) and the transcription of effector genes (5, 6). The Jak/Stat pathway is activated in response to cytokine signaling. Following the neutralization of the pathogen, the restoration of homeostasis requires the inhibition of the inflammatory pathways, which depends on potent negative autoregulatory loops where each pathway activates its own inhibitors (7, 8).

Drosophila hemocytes are myeloid-like cells that respond to inflammatory challenges. Like in vertebrates, they are produced by two hematopoietic waves occurring in different anlagens and times. The first-wave hemocytes originate from the procephalic mesoderm of the embryo and circulate in the larval hemolymph or reside between the muscles and the cuticle (i.e., sessile pockets, dorsal stripes) (Figure 1A) (10, 11). The second wave occurs in the larval lymph gland, which histolyzes and releases a second pool of hemocytes after puparium formation (or already in the larva, upon immune challenge) (10). The Toll and the Jak/Stat pathways activate the hemocytes originating from the two hematopoietic waves, leading to their differentiation into lamellocytes, large cells that encapsulate pathogens too big to be phagocytosed (12, 13).

The transcription factor Glial cell deficient/Glial cell missing (Glide/Gcm, Gcm throughout the article) is specifically expressed in the hemocytes of the first wave and has an anti-inflammatory role that is conserved in evolution (13, 14). Gcm inhibits the pathway by activating Jak/Stat inhibitors (13), raising the question of whether this transcription factor has a general role in the inflammatory response. We here demonstrate that Gcm impacts the Toll pathway. Animals displaying constitutive Toll pathway activation and sensitized hemocytes due to Gcm downregulation produce more lamellocytes than control hemocytes. Transcriptomic analyses reveal that such hemocytes express lower levels of glutathione S-transferase (Gst) and produce higher levels of reactive oxygen species (ROS), which may explain their higher propensity to produce lamellocytes. In addition, our data highlight the expression of several neurotransmitter receptors in these sensitized hemocytes, and we show that these receptors regulate the number of hemocytes in the larva.

In sum, the present work indicates that Gcm acts as a general anti-inflammatory transcription factor inhibiting the Toll pro-inflammatory pathway. Moreover, it highlights a new signaling channel through which neurotransmitters from the nervous system modulate the immune system during inflammation.

Materials and methods

Fly strains and genetics

Drosophila stocks and crosses were maintained on standard fly medium (75 g/L organic corn flour, 7.5 g/L soybean flour, 15 g/L dry yeast, 15 g/L sucrose, 5.5 g/L agar, 5 mL/L propionic acid) at 25°C under 60% humidity with a day/light cycle of 12 h/12 h. The stocks used are detailed in the Supplementary Methods.

Monitoring the tumors and hemocyte phenotypes

The tumor and hemocyte and lymph gland phenotypes were scored as in Bazzi et al. (13). Detailed protocols are available in the Supplementary Methods for the estimation of the penetrance of the melanotic tumors, the hemocyte counting, and the lymph gland immunolabeling.

Stranded RNA sequencing on hemocytes from WL3 larvae

The sample preparation and analysis are detailed in the Supplementary Methods. The RNA sequencing (RNA-seq) data have been deposited in the ArrayExpress database at EMBL-EBI (www.ebi.ac.uk/arrayexpress) under accession number E-MTAB-11970.

RNA extraction and qPCR

For the qPCR validation of the transcriptomic data, 20 WL3 of the indicated genotypes were bled on ice-cold Phosphate Buffered Saline (PBS). The cells were then centrifuged at 1,200 rpm at 4°C, and RNA isolation was performed with TRI Reagent (Sigma) following the manufacturer's protocol. The DNase treatment was done with the TURBO DNA-free kit (Invitrogen) and the reverse transcription (RT) with the SuperScript IV (Invitrogen) using random primers. The qPCR assays were done with FastStart Essential DNA Green Master (Roche) with the primers listed in the Supplementary Methods.

The expression levels were calculated relative to the two housekeeping genes *Rp49* and *Act5C* levels using the ΔCt formula: $2\text{^}(\text{average}(Ct_{Rp49}, Ct_{Act5c}) - Ct_{target})$. Triplicates were done for each genotype, and the levels were compared using bilateral Student's t-test after variance analysis.

DHE, pH3, and Dcp-1 quantification

ROS levels were estimated using dihydroethidium (DHE; Sigma) (15). The DHE intensity averages were compared using bilateral Student's t-test. For the estimation of the number of

10.3389/fimmu.2023.1293766

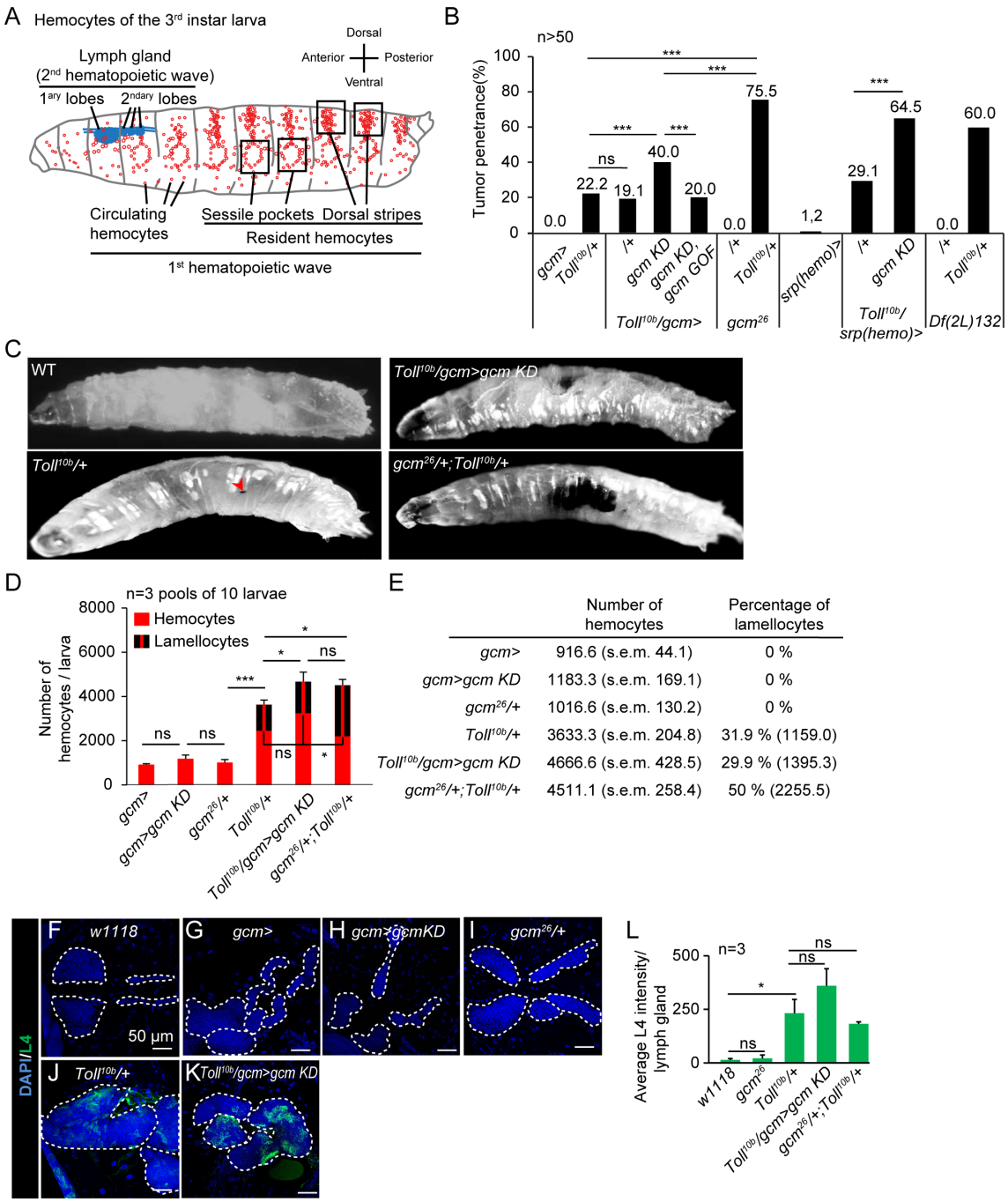

FIGURE 1
Sensitized hemocytes enhance the inflammatory response induced by Toll activation. **(A)** Schematic representation of the hemocytes of the *Drosophila* wandering L3 (WL3). The orientation of the larva is indicated on the right. The larva is mostly populated by hemocytes originating from the first hematopoietic wave during embryogenesis. In the larva, the embryonic hemocytes (in red) are circulating in the hemolymph or become resident and aggregate between the muscles and the cuticle, laterally around the oenocytes to form the sessile pockets or dorsally to form the dorsal stripes. A second hematopoietic wave is taking place at the larval stage in the lymph gland (in blue), composed of successive lobes arranged along the cardiac tube, which produce hemocytes that are released shortly after puparium formation during metamorphosis (9). **(B)** Penetrance of melanotic tumors (n > 50) in WL3 of the indicated genotype. The p-values were estimated with a chi-square test for frequency comparison. **(C)** WL3 of the indicated genotypes. The red arrowhead indicates a small melanotic tumor. **(D, E)** Total number of hemocytes and lamellocyte contribution (n = 3, using 10 larvae/replicate). The p-values were estimated by ANOVA followed by Student's *post-hoc* test. **(F–K)** Lymph glands from WL3 of the following genotypes: *w1118* **(F)**, *gcmGal4* (*gcm>*, **(G)**, *gcmGal4;UAS-gcmRNAi/+* (*gcm>gcm KD*, **(H)**, gcm^{26}*/+* **(I)**, $Toll^{10b}$*/+* **(J)**, and *gcmGal4/+;UAS-gcmRNAi/*$Toll^{10b}$ ($Toll^{10b}$*/gcm>gcm KD*, **(K)**. The lamellocytes are labeled with an antibody anti-L4 (in green) and the nuclei are labeled with DAPI (in blue). The scale bars represent 50 µm. The white dashed lines highlight the lobes of the lymph glands. **(L)** Quantification of the L4 intensity in the lymph glands of the indicated genotypes. The p-values were estimated with Student's t-test. In all figures, *p < 0.05; ***p < 0.001; ns, not significant.

mitotic and apoptotic hemocytes, the hemocytes were labeled for pH3 or Dcp-1, respectively. Detailed protocols are available in the Supplementary Methods.

Results

Sensitizing hemocytes enhances their response to Toll activation

To understand whether Gcm counteracts the Toll pro-inflammatory pathway, we combined a *Toll* mutation (16) and altered Gcm expression. $Toll^{10b}$ is a dominant mutation replacing the amino acid C781Y in the extracellular domain of the receptor, which induces constitutive activation of the Toll pathway (16). Compared to wild type, $Toll^{10b}$/+ animals display a higher number of hemocytes, precocious lymph gland histolysis, and spontaneous differentiation of lamellocytes that aggregate and form melanized black masses called melanotic tumors in 22% of the larvae (Figures 1B–E, F, J) (12, 17–20). In homeostatic conditions, the third larval instar lymph gland is composed of large primary lobes containing progenitors and differentiated hemocytes followed by small secondary lobes composed of undifferentiated hemocytes. In $Toll^{10b}$/+ animals, the primary lobes and some secondary lobes are histolyzed, and the remaining lobes are enlarged and display mature plasmatocytes and lamellocytes (Figures 1F, J; Supplementary Figures S1A, B) (12).

Knocking down Gcm expression in hemocytes using the *gcm-Gal4* driver (*gcm>gcm KD*) does not *per se* affect hemocyte number or nature (Figures 1D, E), but $Toll^{10b}$/*gcm>gcm KD* animals display a considerably enhanced inflammatory phenotype compared to $Toll^{10b}$/+ animals. The number of larvae carrying tumors (~40%) (Figure 1B) and the number of circulating hemocytes and lamellocytes per larva are significantly higher (Figures 1D, E). We did not observe significant differences of lamellocytes' differentiation in the remaining lobes of the double mutant $Toll^{10b}$/*gcm>gcm KD* compared to $Toll^{10b}$/+ lymph glands (Figures 1F–L). A similar strengthening of the melanotic tumor phenotype is observed by driving *gcm KD* with the driver *srp(hemo) Gal4* (*srp(hemo)>* (21) (Figure 1B), which is also specific for the first-wave hemocytes (22). Importantly, the phenotype of the double mutant animals is rescued by the overexpression of Gcm ($Toll^{10b}$/*gcm>gcm KD, gcm GOF*) (Figure 1B).

The response to Toll activation further increases in combination with the *gcm* null alleles (gcm^{26} (23) or the *Df(2L) 132* (24)) in heterozygous conditions. gcm^{26}/+;$Toll^{10b}$/+ and *Df(2L) 132*/+;$Toll^{10b}$/+ display higher penetrance of the melanotic tumor phenotype compared to $Toll^{10b}$/+ (Figure 1B). As in the case of *gcm KD*, the number of hemocytes in gcm^{26}/+ animals is not affected, while it does decrease in homozygous embryos (25, 26) (Figures 1D, E). gcm^{26}/+;$Toll^{10b}$/+ animals display a similar number of hemocytes but a higher proportion of lamellocytes in the hemolymph compared to $Toll^{10b}$/*gcm>gcm KD*, suggesting an even stronger pro-inflammatory phenotype than *gcm>gcm KD* (Figures 1B–E).

In sum, reducing *gcm* expression sensitizes the hemocytes and enhances the response to Toll pathway activation.

Transcriptome analysis of the sensitized hemocytes after Toll pathway activation

To assess the molecular mechanisms underlying the relative impact of Toll and Gcm on the observed phenotypes, we performed pairwise comparisons among the transcriptomes from gcm^{26}/+, from $Toll^{10b}$/+, and from gcm^{26}/+;$Toll^{10b}$/+ wandering third instar larvae (WL3) hemocytes (Supplementary Figures S2A, B).

The comparison of gcm^{26}/+;$Toll^{10b}$/+ with gcm^{26}/+ hemocytes highlights the impact of $Toll^{10b}$ on gene expression: 688 genes are significantly upregulated [mean expression >100, Log2 Fold change (Log2FC) >1, and $p < 0.01$] (Figure 2A, Supplementary Table S1). In line with the known function of the Toll pathway in response to fungi, bacteria, and wasp infestation (27–29), Gene Ontology (GO) analysis indicates the upregulation of genes involved in the innate immune response and more specifically in the Jak/Stat pathway in the defense response to Gram-positive and Gram-negative bacteria (Supplementary Figure S2C). The expression of most core components of the Toll pathway is induced, including that of the transcription factor *dorsal* (*dl*) (Figure 2A', Supplementary Figure S2F), in agreement with the autoregulatory loop shown for the Toll pathway (30). The induction of the core elements of the Jak/Stat pathway (Supplementary Figure S2D) is concordant with chromatin immunoprecipitation (ChIP) data targeting Dorsal (Dl), which indicates that Dl binds the promoters of all Jak/Stat core components (31). The response to Gram-negative bacteria is commonly associated with the activation of the Immune Deficiency (IMD) pathway and illustrates the crosstalk between the Toll and the IMD pathways (32–35). Most core components of the IMD pathways and the majority of antimicrobial peptides are upregulated in gcm^{26}/+;$Toll^{10b}$/+ compared to gcm^{26}/+ (Figures 2A'–A''', B), suggesting that the Toll pathway may activate the IMD pathway. Concordantly, ChIP data targeting Dl and Dorsal-related immunity factor (Dif) show that most genes of the IMD pathway are targeted by Dl/Dif in the larva (36), and a transcriptome analysis of $Toll^{10b}$ animals shows that Relish (Rel) is induced in $Toll^{10b}$ adults (33).

The impact of hemocyte sensitization is shown by comparing the transcriptomes from gcm^{26}/+;$Toll^{10b}$/+ and $Toll^{10b}$/+ larvae: 87 genes are downregulated and 161 genes are upregulated by gcm^{26} [mean expression >100, absolute value (Log2FC) >1, and $p < 0.01$] (Supplementary Table S1). Noteworthily, the number of genes affected by gcm^{26} is much lower than that affected by $Toll^{10b}$ (Figures 2A, C). This is likely due to the fact that $Toll^{10b}$ is a dominant gain-of-function (GOF) condition while gcm^{26} is a recessive mutation analyzed in heterozygous conditions, thus, a stronger impact on the transcriptome is expected for $Toll^{10b}$. With such a low number of genes, only a few GO terms were found significantly enriched when gcm^{26}/+;$Toll^{10b}$/+ and $Toll^{10b}$/+ larvae were compared. We did follow one of the GO terms with the lowest p-value, glutathione metabolic process (Supplementary Figure S2E), and found that most associated genes are downregulated in gcm^{26}/

10.3389/fimmu.2023.1293766

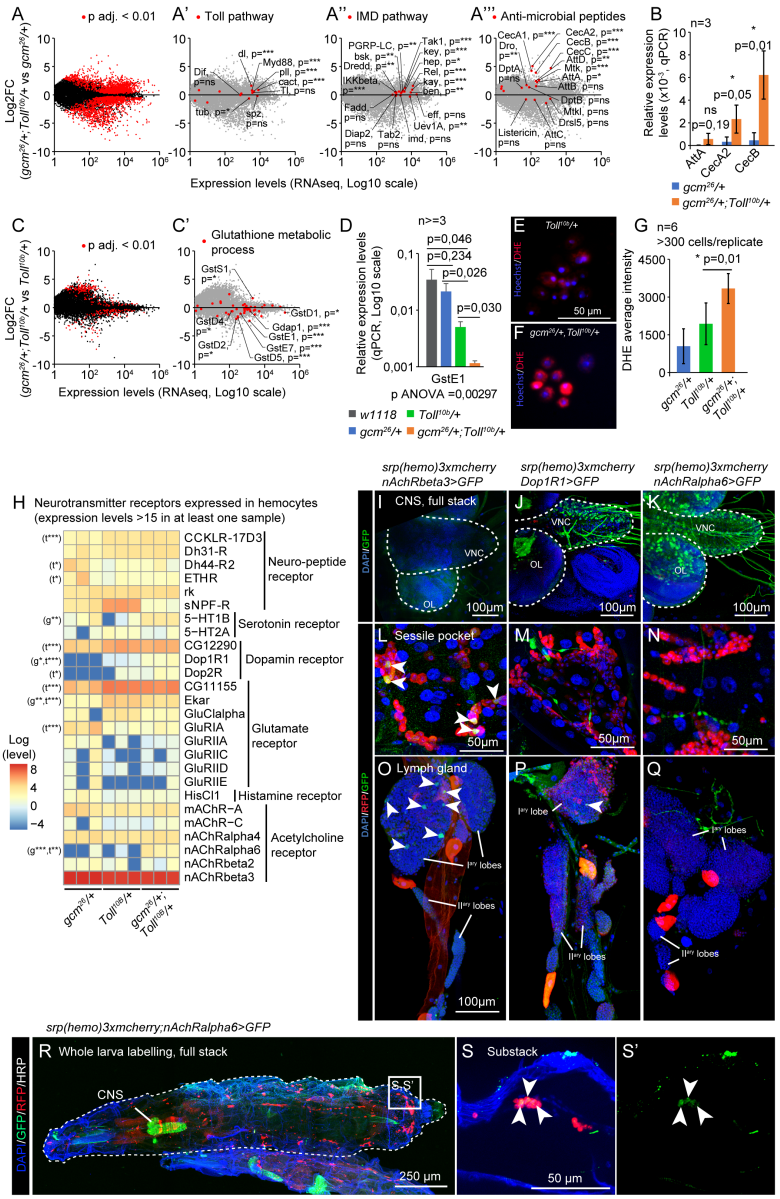

FIGURE 2
The pro-inflammatory condition *gcm*^{26}*/+;Toll*^{10b}*/+* induces the IMD pathway and modulates the ROS metabolism and the expression of neurotransmitter receptors. **(A–A''')** Transcriptome comparison of hemocytes from WL3 *gcm*^{26}*/+* and *gcm*^{26}*/+;Toll*^{10b}*/+*. The x-axis represents the average gene expression levels (n = 3) and the y-axis the Log2 fold change *gcm*^{26}*/+;Toll*^{10b}*/+/gcm*^{26}*/+*. The red dots highlight the genes presenting a significant fold change (adjusted p-values <0.01) in **(A)**, the genes of the Toll pathway in **(A')**, of the Immune Deficiency (IMD) pathway in **(A'')**, and the genes coding for antimicrobial peptides (AMP) in **(A''')**. **(B)** Expression levels of *AttA*, *CecA2*, and *CecB* in hemocytes *gcm*^{26} (in blue) and *gcm*^{26}*/+;Toll*^{10b}*/+* (in orange) estimated by quantitative PCR. N = 3 pools of 10 larvae, p-value estimated by bilateral Student's t-test. **(C, C')** Transcriptome comparison of hemocytes from WL3 *Toll*^{10b} and *gcm*^{26}*/+;Toll*^{10b}*/+*. The x-axis represents the average gene expression levels (n = 3) and the y-axis the Log2 fold change *gcm*^{26}*/+;Toll*^{10b}*/+/Toll*^{10b}. The red dots highlight the genes presenting a significant fold change (adjusted p-values <0.01) in **(C)** and the genes coding for glutathione S-transferase (Gst) in **(C')**. **(D)** Expression levels of *GstE1* in hemocytes *w1118* (wild-type control, in gray), *gcm*^{26}*/+* (in blue), *Toll*^{10b}*/+* (in green), and *gcm*^{26}*/+;Toll*^{10b}*/+* (in orange) estimated by quantitative PCR. N ≥ 3 pools of 10 larvae, p-value estimated by bilateral Student's t-test after ANOVA (p ANOVA = 0.00297). **(E–G)** Live hemocytes from *Toll*^{10b}*/+* **(E)** and *gcm*^{26}*/+;Toll*^{10b}*/+* **(F)** animals labeled for reactive oxygen species (ROS) using DHE (in red). The nuclei are labeled with Hoechst. The levels of oxidized DHE are quantified in **(G)**. N = 6, at least 300 hemocytes were monitored per replicate, the p-value was estimated by bilateral Student's t-test. **(H)** Heatmap representing the expression levels of neurotransmitter and neuropeptide receptors in hemocytes *gcm*^{26}*/+*, *Toll*^{10b}*/+*, and *gcm*^{26}*/+;Toll*^{10b}*/+*. The levels are in log scale. The significant p-values are mentioned on the left side of the heatmap. The comparison of *gcm*^{26}*/+* to *gcm*^{26}*/+;Toll*^{10b}*/+* is indicated by "t" and *Toll*^{10b}*/+* to *gcm*^{26}*/+;Toll*^{10b}*/+* by "g"; p-values: *: 0.05 < p < 0.01; **: 0.01 < p < 0.001; ***: 0.001 < p. **(I–Q)** Central nervous systems **(I–K)**, sessile pockets **(L–N)**, and lymph glands **(O–Q)** from larvae carrying the *T2A-Gal4* reporters of *nAchRbeta3*, *Dop1R1*, or *nAchRalpha6* (in green) and the hemocyte reporter *srp(hemo)3xmcherry* (in red). The nuclei are labeled with DAPI. The images were acquired with confocal microscopy and represent the whole stack projections. Scale bars are 100 µm in **(I–K)** and **(O–Q)** and 50 µm in **(L–N)**. **(R, S)** Whole-mount immunolabelings of L3 larvae *nAchRalpha6-T2A-Gal4/srp(hemo)3xmcherry;UAS-encGFP/+*. The larva is outlined by a white dashed line, the hemocytes are labeled with anti-RFP (in red), and the cells expressing *nAchRalpha6-T2A-Gal4* are labeled with anti-GFP (in green). The complete stack projections are shown in **(R)**, and a substack of the region indicated in panel R is shown in **(S, S')**.

+;$Toll^{10b}$/+ compared to $Toll^{10b}$/+ hemocytes (Figures 2C', D) and belong to the Gst family. Since Gsts are involved in xenobiotic detoxification and in the defense mechanism against oxidative stress (37–39), we assessed the biological relevance of their reduction in hemocytes by estimating the ROS levels in gcm^{26}/+;$Toll^{10b}$/+ and $Toll^{10b}$/+ hemocytes using DHE. DHE is oxidized by intracellular ROS to produce red fluorescent ethidium (40). The quantification of the ethidium levels in hemocytes suggests higher levels of ROS in gcm^{26}/+;$Toll^{10b}$/+ than in $Toll^{10b}$/+ hemocytes, which can be due to the lower levels of Gst (Figures 2E–G). A recent study showed that the ROS produced after injury induces the Toll pathway in hemocytes (41). Thus, we speculate that the low levels of Gst in gcm^{26}/+;$Toll^{10b}$/+ hemocytes (Figure 2D) may increase their level of ROS, hence leading to a stronger response to Toll activation.

Unexpectedly, the GO term enrichment analyses carried out on each dataset highlighted GO terms related to synapse activity enriched in the two comparisons (Supplementary Figures S2C, E). These genes included several neurotransmitter receptors, suggesting an involvement of neurotransmitter-mediated signaling in Toll activation and gcm^{26} sensitization. A targeted analysis of neurotransmitter receptor expression in our dataset revealed the expression of 26 receptors in hemocytes and significant upregulations of the nicotinic acetylcholine receptor alpha 6 (nAchRalpha6), the serotonin receptor 5-hydroxytryptamine receptor 1B (5-HT1B), the dopamine receptor Dopamine 1-like receptor 1 (Dop1R1), and the short neuropeptide F receptor (sNPF-R) by $Toll^{10b}$ and/or by gcm^{26} (Figure 2H, Supplementary Table S1). The expression of nAchRalpha6, 5-HT1B, and Dop1R1 is significantly enhanced in the double mutant gcm^{26}/+;$Toll^{10b}$/+ compared to $Toll^{10b}$/+ and to gcm^{26}/+, with nAchRalpha6 showing the strongest increase. In contrast, sNPF-R is significantly reduced (Figure 2H, Supplementary Table S1). Other neurotransmitter receptors such as nAchRbeta3 are expressed constitutively at high levels in the hemocytes regardless of the genetic background (Figure 2H).

To verify the expression of neurotransmitter receptors in hemocytes, we took advantage of recently produced T2A reporter lines that express intact receptors along with Gal4 under the endogenous promoter of the gene (42, 43). We assessed the expression of *nAchRbeta3*, which presents the highest expression levels and is constitutively expressed in hemocytes (Figure 2H), as well as *Dop1R1* and *nAchRalpha6*, which show the most significant induction in the double mutant gcm^{26}/+;$Toll^{10b}$/+ compared to $Toll^{10b}$/+ and gcm^{26}/+. The *T2A-Gal4* lines were crossed with the double reporter *srp(hemo)-3xmcherry;UAS-GFP* to obtain flies that express Red Fluorescent Protein (RFP) in hemocytes (both lymph gland and first-wave hemocytes) (44) and Green Fluorescent Protein (GFP) in the receptor-T2A-Gal4 expressing cells. The *Dop1R1* and *nAchRalpha6* reporters but not *nAchRbeta3* are expressed in the larval central nervous system (CNS) (Figures 2I–K), consistent with the literature (42, 45).

The *nAchRbeta3* reporter shows GFP signals in hemocytes from the lymph gland and in sessile pockets (Figures 2L, O), and the *Dop1R1* reporter is detected in a few cells of the lymph gland but not in the hemocytes of the sessile pockets (Figures 2M, P) nor in other circulating or resident hemocytes. The *nAchRalpha6-T2A-Gal4* reporter is not detected in the sessile pockets nor in the lymph gland (Figures 2N, Q); however, whole-larva immunolabeling and larval filet preparations show the expression of the receptor in resident hemocytes located in the dorsal stripes (Figure 1A; Figures 2R, S; Supplementary Figures S3A–C). The larva contains on average 1.05% ± 0.49% of nAchRalpha6-positive hemocytes (n = 3, estimated by cytometry on 10 larvae per replicate). Because of the highest effect observed in the double mutant larvae, we focused on *nAchRalpha6* and confirmed its expression profile with a transgenic line expressing a nAchRalpha6-YFP fusion protein (46) (Supplementary Figures S3D–S3F'''). The nAchRalpha6-positive hemocytes express strongly the plasmatocyte markers Nimrod C1 (NimC1 or P1) and Hemese (He) (Supplementary Figures S3C–S3F'''). At last, we profiled nAchRalpha6 in gcm^{26}/+;$Toll^{10b}$/+, $Toll^{10b}$/+, and gcm^{26}/+ larvae by crossing in *nAchRalpha6-T2A-Gal4;UAS-nRFP*. The larval filets show that the double mutants gcm^{26}/+;$Toll^{10b}$/+ have more *nAchRalpha6* hemocytes than control, $Toll^{10b}$/+, and gcm^{26}/+ larvae, confirming the transcriptomic data (Supplementary Figures S3G–K).

Overall, these data suggest that Toll activation regulates the IMD and the Jak/Stat pathways, that sensitized hemocytes display higher ROS levels in response to Toll activation possibly due to suboptimal levels of Gst, and that the hemocytes express neurotransmitter receptors whose expression is modulated by inflammatory conditions.

nAchRalpha6 modulates the proliferation of hemocytes

We next evaluated the impact of the receptors on hemocytes. We focused on *nAchRalpha6* and observed how manipulating its expression levels affects hemocytes. The null mutation $nAchRalpha6^{DAS1}$ alters the splice donor site of the first intron, which produces an inactive truncated protein, and the null mutation $nAchRalpha6^{DAS2}$ converts the codon for the tryptophan 458 to a terminal codon. In both mutations, the number of hemocytes in WL3 is significantly reduced (Figure 3A). Given the impact of *nAchRalpha6* in the nervous system (49), we next determined if the phenotype is cell autonomous by downregulating the expression of *nAchRalpha6* specifically in hemocytes. The expression of a *UAS-RNAi* transgene targeting the receptor was driven by a combination of the two larval hemocyte-specific drivers *HmldeltaGal4* and *PxnGal4* that cover the whole larval hemocyte population (50–52). The *nAchRalpha6* knockdown (*nAchRalpha6-KD*) animals are completely viable and display fewer hemocytes than the control animals (Figure 3B). The hemocyte number is also reduced in *nAchRalpha6-KD* with the driver *PxnGal4* alone (Figure 3C), but not with *HmldeltaGal4* alone (Figure 3D). The two drivers are specific to hemocytes, and while the majority of hemocytes express both drivers, small subsets of hemocytes express exclusively *PxnGal4* (37% in WL3) or *HmldeltaGal4* (10% in WL3) (50). The different hemocyte number observed upon *nAchRalpha6 KD* driven by one or the other driver may depend either on the different hemocyte populations affected or on the different levels of knockdown. To discern between the two possibilities, we stabilized and hence enhanced *HmldeltaGal4*-driven expression levels using the G-trace approach (47). *HmldeltaGal4,Dbgtrace>nAchRalpha6-KD* animals do display

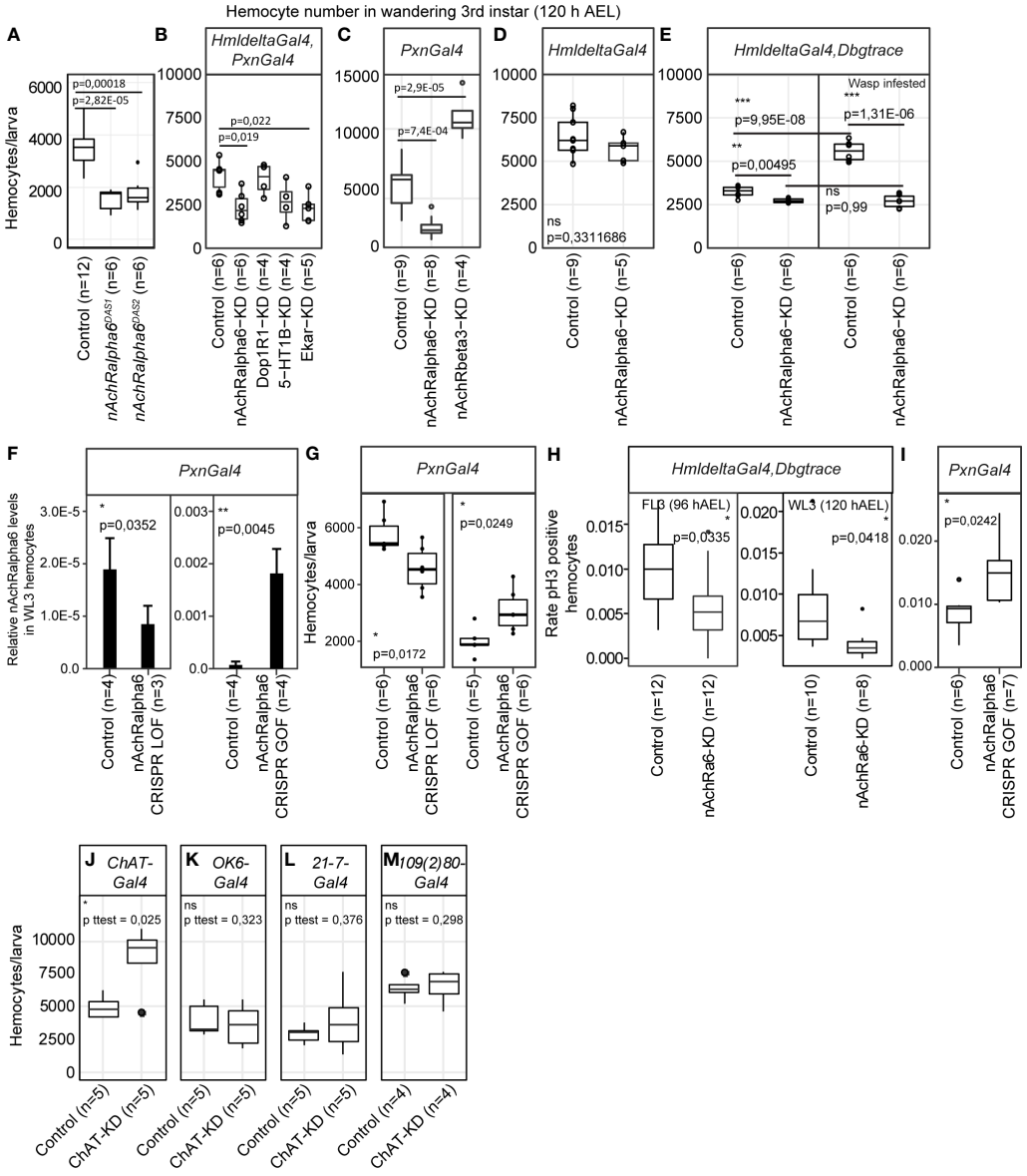

FIGURE 3
nAchRalpha6 modulates hemocyte proliferation, cell autonomously. **(A–E)** Number of hemocytes per WL3 in the indicated genotypes. N ≥ 4, each replicate being a pool of 10 females. Note that in *HmldeltaGal4,Dbgtrace* **(E)**, Gal4 expression was enhanced using lineage tracing *Gal4* transgenes (*Dbgtrace*). *Dbgtrace* includes a flipase cassette under the control of the UAS promoter (*UAS-FLP*) and the *Gal4* gene separated from the *Act5C* constitutive promoter by a stop cassette surrounded by two flipase recognition sites (*Act5C-FRT-STOP-FRT-Gal4*) (47). The expression of the flipase in the hemocytes excises the STOP cassette and leads to constitutive expression of *Gal4* in those cells, strongly enhancing the expression levels of *Gal4*. The p-values were estimated by one-factor ANOVA followed by *post-hoc* Tukey HSD for **(A–C)** (p ANOVA **(A)** = 7.17E-06; **(B)** = 0.0051787; **C** = 5.32E-08) and by Student's t-test after variance analysis for **(D, E)**. **(F)** Expression levels of *nAchRalpha6* in WL3 hemocytes from *Pxn>nAchRalpha6 CRISPR LOF* and *GOF* animals (complete genotypes are indicated in the *Methods* section) measured by quantitative PCR; n = 4 each replicate being a pool of 10 females. Note that the controls are specific to each genetic setup. The full genotypes of the controls are indicated in the *Methods* section *Fly Strains and Genetics*. In *CRISPR LOF* animals, the Cas9 nuclease was expressed specifically in hemocytes using the driver *PxnGal4* and targeted to the coding sequence of *nAchRalpha6* by the constitutive expression of two *nAchRalpha6* specific guide RNA (*nAchRalpha6 CRISPR LOF*) (48). In *CRISPR GOF* animals, a dead Cas9 fused to the activator domain VPR (Zirin et al., 2020) was expressed with the driver *PxnGal4* and guided to the promoter of *nAchRalpha6* with specific guide RNA (*nAchRalpha6 CRISPR GOF*). Note that the two controls are different: *Pxn>nAchRalpha6 CRISPR LOF* Control is *UAS-Cas9/+;PxnGal4/+* and *Pxn>nAchRalpha6 CRISPR GOF* Control is *UAS- dCas9-VPR/+;PxnGal4/+* (see Supplementary Methods). **(G)** Number of hemocytes per WL3 in *Pxn>nAchRalpha6 CRISPR LOF* and *GOF*. N ≥ 5, each replicate being a pool of 10 females. **(H)** Quantification of the proliferative hemocytes in feeding L3 (96 hAEL) and WL3 (120 hAEL) *HmldeltaGal4,Dbgtrace* or *HmldeltaGal4,Dbgtrace, nAchRalpha6-KD*; n ≥ 8, with more than 300 hemocytes scored for each replicate, p-values were estimated by one-factor ANOVA. **(I)** Quantification of the proliferative hemocytes in WL3 (120 hAEL) *Pxn>nAchRalpha6 CRISPR GOF* and control; n ≥ 6, with more than 1,000 hemocytes scored for each replicate, p-value was estimated by one-factor ANOVA. **(J–M)** Number of hemocytes per WL3 (120 hAEL) in the indicated genotypes. ChAT expression was inhibited specifically in cholinergic neurons with ChATGal4 **(J)**, in type I motoneurons with OK6Gal4 **(K)** and in multidendritic neurons with 21-7Gal4 or 109(2)80Gal4 **(L, M)**. N ≥ 4, each replicate being a pool of 10 females.

fewer hemocytes compared to the control WL3 (Figure 3E), indicating that the difference observed upon *PxnGal4* and *HmldeltaGal4*-driven knockdown is due to different levels of Gal4 induction.

To further prove the role of *nAchRalpha6* in hemocytes, we used tissue-specific Clustered Regularly Interspaced Short Palindromic Repeats / CRISPR-associated protein 9 (CRISPR/Cas9)-mediated loss-of-function (LOF) and GOF animals (Figures 3F, G). In *nAchRalpha6 CRISPR LOF* larvae, the expression levels of nAchRalpha6 decrease and so does the number of hemocytes (Figures 3F, G). In *nAchRalpha6 CRISPR GOF*, the expression levels of nAchRalpha6 increase by more than 10-fold and the number of hemocytes increases compared to those of the control (Figures 3F, G). Altogether, these data demonstrate that nAchRalpha6 regulates the number of hemocytes in the larva.

To assess the cause(s) of the different hemocyte numbers in *nAchRalpha6 KD* and *GOF*, we quantified hemocyte proliferation and apoptosis using antibodies against phosphorylated Ser10 of histone 3 (pH3) (53) and cleaved caspase Dcp-1 (54), respectively. No difference was found in the rate of apoptosis (Supplementary Figures S4B–D). A significant reduction of the proliferation rate was observed in *nAchRalpha6-KD* hemocytes in feeding as well as in wandering third instar larvae (FL3, WL3, respectively) and a significant increase in proliferation in *nAchRalpha6 CRISPR GOF* hemocytes compared to control hemocytes (Figures 3H, I; Supplementary Figure S4A). To assess if the impact of nAchRalpha6 on proliferation is cell autonomous, we quantified the number of proliferative hemocytes that express nAchRalpha6 in *nAchRalpha6-T2A-Gal4/+;UAS-GFP/srp(hemo)3xmcherry* larvae. On average, 26.6% ± 2.6% of nAchRalpha6 hemocytes are mitotic according to pH3 labeling compared to 0.6% in the whole population (n = 3, estimated on 10 larvae per replicate, p paired Student's t-test = 0.0038). The nAchRalpha6 hemocytes represent 46% ± 6.5% of the proliferative larval hemocytes, suggesting that the receptor is involved in the cell autonomous regulation of hemocyte proliferation. These results are in agreement with the increase in hemocyte number observed in the gcm^{26}/+;$Toll^{10b}$/+ larvae that also display increased expression of *nAchRalpha6*. We hence assessed the direct impact of nAchRalpha6 on hemocyte number in inflammatory conditions. Given the complexity of the genetic setup to reduce *nAchRalpha6* expression in $Toll^{10b}$ animals, we induced an immune challenge upon infesting larvae with the parasitoid wasp *Leptopilina boulardi*, which is known to trigger the Toll pathway. The rate of lamellocyte differentiation is not affected in *HmldeltaGal4, Dbgtrace>nAchRalpha6-KD* animals, with a percentage of lamellocytes/total hemocytes number of 18.6% (n = 6, stdev. = 2.9%) compared to 18.4% in control animals (n = 6, stdev = 12.3%; p t-test unequal variance = 0.97). However, a striking difference is observed in the number of hemocytes. Control animals display significantly more hemocytes after wasp infestation, while the hemocyte number in *nAchRalpha6-KD* animals remains stable (Figure 3E). Thus, the increase of hemocyte triggered by wasp infestation depends at least in part on *nAchRalpha6* expression in hemocytes.

Overall, these data show that *nAchRalpha6* modulates the proliferation of hemocytes in homeostasis and during the inflammatory response.

Cholinergic signaling regulates hemocyte homeostasis

We evaluated the impact of other neurotransmitter receptors and downregulated 5-HT1B, Dop1R1, nAchRbeta3 or the glutamate receptor Eye-enriched kainate receptor (Ekar) (Figure 3B). In all cases, the KD animals are completely viable (data not shown). In terms of hemocyte number, *5-HT1B-KD* and *Dop1R1-KD* show no difference compared to control WL3. *Ekar-KD* displays less hemocytes (Figure 3B), suggesting that glutamate signaling may also be involved in the regulation of hemocyte homeostasis. *nAchRbeta3-KD* shows a strong increase in the number of hemocytes (Figure 3C), which further highlights the importance of cholinergic signaling in hemocyte homeostasis.

At last, to assess the impact of cholinergic transmission on hemocytes, we monitored the number of larval hemocytes after inhibiting the expression of the choline-acetyltransferase ChAT in neurons. To inhibit ChAT, we used a *UAS-ChAT-RNAi* (55) and a *ChAT-Gal4* to drive *ChAT-RNAi* in the cholinergic neurons (56), which led to a strong increase in the number of hemocytes (Figure 3J), indicating that cholinergic neurons modulate hemocyte homeostasis through the secretion of acetylcholine. As controls, we used *OK6-Gal4* for type 1 motoneurons (57), which mostly secrete glutamate (58, 59), *21-7-Gal4* and *109(2)80-Gal4* drivers for multidendritic neurons, which are cholinergic (56) and regulate hemocyte localization and proliferation at the dorsal stripes through activin signaling (60). Since the multidendritic neurons make synapses at the CNS (61–64), we do not expect an effect using these drivers either (Figures 3K–M). These data indicate that motoneurons or multidendritic neurons are not the source of acetylcholine that affects the hemocyte number.

Taken together, our data show that several neurotransmitter receptors are involved in hemocyte homeostasis, that nAchRalpha6 regulates the proliferation of the hemocyte cell autonomously, and that acetylcholine signaling to the hemocytes likely originates from cholinergic neurons from the CNS.

Discussion

In this study, we show that downregulating Gcm enhances the immune response to Toll activation, calling for a general anti-inflammatory role of this evolutionarily conserved transcriptional cascade. The comparison of the transcriptomes in control and mutant backgrounds reveals that the activation of the Toll pathway induces the expression of core components of the IMD pathway and that sensitizing the hemocytes by Gcm downregulation alters the levels of Gst and ROS metabolism in $Toll^{10b}$ background. Finally, we demonstrate that hemocyte expression of acetylcholine receptor nAchRalpha6 is modulated upon hemocyte sensitizing and Toll activation and that nAchRalpha6 regulates hemocyte proliferation cell autonomously. The finding that cholinergic signaling controls hemocyte proliferation underlines the interaction between the immune and nervous systems.

Sensitized hemocytes display an enhanced response to Toll and Jak/Stat signaling

Gcm acts as a general anti-inflammatory factor, as its downregulation enhances the inflammatory response to challenges of different natures. This phenotype is observed in sensitized hemocytes upon the constitutive activation of the Toll pathway (this study) or of the Jak/Stat pathway (13), two examples of chronic challenges. A similar phenotype is also observed upon wasp infestation, an acute challenge that activates both pathways (13, 29). The inflammatory responses induced by Toll and Jak/Stat are highly similar: increasing hemocyte number and lamellocyte differentiation at comparable levels (13). In both conditions, sensitizing the hemocytes doubles the penetrance of the melanotic tumor phenotype in the larva (13). These strong similarities can be explained by the high interconnection between the two pathways. For example, the Toll pathway acts upstream of Jak/Stat for the regulation of the thiolester-containing protein Tep1 (65). In addition, the Tep protein family regulates the Toll pathway (66) and Jak/Stat modulates the expression of the Toll's ligand Spatzle (67), providing means by which the Jak/Stat pathway can modulate the Toll pathway. At last, recent data show that in hemocytes, Toll activation induces the expression of the pro-inflammatory cytokine Upd3, which activates the Jak/Stat pathway (68). Therefore, the activation of one pathway will likely activate the second one in a feed-forward loop. This hypothesis is supported by the *Toll*^{10b} transcriptome that shows increased levels of several targets regulated by the Jak/Stat pathway, including Ptp61F and Socs36E (69) (Supplementary Figure S2D) as well as Tep1, Tep2, and Tep4 (65, 67) (Supplementary Table S1). Our previous data showed that Gcm inhibits the Jak/Stat pathway (13). Gcm could hence inhibit the Toll pathway at least in part through the inhibition of the Jak/Stat pathway.

A second hypothesis that can explain the impact of Gcm on the inflammatory response is the modulation of the Gst. Our transcriptome analysis on the sensitized animals reveals a significant decrease in the anti-oxidant enzymes Gst, which correlates with higher levels of ROS. The production of ROS is tightly linked to the Toll pathway. On the one hand, ROS are known to activate the Toll and the Jak/Stat pathways (41, 70); on the other hand, Toll activates the production of ROS (71). We speculate that in our sensitized model, the deficit in Gst increases ROS levels, which might enhance the inflammatory response induced by Toll activation.

These data highlight Gcm as a potent anti-inflammatory transcription factor acting at multiple levels, directly on the Jak/Stat pathway, indirectly on Toll and IMD pathway or on ROS levels through the modulation of the Gst. Importantly, the impact of Gcm on the inflammatory response of immune cells is conserved in mammals. In mice, knockout for Gcm2 in microglia, the macrophage of the nervous system leads to the production of microglia in a pro-inflammatory state (14).

Expression of neurotransmitter receptors in hemocytes

The modulation of the immune cells by neurotransmitters is well described in mammals. Numerous neurotransmitter receptors are expressed in immune cells, and cholinergic, dopaminergic, and serotoninergic signaling mediates the function, the inflammatory status, and the proliferation of macrophages [reviewed by (72)]. In *Drosophila*, few studies report neurotransmitter signaling in immune cells. Neuronal gamma aminobutyric acid (GABA) is secreted in the hemolymph after olfactory stimuli induced by parasitoid wasp scent and promotes the differentiation of lamellocytes in the lymph gland (73). Qi et al. (74) showed the impact of serotonin signaling on the phagocytic capacity of the plasmatocytes in the butterfly *Pieris rapae* and in *Drosophila*. Immune challenge in the adult induces the secretion of serotonin by the plasmatocytes, which enhances their phagocytic capacity. This autocrine process is mediated by the receptors 5-HT1B and 5-HT2B (74). At last, dopamine signaling is used by the progenitors in the lymph gland to regulate the cell cycle (75).

Our transcriptome analysis reveals the expression of a dozen neurotransmitter receptors in the hemocytes, some of whose appear to be modulated by the inflammatory state of the larva. We report here the expression of receptors to acetylcholine, glutamate, serotonin, dopamine, and several neuropeptides in the hemocytes patrolling the larva. Our data indicate that the levels of nAchRalpha6 increase in sensitized hemocytes in *Toll*^{10b} background and that nAchRalpha6 is enriched in proliferative hemocytes. Additionally, we have shown that modulating acetylcholine production in the nervous system or the expression of specific subunits of the acetylcholine receptors in the hemocytes has a significant impact on these cells. Repressing cholinergic signaling from the neurons increases the number of hemocytes, similar to the effect of inhibiting *nAchRbeta3* or overexpressing *nAchRalpha6* in hemocytes and opposite to the effect of inhibiting *nAchRalpha6* in hemocytes (Figure 3C). Taken together, these data indicate that cholinergic signaling regulates the proliferation of hemocytes through the activation of nicotinic acetylcholine receptors. The nicotinic acetylcholine receptor is composed of five subunits homomeric or heterodimeric (76), and the subunit composition defines its biochemical properties (77). Our experimental setup modulates the expression of specific subunits, which may modify the composition of the receptors in the hemocytes and lead to two distinct effects (i.e., promotion or inhibition of hemocyte proliferation with nAchRalpha6 or nAchRbeta3, respectively). Thus, modulating the expression of neurotransmitter receptor subunits may represent a novel mechanism by which the hemocyte homeostasis is regulated in response to pro-inflammatory cues.

Altogether, these observations suggest that hemocytes are sensitive to a large panel of neurotransmitters. Our data do not allow to distinguish if the signal is transmitted through direct neuron–hemocyte connection or through systemic acetylcholine secretion. Several neurotransmitters are secreted systemically in the hemolymph (73) and can be produced by the hemocytes themselves (74, 75), but this was never shown for acetylcholine in the hemolymph, and our transcriptomic data indicate that ChAT is not expressed in hemocytes. A recent study in adult *Drosophila* shows that tissues other than neurons produce acetylcholine and that both neuronal and glia-derived acetylcholine regulates the Toll-mediated immune response of hemocytes through nAch receptors (78). Thus, cholinergic signaling appears as a fundamental mechanism of the immune response, providing a direct

communication channel between the nervous system and the immune system. Establishing the prevalence, the localization, and the nature of the receptors expressed in the hemocytes and the source of the neurotransmitters will be key steps to decipher this signaling axis.

Concluding notes

Our study ascertains the anti-inflammatory role of Gcm on several inflammatory pathways, reveals a role for nAchRalpha6 in the regulation of hemocyte proliferation in homeostasis as well as in response to inflammation, and shows the contribution of the neuronal cholinergic signaling to the immune system homeostasis. These data parallel the function of neurotransmitter receptors in mammals, whose activation in macrophages modulates cell proliferation and the activity of inflammatory pathways. Our model paves the way to characterize the role of neurotransmitter signaling in the immune response and to explore the evolutionary conserved mechanisms involved.

Data availability statement

The datasets presented in this study can be found in online repositories. The names of the repository/repositories and accession number(s) can be found below: https://www.ebi.ac.uk/arrayexpress/, E-MTAB-11970.

Ethics statement

Ethical review and approval was not required for the study on animals in accordance with the local legislation and institutional requirements.

Author contributions

WB: Conceptualization, Data curation, Formal Analysis, Investigation, Methodology, Writing – original draft. SM: Data curation, Investigation, Writing – review & editing. CD: Investigation, Methodology, Writing – review & editing. CR: Methodology, Validation, Writing – review & editing. AG: Conceptualization, Formal Analysis, Funding acquisition, Project administration, Resources, Supervision, Validation, Writing – review & editing. PC: Conceptualization, Data curation, Formal Analysis, Funding acquisition, Investigation, Methodology, Project administration, Supervision, Validation, Writing – original draft, Writing – review & editing.

Funding

The author(s) declare financial support was received for the research, authorship, and/or publication of this article. This work was supported by INSERM, CNRS, UDS, Ligue Régionale contre le Cancer, Hôpital de Strasbourg, ARC, CEFIPRA, USIAS, FRM and ANR grants. PC was funded by the ANR and by the ARSEP, WB by the USIAS and by the FRM (FDT20160435111). SM was funded from CEFIPRA and ANR fellowships. This work of the Interdisciplinary Thematic Institute IMCBio, as part of the ITI 2021-2028 program of the University of Strasbourg, CNRS and Inserm, was supported by IdEx Unistra (ANR-10-IDEX-0002), and by SFRI-STRAT'US project (ANR 20-SFRI-0012) and EUR IMCBio (ANR-17-EURE-0023) under the framework of the French Investments for the Future Program.

Acknowledgments

We thank K. Bruckner, D. Siekhaus, D. Hultmark, H. Tanimoto, S. Kondo, S. Russell, V. Honti, I. Ando and P. Soba for providing fly stocks and antibodies. In addition, stocks obtained from the Bloomington *Drosophila* Stock Center (NIH P40OD018537) and antibodies obtained from the Developmental Studies Hybridoma Bank created by the NICHD of the NIH and maintained at The University of Iowa (Department of Biology, Iowa City, IA 52242) were used in this study. We thank F. Stenger, M. Heinis, M. Moog, A. Kucan, A. Bhan, E. Naegelen, G. Zhang for technical assistance. We thank the Imaging Center of the IGBMC for technical assistance. We thank A. Maglott-Roth from the IGBMC screening facility for the hemocyte analysis. The sequencing was performed by the GenomEast platform, a member of the "France Génomique" consortium (ANR-10-INBS-0009).

Conflict of interest

The authors declare that the research was conducted in the absence of any commercial or financial relationships that could be construed as a potential conflict of interest.

Publisher's note

Supplementary material

The Supplementary Material for this article can be found online at: https://www.frontiersin.org/articles/10.3389/fimmu.2023.1293766/full#supplementary-material.

References

1. Nathan C, Ding A. Nonresolving inflammation. *Cell* (2010) 140(6):871–82. doi: 10.1016/j.cell.2010.02.029

2. Greten FR, Grivennikov SI. Inflammation and cancer: triggers, mechanisms, and consequences. *Immunity* (2019) 51(1):27–41. doi: 10.1016/j.immuni.2019.06.025

3. Fakhoury M. Immune-mediated processes in neurodegeneration: where do we stand? *J Neurol* (2016) 263(9):1683–701. doi: 10.1007/s00415-016-8052-0

4. Imler JL. Overview of Drosophila immunity: a historical perspective. *Dev Comp Immunol* (2014) 42(1):3–15. doi: 10.1016/j.dci.2013.08.018

5. Imler JL, Hoffmann JA. Signaling mechanisms in the antimicrobial host defense of Drosophila. *Curr Opin Microbiol* (2000) 3(1):16–22. doi: 10.1016/S1369-5274(99)00045-4

6. Lemaitre B, Hoffmann J. The host defense of Drosophila melanogaster. *Annu Rev Immunol* (2007) 25:697–743. doi: 10.1146/annurev.immunol.25.022106.141615

7. Arbouzova NI, Zeidler MP. JAK/STAT signalling in Drosophila: insights into conserved regulatory and cellular functions. *Development* (2006) 133(14):2605–16. doi: 10.1242/dev.02411

8. Lang T, Mansell A. The negative regulation of Toll-like receptor and associated pathways. *Immunol Cell Biol* (2007) 85(6):425–34. doi: 10.1038/sj.icb.7100094

9. Gold KS, Bruckner K. Macrophages and cellular immunity in Drosophila melanogaster. *Semin Immunol* (2015) 27(6):357–68. doi: 10.1016/j.smim.2016.03.010

10. Banerjee U, Girard JR, Goins LM, Spratford CM. Drosophila as a genetic model for hematopoiesis. *Genetics* (2019) 211(2):367–417. doi: 10.1534/genetics.118.300223

11. Mase A, Augsburger J, Bruckner K. Macrophages and their organ locations shape each other in development and homeostasis - A drosophila perspective. *Front Cell Dev Biol* (2021) 9:630272. doi: 10.3389/fcell.2021.630272

12. Davidson CJ, Tirouvanziam R, Herzenberg LA, Lipsick JS. Functional evolution of the vertebrate Myb gene family: B-Myb, but neither A-Myb nor c-Myb, complements Drosophila Myb in hemocytes. *Genetics* (2005) 169(1):215–29. doi: 10.1534/genetics.104.034132

13. Bazzi W, Cattenoz PB, Delaporte C, Dasari V, Sakr R, Yuasa Y, et al. Embryonic hematopoiesis modulates the inflammatory response and larval hematopoiesis in Drosophila. *Elife* (2018) 7. doi: 10.7554/eLife.34890

14. Pavlidaki A, Panic R, Monticelli S, Riet C, Yuasa Y, Cattenoz PB, et al. An anti-inflammatory transcriptional cascade conserved from flies to humans. *Cell Rep* (2022) 41(3):111506. doi: 10.1016/j.celrep.2022.111506

15. Zhao H, Joseph J, Fales HM, Sokoloski EA, Levine RL, Vasquez-Vivar J, et al. Detection and characterization of the product of hydroethidine and intracellular superoxide by HPLC and limitations of fluorescence. *Proc Natl Acad Sci U S A* (2005) 102(16):5727–32. doi: 10.1073/pnas.0501719102

16. Schneider DS, Hudson KL, Lin TY, Anderson KV. Dominant and recessive mutations define functional domains of Toll, a transmembrane protein required for dorsal-ventral polarity in the Drosophila embryo. *Genes Dev* (1991) 5(5):797–807. doi: 10.1101/gad.5.5.797

17. Minakhina S, Steward R. Melanotic mutants in Drosophila: pathways and phenotypes. *Genetics* (2006) 174(1):253–63. doi: 10.1534/genetics.106.061978

18. Huang L, Ohsako S, Tanda S. The lesswright mutation activates Rel-related proteins, leading to overproduction of larval hemocytes in Drosophila melanogaster. *Dev Biol* (2005) 280(2):407–20. doi: 10.1016/j.ydbio.2005.02.006

19. Remillieux-Leschelle N, Santamaria P, Randsholt NB. Regulation of larval hematopoiesis in Drosophila melanogaster: a role for the multi sex combs gene. *Genetics* (2002) 162(3):1259–74. doi: 10.1093/genetics/162.3.1259

20. Zettervall CJ, Anderl I, Williams MJ, Palmer R, Kurucz E, Ando I, et al. A directed screen for genes involved in Drosophila blood cell activation. *Proc Natl Acad Sci U S A* (2004) 101(39):14192–7. doi: 10.1073/pnas.0403789101

21. Bruckner K, Kockel L, Duchek P, Luque CM, Rorth P, Perrimon N. The PDGF/VEGF receptor controls blood cell survival in Drosophila. *Dev Cell* (2004) 7(1):73–84. doi: 10.1016/j.devcel.2004.06.007

22. Cattenoz PB, Sakr R, Pavlidaki A, Delaporte C, Riba A, Molina N, et al. Temporal specificity and heterogeneity of Drosophila immune cells. *EMBO J* (2020) 39(12):e104486. doi: 10.15252/embj.2020104486

23. Vincent S, Vonesch JL, Giangrande A. Glide directs glial fate commitment and cell fate switch between neurones and glia. *Development* (1996) 122(1):131–9. doi: 10.1242/dev.122.1.131

24. Kammerer M, Giangrande A. Glide2, a second glial promoting factor in Drosophila melanogaster. *EMBO J* (2001) 20(17):4664–73. doi: 10.1093/emboj/20.17.4664

25. Bernardoni R, Vivancos V, Giangrande A. glide/gcm is expressed and required in the scavenger cell lineage. *Dev Biol* (1997) 191(1):118–30. doi: 10.1006/dbio.1997.8702

26. Alfonso TB, Jones BW. gcm2 promotes glial cell differentiation and is required with glial cells missing for macrophage development in Drosophila. *Dev Biol* (2002) 248(2):369–83. doi: 10.1006/dbio.2002.0740

27. Rutschmann S, Kilinc A, Ferrandon D. Cutting edge: the toll pathway is required for resistance to gram-positive bacterial infections in Drosophila. *J Immunol* (2002) 168(4):1542–6. doi: 10.4049/jimmunol.168.4.1542

28. Louradour I, Sharma A, Morin-Poulard I, Letourneau M, Vincent A, Crozatier M, et al. Reactive oxygen species-dependent Toll/NF-kappaB activation in the Drosophila hematopoietic niche confers resistance to wasp parasitism. *Elife* (2017) 6. doi: 10.7554/eLife.25496

29. Kim-Jo C, Gatti JL, Poirie M. Drosophila cellular immunity against parasitoid wasps: A complex and time-dependent process. *Front Physiol* (2019) 10:603. doi: 10.3389/fphys.2019.00603

30. Mrinal N, Nagaraju J. Dynamic repositioning of dorsal to two different kappaB motifs controls its autoregulation during immune response in Drosophila. *J Biol Chem* (2010) 285(31):24206–16. doi: 10.1074/jbc.M109.097196

31. MacArthur S, Li XY, Li J, Brown JB, Chu HC, Zeng L, et al. Developmental roles of 21 Drosophila transcription factors are determined by quantitative differences in binding to an overlapping set of thousands of genomic regions. *Genome Biol* (2009) 10(7):R80. doi: 10.1186/gb-2009-10-7-r80

32. Valanne S, Wang JH, Ramet M. The Drosophila Toll signaling pathway. *J Immunol* (2011) 186(2):649–56. doi: 10.4049/jimmunol.1002302

33. De Gregorio E, Spellman PT, Tzou P, Rubin GM, Lemaitre B. The Toll and Imd pathways are the major regulators of the immune response in Drosophila. *EMBO J* (2002) 21(11):2568–79. doi: 10.1093/emboj/21.11.2568

34. Nishide Y, Kageyama D, Yokoi K, Jouraku A, Tanaka H, Futahashi R, et al. Functional crosstalk across IMD and Toll pathways: insight into the evolution of incomplete immune cascades. *Proc Biol Sci* (2019) 286(1897):20182207. doi: 10.1098/rspb.2018.2207

35. Alejandro AD, Lilia JP, Jesus MB, Henry RM. The IMD and Toll canonical immune pathways of Triatoma pallidipennis are preferentially activated by Gram-negative and Gram-positive bacteria, respectively, but cross-activation also occurs. *Parasit Vectors* (2022) 15(1):256. doi: 10.1186/s13071-022-05363-y

36. Kudron MM, Victorsen A, Gevirtzman L, Hillier LW, Fisher WW, Vafeados D, et al. The modERN resource: genome-wide binding profiles for hundreds of drosophila and caenorhabditis elegans transcription factors. *Genetics* (2018) 208(3):937–49. doi: 10.1534/genetics.117.300657

37. Hurst R, Bao Y, Jemth P, Mannervik B, Williamson G. Phospholipid hydroperoxide glutathione peroxidase activity of human glutathione transferases. *Biochem J* (1998) 332(Pt 1):97–100. doi: 10.1042/bj3320097

38. Armstrong RN. Glutathione S-transferases: reaction mechanism, structure, and function. *Chem Res Toxicol* (1991) 4(2):131–40. doi: 10.1021/tx00020a001

39. Sawicki R, Singh SP, Mondal AK, Benes H, Zimniak P. Cloning, expression and biochemical characterization of one Epsilon-class (GST-3) and ten Delta-class (GST-1) glutathione S-transferases from Drosophila melanogaster, and identification of additional nine members of the Epsilon class. *Biochem J* (2003) 370(Pt 2):661–9. doi: 10.1042/bj20021287

40. Dikalov S, Griendling KK, Harrison DG. Measurement of reactive oxygen species in cardiovascular studies. *Hypertension* (2007) 49(4):717–27. doi: 10.1161/01.HYP.0000258594.87211.6b

41. Chakrabarti S, Visweswariah SS. Intramacrophage ROS primes the innate immune system *via* JAK/STAT and toll activation. *Cell Rep* (2020) 33(6):108368. doi: 10.1016/j.celrep.2020.108368

42. Kondo S, Takahashi T, Yamagata N, Imanishi Y, Katow H, Hiramatsu S, et al. Neurochemical organization of the drosophila brain visualized by endogenously tagged neurotransmitter receptors. *Cell Rep* (2020) 30(1):284–97 e5. doi: 10.1016/j.celrep.2019.12.018

43. Diao F, White BH. A novel approach for directing transgene expression in Drosophila: T2A-Gal4 in-frame fusion. *Genetics* (2012) 190(3):1139–44. doi: 10.1534/genetics.111.136291

44. Gyoergy A, Roblek M, Ratheesh A, Valoskova K, Belyaeva V, Wachner S, et al. Tools allowing independent visualization and genetic manipulation of drosophila melanogaster macrophages and surrounding tissues. *G3 (Bethesda)* (2018) 8(3):845–57. doi: 10.1534/g3.117.300452

45. Chintapalli VR, Wang J, Dow JA. Using FlyAtlas to identify better Drosophila melanogaster models of human disease. *Nat Genet* (2007) 39(6):715–20. doi: 10.1038/ng2049

46. Korona D, Dirnberger B, Giachello CNG, Queiroz RML, Minde D-P, Deery MJ, et al. Drosophila nicotinic acetylcholine receptor subunits and their native interactions with insecticidal peptide toxins. *bioRxiv* (2021). 2021.08.13.456240. doi: 10.1101/2021.08.13.456240

47. Honti V, Csordas G, Markus R, Kurucz E, Jankovics F, Ando I. Cell lineage tracing reveals the plasticity of the hemocyte lineages and of the hematopoietic compartments in Drosophila melanogaster. *Mol Immunol* (2010) 47(11-12):1997–2004. doi: 10.1016/j.molimm.2010.04.017

48. Zirin J, Hu Y, Liu L, Yang-Zhou D, Colbeth R, Yan D, et al. Large-scale transgenic drosophila resource collections for loss- and gain-of-function studies. *Genetics* (2020) 214(4):755–67. doi: 10.1534/genetics.119.302964

49. Watson GB, Chouinard SW, Cook KR, Geng C, Gifford JM, Gustafson GD, et al. A spinosyn-sensitive Drosophila melanogaster nicotinic acetylcholine receptor

identified through chemically induced target site resistance, resistance gene identification, and heterologous expression. *Insect Biochem Mol Biol* (2010) 40 (5):376–84. doi: 10.1016/j.ibmb.2009.11.004

50. Shin M, Cha N, Koranteng F, Cho B, Shim J. Subpopulation of macrophage-like plasmatocytes attenuates systemic growth *via* JAK/STAT in the drosophila fat body. *Front Immunol* (2020) 11:63. doi: 10.3389/fimmu.2020.00063

51. Stramer B, Wood W, Galko MJ, Redd MJ, Jacinto A, Parkhurst SM, et al. Live imaging of wound inflammation in Drosophila embryos reveals key roles for small GTPases during in *vivo* cell migration. *J Cell Biol* (2005) 168(4):567–73. doi: 10.1083/jcb.200405120

52. Sinenko SA, Mathey-Prevot B. Increased expression of Drosophila tetraspanin, Tsp68C, suppresses the abnormal proliferation of ytr-deficient and Ras/Raf-activated hemocytes. *Oncogene* (2004) 23(56):9120–8. doi: 10.1038/sj.onc.1208156

53. Perez-Cadahia B, Drobic B, Davie JR. H3 phosphorylation: dual role in mitosis and interphase. *Biochem Cell Biol* (2009) 87(5):695–709. doi: 10.1139/O09-053

54. Song Z, McCall K, Steller H. DCP-1, a Drosophila cell death protease essential for development. *Science* (1997) 275(5299):536–40. doi: 10.1126/science.275.5299.536

55. Rotelli MD, Bolling AM, Killion AW, Weinberg AJ, Dixon MJ, Calvi BR. An RNAi screen for genes required for growth of drosophila wing tissue. *G3 (Bethesda)* (2019) 9(10):3087–100. doi: 10.1534/g3.119.400581

56. Salvaterra PM, Kitamoto T. Drosophila cholinergic neurons and processes visualized with Gal4/UAS-GFP. *Brain Res Gene Expr Patterns* (2001) 1(1):73–82. doi: 10.1016/S1567-133X(01)00011-4

57. Sanyal S. Genomic mapping and expression patterns of C380, OK6 and D42 enhancer trap lines in the larval nervous system of Drosophila. *Gene Expr Patterns* (2009) 9(5):371–80. doi: 10.1016/j.gep.2009.01.002

58. Johansen J, Halpern ME, Johansen KM, Keshishian H. Stereotypic morphology of glutamatergic synapses on identified muscle cells of Drosophila larvae. *J Neurosci* (1989) 9(2):710–25. doi: 10.1523/JNEUROSCI.09-02-00710.1989

59. Lacin H, Chen HM, Long X, Singer RH, Lee T, Truman JW. Neurotransmitter identity is acquired in a lineage-restricted manner in the Drosophila CNS. *Elife* (2019) 8. doi: 10.7554/eLife.43701

60. Makhijani K, Alexander B, Rao D, Petraki S, Herboso L, Kukar K, et al. Regulation of Drosophila hematopoietic sites by Activin-beta from active sensory neurons. *Nat Commun* (2017) 8:15990. doi: 10.1038/ncomms15990

61. Cheng LE, Song W, Looger LL, Jan LY, Jan YN. The role of the TRP channel NompC in Drosophila larval and adult locomotion. *Neuron* (2010) 67(3):373–80. doi: 10.1016/j.neuron.2010.07.004

62. Song W, Onishi M, Jan LY, Jan YN. Peripheral multidendritic sensory neurons are necessary for rhythmic locomotion behavior in Drosophila larvae. *Proc Natl Acad Sci U S A* (2007) 104(12):5199–204. doi: 10.1073/pnas.0700895104

63. Hughes CL, Thomas JB. A sensory feedback circuit coordinates muscle activity in Drosophila. *Mol Cell Neurosci* (2007) 35(2):383–96. doi: 10.1016/j.mcn.2007.04.001

64. Hwang RY, Zhong L, Xu Y, Johnson T, Zhang F, Deisseroth K, et al. Nociceptive neurons protect Drosophila larvae from parasitoid wasps. *Curr Biol* (2007) 17 (24):2105–16. doi: 10.1016/j.cub.2007.11.029

65. Lagueux M, Perrodou E, Levashina EA, Capovilla M, Hoffmann JA. Constitutive expression of a complement-like protein in toll and JAK gain-of-function mutants of Drosophila. *Proc Natl Acad Sci U S A* (2000) 97(21):11427–32. doi: 10.1073/pnas.97.21.11427

66. Dostalova A, Rommelaere S, Poidevin M, Lemaitre B. Thioester-containing proteins regulate the Toll pathway and play a role in Drosophila defence against microbial pathogens and parasitoid wasps. *BMC Biol* (2017) 15(1):79. doi: 10.1186/s12915-017-0408-0

67. Irving P, Ubeda JM, Doucet D, Troxler L, Lagueux M, Zachary D, et al. New insights into Drosophila larval haemocyte functions through genome-wide analysis. *Cell Microbiol* (2005) 7(3):335–50. doi: 10.1111/j.1462-5822.2004.00462.x

68. Evans CJ, Liu T, Girard JR, Banerjee U. Injury-induced inflammatory signaling and hematopoiesis in Drosophila. *bioRxiv* (2021). 2021.10.13.464248. doi: 10.1101/2021.10.13.464248

69. Baeg GH, Zhou R, Perrimon N. Genome-wide RNAi analysis of JAK/STAT signaling components in Drosophila. *Genes Dev* (2005) 19(16):1861–70. doi: 10.1101/gad.1320705

70. Ramond E, Jamet A, Ding X, Euphrasie D, Bouvier C, Lallemant L, et al. Reactive oxygen species-dependent innate immune mechanisms control methicillin-resistant staphylococcus aureus virulence in the drosophila larval model. *mBio* (2021) 12(3): e0027621. doi: 10.1128/mBio.00276-21

71. Li Z, Wu C, Ding X, Li W, Xue L. Toll signaling promotes JNK-dependent apoptosis in Drosophila. *Cell Div* (2020) 15:7. doi: 10.1186/s13008-020-00062-5

72. Hodo TW, de Aquino MTP, Shimamoto A, Shanker A. Critical neurotransmitters in the neuroimmune network. *Front Immunol* (2020) 11:1869. doi: 10.3389/fimmu.2020.01869

73. Madhwal S, Shin M, Kapoor A, Goyal M, Joshi MK, Ur Rehman PM, et al. Metabolic control of cellular immune-competency by odors in Drosophila. *Elife* (2020) 9. doi: 10.7554/eLife.60376

74. Qi YX, Huang J, Li MQ, Wu YS, Xia RY, Ye GY. Serotonin modulates insect hemocyte phagocytosis via two different serotonin receptors. *Elife* (2016) 5. doi: 10.7554/eLife.12241

75. Kapoor A, Padmavathi A, Mukherjee T. Dual control exerted by dopamine in blood-progenitor cell cycle regulation in Drosophila. *bioRxiv* (2021). 2021.03.29.437463. doi: 10.1101/2021.03.29.437463

76. Dupuis J, Louis T, Gauthier M, Raymond V. Insights from honeybee (Apis mellifera) and fly (Drosophila melanogaster) nicotinic acetylcholine receptors: from genes to behavioral functions. *Neurosci Biobehav Rev* (2012) 36(6):1553–64. doi: 10.1016/j.neubiorev.2012.04.003

77. Rosenthal JS, Yuan Q. Constructing and tuning excitatory cholinergic synapses: the multifaceted functions of nicotinic acetylcholine receptors in drosophila neural development and physiology. *Front Cell Neurosci* (2021) 15:720560. doi: 10.3389/fncel.2021.720560

78. Giordani G, Cattabriga G, Becchimanzi A, Di Lelio I, De Leva G, Gigliotti S, et al. Role of neuronal and non-neuronal acetylcholine signaling in Drosophila humoral immunity. *Insect Biochem Mol Biol* (2023) 153:103899. doi: 10.1016/j.ibmb.2022.103899

frontiers | Frontiers in Immunology

TYPE Perspective
PUBLISHED 06 December 2023
DOI 10.3389/fimmu.2023.1330312

OPEN ACCESS

EDITED BY
Laura Vesala,
Tampere University, Finland

REVIEWED BY
Bregje Wertheim,
University of Groningen, Netherlands
Jin Li Hua,
Northeast Forestry University, China

*CORRESPONDENCE
Tomas Dolezal
tomas.dolezal@prf.jcu.cz

RECEIVED 30 October 2023
ACCEPTED 22 November 2023
PUBLISHED 06 December 2023

CITATION
Dolezal T (2023) How to eliminate pathogen without killing oneself? Immunometabolism of encapsulation and melanization in *Drosophila*. *Front. Immunol.* 14:1330312. doi: 10.3389/fimmu.2023.1330312

How to eliminate pathogen without killing oneself? Immunometabolism of encapsulation and melanization in *Drosophila*

Tomas Dolezal*

Faculty of Science, University of South Bohemia, Ceske Budejovice, Czechia

Cellular encapsulation associated with melanization is a crucial component of the immune response in insects, particularly against larger pathogens. The infection of a *Drosophila* larva by parasitoid wasps, like *Leptopilina boulardi*, is the most extensively studied example. In this case, the encapsulation and melanization of the parasitoid embryo is linked to the activation of plasmatocytes that attach to the surface of the parasitoid. Additionally, the differentiation of lamellocytes that encapsulate the parasitoid, along with crystal cells, is accountable for the melanization process. Encapsulation and melanization lead to the production of toxic molecules that are concentrated in the capsule around the parasitoid and, at the same time, protect the host from this toxic immune response. Thus, cellular encapsulation and melanization represent primarily a metabolic process involving the metabolism of immune cell activation and differentiation, the production of toxic radicals, but also the production of melanin and antioxidants. As such, it has significant implications for host physiology and systemic metabolism. Proper regulation of metabolism within immune cells, as well as at the level of the entire organism, is therefore essential for an efficient immune response and also impacts the health and overall fitness of the organism that survives. The purpose of this "perspective" article is to map what we know about the metabolism of this type of immune response, place it in the context of possible implications for host physiology, and highlight open questions related to the metabolism of this important insect immune response.

KEYWORDS

melanization, encapsulation, immunometabolism, parasitoid wasp, ROS, hemocyte, lamellocyte, phenoloxidase

Introduction

Insects possess primarily innate immunity, which includes both humoral and cellular immunity. Antimicrobial peptides and the melanization cascade constitute humoral immunity, while hemocytes, which perform various immune functions such as phagocytosis, encapsulation, and melanization, provide cellular immunity. Thus, melanization, which occurs in both humoral and cellular responses, is an essential component of insect immunity, as we have learned especially from the work of Anthony Nappi (1, 2). Melanization is a process that involves the oxidation of tyrosine and the production of quinones, which polymerize to form melanin (3). The process has several roles, including a developmental role in cuticle pigmentation and the nervous system, an immune role in clot formation during wounding, and a role in phagocytosis, nodulation, or encapsulation of bacteria, fungi, and parasites (4). Cellular melanization is particularly utilized in the encapsulation of multicellular pathogens. I focus here on the infection of the *Drosophila* larva by a parasitoid wasp, which is the most extensively studied model (5).

An effective immune response requires appropriate changes in immune cell metabolism and associated changes in systemic metabolism (6–9). Although immunometabolism has been a popular topic in recent years, research on immunometabolism in insects has somewhat lagged (10). Very little is known about the metabolic changes associated with cellular encapsulation and melanization, which is primarily a metabolic response. The enormous nutrient requirements of this response have a major impact on the entire organism, and regulation of metabolism therefore affects not only the efficiency of the response, but also the development and physiology of the surviving organism (11). The production of toxic molecules is essential to eliminate the pathogen, but is harmful to the host (3, 12). Adjusting the strength of the response while protecting the host has significant evolutionary and ecological implications (13, 14). The pathogen interferes with the host's immune response by targeting the metabolism of the response (15). A thorough understanding of all these relationships cannot be achieved without examining the complex metabolic changes that support this response. This article focuses on what is known about these changes and the open questions that remain.

During the reaction of the *Drosophila* larva to the parasitoid wasp egg (Figure 1), circulating plasmocytes are the first to recognize the parasitoid egg and activate immune response. This results in the mobilization of "sessile" hemocytes into the circulation (16), some of which attach to the egg, while others along with the originally circulating hemocytes trans-differentiate into lamellocytes (17). Once fully differentiated, the lamellocytes attach to the egg and encapsulate it in multiple layers. Additional lamellocytes are produced in the lymph gland. Encapsulation is associated with melanization, which is facilitated by the expression of prophenoloxidase PPO2 in crystal cells and PPO3 in lamellocytes

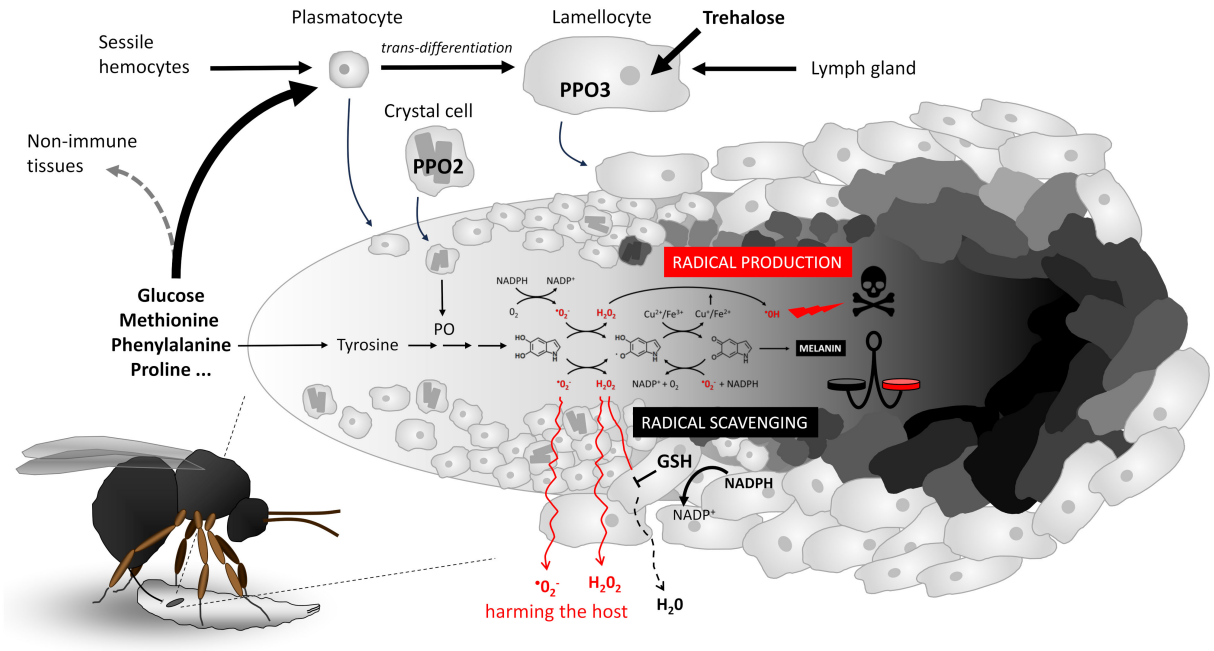

FIGURE 1
Cellular melanizing encapsulation response of *Drosophila* larvae to the egg of the parasitoid wasp *Leptopilina boulardi*. Schematic representation of hemocyte response, nutrient requirement, activation and differentiation, progressive adherence, encapsulation of the egg in multiple layers, and melanization (schematically shown from left to right on the egg). A simplified melanization reaction is shown in the middle, with the most critical redox interconversions between 5,6-dihydroxyindole, indole-semiquinone, and indole-quinone (shown by chemical formulas from left to right), the generation of reactive oxygen species to destroy the parasitoid (shown above the reaction), or the scavenging of radicals in cooperation with glutathione GSH to protect the host from the escape of radicals (shown below the reaction). The balance between radical generation and radical scavenging (indicated by the scale symbol) determines host resistance and protection. GSH, glutathione; PPO2/3, prophenoloxidase 2/3; PO, phenoloxidase.

(18). On the one hand, encapsulation and melanization ensure the elimination of the parasitoid by generating toxic molecules that are localized and concentrated on the egg inside the capsule, and on the other hand, they are presumed to protect the host by keeping this toxic reaction inside the capsule.

What are the metabolic requirements of hemocytes during parasitoid encapsulation and melanization (Figure 2)? Hemocytes maintain their basic vital functions in the resting state, i.e. without infection, and generate ATP with maximum efficiency from glucose by glycolysis and from fatty acids by beta-oxidation coupled to oxidative phosphorylation in mitochondria (19). This process allows them to produce up to 38 ATPs per molecule of glucose, although in reality it is lower. Once activated by the detection of a parasitoid, previously dormant processes are initiated in hemocytes. Unlike, for example, the activation of mammalian T lymphocytes, which require nutrient support for cell division, there is minimal hemocyte proliferation in this response (17, 19, 20). However, over a thousand genes undergo changes (9) that lead to intense transcription and translation, requiring nucleotide production and amino acid uptake to support them. During cellular differentiation, epigenetic modifications occur that require methylation. Methylation is also required for post-translational modification of new proteins. The methylation cycle intensifies during immune response, resulting in increased consumption of ATP and methionine, from which S-adenosylmethionine (SAM) is formed as a source of methyl groups (21). Differentiation of lamellocytes and encapsulation of the parasitoid by plasmatocytes and lamellocytes requires changes in the cytoskeleton and membrane, with cells adhering to the surface of the parasitoid where they interconnect to form layers of the capsule (22). Metabolically demanding is the production of reactive oxygen species (ROS) and other toxic molecules to destroy the parasitoid, but also the production of antioxidants to protect the host. Both actions are redox reactions that consume significant amounts of NADPH. NADPH is generated primarily by oxidative PPP, which uses glucose as its source (23), or by malic enzyme and isocitrate

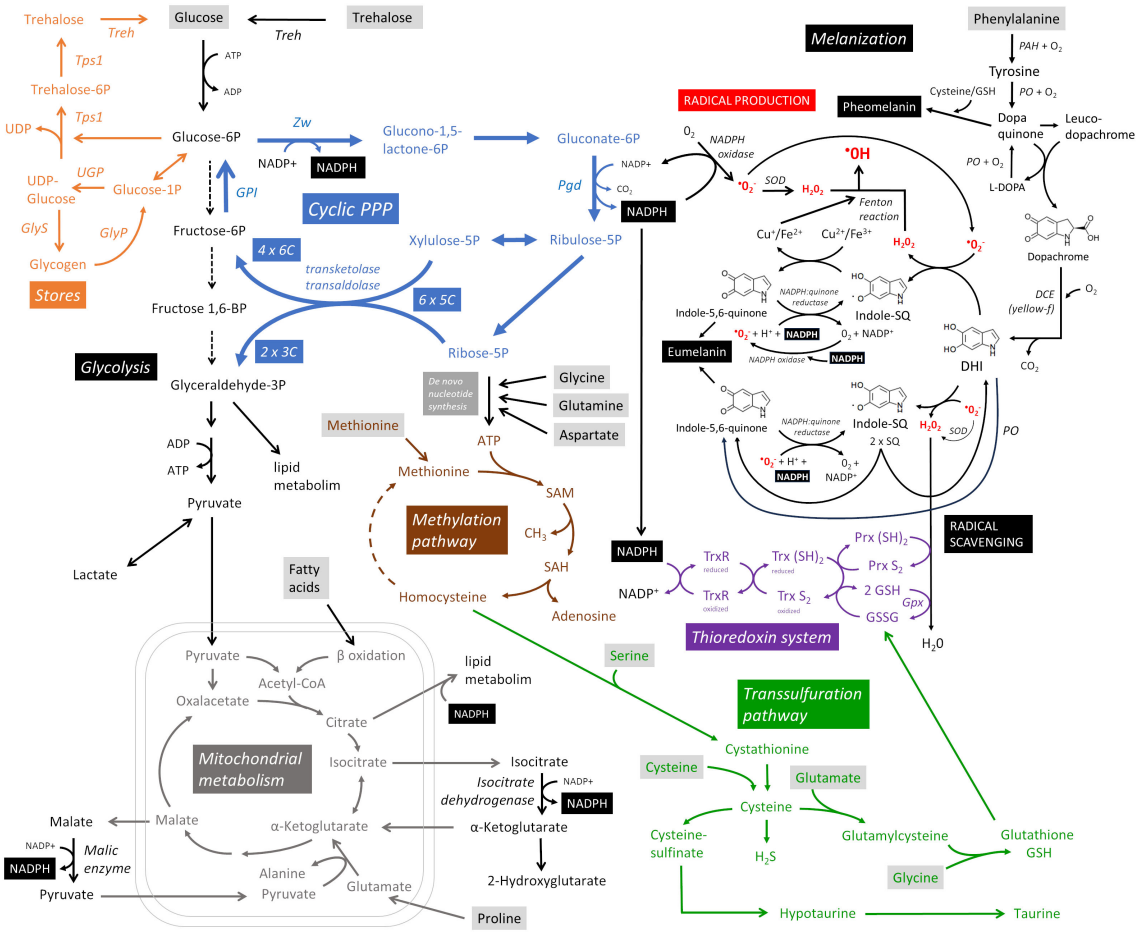

FIGURE 2
Metabolic pathways supporting cellular melanizing encapsulation. A detailed description is provided throughout the main text. Metabolites in gray boxes represent the predicted nutritional requirements of hemocytes during the response. Cyclic PPP, cyclic pentose phosphate pathway; DCE, dopachrome conversion enzyme; DHI, 5,6-dihydroxyindole; GlyP, glycogen phosphorylase; GlyS, glycogen synthase; GPI, glucose-6-phosphate isomerase; Gpx, glutathione peroxidase; Indole-SQ, Indole-semiquinone; GSH, glutathione; GSSG, glutathione disulfide; PAH, phenylalanine hydroxylase; Pgd, Phosphogluconate dehydrogenase; PO, phenoloxidase; Prx, thioredoxin peroxidase; SAM, S-adenosylmethionine; SOD, superoxide dismutase; Tps1, trehalose-6-phosphate synthase 1; Treh, trehalase; Trx, thioredoxin; TrxR, thioredoxin reductase; UGP, UDP-glucose pyrophosphorylase; Zw, Zwischenferment (glucose-6-phosphate dehydrogenase).

dehydrogenase, which require citric acid cycle intermediates (24). For melanization, the source is tyrosine, but this is more likely to be supplied to cells as phenylalanine and converted to tyrosine by phenylalanine hydroxylase (14). The role of mitochondrial function and ATP production in hemocytes during this immune response remains uncertain. However, lactate production is increased in hemocytes (9, 10), suggesting increased ATP production by glycolysis, which is much less efficient (2 ATP per glucose molecule) and consequently requires more glucose.

The primary purpose of cellular encapsulation and melanization is to produce toxic molecules that will eliminate the parasitoid, while localizing this production to the surface of the parasitoid and protecting the host (3). All processes are ultimately directed toward this goal. Both ROS and antioxidant production require NADPH. NADPH oxidase transfers electrons from NADPH to molecular oxygen, resulting in a one-electron reduction to the superoxide anion O_2^-. Of the three NADPH oxidases, most hemocyte types express *AIF*, but very little *Nox* or *Duox* genes (9, 19, 20). The conversion of O_2^- to H_2O_2 occurs spontaneously or with the assistance of superoxide dismutase [the *SOD1* and *SOD2* genes are both strongly expressed in most hemocytes (9, 19, 20)]. These primary ROS (O_2^- and H_2O_2) can be further processed to the much more reactive hydroxyl radical ($^{\bullet}OH$) or hypochlorous acid (HOCl) (3). The cyclic pentose phosphate pathway (PPP) is the most efficient mechanism for reducing $NADP^+$ to NADPH, yielding up to six NADPH per glucose during the re-oxidation of glucose 6-phosphate (G6P) (23). In cyclic PPP, G6P is oxidized to phosphogluconolactone by glucose-6-phosphate dehydrogenase, reducing one $NADP^+$. In the following step, 6-phosphogluconate dehydrogenase reduces another $NADP^+$ while catalyzing the oxidation and decarboxylation of phosphogluconate to produce ribulose 5-phosphate pentose. The pentoses can be used for *de novo* nucleotide synthesis, but if more NADPH is needed, xylulose 5-phosphate and ribose 5-phosphate can be converted by transketolase and transaldolase to glyceraldehyde 3-phosphate (GAP) and fructose 6-phosphate. This hexose can be converted back to G6P by the reversed action of glucose-6-phosphate isomerase and oxidized again to produce more NADPH, forming a pentose cycle (cyclic PPP). Through the action of transketolases and transaldolases, six pentoses are recycled to four hexoses and two GAPs. Transketolases and transaldolases can also work in the opposite direction (25), using non-oxidative PPP to form pentoses from hexoses when the cell primarily needs to produce nucleotides.

Drosophila larval hemocytes metabolize glucose by cyclic PPP, and this metabolism is greatly increased during parasitoid infection (9) [detailed analysis of the expression of glycolytic and PPP enzymes in hemocytes is presented in (9)]. Another possibility for the formation of cytosolic NADPH is the utilization of the citric acid cycle intermediates, isocitrate and malate, which are transported from the mitochondria to the cytoplasm and metabolized by isocitrate dehydrogenase [*Idh* is strongly expressed in plasmatocytes, less in lamellocytes (9, 19, 20)] or malic enzyme [*Men* is strongly expressed in hemocytes, especially in crystal cells (9, 19, 20)] to alpha-ketoglutarate and pyruvate, respectively, with concomitant reduction of $NADP^+$ to NADPH. The source in this case may be pyruvate from glycolysis, beta-oxidation of fatty acids, or proline (or possibly glutamine), which is converted in the mitochondria to glutamate and alpha-ketoglutarate, which may be converted in one direction to isocitrate and in the other to malate, thus serving as a source for NADPH formation. Proline is one of the most abundant amino acids in insect hemolymph (26–28), but it is not known whether it is used as an alternative source of NADPH in hemocytes during encapsulation/melanization. *P5cr* and *P5cr-2*, which are predicted to convert proline to pyrroline-5-carboxylate, and *P5CDh1*, which is predicted to convert L-glutamate 5-semialdehyde to glutamate, are expressed in hemocytes with stronger expression in lamellocytes (9, 19, 20). GAP formed by glycolysis or cyclic PPP, citrate and NADPH are also important for lipid metabolism, which is most likely essential during this reaction, at least for membrane remodeling during lamellocyte differentiation. All this can be provided by glucose metabolism and the coupling of cyclic PPP with downstream glycolysis and pyruvate metabolized in the citric acid cycle, or supplemented by proline metabolism in mitochondria. It is not known whether rewiring of mitochondrial metabolism, either for additional NADPH production by isocitrate dehydrogenase and malic enzyme or to support lipid metabolism, reduces ATP production by oxidative phosphorylation and thus the cell produces more ATP by glycolysis ending in lactate, whose increased production we detected during this response (9). The role of mitochondrial metabolism requires further investigation.

Melanization begins with the oxidation of tyrosine by phenol oxidase (PO) in the presence of O_2 (29). Tyrosine is replenished in cells from phenylalanine by phenylalanine hydroxylase [*Hn* is expressed in hemocytes, more in plasmatocytes, less in lamellocytes (9, 19, 20)], so phenylalanine or tyrosine are essential sources for melanization. PO oxidizes tyrosine to dopaquinone, which is converted by intramolecular cyclization to leucodopachrome. The latter is oxidized to dopachrome by dopaquinone, while dopaquinone is reduced to L-DOPA, which is oxidized back to dopaquinone by PO. In an environment with cysteine or glutathione (GSH), cysteinyldopa and red pheomelanin can be formed (4). Whether this type of melanization plays a role in this immune response is unknown (30). Dopachrome is a substrate for the enzyme yellow-f (31), which decarboxylates it to 5,6-dihydroxyindole (DHI). *yellow-f* is one of the genes with the highest up-regulation in hemocytes after parasitoid challenge due to a strong expression in lamellocytes (9, 19, 20). In mammals, the tautomerization of dopachrome to DHICA (no decarboxylation), which is the basis of DHICA eumelanin, is also known; in insects, the formation of DHICA is unclear (4). The highly diffusible DHI and its redox conversion between DHI, indole-semiquinone and indolequinone probably represent the essential role that melanization plays in this type of immune response (3). Depending on the environment in which these redox conversions occur (pH, redox state, presence of antioxidants), this part of the melanization cascade can either greatly enhance the production of toxic radicals or, conversely, scavenge them. DHl is converted to indole-semiquinone in the presence of oxygen radicals to form H_2O_2. In addition to NADPH oxidase, the source of the oxygen radical may be the conversion of indole-semiquinone to

indolequinone (3). Indole-semiquinone is further converted to indolequinone in the presence of Cu^{2+}/Fe^{3+}, reducing the ions to Cu^{+} and Fe^{2+}, respectively. Cu^{+} and Fe^{2+} can convert H_2O_2 to a highly reactive hydroxyl radical (Fenton reaction), which locally damages various biomolecules at the site of its formation. When this reaction is directed to the surface of the parasitoid, it destroys it. Indolequinone can be reduced by NADPH:quinone reductase to indole-semiquinone (one-electron reduction) or DHI (two-electron reduction) (32), and the next round of oxidation could produce additional H_2O_2, ions, and ultimately $^{\bullet}OH$. Unfortunately, it is not known whether NADPH:quinone reductase plays a role in melanization, so possible interconversion using NADPH is speculative.

However, in an environment with GSH, the same interconversions can scavenge radicals (3). DHI converts O_2^- to H_2O_2, which is converted to H_2O by GSH. Indolequinone, presumably involving NADPH:quinone reductase, scavenges O_2^- to O_2. In both cases, reactive indole-semiquinone is formed. The two indole-semiquinones can react with each other to form DHI (reduction) and indolequinone (oxidation), which can scavenge other O_2^- radicals. Thus, in an environment where Cu and Fe ions are present, DHI-semiquinone-quinone interconversion can lead to radical production, whereas in an environment with GSH, it can scavenge radicals. Finally, indolequinone can polymerize into visible black eumelanin. DHI-semiquinone-quinone interconversions can occur spontaneously without enzymatic action. However, it is likely that enzymes (PO, NADPH:quinone reductase, NADPH oxidase) and the supply of Cu/Fe ions can direct these conversions in the desired direction. Whether NADPH is needed only for the input (NADPH oxidase) and for antioxidant formation (thioredoxin system), or whether it is also involved in melanization itself, is a question. In any case, the production and scavenging of radicals, the essence of this immune response, depends on sufficient NADPH production.

The parasitoid is destroyed by the production of radicals, and although their production appears to be tightly regulated and somehow localized and targeted to the parasitoid, the escaping radicals still threaten the host itself. Therefore, host protection by antioxidant production and ROS scavenging is an integral part of this immune response. We found increased levels of the reduced form of glutathione and taurine in hemocytes (9). Diptera lack glutathione reductase and therefore utilize a thioredoxin system in which the protein thioredoxin Trx S_2 is reduced to the dithiol form Trx $(SH)_2$ by NADPH-dependent thioredoxin reductase (TrxR) (33). Hemocytes strongly express *Trxr1* and *Trx-2*, many different peroxiredoxins and glutathione peroxidase *dj-1beta*, with increasing expression in lamellocytes (9, 19, 20). The reduced thioredoxin then reduces glutathione disulfide (GSSG) to GSH. GSH reduces H_2O_2 to water, which can also be reduced by thioredoxin peroxidase (Prx), which is also reduced by thioredoxin. Hemocytes express each component of this system very strongly, and lamellocytes appear to further increase expression, consistent with increased GSH production in hemocytes after infection. Thus, the thioredoxin system appears to be another major consumer of NADPH.

Increased glutathione and taurine must be newly produced in the hemocytes. The source is cysteine, which, if insufficient, is produced by the transsulfuration pathway from homocysteine, the source of which is methionine and the methylation pathway (SAM cycle) (34). Activated immune cells take up large amounts of methionine and significantly increase the methylation pathway (21). After ATP, SAM is one of the most abundant molecules in the cell. SAM is the source of the methyl group for the vast majority of methylation in the cell, both for the regulation of gene expression and for the methylation of newly generated biomolecules, especially proteins. In addition, the methylation pathway is the source of homocysteine for transsulfuration and the formation of GSH and taurine (34). The methylation pathway starts with the coupling of methionine and ATP, so its increase depends on the *de novo* production of ATP (the source is glucose and PPP) and the uptake of methionine. Thus, methylation and antioxidant production, which seems to be important for this immune response, are another reason for the need for glucose and amino acids such as methionine, glutamine, glycine, and serine in hemocytes.

Activation and differentiation of hemocytes takes place in the circulation, in sessile pockets or in the lymph gland, i.e. in environments with easy access to sugars and amino acids. However, melanization and related processes take place on the surface of the parasitoid and later in the capsule, which is formed by many layers of encapsulating cells that gradually die. In this environment, they probably have limited access to nutrients. Nevertheless, they must still metabolize intensively for several hours, certainly at least reducing $NADP^+$ to NADPH. Therefore, it can be assumed that prior to encapsulation, hemocytes accumulate reserves of sugars and possibly other biomolecules (e.g., as a source of amino acids) for later use in NADPH production and melanization reactions. For example, mammalian neutrophils accumulate glycogen from which they then liberate glucose at their site of action, where sugars are no longer readily available (35). Insect hemocytes can potentially form glycogen or trehalose-6-phosphate stores (36) because they express the necessary enzymes (UGP, GlyS, Tps1) (9). They also express the enzymes required to release glucose from these stores (GlyP and Treh) (9), and the expression of these enzymes is markedly increased in differentiated lamellocytes (19, 20).

Although we have learned a lot about the melanization cascade through Nappi's work, and more recently about supporting metabolism, especially cyclic PPP, there are still many unanswered questions:

1. How to achieve a localized toxic response that kills the pathogen but not the host? Do different types of hemocytes play different roles in this response? For example, are plasmatocytes and crystal cells primarily responsible for radical generation because they are the first to adhere to the parasitoid surface (37), whereas lamellocytes, which adhere later and form the outer layers of the capsule, are more likely to be responsible for protective functions and radical scavenging? If so, how are similar effects achieved in insect species that do not produce lamellocytes (5)?
2. Do Fe and Cu ions and Fenton reactions play an important role in melanization as suggested by Nappi? If so, how is

their enrichment and controlled release on the pathogen surface achieved? Do Fe-transporting proteins such as transferrin (38, 39) play a role?

3. Do hemocytes store glycogen and trehalose, and is this essential for this response? Do they also store amino acids, e.g. in the form of storage proteins such as Lsp (40)?
4. Metabolism is very flexible. Does the metabolism of this reaction change based on the current nutritional status of the organism? Can proline or glutamine and NADPH production by isocitrate dehydrogenase and/or malic enzyme replace NADPH production by glucose metabolism via cyclic PPP?
5. How is the host protected against this reaction? Is there an essential role for the thioredoxin system in the production of antioxidants? Is the cysteine source or the methylation cycle and transsulfuration pathway essential?
6. How is the balance between producing and scavenging toxic radicals established? Too little production and/or too much scavenging will reduce resistance, the opposite will lead to more host damage. Thus, the balance is of great evolutionary importance.
7. All of these processes are potential targets for pathogen interference with the host immune response. How do they affect host-pathogen coevolution, and which ones become targets for perturbation by the pathogen?

Data availability statement

Publicly available datasets were analyzed in this study. This data can be found here: https://www.flyrnai.org/scRNA/blood/; https://www.flyrnai.org/tools/single_cell/web.

Author contributions

TD: Funding acquisition, Visualization, Writing – original draft, Writing – review & editing.

Funding

The author(s) declare financial support was received for the research, authorship, and/or publication of this article. This work was supported by the Grant Agency of the Czech Republic (Project 20-09103S; www.gacr.cz).

Conflict of interest

The author declares that the research was conducted in the absence of any commercial or financial relationships that could be construed as a potential conflict of interest.

Publisher's note

References

1. Nappi AJ, Vass E. Cytotoxic reactions associated with insect immunity. In: Beck G, Sugumaran M, Cooper EL, editors. *Phylogenetic Perspectives on the Vertebrate Immune System*. Boston, MA: Springer US (2001). p. 329–48. Available at: http://link.springer.com/10.1007/978-1-4615-1291-2_33. (Advances in Experimental Medicine and Biology; vol. 484).

2. Yang L, Qiu L, Fang Q, Stanley DW, Ye G. Cellular and humoral immune interactions between *Drosophila* and its parasitoids. *Insect Sci* (2021) 28(5):1208–27. doi: 10.1111/1744-7917.12863

3. Nappi AJ, Christensen BM. Melanogenesis and associated cytotoxic reactions: Applications to insect innate immunity. *Insect Biochem Mol Biol* (2005) 35(5):443–59. doi: 10.1016/j.ibmb.2005.01.014

4. Sugumaran M, Barek H. Critical analysis of the melanogenic pathway in insects and higher animals. *Int J Mol Sci* (2016) 17(10):1753. doi: 10.3390/ijms17101753

5. Kim-Jo C, Gatti JL, Poirié M. Drosophila cellular immunity against parasitoid wasps: A complex and time-dependent process. *Front Physiol* (2019) 10:603/full. doi: 10.3389/fphys.2019.00603/full

6. Krejčová G, Danielová A, Nedbalová P, Kazek M, Strych L, Chawla G, et al. Drosophila macrophages switch to aerobic glycolysis to mount effective antibacterial defense. *eLife* (2019) 8:e50414. doi: 10.7554/eLife.50414

7. Krejčová G, Morgantini C, Zemanová H, Lauschke VM, Kovářová J, Kubásek J, et al. Macrophage-derived insulin antagonist ImpL2 induces lipoprotein mobilization upon bacterial infection. *EMBO J* (2023) e114086. doi: 10.15252/embj.2023114086

8. McMullen E, Strych L, Chodáková L, Krebs A, Dolezal T. JAK/STAT mediated insulin resistance in muscles is essential for effective immune response. *bioRxiv* (2023) 10.04.560867. doi: 10.1101/2023.10.04.560867

9. Kazek M, Chodáková L, Lehr K, Strych L, Nedbalová P, McMullen E, et al. Metabolism of glucose and trehalose by cyclic pentose phosphate pathway is essential for effective immune response in Drosophila. *bioRxiv* (2023) 08.17.553657. doi: 10.1101/2023.08.17.553657

10. Dolezal T, Krejcova G, Bajgar A, Nedbalova P, Strasser P. Molecular regulations of metabolism during immune response in insects. *Insect Biochem Mol Biol* (2019) 109:31–42. doi: 10.1016/j.ibmb.2019.04.005

11. Bajgar A, Kucerova K, Jonatova L, Tomcala A, Schneedorferova I, Okrouhlik J, et al. Extracellular adenosine mediates a systemic metabolic switch during immune response. *PloS Biol* (2015) 13(4):e1002135. doi: 10.1371/journal.pbio.1002135

12. DeJong RJ, Miller LM, Molina-Cruz A, Gupta L, Kumar S, Barillas-Mury C. Reactive oxygen species detoxification by catalase is a major determinant of fecundity in the mosquito *Anopheles Gambiae*. *Proc Natl Acad Sci* (2007) 104(7):2121–6. doi: 10.1073/pnas.0608407104

13. Schulenburg H, Kurtz J, Moret Y, Siva-Jothy MT. Introduction. Ecological immunology. *Philos Trans R Soc B: Biol Sci* (2008) 364(1513):3–14. doi: 10.1098/rstb.2008.0249

14. Fuchs S, Behrends V, Bundy JG, Crisanti A, Nolan T. Phenylalanine metabolism regulates reproduction and parasite melanization in the malaria mosquito. *PloS One* (2014) 9(1):e84865. doi: 10.1371/journal.pone.0084865

15. Kohler LJ, Carton Y, Mastore M, Nappi AJ. Parasite suppression of the oxidations of eumelanin precursors inDrosophila melanogaster. *Arch Insect Biochem Physiol* (2007) 66(2):64–75. doi: 10.1002/arch.20199

16. Schmid MR, Anderl I, Vesala L, Vanha-aho LM, Deng XJ, Rämet M, et al. Control of drosophila blood cell activation *via* toll signaling in the fat body. *PloS One* (2014) 9(8):e102568. doi: 10.1371/journal.pone.0102568

17. Anderl I, Vesala L, Ihalainen TO, Vanha-aho LM, Andó I, Rämet M, et al. Transdifferentiation and Proliferation in Two Distinct Hemocyte Lineages in Drosophila melanogaster Larvae after Wasp Infection. *PloS Pathog* (2016) 12(7): e1005746. doi: 10.1371/journal.ppat.1005746

18. Dudzic JP, Kondo S, Ueda R, Bergman CM, Lemaitre B. Drosophila innate immunity: regional and functional specialization of prophenoloxidases. *BMC Biol* (2015) 13(1):81. doi: 10.1186/s12915-015-0193-6

19. Cattenoz PB, Sakr R, Pavlidaki A, Delaporte C, Riba A, Molina N, et al. Temporal specificity and heterogeneity of Drosophila immune cells. *EMBO J* (2020) 39(12): e104486. doi: 10.15252/embj.2020104486

20. Tattikota SG, Cho B, Liu Y, Hu Y, Barrera V, Steinbaugh MJ, et al. A single-cell survey of Drosophila blood. *eLife* (2020) 9:e54818. doi: 10.7554/eLife.54818

21. Yu W, Wang Z, Zhang K, Chi Z, Xu T, Jiang D, et al. One-carbon metabolism supports S-adenosylmethionine and histone methylation to drive inflammatory macrophages. *Mol Cell* (2019) 75(6):1147–1160.e5. doi: 10.1016/j.molcel.2019.06.039

22. Williams MJ, Ando I, Hultmark D. Drosophila melanogaster Rac2 is necessary for a proper cellular immune response. *Genes To Cells: Devoted to Mol Cell Mechanisms* (2005) 10(8):813–23. doi: 10.1111/j.1365-2443.2005.00883.x

23. Britt EC, Lika J, Giese MA, Schoen TJ, Seim GL, Huang Z, et al. Switching to the cyclic pentose phosphate pathway powers the oxidative burst in activated neutrophils. *Nat Metab* (2022) 4(3):389–403. doi: 10.1038/s42255-022-00550-8

24. Merritt TJS, Kuczynski C, Sezgin E, Zhu CT, Kumagai S, Eanes WF. Quantifying interactions within the NADP(H) enzyme network in Drosophila melanogaster. *Genetics* (2009) 182(2):565–74. doi: 10.1534/genetics.109.100677

25. Katz J, Rognstad R. The labeling of pentose phosphate from glucose-14C and estimation of the rates of transaldolase, transketolase, the contribution of the pentose cycle, and ribose phosphate synthesis*. *Biochemistry* (1967) 6(7):2227–47. doi: 10.1021/bi00859a046

26. Des Marteaux L, Kučera L, Moos M, Štětina T, Korbelová J, Des Marteaux L, et al. A mixture of innate cryoprotectants is key for freeze tolerance and cryopreservation of a drosophilid fly larva. *J Exp Biol* (2022) 225(8):jeb243934. doi: 10.1242/jeb.243934

27. Teulier L, Weber JM, Crevier J, Darveau CA. Proline as a fuel for insect flight: enhancing carbohydrate oxidation in hymenopterans. *Proc R Soc B: Biol Sci* (2016) 283 (1834):20160333. doi: 10.1098/rspb.2016.0333

28. Piyankarage SC, Augustin H, Featherstone DE, Shippy SA. Hemolymph amino acid variations following behavioral and genetic changes in individual Drosophila larvae. *Amino Acids* (2010) 38(3):779–88. doi: 10.1007/s00726-009-0284-1

29. González-Santoyo I, Córdoba-Aguilar A. Phenoloxidase: a key component of the insect immune system. *Entomol Experimentalis Applicata* (2012) 142(1):1–16. doi: 10.1111/j.1570-7458.2011.01187.x

30. Galván I, Jorge A, Edelaar P, Wakamatsu K. Insects synthesize pheomelanin. *Pigment Cell Melanoma Res* (2015) 28(5):599–602. doi: 10.1111/pcmr.12397

31. Han Q, Fang J, Ding H, Johnson JK, Christensen BM, Li J. Identification of Drosophila melanogaster yellow-f and yellow-f2 proteins as dopachrome-conversion enzymes. *Biochem J* (2002) 368(Pt 1):333–40. doi: 10.1042/bj20020272

32. Vasiliou V, Ross D, Nebert DW. Update of the NAD(P)H:quinone oxidoreductase (NQO) gene family. *Hum Genomics* (2006) 2(5):329–35. doi: 10.1186/1479-7364-2-5-329

33. Bauer H, Kanzok SM, Schirmer RH. Thioredoxin-2 but Not Thioredoxin-1 Is a Substrate of Thioredoxin Peroxidase-1 from Drosophila melanogaster. *J Biol Chem* (2002) 277(20):17457–63. doi: 10.1074/jbc.M200636200

34. Parkhitko AA, Jouandin P, Mohr SE, Perrimon N. Methionine metabolism and methyltransferases in the regulation of aging and lifespan extension across species. *Aging Cell* (2019) 18(6):e13034. doi: 10.1111/acel.13034

35. Sadiku P, Willson JA, Ryan EM, Sammut D, Coelho P, Watts ER, et al. Neutrophils fuel effective immune responses through gluconeogenesis and glycogenesis. *Cell Metab* (2021) 33(2):411–423.e4. doi: 10.1016/j.cmet.2020.11.016

36. Yamada T, Habara O, Kubo H, Nishimura T. Fat body glycogen serves as a metabolic safeguard for the maintenance of sugar levels in Drosophila. *Development* (2018) 145(6):dev158865. doi: 10.1242/dev.158865

37. Nappi AJ, Vass E. Hydrogen peroxide production in immune-reactive Drosophila melanogaster. *J Parasitol* (1998) 84(6):1150. doi: 10.2307/3284664

38. Wu S, Yin S, Zhou B. Molecular physiology of iron trafficking in Drosophila melanogaster. *Curr Opin Insect Sci* (2022) 50:100888. doi: 10.1016/j.cois.2022.100888

39. Iatsenko I, Marra A, Boquete JP, Peña J, Lemaitre B. Iron sequestration by transferrin 1 mediates nutritional immunity in Drosophila melanogaster. *Proc Natl Acad Sci* (2020) 117(13):7317–25. doi: 10.1073/pnas.1914830117

40. Handke B, Poernbacher I, Goetze S, Ahrens CH, Omasits U, Marty F, et al. The hemolymph proteome of fed and starved Drosophila larvae. *PloS One* (2013) 8(6): e67208–8. doi: 10.1371/journal.pone.0067208

frontiers | Frontiers in Immunology

TYPE Original Research
PUBLISHED 07 December 2023
DOI 10.3389/fimmu.2023.1275923

OPEN ACCESS

EDITED BY
Laura Vesala,
Tampere University, Finland

REVIEWED BY
Sheena Cotter,
University of Lincoln, United Kingdom
Kwang-Zin Lee,
Fraunhofer Society (FHG), Germany
Viktor Honti,
Hungarian Academy of Sciences, Hungary

*CORRESPONDENCE
Francis M. Jiggins
fmj1001@cam.ac.uk
Alexandre B. Leitão
alexandre.leitao@research.fchampalimaud.org

†These authors have contributed equally to this work

RECEIVED 10 August 2023
ACCEPTED 14 November 2023
PUBLISHED 07 December 2023

CITATION
Leitão AB, Geldman EM and Jiggins FM (2023) Activation of immune defences against parasitoid wasps does not underlie the cost of infection.
Front. Immunol. 14:1275923.
doi: 10.3389/fimmu.2023.1275923

Activation of immune defences against parasitoid wasps does not underlie the cost of infection

Alexandre B. Leitão[1,2*†], Emma M. Geldman[1†] and Francis M. Jiggins[1*]

[1]Department of Genetics, University of Cambridge, Cambridge, United Kingdom, [2]Champalimaud Neuroscience Progamme, Champalimaud Centre for the Unknown, Champalimaud Foundation, Lisbon, Portugal

Parasites reduce the fitness of their hosts, and different causes of this damage have fundamentally different consequences for the evolution of immune defences. Damage to the host may result from the parasite directly harming its host, often due to the production of virulence factors that manipulate host physiology. Alternatively, the host may be harmed by the activation of its own immune defences, as these can be energetically demanding or cause self-harm. A well-studied model of the cost of infection is *Drosophila melanogaster* and its common natural enemy, parasitoid wasps. Infected *Drosophila* larvae rely on humoral and cellular immune mechanisms to form a capsule around the parasitoid egg and kill it. Infection results in a developmental delay and reduced adult body size. To disentangle the effects of virulence factors and immune defences on these costs, we artificially activated anti-parasitoid immune defences in the absence of virulence factors. Despite immune activation triggering extensive differentiation and proliferation of immune cells together with hyperglycaemia, it did not result in a developmental delay or reduced body size. We conclude that the costs of infection do not result from these aspects of the immune response and may instead result from the parasite directly damaging the host.

KEYWORDS

***Drosophila*, parasitoid, immunity, cost, tradeoff**

Introduction

The reduction in host fitness during infection can be attributed to two major mechanisms. First, parasites may directly harm their hosts, frequently due to virulence factors that manipulate host physiology. For example, cholera toxin produced by *Vibrio cholerae* leads to an imbalance of electrolyte movement in enterocytes, which results in cellular water loss (1). Second, activation of immune defences can be costly. In insects, immune activation without infection can reduce fecundity [reviewed in (2)] and longevity (3). Immune responses can be costly for different reasons. Energy can be relocated from

other physiological processes and development to the immune response (4). For example, when mice are injected with lipopolysaccharide, a potent immune stimulant, the energetic cost of the response causes them to enter a hypometabolic state accompanied by a decrease in body temperature (5). Immune responses can also cause self-harm (immunopathology), as exemplified by the activation of the melanisation cascade, an immune response in insects that damages self-tissues (6). Immune activation can also cause other physiological or behavioural changes, such as anorexia, that reduce fitness (7).

Because natural selection will favour traits that reduce the cost of infection, whether parasites harm their hosts directly or indirectly through a costly immune response has important evolutionary consequences. If the main cost of infection is the immune response itself, selection may favour a reduction in the magnitude of this response even if this increases susceptibility to infection (8). Such 'immune restraint' is unlikely if the direct harm caused by the parasite greatly outweighs the cost of mounting an immune response. Immune systems will also evolve adaptations to reduce costs, such as making immune responses inducible so that the cost of immunity is only incurred when infected (9, 10). For example, we recently demonstrated that aspects of the antiparasitoid immune response that are inducible when flies evolve under low parasitism conditions evolve to be constitutive when parasitism rates are high (11). This is predicted to be the case when immune responses are costly. Hence, to understand how immune defences evolve, we must understand why infection is costly.

When *Drosophila melanogaster* is infected with parasitoid wasps, larvae take longer to develop (12), and adults that survive the infection have reduced body size and fecundity (13). The immune response against parasitoids relies on both the humoral and cellular arms of the innate immune system. The humoral immune response includes upregulating complement-like proteins called TEPs (thioester-containing proteins) in the fat body (14, 15). The cellular immune response involves the proliferation and differentiation of different immune cell types. Large circulating immune cells called lamellocytes, which are rarely seen in healthy larvae, increase drastically in number after parasitoid infection (16). Together with plasmatocytes, they form a multi-layered capsule around the parasitoid egg to kill it. During the final stages of infection, lamellocytes activate prophenoloxidase 3 (PPO3), which is essential for the complete melanisation of the capsule around the parasitoid egg (17).

To manipulate the host immune response, parasitoid females frequently inject a cocktail of venoms into the larval haemocoel (18). In the genus *Leptopilina*, venom composition evolves very fast, allowing the diversification of strategies used by different wasp species. For example, the generalist species *L. heterotoma* uses protein with a hydrolase-like structure to lyse the lymph gland, the hematopoietic organ responsible for producing lamellocytes (19). A closely related species, *L. boulardi*, does not affect lymph gland structure, but it uses a RhoGAP protein to alter lamellocyte morphology, impairing the cell's ability to encapsulate the wasp egg (20). Other proteins present in *L. boulardi* venom glands are predicted to affect glycolysis and other physiological processes (21).

Parasitoid infection is associated with major changes in metabolism, with infected larvae entering a state of hyperglycaemia triggered by the release of extracellular adenosine from immune cells (12). This metabolic switch is necessary to produce lamellocytes and the ability to encapsulate parasitoid eggs. It has been argued that the developmental delay and reduction in body size observed during parasitoid infection are caused by this metabolic shift and are therefore a cost of immune activation (12). However, parasite infection both exposes the host to virulence factors and activates the immune response, so either of these could be harming the fly. Here, we investigate whether reductions in body size and developmental delay are caused by the cost of mounting the encapsulation response.

Results

Injection of parasitoid wasp homogenate recapitulates the immune response to infection

To investigate the impact of immune activation on *D. melanogaster* physiology and life history, we compared larvae infected by the parasitoid wasp *L. boulardi* with larvae injected with 'wasp homogenate'. Wasp homogenate is prepared by homogenising adult parasitoid wasps in paraffin oil, which is then injected into a *Drosophila* larva's haemocoel. This induces the antiparasitoid immune response (22), with the oil droplet frequently being melanised similarly to wasp eggs [(22); Supplementary Figures 1C, D]. Virtually all fly larvae mount this response (22). However, because the homogenate is prepared from male wasps that do not have a venom gland, it does not include virulence factors. If paraffin oil is injected alone into larvae, it stays as a sphere and is not melanised [(22); Supplementary Figure 1B].

Melanisation of the parasitoid egg occurs when it is surrounded by layers of plasmatocytes and lamellocytes that form a cellular capsule (16). When larvae were injected with wasp homogenate, the number of haemocytes in circulation at 24h increased to a level indistinguishable from that in infected larvae for both lamellocytes (Figure 1A, main effect of treatment: $\chi^2 = 298.75$, d.f = 3, $p < 2 \times 10^{-16}$; wasp homogenate vs. infection: z = 2.15, $p = 0.19$) and plasmatocytes (main effect of treatment: $\chi^2 = 87.17$, d.f = 3, $p < 2 \times 10^{-16}$; wasp homogenate vs. infection: z = 0.59, $p = 1$). In contrast, injection of oil caused a modest increase in lamellocytes (oil vs. unchallenged: difference in mean lamellocyte number = 1.85, z = 2.62, $p = 0.05$) and no increase in plasmatocytes (main effect of treatment: $\chi^2 = 87.17$, d.f = 3, $p < 2 \times 10^{-16}$; oil vs. unchallenged: z = 0.26, $p = 1$). The melanisation response relies on the expression of *PPO3* in lamellocytes, and this gene was upregulated to a similar extent following the injection of wasp homogenate and infection (Figure 1B; main effect of treatment: $F = 62.73$, d.f = 3, $p = 6.24 \times 10^{-16}$; wasp homogenate vs. infection: t = 0.38, d.f. = 44, $p = 1$). Injection of oil alone caused a small increase in the expression of *PPO3* (oil vs. unchallenged: difference in Ct values = 1.13, $t = 3.57$, d.f. = 44, $p = 0.005$).

Alongside the cellular response, there is a humoral immune response to wasp infection that relies on the production of immune

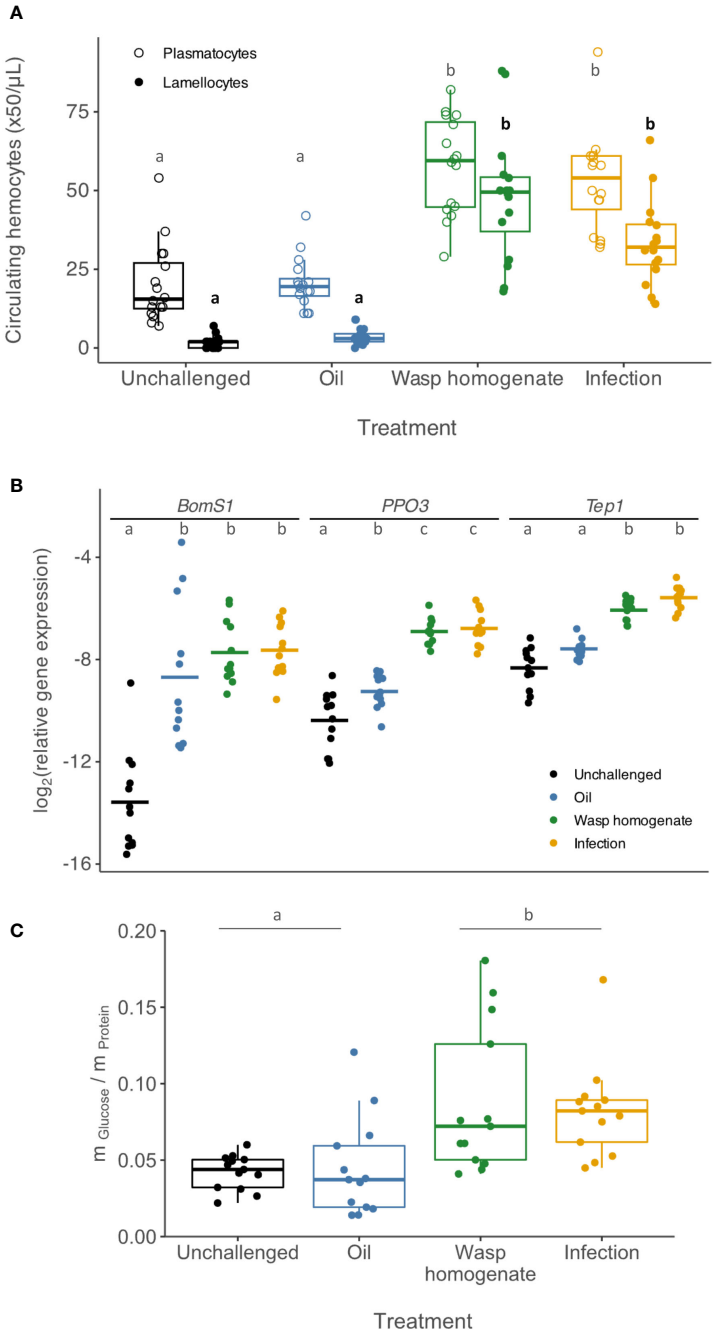

FIGURE 1
Effect of immune challenge on immunity and metabolism. Third instar larvae were injected with paraffin oil (blue), wasp homogenate (green) or parasitised (orange). **(A)** The concentrations of circulating plasmatocytes (open circles) and lamellocytes (dots) (16 pools of 8 – 10 larvae/treatment) 24h post-treatment. **(B)** Expression of three genes normalised to *RpL32* expression (n=11-12) 18h post-treatment. **(C)** The concentration of glucose relative to total protein was measured in cell-free hemolymph samples (13 pools of 40 larvae per treatment) 24h post-treatment. Boxes represent the 25th and 75th percentiles, and the line represents the median. In all cases, letters show significantly different groups (Tukey's test, p <.05) In **(A)**, comparisons between lamellocytes are represented in bold.

molecules by the fat body. This is characterised by the upregulation of the complement-like gene *thioester-containing protein 1* (*Tep1*), and this is induced to similar levels by both infection and wasp homogenate at 24h post-treatment (Figure 1B, main effect of treatment: F = 35.52, d.f = 3, p = 8.06 x 10^{-12}; wasp homogenate vs. infection: t = 2.62, d.f. = 44, p = 0.07). Injection of oil alone caused only a small increase in *Tep1* expression (oil vs. unchallenged: difference in Ct values = 0.74, t = 2.55, d.f. = 44, p = 0.086). Wounding alone can induce a transcriptional change in the fat body (23), including genes involved in microbial killing, such as *Bomanin Short 1* (*BomS1*). Both wasp infection and injection result in a wound from the ovipositor or needle, and the induction of *BomS1* occurs to a similar level in all challenges (Figure 1B, main effect of treatment: F = 26.76, d.f = 3, p = 5.26 x 10^{-10}; wasp

homogenate vs. oil: $t = 1.25$, d.f. = 44, $p = 1$; infection vs. oil: $t = 1.37$, d.f. = 44, $p = 1$; infection vs. wasp homogenate: $t = 0.118$, d.f. = 44, $p = 1$).

Infection by parasitoid wasps causes a metabolic change characterised by a state of hyperglycaemia (12). Injection of wasp homogenate increased the concentration of circulating glucose to the same levels as infection at 18h (Figure 1C; main effect of treatment: $\chi^2 = 35.69$, d.f = 3, $p = 8.69 \times 10^{-8}$; wasp homogenate vs. infection: z = 0.58, $p = 1$), while oil injection had similar levels to unchallenged larvae (oil vs. unchallenged: z = 0.223, $p = 1$). Overall, these results indicate that the injection of wasp homogenate induces similar physiological responses to parasitoid infection.

Developmental delay and body size reduction results from infection but not experimental induction of the immune response

As previously reported (13), infection by parasitoid wasps reduced thorax length by ~5% in females (Figure 2A, unchallenged vs. infection: $t = 7.05$, $p = 3.9 \times 10^{-10}$) and ~4% in males (unchallenged vs. infection: $t = 5.77$, $p = 2.9 \times 10^{-7}$). However, the thorax length of flies that were injected with wasp homogenate was indistinguishable from that of unchallenged larvae (females: $t = 0.78$, $p = 1$, males: $t = 0.34$, $p = 1$) and larvae injected with oil (females: $t = 0.25$, $p = 1$, males: $t = 0.32$, $p = 1$).

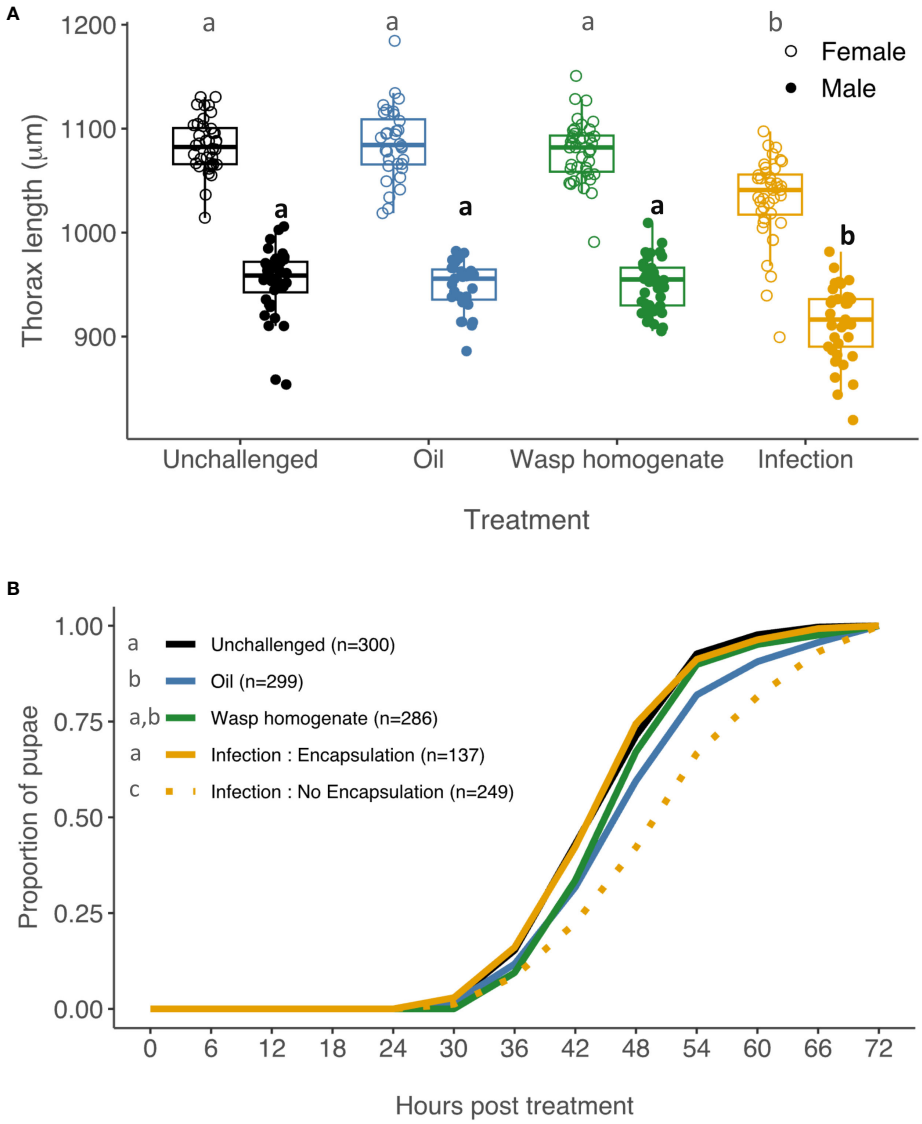

FIGURE 2
Effect of wasp infection and immune activation on body size and development time. Third instar larvae were injected with paraffin oil (blue), wasp homogenate (green) or parasitised by a female wasp (orange). **(A)** Thorax length was measured in females (open circles) and males (filled circles), *n*=27-40. **(B)** The number of larvae that pupated was recorded every 6 hours for 72 hours. Infected pupae were maintained to determine if the fly survived having successfully killed the parasitoid (Encapsulation, orange solid line) or if the wasp survived (No Encapsulation, orange dashed line). Number of tested larvae in parentheses. In all cases, letters show significantly different groups (Tukey's test, $p < 0.05$). In **(A)**, comparisons between males are represented in bold.

Therefore, the immune responses triggered by wasp homogenate cannot explain the reduction in body size following infection.

Infection by parasitoid wasps also causes a developmental delay (12). By the time they pupate, *Drosophila* that were infected as larvae have either mounted a successful immune response and encapsulated the parasitoid egg, or they have a living wasp larva feeding on their hemolymph. For this reason, when measuring the pupation timing of infected larvae, we distinguished between these two phenotypes. Interestingly, we observed that larvae that were successful in encapsulating the parasitoid egg did not have a developmental delay (Figure 2B, orange solid line, unchallenged vs. encapsulation: z = 0.04, p = 1). Larvae where the immune response failed and the parasite survived had a significant developmental delay of ~6 h (Figure 2B, orange dashed line, unchallenged vs. no encapsulation: z = 7.96, p = 1.78 x 10^{-14}). This developmental delay was also highly significant when compared to larvae injected with either oil or oil and wasp homogenate (Figure 2B).

There was also a smaller cost to injecting oil, which may reflect harm caused by our injection protocol. The injection of oil caused a small developmental delay (Figure 2B; unchallenged vs. oil: z = 4.85, p = 1.25 x 10^{-5}). The development time of the oil-injected flies did not differ significantly from larvae injected with oil containing wasp homogenate (wasp homogenate vs. oil: z = 2.35, p = 0.18).

Discussion

Immune responses require drastic changes in gene expression and cell differentiation, and the energy necessary for these processes must be redirected from other traits. In addition, immune responses can damage the host's own tissues. Both effects can result in trade-offs between immune competence and other fitness-related traits. However, to detect and quantify these trade-offs, it is necessary to have an artificial system to trigger the immune response, excluding the negative effects of virulence factors delivered by parasites. For example, the antibacterial immune response in mammals can be triggered by injecting LPS (5). In insects, the encapsulation response has been activated using materials such as nylon strings (24). In *Drosophila*, paraffin oil can activate the encapsulation response in some species (25), but this is less successful in *D. melanogaster* (26). Here, we exploited a technique we developed recently that involves injecting paraffin oil containing wasp homogenate (available as a preprint, 22). We found that the wasp homogenate in the oil triggers physiological changes that have been associated with costly immune responses, and the magnitude of these immune responses is similar to the response to natural infection by a parasitoid wasp. First, injection of wasp homogenate induces melanisation, which in other insect species is known to damage host tissues (6). Second, it induces an increase in the number of circulating hemocytes and the differentiation of lamellocytes. Finally, the injection of wasp homogenate causes flies to become hyperglycaemic. This is a signature of a metabolic switch previously reported with parasitoid infection (12), which is thought to underlie the reallocation of energy from development to the immune system. Importantly, our data demonstrate that this metabolic shift is triggered by immune challenge and is neither a manipulation by the parasitoid wasp nor an indirect effect of the wasp damaging host tissues.

The development of a technique to trigger the immune response allowed us to investigate whether the reduction in fitness suffered by flies that survive infection is a consequence of a costly immune response. The induction of the immune response is likely due to a pathogen associated molecular pattern (PAMP) present in adult wasps and not in the venom, since immune readouts are similar between wasp homogenate prepared with males or females. While the injection of oil droplets induces little transcriptional response in the fat body, injection of wasp homogenate induces a transcriptional response that resembles the one induced by parasitoid infection (22).

In agreement with past work, we found that infection by parasitoid wasps causes a reduction in body size (13). This is likely to reflect a reduction in fitness—for example, artificial selection experiments have found that smaller *D. melanogaster* males have lower fecundity and longevity (27). However, when we activated the immune response by injecting wasp homogenate, it did not affect body size. As we observed a reduction in body size in infected animals held under the same conditions, this suggests that this is not being caused by the immune responses triggered by wasp extract, which includes lamellocyte differentiation, a humoral response and hyperglycemia. Alternatively, smaller larvae could be more resistant to parasitoid infection, resulting in smaller adult in parasitized conditions. However, this scenario is unlikely since selection for *L. boulardi* resistance in *D. melanogaster* does not change body size over the generations (28).

This suggests that the cost of infection is caused by the parasite directly harming its host. As we are studying flies that succeed in killing the parasite, the parasite is normally killed as an egg before it can directly damage host tissues by feeding at the larval stage. Instead, the likely causes of reduced body size are the virulence factors injected by the female wasp at the time of infection or secreted by the developing wasp embryo. Similar reductions in body size have been observed with infections by another parasitoid species, *Asobara tabida* (13), which is very distantly related to *L. boulardi*. As these species have very different venom compositions (29), it is unclear whether there is a common mechanism for the reduction in body size caused by these different parasites. Combined with efforts to describe venom composition in parasitoid wasps (21, 30), it is now worth pursuing which venoms affect the fitness-related traits in the host.

An alternative explanation of why the wasp homogenate injection does not carry the same costs as infection is that it does not trigger the same immune response as a wasp egg. This was not the case for the traits we measured. Most notably, the wasp homogenate and infection induced similar levels of hyperglycaemia and lamellocyte differentiation, and these are the responses that have previously been thought to underlie the cost of infection (12). In a separate study we have used RNA sequencing (RNAseq) to investigate the effect of wasp homogenate on gene expression (22). In hemocytes, the treatment significantly altered the expression of 3886 genes, which allowed us to use our published single-cell RNAseq data to infer how the hemocyte population had

changed (11, 22). This revealed a response to wasp homogenate that resembles the response to wasp infection (11). Not only did mature lamellocytes differentiate, but there are also increases in the proportion of immature lamellocytes—cells that morphologically resemble plasmatocytes and therefore could not be detected in the experiments reported here (11). We also used RNAseq and quantitative PCR (qPCR) to measure gene expression in the fat body, which is the primary organ in the humoral immune response (11). This confirmed that wasp homogenate upregulates Bomanins, which are a family of genes regulated by the Toll pathway (31). *Tep1* and *Tep2*, which are regulated by the JAK-STAT and Toll pathways (32), also increased in expression. Similarly, *IBIN*, which is regulated by the Toll and IMD pathways (33), was upregulated, as was *TotC*, which is regulated by the JAK-STAT pathway (34). Together these results indicate that the JAK-STAT and Toll pathways, which play a key role in the immune response to parasitoid wasps, are upregulated by wasp extract. Furthermore, upregulated genes are known to have important functions. Wasp extract increased the expression of both *Tep1* and *Lectin-24a* (35), which play a role in killing parasitoids, and *IBIN*, which affects blood sugar levels (33). However, it is possible that the duration of these responses or some other response that we did not measure may differ between natural infection and our experimental induction of the immune response. Moreover, it would be valuable to investigate whether the translation of upregulated immune genes is similar in both conditions, as transcription and translation do not always display a linear relationship during the insect immune response (36) and can underpin different costs.

Apart from the costs of deploying an immune response, that are manifested following infection, there can also be costs of maintenance of immune defences, that are manifested in the absence of infection. *D. melanogaster* populations selected to resist parasitoid infection have reduced competitive ability in low food conditions (37, 38), demonstrating that resistance to parasitoid wasps is costly to maintain. These populations show altered hemocyte composition in circulation, which is believed to be the cause for higher resistance and possibly for the cost of maintenance. It would be interesting to understand if immune activation with wasp homogenate induces costs in larva competitive ability with low food availability.

In line with past work, we found that flies that had been parasitised developed slower than uninfected controls. Again, we were unable to mimic this effect by upregulating the immune response. Here, the explanation was straightforward, as the developmental delay was found only in larvae that had failed to mount a successful immune response and contained a live parasite. This suggests that the developmental delay may be due to direct damage caused by the parasite. Developmental delay of the host can be beneficial for some parasitoid wasps (18). This could be the case for *L. boulardi*, for example, to guarantee that the host larva reaches an appropriate size. Alternatively, the developmental delay can be caused by an immune response that continued for a longer period in the larvae that failed to kill the parasite. Regardless, the developmental delay is of little evolutionary relevance for the host, as the flies will all be killed during the pupal stage by the parasite.

In an elegant study, Bajgar and colleagues showed that during parasitoid infection, nutrients are relocated from development into the differentiation of new immune cell types, particularly lamellocytes (12). This metabolic switch is dependent on sensing extracellular adenosine taken up by the adenosine receptor (AdoR). *AdoR* mutants produce fewer lamellocytes upon infection and, strikingly, show no developmental delay or reduction in body size (12). This result is surprising considering our data, as their results suggest that the reallocation of resources to the immune response underlies the costs of infection. One explanation of the apparent conflict between this result and our observations is that these costs result from an interaction between the effects of wasp infection and the host response, which is dependent on AdoR. For example, virulence factors may damage hosts only when there is an AdoR-mediated change to host metabolism. Alternatively, the genetic background of the *AdoR* mutants may have made them respond differently to infection. As fewer flies survive infection in the absence of the AdoR-mediated reallocation of resources to immunity, it is possible that those that do survive manage to kill the parasite larva immediately upon infection and are less seriously affected by parasite-secreted virulence factors.

Our results indicate that the large cost of infection seen in flies that survive parasitoid attack is not reproduced by experimental immune activation. Therefore, there may not be selection to moderate the magnitude of this aspect of the immune response if that reduces the probability of killing the parasite. This is particularly the case for this system, as failure to kill the parasite inevitably results in death. However, it is still possible that the activation of immune defences against parasitoid wasps may carry costs we were not able to measure. First, if we had measured the immune response at different times or other immune traits, we may have found a larger response in the presence of the wasp. This could be addressed by directly testing the fitness effects of exposure to virulence factors. Second, immune induction may affect fitness components we did not measure, or costs may only become apparent in certain environments. For example, our experiments were performed with food *ad libitum*, and some costs associated with immune defence are only visible with limited food resources (39).

Methods

D. melanogaster and *L. boulardi* maintenance

A wild-type *D. melanogaster* population was maintained with nonoverlapping generations with 200 flies per generation (11). Flies in this population encapsulate approximately 10% of the wasp strain used in our experiments (11). In each generation, flies were allowed to lay eggs overnight in 90 mm diameter agar plates (per 1500 ml water: 45 g agar, 50 g dextrose, 500 ml apple juice, 30 ml Nipagin 10% w/v) spread with a thin layer of yeast paste (Saccharomyces cerevisiae – Sigma–Aldrich #YSC2). Eggs were washed and removed with phosphate buffered saline (PBS) and a paintbrush, collected in 15 ml centrifuge tubes and allowed to settle

on the bottom of the tube. Five hundred microliters of egg solution was transferred into a 1.5 ml microcentrifuge tube. Five microliters of egg suspension was transferred into plastic vials with cornmeal food (per 1200 ml water: 13 g agar, 105 g dextrose, 105 g maize, 23 g yeast, 35 ml Nipagin 10% w/v) and incubated at 25°C for 12-15 days in a 14-hr light/10-hr dark cycle and 70% humidity.

Leptopilina boulardi strain G486 (40) was maintained in a susceptible *D. melanogaster* outcrossed population named CAMOP2. Cornmeal vials were prepared with 6 µl of eggs as described above. Two female wasps and one male were added to each vial. Vials were incubated for 24 days at 25°C in a 14-hr light/10-hr dark cycle and 70% humidity. Adult wasps were collected and maintained in cornmeal vials with a drop of honey.

Immune challenge treatments

To prepare wasp homogenate, 20 *L. boulardi* males were collected into a 0.5 mL microcentrifuge tube and homogenised in 200 µL of paraffin oil with a pestle. The wasp homogenate was centrifuged for 2 minutes at 300xg, and the supernatant was transferred into a new 0.5 mL microcentrifuge tube. Centrifugation was repeated, and the supernatant was transferred into a new 0.5 mL microcentrifuge tube.

Flies were allowed to lay eggs for four hours, and egg suspensions were prepared as described above. Fifteen microliters of eggs in PBS were then pipetted onto 50 mm diameter cornmeal plates and incubated at 25°C for 72 hours. Using forceps, 40 early 3rd instar larvae per sample were gently collected and transferred onto filter paper. For unchallenged controls, larvae were directly transferred into a cornmeal vial by wetting the filter paper with double-distilled water (ddH_2O) and collecting the larvae with forceps. For parasitism, the larvae were transferred into a cornmeal vial and exposed to three female G486-strain wasps for three hours. For injections, glass needles were prepared from 3.5" long borosilicate glass capillaries (Drummond Scientific Co. 3-000-203-G/X) pulled in a needle puller (Narishige PC-10). The needles were backfilled with paraffin oil or wasp homogenate, and 4.6 nL was injected into each of the 40 early third instar larvae that had been collected onto filter paper. The larvae were then transferred into a cornmeal vial. All vials were incubated at 25°C, 70% humidity and a 14-hour light/10-hour dark cycle.

Hemocyte counts

A 15% w/v sugar solution was added to the vials to suspend the larvae, and 10-12 larvae were collected from each vial. The larvae were washed in double-distilled water (ddH2O), dried on filter paper and transferred into a cavity of a porcelain spot plate. The larvae were bled by tearing the cuticle of their ventral side, and 2 µL of hemolymph was diluted into 8 µL of Neutral Red staining solution (1.65 g/L PBS – Sigma–Aldrich #N2889). The stained hemolymph samples were loaded into hemocytometers (Thoma), and the numbers of plasmatocytes and lamellocytes in 0.1 µL were recorded. Hemocyte counts were performed at 24 hours post-treatment.

Quantitative PCR

Larvae were transferred into cornmeal vials to be incubated in the constant temperature (CT) room for an additional 18 hours. The larvae were suspended in 15% w/v sugar solution, and 30 larvae from each vial were collected using forceps. The larvae were washed with ddH2O and dried on filter paper. Ten larvae from each vial were collected into 0.5 mL microcentrifuge tubes containing 1.0 mm diameter zirconia beads. Then, 250 µL of TRIzol reagent was added to each sample, and the samples were homogenised using a Qiagen Retsch MM300 TissueLyser set at a vibrational frequency of 25 Hz for 2 minutes. Samples were stored at -80°C.

For RNA extraction, samples were defrosted at room temperature and centrifuged for 10 minutes at 12,000xg and 4°C. Then, 160 µL of the supernatant was pipetted into a new 1.5 mL microcentrifuge tube, and 62.5 µL of chloroform was added to each tube. The tubes were shaken for 15 seconds and incubated at room temperature for 3 minutes. Following this, samples were then centrifuged for 10 minutes at 12,000xg and 4°C. A total of 66 µL of the aqueous phase was transferred into a new 1.5 mL microcentrifuge tube, and 156 µL of isopropanol was added to each sample. Tubes were inverted 5 times to mix the components thoroughly and incubated at room temperature for 10 minutes. Samples were then centrifuged for 10 minutes at 12,000xg and 4°C, and the supernatant of each sample was discarded. The pellets were washed with 250 µL of 70% ethanol and centrifuged for 2 minutes at 12,000xg and 4°C. The ethanol was discarded, and the pellet was dried. Then, 20 µL of nuclease-free water was added, and the samples were incubated at 45°C for 10 minutes. Samples were stored at -80°C.

For cDNA synthesis, samples were defrosted and kept on ice. cDNA was synthesised using the GoScript Reverse Transcription System Kit (Promega) following the manufacturer's instructions. For quantitative real-time PCR (qPCR) on an Applied Biosystems StepOnePlus system, the SensiFASTTM Hi-Rox® SYBR kit (Bioline) was used. Primers used for the genes of interest: BomS1 (BomS1_Fw: 5'-ACCGGAGAAATCCATCCAGA-3'; BomS1_Rev: 5'-CGACAGTGGAACAGCATTGG-3'), Tep1 (Tep1_Fw: 5'-ACTGGAAGCCTCATTGGTCG-3'; Tep1_Rev: 5'-ACCGACAATGGGAACAGGAC-3') and PPO3 (PPO3_Fw: 5'-GATGTGGACCGGCCTAACAA-3'; PPO3_Rev: 5'-GATGCCCTTAGCGTCATCCA-3'), and for *RpL32* (RpL32_Fw: 5'-TGCTAAGCTGTCGCACAAATGG-3'; RpL32_Rev: 5'-TGCGCTTGTTCGATCCGTAAC-3') to normalise gene expression. A technical replicate was completed for each biological sample.

Thorax measurements

Emerging adult fruit flies were collected and frozen at -20°C in 50 mm plates. The right wing of each fly was removed. Each fly was then positioned on a microscope slide, resting on their left side. Using a Leica Brightfield stereoscope mounted with a GXCapture camera, images of the thorax were taken, and measurements were

recorded using ImageJ software. The thorax was measured as shown in Supplementary Figure 2.

Circulating glucose quantification

The larvae were transferred into cornmeal vials and incubated in the CT room for an additional 24 hours. The larvae were suspended in 15% w/v sugar solution and collected using forceps. All 40 larvae from each vial were washed with ddH2O and dried on filter paper.

They were then transferred into a cavity of a porcelain spot plate and rapidly bled by tearing the cuticle of the ventral side. Eight microliters of hemolymph was collected and added to a 0.5 mL microcentrifuge tube containing 8 µL of PBS (pH 7.2). The samples were centrifuged for 5 minutes at 800xg and 4°C. Then, 4 µL of each sample was pipetted into a new 0.5 mL microcentrifuge tube to be used for protein quantification. Ten microliters of each sample was pipetted into another 0.5 mL microcentrifuge tube and heat-shocked at 75°C for 5 minutes. These were used for glucose quantification. If not for immediate use, samples were frozen at -80°C.

To measure the glucose concentration of each sample from a standard curve, 16 µL of 1 mg/mL glucose standard was diluted in 84 µL of PBS (pH 7.2) to a concentration of 0.16 mg/mL. From this, four 2-fold serial dilutions were made, resulting in standards ranging from 0.01 mg/mL to 0.16 mg/mL. Then, 30 µL of the glucose standards and a PBS blank were pipetted into the wells of a Falcon 96 Well U-Bottom Tissue Culture Treated plate. The hemolymph samples were centrifuged for 5 minutes at 10,000xg and 4°C. The samples were further diluted by adding 5 µL of each sample to 25 µL of PBS. Then, 30 µL of each diluted sample was pipetted into the same plate. The GO assay reagent was prepared from the Glucose (GO) Assay Kit (Sigma–Aldrich®) following the manufacturer's instructions and maintained on ice. Then, 100 µL of the reagent was added to each well containing the glucose standards and the samples. The plate was covered with a lid and incubated at 37°C for 30 minutes. The reactions in the plate were stopped by adding 100 µL of 12 N H2SO4 to the wells. The plate was centrifuged in a swing bucket motor to remove bubbles. Using a SpectraMax id3 Multi-Mode Microplate Reader, the absorbance of each sample was measured at 540 nm. A standard curve for glucose concentrations was created using the absorbance readings of the standards, and the glucose concentrations of the undiluted hemolymph samples were calculated.

To measure the protein concentration of each sample from a standard curve, standards ranging from 0.2 mg/mL to 1.4 mg/mL bovine serum albumin (BSA), which increased in increments of 0.2 mg/mL, were made by diluting 2 mg/mL BSA standard in PBS (pH 7.2). Ten microliters of the BSA standards and a PBS blank were pipetted into the wells of a Falcon 96 Well U-Bottom Tissue Culture Treated plate. The hemolymph samples were centrifuged for 5 minutes at 10,000xg and 4°C. The samples were further diluted by adding 2 µL of each sample to 198 µL of PBS. Then, 10 µL of each diluted sample was pipetted into the same plate. Bradford reagent (200 µL) was added to each well containing the BSA standards and the samples. After 5 minutes, the absorbance of each sample was measured at 595 nm using a SpectraMax id3 Multi-Mode Microplate Reader. A standard curve for protein concentrations was created using the absorbance readings of the standards, and the protein concentrations of undiluted hemolymph samples were calculated. The circulating glucose in the hemolymph of 40 larvae was calculated by dividing the glucose concentration of each sample by the protein concentration.

Data availability statement

The datasets presented in this study can be found in online repositories. The names of the repository/repositories and accession number(s) can be found below: https://www.repository.cam.ac.uk; https://doi.org/10.17863/CAM.104190.

Ethics statement

The manuscript presents research on animals that do not require ethical approval for their study.

Author contributions

AL: Conceptualization, Funding acquisition, Supervision, Writing – original draft, Data curation, Formal Analysis, Investigation, Methodology, Visualization. EG: Investigation, Writing – review & editing. FJ: Conceptualization, Funding acquisition, Supervision, Writing – original draft.

Funding

The author(s) declare financial support was received for the research, authorship, and/or publication of this article. This work was funded by a Natural Environment Research Council grant (NE/P00184X/1) to FJ and AL. AL was also supported by the European Molecular Biology Organization fellowship (ALT-1556).

Conflict of interest

The authors declare that the research was conducted in the absence of any commercial or financial relationships that could be construed as a potential conflict of interest.

Publisher's note

that may be evaluated in this article, or claim that may be made by its manufacturer, is not guaranteed or endorsed by the publisher.

Supplementary material

The Supplementary Material for this article can be found online at: https://www.frontiersin.org/articles/10.3389/fimmu.2023.1275923/full#supplementary-material

SUPPLEMENTARY FIGURE 1
Outcome of immune challenges. 3rd instar larvae were injected with paraffin oil (blue), wasp homogenate (green) or parasitized by a female wasp (orange). 48h post treatment, oil droplets injected with wasp homogenate become melanized **(C´)**, while oil droplets injected alone remain un-melanized **(B´)**. Cuticle melanization of the wound caused by the needle can be observed (arrows in **(B)** and **(C)**). When infected by a wasp, a wasp larva **(D')** or a melanized capsule **(D'')** can be observed.

SUPPLEMENTARY FIGURE 2
Measurement of thorax length.

References

1. Sánchez J, Holmgren J. Cholera toxin structure, gene regulation and pathophysiological and immunological aspects. *Cell Mol Life Sci* (2008) 65:1347–60. doi: 10.1007/s00018-008-7496-5

2. Schwenke RA, Lazzaro BP, Wolfner MF. Reproduction-immunity trade-offs in insects. *Annu Rev Entomology* (2016) 61:239–56. doi: 10.1146/annurev-ento-010715-023924

3. Libert S, Chao Y, Chu X, Pletcher SD. Trade-offs between longevity and pathogen resistance in *Drosophila melanogaster* are mediated by NFκB signaling. *Aging Cell* (2006) 5:533–43. doi: 10.1111/j.1474-9726.2006.00251.x

4. Sadd BM, Schmid-Hempel P. Principles of ecological immunology. *Evolutionary Appl* (2009) 2:113–21. doi: 10.1111/j.1752-4571.2008.00057.x

5. Ganeshan K, Nikkanen J, Man K, Leong YA, Sogawa Y, Maschek JA, et al. Energetic trade-offs and hypometabolic states promote disease tolerance. *Cell* (2019) 177:399–413.e12. doi: 10.1016/j.cell.2019.01.050

6. Sadd BM, Siva-Jothy MT. Self-harm caused by an insect's innate immunity. *Proc R Soc B: Biol Sci* (2006) 273:2571–4. doi: 10.1098/rspb.2006.3574

7. Bashir-Tanoli S, Tinsley MC. Immune response costs are associated with changes in resource acquisition and not resource reallocation. *Funct Ecol* (2014) 28:1011–9. doi: 10.1111/1365-2435.12236

8. Cressler CE, Graham AL, Day T. Evolution of hosts paying manifold costs of defence. *Proc R Soc B: Biol Sci* (2015) 282:20150065. doi: 10.1098/rspb.2015.0065

9. Boots M, Best A. The evolution of constitutive and induced defences to infectious disease. *Proc R Soc B: Biol Sci* (2018) 285:20180658. doi: 10.1098/rspb.2018.0658

10. Shudo E, Iwasa Y. Inducible defense against pathogens and parasites: Optimal choice among multiple options. *J Theor Biol* (2001) 209:233–47. doi: 10.1006/jtbi.2000.2259

11. Leitão AB, Arunkumar R, Day JP, Geldman EM, Morin-Poulard I, Crozatier M, et al. Constitutive activation of cellular immunity underlies the evolution of resistance to infection in *Drosophila*. *eLife* (2020) 9:e59095. doi: 10.7554/eLife.59095

12. Bajgar A, Kucerova K, Jonatova L, Tomcala A, Schneedorferova I, Okrouhlik J, et al. Extracellular adenosine mediates a systemic metabolic switch during immune response. *PloS Biol* (2015) 13:1–23. doi: 10.1371/journal.pbio.1002135

13. Fellowes MDE, Kraaijeveld AR, Godfray HCJ. The relative fitness of *Drosophila melanogaster* (Diptera , Drosophilidae) that have successfully defended themselves against the parasitoid Asobara tabida (Hymenoptera , Braconidae). *J evolutionary Biol* (1999) 12:123–8. doi: 10.1046/j.1420-9101.1999.00018.x

14. Wertheim B, Kraaijeveld AR, Schuster E, Blanc E, Hopkins M, Pletcher SD, et al. Genome-wide gene expression in response to parasitoid attack in *Drosophila*. *Genome Biol* (2005) 6:R94. doi: 10.1186/gb-2005-6-11-r94

15. Schlenke TA, Morales J, Govind S, Clark AG. Contrasting infection strategies in generalist and specialist wasp parasitoids of *Drosophila melanogaster*. *PloS Pathog* (2007) 3:1486–501. doi: 10.1371/journal.ppat.0030158

16. Kim-Jo C, Gatti JL, Poirié M. *Drosophila* cellular immunity against parasitoid wasps: A complex and time-dependent process. *Front Physiol* (2019) 10:603. doi: 10.3389/fphys.2019.00603

17. Dudzic JP, Kondo S, Ueda R, Bergman CM, Lemaitre B. *Drosophila* innate immunity: regional and functional specialization of prophenoloxidases. *BMC Biol* (2015) 13:81–97. doi: 10.1186/s12915-015-0193-6

18. Moreau SJM, Asgari S. Venom proteins from parasitoid wasps and their biological functions. *Toxins* (2015) 7:2385–412. doi: 10.3390/toxins7072385

19. Huang J, Chen J, Fang G, Pang L, Zhou S, Zhou Y, et al. Two novel venom proteins underlie divergent parasitic strategies between a generalist and a specialist parasite. *Nat Commun* (2021) 12(1):234. doi: 10.1038/s41467-020-20332-8

20. Labrosse C, Eslin P, Doury G, Drezen JM, Poirié M. Haemocyte changes in *D. Melanogaster* in response to long gland components of the parasitoid wasp *Leptopilina boulardi*: a Rho-GAP protein as an important factor. *J Insect Physiol* (2005) 51:161–70. doi: 10.1016/j.jinsphys.2004.10.004

21. Goecks J, Mortimer NT, Mobley JA, Bowersock GJ, Taylor J, Schlenke TA. Integrative approach reveals composition of endoparasitoid wasp venoms. *PloS One* (2013) 8:e64125. doi: 10.1371/journal.pone.0064125

22. Leitão AB, Arunkumar R, Day JP, Hanna N, Devi A, Hayes MP, et al. Recognition of non-self is necessary to activate *Drosophila*'s immune response against an insect parasite. *bioRxiv* (2022) 2022:6.28.497890. doi: 10.1101/2022.06.28.497890

23. Kenmoku H, Hori A, Kuraishi T, Kurata S. A novel mode of induction of the humoral innate immune response in *Drosophila larvae*. *Dis Models Mech* (2017) 10:271–81. doi: 10.1242/dmm.027102

24. Siva-Jothy MT. A mechanistic link between parasite resistance and expression of a sexually selected trait in a damselfly. *Proc R Soc B: Biol Sci* (2000) 267:2523–7. doi: 10.1098/rspb.2000.1315

25. Dubuffet A, Doury G, Labrousse C, Drezen J-M, Carton Y, Marylène P. Variation of success of *Leptopilina boulardi* in *Drosophila yakuba* : The Variation of success of *Leptopilina boulardi* in *Drosophila yakuba* : The mechanisms explored. *Dev Comp Immunol* (2008) 32:597–602. doi: 10.1016/j.dci.2007.10.009

26. Moreau SJM, Eslin P, Giordanengo P, Doury G. Comparative study of the strategies evolved by two parasitoids of the genus Asobara to avoid the immune response of the host, *Drosophila melanogaster*. *Dev Comp Immunol* (2003) 27:273–82. doi: 10.1016/S0145-305X(02)00101-5

27. Reeve MW, Fowler K, Partridge L. Increased body size confers greater fitness at lower experimental temperature in male *Drosophila melanogaster*. *J Evolutionary Biol* (2000) 13:836–44. doi: 10.1046/j.1420-9101.2000.00216.x

28. Fellowes MD, Kraaijeveld a R, Godfray HC. Trade-off associated with selection for increased ability to resist parasitoid attack in *Drosophila melanogaster*. *Proc Biol Sci / R Soc* (1998) 265:1553–8. doi: 10.1098/rspb.1998.0471

29. Eslin P, Giordanengo P, Fourdrain Y, Prevost G. Avoidance of encapsulation in the absence of VLP by a braconid parasitoid of *Drosophila larvae*: An ultrastructural study. *Can J Zoology* (1996) 74(12):2193–8. doi: 10.1139/z96-248

30. Cavigliasso F, Mathé-Hubert H, Kremmer L, Rebuf C, Gatti J-L, Malausa T, et al. Rapid and differential evolution of the venom composition of a parasitoid wasp depending on the. *Toxins* (2019) 11:629. doi: 10.3390/toxins11110629

31. Clemmons AW, Lindsay SA, Wasserman SA. An effector peptide family required for *drosophila* toll-mediated immunity. *PloS Pathog* (2015) 11:e1004876. doi: 10.1371/journal.ppat.1004876

32. Lagueux M, Perrodou E, Levashina EA, Capovilla M, Hoffmann JA. Constitutive expression of a complement-like protein in Toll and JAK gain-of-function mutants of *Drosophila*. *Proc Natl Acad Sci* (2002) 97:11427–32. doi: 10.1073/pnas.97.21.11427

33. Valanne S, Salminen TS, Järvelä-Stölting M, Vesala L, Rämet M. Immune-inducible non-coding RNA molecule lincRNA-IBIN connects immunity and metabolism in *Drosophila melanogaster*. *PLoS Pathog* (2019), e1007504. doi: 10.1371/journal.ppat.1007504

34. Kinoshita Y, Shiratsuchi N, Araki M, Inoue YH. Anti-Tumor Effect of Turandot Proteins Induced *via* the JAK/STAT Pathway in the mxc Hematopoietic Tumor Mutant in *Drosophila*. *Cells* (2023) 12:2047. doi: 10.3390/cells12162047

35. Arunkumar R, Zhou SO, Day JP, Bakare S, Pitton S, Zhang Y, et al. Natural selection has driven the recurrent loss of an immunity gene that protects *Drosophila* against a major natural parasite. *Proc Natl Acad Sci USA* (2023) 120:e2211019120. doi: 10.1073/pnas.2211019120

36. Cotter SC, Reavey CE, Tummala Y, Randall JL, Holdbrook R, Ponton F, et al. Diet modulates the relationship between immune gene expression and functional immune responses. *Insect Biochem Mol Biol* (2019) 109:128–41. doi: 10.1016/j.ibmb.2019.04.009

37. Kraaijeveld AR, Godfray HCJ. Trade-off between parasitoid resistance and larval competitive ability in *Drosophila Melanogaster*. *Nature* (1997) 389:278–80. doi: 10.1038/38483

38. McGonigle JE, Leitão AB, Ommeslag S, Smith S, Day P, Jiggins FM. Parallel and costly changes to cellular immunity underlie the evolution of parasitoid resistance in three *Drosophila* species. *PloS Pathog* (2017) 13(10):1–20. doi: 10.1371/journal.ppat.1006683

39. Moret Y, Schmid-Hempel P. Survival for immunity: The price of immune system activation for bumblebee workers. *Science* (2000) 290:1166–8. doi: 10.1126/science.290.5494.1166

40. Dupas S, Brehelin M, Frey F, Carton Y. Immune suppressive virus-like particles in a Drosophila parasitoid: Significance of their intraspecific morphological variations. *Parasitology* (1996) 113:207–212. doi: 10.1017/S0031182000081981

frontiers | Frontiers in Immunology

TYPE Original Research
PUBLISHED 21 December 2023
DOI 10.3389/fimmu.2023.1322381

OPEN ACCESS

EDITED BY
Shoichiro Kurata,
Tohoku University, Japan

REVIEWED BY
Lolitika Mandal,
Indian Institute of Science Education and Research Mohali, India
Ryohei Furukawa,
Keio University, Japan

*CORRESPONDENCE
István Andó
ando@brc.hu

†These authors share last authorship

RECEIVED 16 October 2023
ACCEPTED 04 December 2023
PUBLISHED 21 December 2023

CITATION
Cinege G, Magyar LB, Kovács H, Varga V, Bodai L, Zsindely N, Nagy G, Hegedűs Z, Hultmark D and Andó I (2023) Distinctive features of *Zaprionus indianus* hemocyte differentiation and function revealed by transcriptomic analysis.
Front. Immunol. 14:1322381.
doi: 10.3389/fimmu.2023.1322381

Distinctive features of *Zaprionus indianus* hemocyte differentiation and function revealed by transcriptomic analysis

Gyöngyi Cinege[1], Lilla B. Magyar[1,2], Henrietta Kovács[1], Viktória Varga[1], László Bodai[3], Nóra Zsindely[3], Gábor Nagy[3], Zoltán Hegedűs[4,5], Dan Hultmark[6†] and István Andó[1*†]

[1]Innate Immunity Group, Institute of Genetics, HUN-REN Biological Research Centre, Szeged, Hungary, [2]Doctoral School of Biology, University of Szeged, Szeged, Hungary, [3]Department of Biochemistry and Molecular Biology, University of Szeged, Szeged, Hungary, [4]Laboratory of Bioinformatics, HUN-REN Biological Research Centre, Szeged, Hungary, [5]Department of Biochemistry and Medical Chemistry, Medical School, University of Pécs, Pécs, Hungary, [6]Department of Molecular Biology, Umea University, Umea, Sweden

Background: Insects have specialized cell types that participate in the elimination of parasites, for instance, the lamellocytes of the broadly studied species *Drosophila melanogaster*. Other drosophilids, such as *Drosophila ananassae* and the invasive *Zaprionus indianus*, have multinucleated giant hemocytes, a syncytium of blood cells that participate in the encapsulation of the eggs or larvae of parasitoid wasps. These cells can be formed by the fusion of hemocytes in circulation or originate from the lymph gland. Their ultrastructure highly resembles that of the mammalian megakaryocytes.

Methods: Morphological, protein expressional, and functional features of blood cells were revealed using epifluorescence and confocal microscopy. The respective hemocyte subpopulations were identified using monoclonal antibodies in indirect immunofluorescence assays. Fluorescein isothiocyanate (FITC)-labeled *Escherichia coli* bacteria were used in phagocytosis tests. Gene expression analysis was performed following mRNA sequencing of blood cells.

Results: *D. ananassae* and *Z. indianus* encapsulate foreign particles with the involvement of multinucleated giant hemocytes and mount a highly efficient immune response against parasitoid wasps. Morphological, protein expressional, and functional assays of *Z. indianus* blood cells suggested that these cells could be derived from large plasmatocytes, a unique cell type developing specifically after parasitoid wasp infection. Transcriptomic analysis of blood cells, isolated from naïve and wasp-infected *Z. indianus* larvae, revealed several differentially expressed genes involved in signal transduction, cell movements, encapsulation of foreign targets, energy production, and melanization, suggesting their role in the anti-parasitoid response. A large number of genes that encode proteins associated with coagulation and wound healing, such as phenoloxidase activity factor-like

proteins, fibrinogen-related proteins, lectins, and proteins involved in the differentiation and function of platelets, were constitutively expressed. The remarkable ultrastructural similarities between giant hemocytes and mammalian megakaryocytes, and presence of platelets, and giant cell-derived anucleated fragments at wound sites hint at the involvement of this cell subpopulation in wound healing processes, in addition to participation in the encapsulation reaction.

Conclusion: Our observations provide insights into the broad repertoire of blood cell functions required for efficient defense reactions to maintain the homeostasis of the organism. The analysis of the differentiation and function of multinucleated giant hemocytes gives an insight into the diversification of the immune mechanisms.

KEYWORDS

hemocyte, multinucleated giant hemocyte, immune response, *Drosophila*, wound healing, invasive, transcriptome, *Zaprionus indianus*

1 Introduction

Over the course of evolution, mechanisms of the innate immune system have diversified into a broad repertoire of various effector cells, which participate in the production of antimicrobial peptides, phagocytosis of microbes, encapsulation of large particles, blood clotting, wound healing, regeneration, and tissue remodeling. As the transcriptional and epigenetic regulators and the signal transduction pathways are all phylogenetically conserved between insects and vertebrates (1, 2), *Drosophila* has become a well-established model organism for the analysis of cellular innate immune reactions and host–pathogen interactions.

In *Drosophila melanogaster*, four main classes of effector blood cells, called hemocytes, were described: the phagocytic plasmatocytes, the melanizing crystal cells, the encapsulating lamellocytes, and the recently discovered primocytes (PSC-like cells) (3–9). The lamellocytes attach to and spread around large particles, including eggs and larvae of parasitoids, and form a multilayered capsule to block parasitoid development. Genetic variation among fly species for resistance against invaders, and variation in virulence of wasp species against the flies, will determine the effectiveness and success of the defense against parasitoids. We have previously found that several fly species, such as those of the *ananassae* subgroup and *Zaprionus indianus* of the *vittiger* subgroup of Drosophilidae, produce a new encapsulating hemocyte type, a syncytium of blood cells: the highly motile multinucleated giant hemocyte (MGH) (10–12).

Multinucleation is a form of endomitosis, where the completion of mitotic events through nuclear division in the absence of cytokinesis leads to multinucleated cells. Generally, most cells maintain a diploid state, but when there is a demand for high rates of metabolic activity and biosynthesis, amplification of the genome provides an advantage. In many cases, multinucleated cells are of hematopoietic origin (13, 14), and their presence is often associated with infections (15–17). Moreover, multinucleated epidermal cells have been detected around wounds in *Drosophila* larvae, which eliminated intracellular spaces and helped seal the wound site (18). It is clear that multinucleation results in an increase of genetic material, which permits these cells to react quickly and robustly, contributing to an efficient effector function.

Combined immuno-electron microscopic and transcriptomic analysis of *Drosophila ananassae* MGHs revealed that these cells possess a characteristic cellular ultrastructure, which is highly supported by their gene expression profile (12), ensuring efficient defense. Similarly, in the cytoplasm of the *Z. indianus* MGHs, we detected a large number of canals and sinuses that communicate with the extracellular space (11), providing a substantial contact surface between the cell and the environment, which is a considerable metabolic advantage.

We previously showed that MGHs of *Z. indianus* belong to a cell type named giant hemocytes, defined by staining with the 4G7 antibody. In addition to the multinucleated cells, the 4G7-positive cell fraction also comprised elongated, single-nucleated blood cells, named nematocytes (19), and anucleated cell fragments surrounded by the plasma membrane, released from the previous two (11). Giant hemocytes and their anucleated cytoplasmic derivatives are also present in naïve larvae (11). We observed that MGHs of *D. ananassae* and *Z. indianus* formed *via* cell fusion in the circulation (10, 11); however, the hematopoietic organ, the lymph gland of *Z. indianus* also contributed to the formation of these cells (11).

In this study, we aimed to obtain deeper insights into the differentiation and function of the MGHs. We show that *D. ananassae* and *Z. indianus*, species developing MGHs, are highly resistant to parasitoid wasps. Furthermore, in *Z. indianus*, we

identified a novel multinucleated cell type, the spherical "large plasmatocyte", developing specifically after parasitoid wasp infection and representing a new source for differentiation of giant hemocytes responsible for encapsulation of the invader. Transcriptomic analysis revealed differential expression of several genes in the hemocytes of parasitoid wasp-infected samples, which encode for proteins involved in biological processes required in anti-parasitoid defense reactions. In a comparative analysis of *D. melanogaster*, *D. ananassae*, and *Z. indianus* transcriptomes, we present several sets of genes that are responsible for the characteristic features of the highly effective defense against parasitoids and highlight the involvement of an ancient mechanism with the contribution of MGHs.

Moreover, here, we found that the 4G7-positive anucleated fragments released from the giant hemocytes accumulate at the wound sites of both naïve and wasp-induced animals. In line with this, we identified several genes expressed in both uninduced and induced blood cell samples, which possess orthologs of genes involved in the wound healing processes of *D. melanogaster* and mammalian species.

The analysis of MGHs in the highly resistant fruit fly species gives insight into the diversification of the immune mechanisms, which likely have provided evolutionary advantages in a broad range of organisms that develop MGHs.

2 Materials and methods

2.1 Insect stocks and culturing

D. ananassae wild type (14024-0371.13) was obtained from the UC San Diego *Drosophila* stock center. *Z. indianus* wild-type strain #3 (19) was kindly provided by Bálint Z. Kacsoh (University of Pennsylvania, USA). *D. melanogaster* wild type (Oregon-R) was ordered from Bloomington Drosophila Stock Center. Each strain was kept at 25°C on standard yeast-cornmeal food. The *Leptopilina heterotoma* (14) and *Leptopilina victoriae* (UNK) wasp strains were kindly provided by Prof. Todd Schlenke (University of Arizona, USA). Wasps were maintained on *D. melanogaster* Oregon-R.

2.2 Parasitization assay

For infection with the parasitic wasps, 60 early second instar larvae were placed together on vials containing standard yeast-cornmeal food with 15 female wasps for 6 hours at 25°C. For eclosion experiments, 48 h after the wasp infection, 10 larvae were dissected from each vial and scored for the presence of the parasitoid eggs or larvae. If each of the 10 tested larvae carried parasitoids, we considered the rest of the samples from the respective vial 100% infected. Following pupariation, the number of eclosed fly and wasp adults was counted, and their proportion was determined. The results of four independent experiments are shown.

2.3 Injury and microbead injection

Early second instar larvae were washed in *Drosophila* Ringer solution and one by one placed on a sterile Petri dish for the respective treatment, which was carried out on the dorsal part of the fifth segment, using sterile, 100-µm-diameter minutien pins or a glass capillary. For septic injury, before treatment, the sterile minutien pins were dipped in a 1:1 mixture of concentrated overnight grown Gram-positive (*Bacillus subtilis*, SzMC 0209) and Gram-negative (*Escherichia coli*, SzMC 0582) bacterial suspension (both bacteria obtained from the Szeged Microbial Collection, University of Szeged, Hungary) or a 50% concentrated suspension of *Beauveria bassiana* entomopathogenic fungus spores (Kwizda Agro, Artis Pro) in sterile phosphate-buffered saline (PBS). For injection, a volume of 0.1 µl of 15-µm-diameter FluoSpheres polystyrene microbeads (Invitrogen, Carlsbad, CA, USA) in sterile *Drosophila* Ringer solution was injected into the larvae at the dorsal part of the fifth segment. A control sterile *Drosophila* Ringer solution was used. After injury or injection, the larvae were carefully transferred into a vial with standard yeast-cornmeal food and used after 48 h for blood cell differentiation assays. For wound healing experiments, early third instar naïve or *L. victoriae*-infected larvae were wounded using a sterile minutien needle as described above, and after a 2-h incubation time, cuticle samples were prepared and immunostaining was carried out.

2.4 Video microscopy

Seventy-two hours after *L. victoriae* wasp infection, larvae were dissected in Complete Schneider's medium (CSM): Schneider's medium (Lonza, Basel, Switzerland) supplemented with 5% fetal bovine serum (GIBCO, Grand Island, NY, USA) and 0.01% 1-phenyl-2-thiourea (Sigma, Darmstadt, Germany). The live hemocytes were analyzed using an Alpha XDS-1T inverted microscope at room temperature. Photographs were taken using a Nikon D5300 DSLR camera. Shooting duration was 75 min with 13-s intervals (Supplementary Movie 1). The images were edited using the Adobe Lightroom CC 2015 program, and the movie was made using FIJI (https://fiji.sc/). Olympus Fluoview and Olympus 3D viewer software were used to prepare the 3D animation of the 4G7 and DAPI-stained wound site.

2.5 Preparation of hemocyte and cuticle samples

For hemocyte samples, larvae were dissected at respective time points in CSM on glass microscope slides. Blood cells were adhered to the glass surface for 1 h, followed by fixation with acetone for 6 min, air-dried, and blocked with 0.1% bovine serum albumin (BSA) in PBS for 20 min. For cuticle preparations, larvae were opened in CSM along the longitudinal axis, and the digestive tracts and fat bodies were removed. The carcasses were then fixed in 2%

paraformaldehyde for 10 min, washed three times for 5 min in PBS, and blocked with 0.1% BSA in PBS supplemented with 0.01% Triton X-100 for 20 min. Samples were incubated with the antibodies as described below.

2.6 Antibodies and indirect immunofluorescence

After blocking, hemocytes and cuticle preparations were incubated with the primary antibodies for 1 h at room temperature. The 5C3 antibody reacted with spherical cells of different sizes, the plasmatocytes, the 4G7 specific for the giant hemocytes, a subpopulation of cells including bi- or multinucleated giant hemocytes, nematocytes (elongated blood cells with a single nucleus), and filariform anucleated structures (11). The anti-human CD45, T2/48 antibody (20) was used as the negative control. The monoclonal antibodies were generally used as undiluted hybridoma supernatants. Following incubation with the primary antibodies, samples were washed three times for 5 min in PBS and incubated with the secondary antibodies for 45 min. As a secondary antibody, the anti-mouse Alexa Fluor 488 goat antibody (Invitrogen, 1:1,000 dilution) was used. For double staining, a 1:1 mixture of the anti-mouse IgM Cross-Adsorbed fluorescein isothiocyanate (FITC) (P.A.R.I.S. 1:1,000 dilution) and anti-mouse IgG2a Cross-Adsorbed Alexa Fluor 568 (Invitrogen, 1:1,000 dilution) secondary antibodies were used. To visualize the nuclei, DAPI (Sigma) at a concentration of 2.5 µg/ml was added to the secondary antibodies. After incubation with the secondary antibodies, samples were washed three times for 5 min and covered with Fluoromount-G medium and a coverslip. Samples were analyzed using a Zeiss Axioscope 2MOT epifluorescence or an Olympus FV1000 confocal microscope.

2.7 Cell measurements, detection of the large plasmatocytes, and statistics

For each sample, hemocyte images of two randomly selected areas were acquired using the 20× objective of a Zeiss Axioscope 2MOT epifluorescence microscope. Cell measurements and hemocyte counts were determined with the ImageJ program (http://imagej.nih.gov/ij/) using microscopic images with standard size, resolution, and magnification. The cell areas were normalized to that of naïve plasmatocytes; therefore, the average area of plasmatocytes was set to 1. As the naïve plasmatocytes possessed lower relative areas than 5 (5 times the average size of naïve plasmatocytes), 5C3-positive cells, which exhibited larger areas, were considered to be large plasmatocytes. Images captured in three independent experiments were analyzed using at least 30 larvae in each. A relative area of 2,000 randomly selected cells is shown. The significance of the differences was determined by Student's *t*, one-way ANOVA, and Tukey's honestly significant difference (HSD) tests.

2.8 *In vivo* phagocytosis assay

The phagocytosis assay was carried out on *L. victoriae* parasitoid wasp-induced *Z. indianus* larvae as described previously (11). The results of three independent experiments, with 24 larvae in each, were combined.

2.9 Collection of samples for sequencing library preparation, RNA sequencing, and bioinformatic analysis of transcriptome data

For transcriptomic analysis, blood cells from 100 age-matched uninduced and 100 *L. victoriae*-induced (72 hours after the parasitoid wasp infection) *Z. indianus* larvae were harvested, and RNA was isolated using an RNeasy mini kit (Qiagen, Valencia, CA, USA). Three parallel samples were used for each group. The quantity and integrity of total RNA samples were determined by capillary gel electrophoresis using a 2100 Bioanalyzer instrument (Agilent, Santa Clara, CA, USA) using Agilent RNA 6000 Nano Kit. For RNA sequencing, mRNA was isolated from 220 ng total RNA per sample using a NEBNext Poly(A) mRNA Magnetic Isolation Module (New England Biolabs (NEB), Ipswich, MA, USA); then, strand-specific sequencing libraries were generated using a NEBNext Ultra II Directional RNA Library Prep Kit for Illumina (NEB) with NEBNext Multiplex Oligos for Illumina (NEB) following the protocol of the manufacturer. Indexed sequencing libraries were validated and quantitated using an Agilent DNA 1000 kit in a 2100 Bioanalyzer instrument; then, libraries were pooled in equimolar ratios. After denaturing, the library pool was diluted to 15-pM concentration and sequenced in a MiSeq DNA sequencer (Illumina, San Diego, CA, USA) using a MiSeq Reagent Kit v3 (150-cycle) producing 2 × 75 bp paired-end reads. Base calling and generation of FASTQ sequence files were performed using BaseSpace Sequence Hub (https://basespace.illumina.com) algorithms. FASTQ files were quality trimmed using the TrimGalore software and then aligned to the *Z. indianus* reference genome (21) using HISAT2. To determine the number of sequence reads mapped to each gene, the reference transcriptome was imported to the R software using the GenomicFeatures package, and then read counts were calculated using the GenomicAlignments R package. DESeq2 analysis was carried out for data normalization and differential gene expression analysis. Genes with a read count <10 were filtered out from the analysis. Only those genes were considered significantly differentially expressed in uninduced and *L. victoriae*-induced *Z. indianus* blood cells, where the Benjamini–Hochberg adjusted p-value was <0.05 and the absolute $\log_2$FoldChange was ≥1. A gene was considered expressed in a given sample if the Fragments per kilobase of exon model per million reads mapped (FPKM) values were >1. Furthermore, a protein was considered ortholog when the coverage was at least 20%, the identity was higher than 40%, and the E-value representing the quality of the alignment was lower than

0.0001. The National Center for Biotechnology Information (NCBI) database was used to find ortholog sequences. Functional data regarding *D. melanogaster* orthologs were acquired using Flybase, those of mammalian orthologs were acquired using Ingenuity Pathways Analysis (IPA), and other gene information was collected from the http://datadryad.org/stash/dataset/doi:10.5061/dryad.866t1g1n3 database. Gene ontology (GO) enrichment analysis for the differentially expressed genes was carried out with the software R, using the clusterProfiler package: https://bioconductor.org/packages/devel/bioc/vignettes/clusterProfiler/inst/doc/clusterProfiler.html. As there is no information available concerning the *Z. indianus* genes and proteins, their *D. melanogaster* orthologs were used.

3 Results

3.1 Species developing MGHs are highly resistant to parasitoids

The fly and wasp eclosion rates of parasitized *D. ananassae*, *Z. indianus*, and *D. melanogaster* were compared (Figure 1). Infections were carried out using two generalist parasitoid wasp species, *L. heterotoma* and *L. victoriae*. The proportional outcome of wasp-attacked flies was analyzed. We observed that both wasp species eclosed at a rate of approximately 40% from *D. melanogaster*, but they eclosed at a significantly lower rate from *D. ananassae* and *Z. indianus*; meanwhile, the fly survival rate of these species was in general higher than in *D. melanogaster* (Figure 1).

3.2 Parasitoid wasp infection induces differentiation of large plasmatocytes

We previously observed that multinucleation in *Z. indianus* was not restricted to MGHs, as a novel cell type appeared after parasitic infection: a class of plasmatocytes, spherical large cells, hereafter called large plasmatocytes, which occasionally had numerous nuclei. To reveal the dynamics of the appearance of large plasmatocytes, we carried out a time-lapse analysis. We infected *Z. indianus* larvae with *L. heterotoma* and *L. victoriae*; we isolated blood cells 24 h, 48 h, and 72 h after the wasp infection and stained them with the plasmatocyte-specific 5C3 antibody (11); and we determined the relative area of the 5C3-positive hemocytes. We detected the large plasmatocytes 48 h and 72 h after infection, and the relative area of these cells was significantly higher at 48 h compared to 72 h after *L. heterotoma* parasitization (Figure 2). By comparison, the size of the plasmatocytes of age-matched uninduced animals remained constant.

Next, we tested whether other immune stimuli, in addition to the parasitoid wasp attacks, could trigger the formation of large plasmatocytes. We used suspensions of *B. subtilis* (Gram-positive), *E. coli* (Gram-negative) bacteria, and an entomopathogenic fungus *B. bassiana* for infection. We applied sterile wounding as the control. Furthermore, we tested whether the presence of large foreign particles could stimulate the development of this cell type. Hence, we injected inert microbeads in sterile *Drosophila* Ringer solution into the hemocoel of second instar *Z. indianus* larvae. We injected sterile *Drosophila* Ringer solution as the control. We carried out the analysis 48 h after the respective treatments, which was the peak of large plasmatocyte differentiation after parasitoid wasp infection. We found that septic injury, sterile wounding, or injection of microbeads did not induce differentiation of large plasmatocytes (Figure 3). Although the injection of *Drosophila* Ringer, with or without microbeads, triggered a slightly increased relative area of plasmatocytes, we concluded that the appearance of large plasmatocytes is specifically connected to parasitic wasp infection (Figure 3).

3.3 Large plasmatocytes display a binary immune phenotype

The phenotypic analysis of large plasmatocytes revealed that a fraction of these cells expressed the 4G7 giant cell-specific antigen. As mentioned before, the giant cell fraction of *Z. indianus* includes

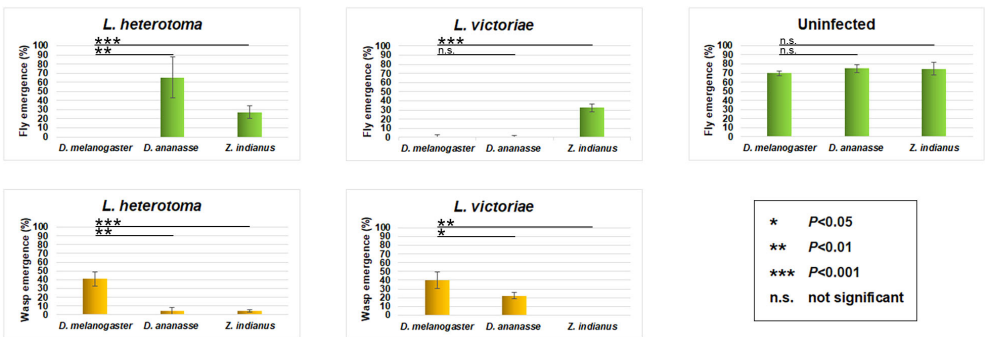

FIGURE 1
Eclosion success of two generalist wasp species. *Drosophila ananassae*, *Zaprionus indianus*, and *Drosophila melanogaster* larvae were infected with *Leptopilina heterotoma* and *Leptopilina victoriae* parasitoid wasps. The data of four independent experiments were cropped, with 50 larvae in each. The error bars indicate the standard deviation. Student's *t*-test was used for statistical analysis.

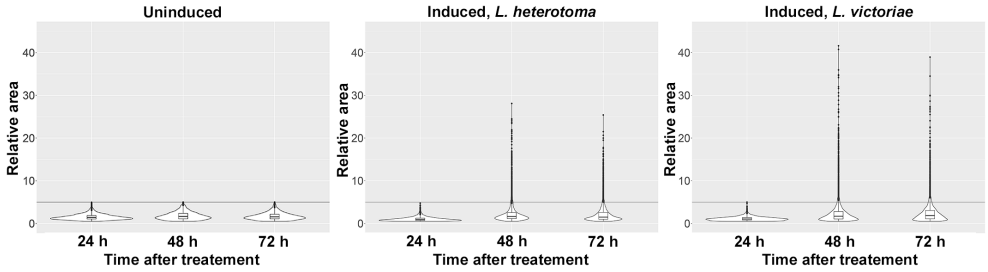

FIGURE 2
Time-lapse analysis of large plasmatocyte differentiation following parasitoid wasp infection. *Leptopilina heterotoma* and *Leptopilina victoriae* parasitoids were used to infect early second instar *Zaprionus indianus* larvae. Blood cells were harvested 24 h, 48 h, and 72 h after infection. As controls, age-matched uninduced larvae were used. Violin plots were generated in RStudio to interpret data distribution. For each plot, relative area of 2,000 randomly selected 5C3-positive cells was applied. The first quartile, the median, and the third quartile are shown.

MGHs, elongated cells with a single nucleus (nematocytes), and anucleated cytoplasmic fragments derived from the previous two, all involved in the encapsulation of parasitoids (11, 19). Expression of the 4G7 antigen on certain large plasmatocytes is suggestive of a transient state between the large plasmatocytes and giant hemocytes; hence, we applied double staining with the combinations of the 5C3 plasmatocyte-specific antibodies and the 4G7 giant hemocyte-specific antibodies in the same samples to analyze the expression rate of cell type-specific antigens. Hemocytes were isolated 48 h after *L. victoriae* parasitoid wasp infection. Our data showed that while 96.1% of the large plasmatocytes were only 5C3-positive, 0.1% presented the 4G7 antigen exclusively, and 3.8% were double-positive (Figure 4A). Each cell category included mononucleated, binucleated, and multinucleated cells. While the size of the nuclei in the 5C3-positive large plasmatocytes varied, the 4G7-positive large plasmatocytes carried exclusively enlarged nuclei (Figure 4A), a characteristic feature of the giant hemocytes in the wasp-infected larvae (11) (Figure 4B).

Plasmatocytes engulf bacteria, but encapsulating giant hemocytes are not phagocytic (11), so we compared the phagocytic capacity of the normal-sized and the large plasmatocytes in relation to their antigen expression phenotypes. We infected second instar larvae with *L. victoriae* parasitoids, and 48 h after wasp infection, we injected larvae with FITC-labeled *E. coli* bacteria. One hour after the injection of bacteria, we isolated and subjected hemocytes to indirect immunofluorescence analysis using the 5C3 and 4G7 discriminative antibodies. We found that 4.3% of the 5C3-positive normal-sized plasmatocytes did not engulf bacteria (Figure 5A), while 13.4% of the 5C3-positive large plasmatocytes and 14.6% of the 4G7-positive large plasmatocytes did not take up bacteria (Figure 5B). Although there was no considerable difference between the phagocytic capacities of 5C3-

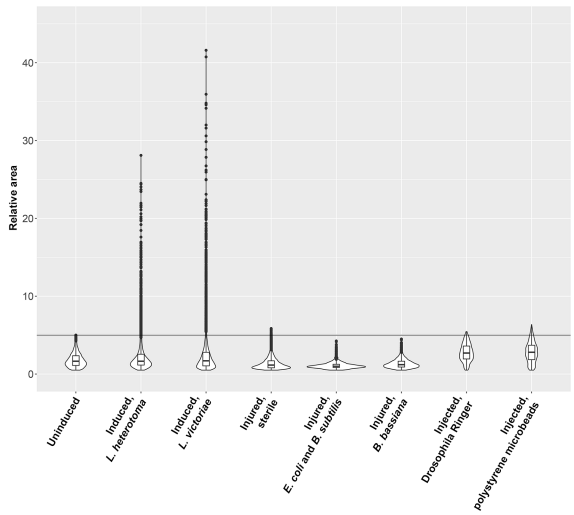

FIGURE 3
Parasitic wasp infection induces differentiation of large plasmatocytes. The respective treatments were carried out on second instar *Zaprionus indianus* larvae, and 5C3-positive blood cells were analyzed after 48 h. Naïve, sterile wounded, and *Drosophila* Ringer-injected larvae were used as controls. Violin plots were generated in RStudio using relative area of 2,000 randomly selected cells for each plot. The first quartile, the median, and the third quartile are shown.

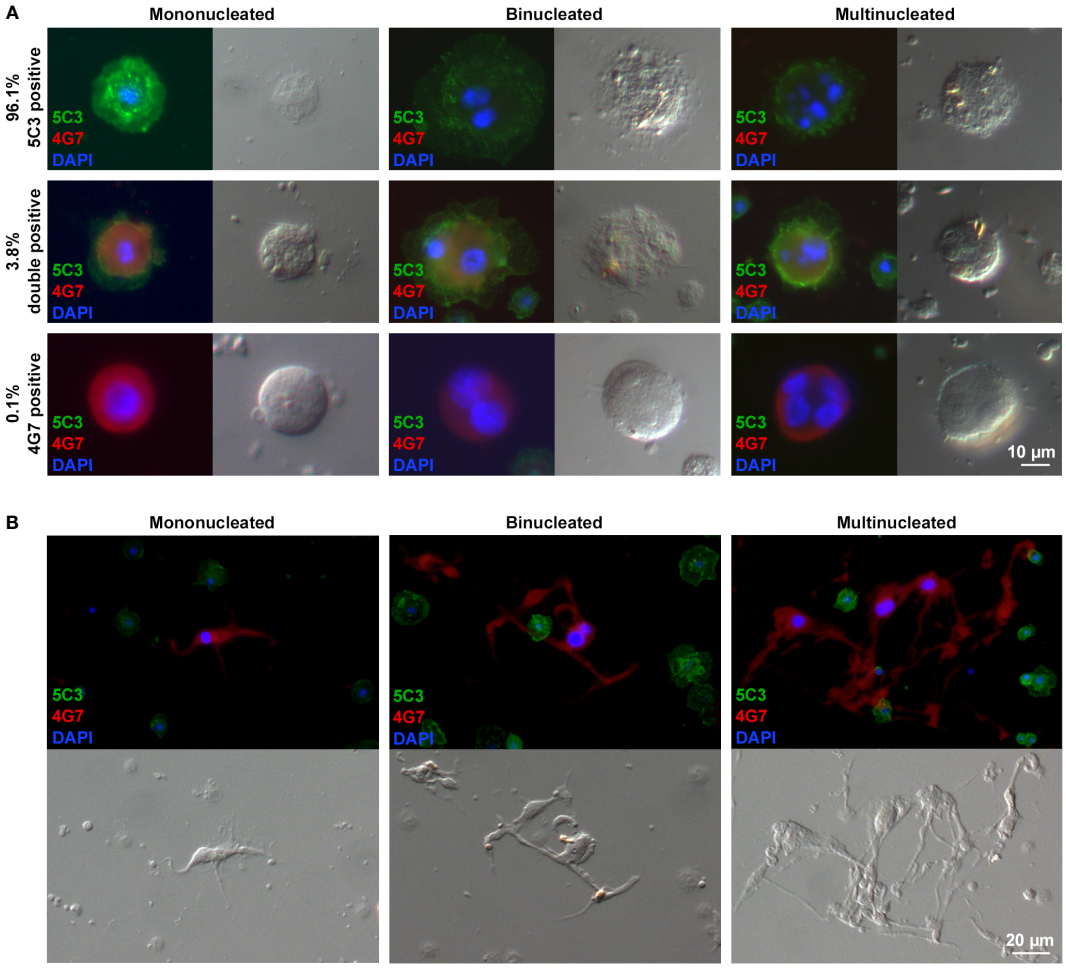

FIGURE 4
Certain large plasmatocytes display binary immune phenotypes or express the giant cell-specific antigen. Forty-eight hours after *Leptopilina victoriae* infection, hemocytes were double stained, using the plasmatocyte-specific 5C3 (IgM), the giant cell-specific 4G7 (IgG2a) monoclonal antibodies, and the respective isotype-specific secondary antibodies. **(A)** The giant cell-specific 4G7 antigen was presented by 3.9% of the large plasmatocytes. Mono-, bi-, and multinucleation were detected in each cell type. The large plasmatocytes carrying exclusively the 4G7 antigen possessed enlarged nuclei **(B)**. The giant cells 72 h after wasp infection carried one, two, or more enlarged nuclei. Detection was performed using an epifluorescence microscope (Zeiss Axioscope 2 MOT).

and 4G7-positive large plasmatocytes, this finding shows that large plasmatocytes are less phagocytic than normal-sized plasmatocytes.

Video microscopic analysis of *L. victoriae*-infected larval hemocytes revealed that large spherical cells changed shape and became elongated cells, morphologically corresponding to the giant hemocytes (Supplementary Movie 1). This finding indicates the phenotypic plasticity of the large plasmatocytes differentiating after parasitoid wasp infection.

3.4 Anucleated fragments accumulate at wound sites

We previously found that the giant hemocytes of *Z. indianus*, including MGHs, are constitutively present in the hemolymph, possess a characteristic ultrastructure as they carry an elaborate system of canals and sinuses in their cytoplasm, and release a large number of anucleated cytoplasmic fragments (11). We observed that mammalian megakaryocytes, which release anucleated cytoplasmic fragments, the platelets, involved in blood clotting and wound remediation, share similar ultrastructural characteristics with the encapsulating 4G7-positive giant hemocytes of *Z. indianus* (12) because they possess a highly tortuous, invaginated membrane system (22, 23). Hence, we considered whether, by analogy, the anucleated fragments derived from the giant hemocytes of *Z. indianus* could be involved in wound healing. To test this idea, we wounded early third instar naïve or *L. victoriae*-infected larvae, and 2 h later, we examined the wound sites by indirect immunofluorescence assay using the giant cell-specific 4G7 antigen. We observed that the 4G7-positive fragments accumulated at wound sites of both naïve and *L. victoriae*-infected *Z. indianus* larvae (Figure 6). This is also supported by 3D confocal picture reconstruction of a 4G7- and DAPI-stained naïve larval sample (Supplementary Movie 2,

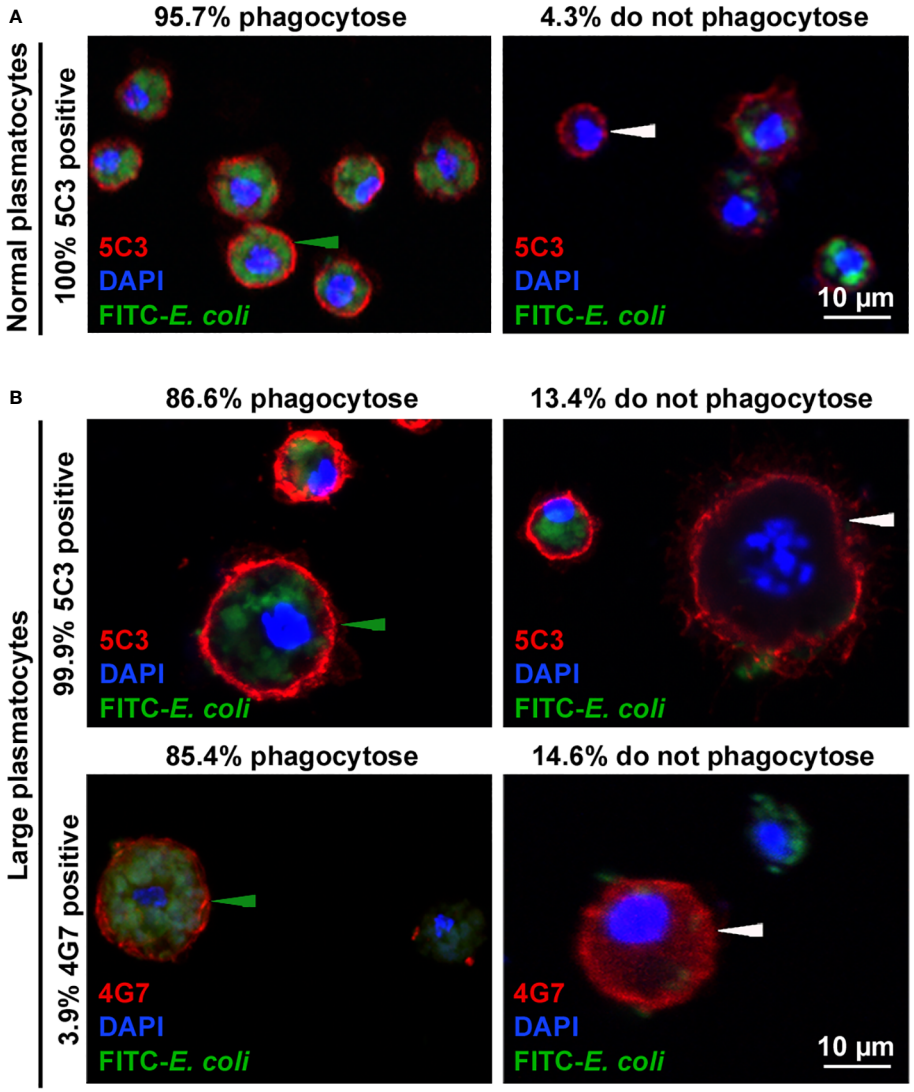

FIGURE 5
Phagocytic ratio of large plasmatocytes decreased when compared to that of normal plasmatocytes. Fluorescein isothiocyanate (FITC)-labeled *Escherichia coli* bacteria were used in combination with the respective antibodies. Green arrowheads point to the plasmatocytes that phagocytosed *E coli*, and white arrowheads show those that did not. Analysis was performed using an Olympus FV1000 confocal LSM microscope, and images in the nucleus plane were used. Results of three independent experiments were considered, each with 24 larvae. **(A)** High ratio of the normal plasmatocytes engulfed bacteria. **(B)** Lower ratio of large plasmatocytes with both immunological phenotypes possessed phagocytic capacity.

Supplementary Figure 1). Although we detected extensive accumulation of the anucleated fragments at the wound sites, the presence of nucleated giant hemocytes cannot be excluded. We suppose therefore that this cell type fulfills an important, so far unrecognized role in cuticle remediation.

3.5 Gene expression patterns of hemocytes underlie their functional characteristics

To gain insights into the molecular mechanisms accountable for effective immune defense reactions and to recognize feasible factors involved in wound healing processes, we analyzed the transcriptomic content of hemocytes isolated from age-matched naïve and *L. victoriae*-infected *Z. indianus* larvae. In total, 7,052 different gene transcripts were detected (Supplementary Table 1). As there is no available information on *Z. indianus* proteins, the possible function of the genes expressed in blood cells of this species was generally considered on the basis of their *D. melanogaster* orthologs.

First, to identify genes that could participate in the immune defense of *Z. indianus* against parasitoids, we compared the gene expression profile of naïve and wasp-induced hemocyte samples. After normalization, 648 genes were differentially expressed between the induced and uninduced samples (Supplementary Table 2). Of these, 374 and 274 genes were expressed at significantly higher and lower levels, in induced and uninduced blood cells, respectively, including 37 genes that were detected exclusively in induced and 12 genes exclusively in uninduced hemocytes (Supplementary Table 2). *D. melanogaster* orthologs for 574 of the differentially expressed genes could be identified. Among these, several encode proteins with a role in

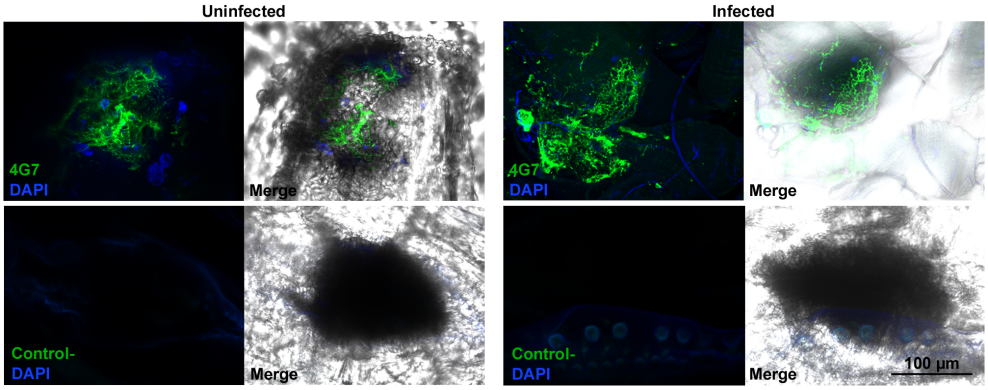

FIGURE 6
Anucleated 4G7-positive fragments accumulated at the wound sites. Cuticle preparations were performed 2 h after wounding of naïve and wasp-induced larvae and stained with the 4G7 antibody. As a negative control, the T2/48 monoclonal antibody was used. Detection was performed using an Olympus FV1000 confocal LSM microscope.

signal transduction, cell movement, encapsulation of foreign particles, melanization, anabolism, and elimination of microbes (Table 1). GO enrichment for "biological process" revealed high expression of genes whose protein products were mainly involved in innate immune defense reactions, amino acid biosynthesis, actin cytoskeleton organization, and cell–cell junctions (Supplementary Figure 2). These enrichments are possibly due to the high energy demand, motility, and fusion of the giant hemocytes, processes required for effective parasitoid encapsulation. Furthermore, GO enrichment analysis in the "cellular component" category revealed that genes overexpressed in hemocytes of parasitoid wasp-infected samples encode for proteins that are mostly localized in the actin cytoskeleton, plasma membrane, and cell junctions (Supplementary Figure 3), which in addition suggest the importance of the encapsulation reaction, involving cellular contacts, cytoskeletal rearrangements, and adhesion to the parasitoid. Both the up- and downregulated genes could have essential functions in immune responses mediated by the activated blood cells (Supplementary Table 2). No orthologs were identified for 74 of the 648 differentially expressed genes, either because they lacked recognizable *D. melanogaster* homologies or because they belong to expanded and rapidly evolving gene families, such as serine proteases, fibrinogen-related proteins (FREPs), and C-type lectins, with uncertain orthology relationships.

Second, because the derivatives of the giant hemocytes, the anucleated fragments, detected at the wound sites are present in both the uninduced and induced samples, we searched for constitutively expressed genes that could potentially be involved in wound healing processes. On the one hand, we selected those genes that had *D. melanogaster* orthologs known to be involved in blood coagulation, wound healing, and cuticle remediation (Table 2). On the other hand, we selected those constitutively expressed *Z. indianus* genes that had mammalian orthologs involved in the function of megakaryocytes and platelets (Supplementary Table 3).

As mentioned above, three of the expanded and rapidly evolving gene families, expressed either differentially or constitutively in the blood cells, are of special interest: the serine proteases, the FREPs, and the C-type lectins. The serine proteases (24–26) comprise a highly expanded class, and some of them act in complement-like cascades to activate Toll signaling, melanization, or coagulation. The FREPs (27–30) and the C-type lectins (31, 32) are pathogen-binding proteins that play important roles in the immune defense of many animals. Of the 90 expressed *Z. indianus* serine proteases, 54 have specific *D. melanogaster* orthologs (Supplementary Table 4). The identified orthologs include genes with known roles in immunity, such as *Hayan*, *Sp7* in PPO1/2 activation, and *grass* and *modSP* in Toll signaling. The remaining 36 genes belong to *Z. indianus*-specific clades, similar to the immunity-related serine proteases, but lack obvious 1:1 orthology relationships with *D. melanogaster* homologs. Of the 51 FREP genes, only 22 have *D. melanogaster* orthologs, and most of these genes have not been characterized so far (Supplementary Table 4). The situation is similar for the 18 *Z. indianus* lectin genes, as only five have *D. melanogaster* orthologs (Supplementary Table 4). The differentially expressed serine proteases, FREPs, and C-type lectins could be involved in the efficient parasitoid-killing processes of *Z. indianus* (Supplementary Table 4).

Furthermore, regarding signaling pathways involved in blood cell differentiation and function, we found components of the JNK pathway (Alg-2, bsk, CYLD, Cdc37, jra, msn, and Pvr) and elements of the JAK–STAT pathway (hop, Stat92E, dome, Ptp61F, and Socs36E) constitutively expressed in blood cells isolated from both naïve and induced larvae (Supplementary Table 1). However, upd1 and upd3 genes, which encode the ligands of the JAK–STAT signaling, had no or very low expression, and the upd2 ortholog is not encoded in the genome of *Z. indianus* (21).

3.6 Comparison to wasp-induced genes in *D. melanogaster* and *D. ananassae* hemocytes

Although the morphological features of lamellocytes in wasp-infected *D. melanogaster* larvae are very different from those of the MGHs and large plasmatocytes in *Z. indianus*, we were interested in whether the genes that were upregulated in *Z. indianus* include orthologs of lamellocyte-specific genes of *D. melanogaster*. Genes that

TABLE 1 Predicted function of those *Zaprionus indianus* genes that were up- or downregulated in parasitoid wasp-induced samples and possessed *Drosophila melanogaster* orthologs (listed).

Signal transduction ***Upregulated*:** Lgr4 (ZIND16G_00006424), mAChR-C (ZIND16G_00004427), CG7497 (ZIND16G_00008737), Proc-R (ZIND16G_00002261), AdoR (ZIND16G_00000124), Galphaf (ZIND16G_00000435), moody (ZIND16G_00002695), Rgk2 (ZIND16G_00005366), Ir8a (ZIND16G_00007061), CG34393 (ZIND16G_00006027), hh (ZIND16G_00003155), Pvf3 (ZIND16G_00008540), Coop (ZIND16G_00006309), p130CAS (ZIND16G_00006792), fs(1)M3 (ZIND16G_00000600), trio (ZIND16G_00001152), Ac78C (ZIND16G_00006086), RSG7 (ZIND16G_00000004), Pld (ZIND16G_00002971), homer (ZIND16G_00004599), gwl (ZIND16G_00009480), PGRP-SC2 (ZIND16G_00004509), PGRP-LB (ZIND16G_00003503), ImpL2 (ZIND16G_00002042), chrb (ZIND16G_00000283), Mnr (ZIND16G_00002683), pigs (ZIND16G_00003317), ric8a (ZIND16G_00002142), CG10359 (ZIND16G_00000441), I-2 (ZIND16G_00000398), P32 (ZIND16G_00004766), Rab32 (ZIND16G_00008079), tum (ZIND16G_00006586), dlp (ZIND16G_00006167), S6k (ZIND16G_00001109), cGlr1 (ZIND16G_00005284), trbd (ZIND16G_00008915), Rala (ZIND16G_00002638), Cp1 (ZIND16G_00005802) ***Downregulated*:** hec (ZIND16G_00005861), Ant2 (ZIND16G_00004162), Alk (ZIND16G_00007368), CG32944 (ZIND16G_00003953), CG4950 (ZIND16G_00002356), CG9391 (ZIND16G_00006079), REPTOR (ZIND16G_00001021), unc-5 (ZIND16G_00007900), sev (ZIND16G_00003697), PGRP-LC (ZIND16G_00008135), Dok (ZIND16G_00004125), magu (ZIND16G_00006621), Men (ZIND16G_00007840), LKRSDH (ZIND16G_00005353), Mob2 (ZIND16G_00001509), Ptp4E (ZIND16G_00004064), Tab2 (ZIND16G_00007372), Doa (ZIND16G_00004009), aru (ZIND16G_00002198), mthl10 (ZIND16G_00001945), CG46491 (ZIND16G_00007929), Pkc98E (ZIND16G_00000763), Thor (ZIND16G_00005322), melt (ZIND16G_00001114), spz (ZIND16G_00008556), Lar (ZIND16G_00009598), Eip75B (ZIND16G_00002603), Lk6 (ZIND16G_00002815), grh (ZIND16G_00005303), ebd1 (ZIND16G_00000358), foxo (ZIND16G_00008428), Ziz (ZIND16G_00008832), Cirl (ZIND16G_00004761), TP53INP (ZIND16G_00006652), gcl (ZIND16G_00003057), myo (ZIND16G_00001094), robo2 (ZIND16G_00008188), loco (ZIND16G_00001880), wit (ZIND16G_00000511), CG33958 (ZIND16G_00004664), Duox (ZIND16G_00005661), numb (ZIND16G_00007698)
Cell movements and encapsulation of foreign target ***Upregulated*:** Strn-Mlck (ZIND16G_00004905), hh (ZIND16G_00003155), Pvf3 (ZIND16G_00008540), Itgbn (ZIND16G_00009296), p130CAS (ZIND16G_00006792), if (ZIND16G_00005558), Dhc16F (ZIND16G_00008232), AdamTS-A (ZIND16G_00003414), trio (ZIND16G_00001152), cher (ZIND16G_00004253), CycB (ZIND16G_00004885), unc-104 (ZIND16G_00004506), ncd (ZIND16G_00005467), mew (ZIND16G_00004434), scb (ZIND16G_00007892), trbd (ZIND16G_00008915), Rala (ZIND16G_00002638), Nrg (ZIND16G_00002077), Eb1 (ZIND16G_00006903) ***Downregulated*:** m (ZIND16G_00004819), unc-5 (ZIND16G_00007900), ena (ZIND16G_00003069), Invadolysin (ZIND16G_00005474), Lar (ZIND16G_00009598), robo2 (ZIND16G_00008188), stai (ZIND16G_00001760)
Production of energy source ***Upregulated*:** CG5171 (ZIND16G_00007239), Treh (ZIND16G_00009882), Men-b (ZIND16G_00000144), beta-Man (ZIND16G_00007729), Ldh (ZIND16G_00008314), Gnmt (ZIND16G_00004579) ***Downregulated:*** Oscillin (ZIND16G_00006234), Pdk (ZIND16G_00009519), Gfat1 (ZIND16G_00003438), fbp (ZIND16G_00009604), foxo (ZIND16G_00008428)
Melanization ***Upregulated*:** Sp7 (ZIND16G_00001050) ***Downregulated:*** modSP (ZIND16G_00002867), PGRP-LC (ZIND16G_00008135)
Elimination of microorganisms ***Upregulated*:** grass (ZIND16G_00000143), PGRP-SB1 (ZIND16G_00000431), CecC (ZIND16G_00002978), DptB (ZIND16G_00002658), AttD (ZIND16G_00001258), Sp7 (ZIND16G_00001050), Tep2 (ZIND16G_00008527), IM33 (ZIND16G_00009971), Bbd (ZIND16G_00006553), slif (ZIND16G_00005220), CG16799 (ZIND16G_00006321), Tep3 (ZIND16G_00009332), PGRP-SC2 (ZIND16G_00004509), PGRP-LB (ZIND16G_00003503), Der-2 (ZIND16G_00003566), Rala (ZIND16G_00002638) ***Downregulated:*** PGRP-LC (ZIND16G_00008135), modSP (ZIND16G_00002867), Tab2 (ZIND16G_00007372), CG13551 (ZIND16G_00005409), spz (ZIND16G_00008556), NimC1 (ZIND16G_00002951), Duox (ZIND16G_00005661)

(Continued)

TABLE 1 Continued

are specific to different *D. melanogaster* hemocyte classes have recently been identified in six independent single-cell sequencing projects (33–38), and consensus lists of these data have been compiled (9). *Z. indianus* homologs of 21 *D. melanogaster* lamellocyte marker genes were indeed upregulated in hemocytes after wasp infection, while three were downregulated (Supplementary Table 5). Thus, there seems to be some correlation between the activity of activated *Z. indianus* hemocytes and *D. melanogaster* lamellocytes. The upregulated genes include orthologs of classical lamellocyte markers such as *atilla*, *cher*, and the integrins *Itgbn* and *mew*, as well as several genes involved in cytoskeletal organization and sugar import.

In contrast to the lamellocyte markers, many plasmatocyte and crystal cell marker homologs were downregulated in *Z. indianus* hemocytes after wasp infection (Supplementary Table 5), albeit modestly so. This may reflect a decreased relative proportion of the corresponding cell classes in the infected animal.

We also compared the differentially expressed genes in *D. ananassae* MGHs and activated plasmatocytes (12) with the differentially expressed *Z. indianus* genes. We noted that expression of six of the lamellocyte markers, *atilla*, *Itgbn*, *Trehalase*, the sugar transporter *CG1208*, *Esyt2*, and Gdap2, were highly expressed in wasp-infected blood cells of *Z. indianus* and also showed increased expression in MGHs of *D. ananassae*, while three of the highly expressed *Z. indianus* genes, *Trehalase*, *Esyt2*, and *aru*, were also upregulated in the activated plasmatocytes of *D. ananassae* (Supplementary Table 6). However, at present, it is hard to say if this overlap in gene expression in effector hemocytes from these three species is due to convergent evolution or if it reflects a common origin of the involved cell types, despite their very different appearances.

4 Discussion

Drosophilids have developed different strategies to circumvent parasitoid attack, which usually involves the transdifferentiation of phagocytic plasmatocytes to non-phagocytic, encapsulating cell types. Several specialized cell types have been described as lamellocytes in *D. melanogaster* (3), MGHs in *Z. indianus* (11), and species of the *ananassae* subgroup (10), giant hemocytes, and nematocytes in *Z. indianus* (11, 19) that encapsulate parasitoids. However, it is not yet known how they are related to each other. When the hosts co-evolve with their local parasite communities, they may acquire novel elements in the arms race, e.g., different types of effector cells develop against the co-evolving parasitoid. This study was carried out with the aim to test the specific features of defense in an invasive *Drosophila* species, *Z. indianus*, which

10.3389/fimmu.2023.1322381

TABLE 2 Set of constitutively expressed *Zaprionus indianus* genes encoding for orthologs of *Drosophila melanogaster* proteins involved in wound healing and hemolymph clotting.

Z. indianus gene ID	D. melanogaster ortholog	Role in D. melanogaster
ZIND16G_00008476	fon	Fat body-secreted hemolymph clotting factor.
ZIND16G_00008262	Hml	Hemolymph clotting.
ZIND16G_00006641	PPO2	Melanization of wounds and capsules.
ZIND16G_00006889	PPO1	Melanization of wounds.
ZIND16G_00008507	CG42259	Involved in response to wounding.
ZIND16G_00003920	Glt	Cross-links blood clot.
ZIND16G_00001938	pbl	Wound healing.
ZIND16G_00006474	Tg	Cuticle development. Hemolymph coagulation, wound healing.
ZIND16G_00002297	Cht2	Cuticle development. Wound healing.
ZIND16G_00006825	Fhos	Plasmatocyte migration during immune response, autophagic programmed cell death.
ZIND16G_00007154	CG15170	Wound healing.
ZIND16G_00008356	TTLL4A	Wound healing.
ZIND16G_00007461	Mtl	Dorsal closure, wound healing, cell migration.
ZIND16G_00005073	Coq3	Wound healing.
ZIND16G_00008371	holn1	Wound healing.
ZIND16G_00004207	CG11089	Wound repair.
ZIND16G_00000950	CG6005	Wound healing.
ZIND16G_00009846	Mmp2	Cleaves proteins in the extracellular matrix. Wound healing.
ZIND16G_00001627	Idgf3	Component of hemolymph clot.
ZIND16G_00006536	CG3294	Splicing factor involved in wound healing.
ZIND16G_00001159	Cht7	Chitin-based cuticle development.
ZIND16G_00003151	Hmu	Wound healing.

develops different types of multinucleated cells in response to parasitoid attack.

We found that *D. ananassae* and *Z. indianus*, using MGHs in the defense against parasitoid wasps, generated highly effective innate immune responses when compared to *D. melanogaster*, which uses lamellocytes to protect against the invaders (Figure 1). The presence of multinucleated hemocytes among Drosophilidae, apart from species of the *ananassae* subgroup (10), and *Z. indianus* (11) was also detected in *Drosophila falleni* and *Drosophila phalerata* (39). The broad distribution of multinucleated hemocytes within the family suggests that this cell type could be present in a common ancestor of Drosophilidae, and the lamellocytes in the *melanogaster* subgroup possibly have turned up as a novelty, where they have replaced the MGHs (9). Previously, we observed that MGHs, a syncytium of blood cells with several nuclei in *D. ananassae* and *Z. indianus*, could develop by fusion of elongated hemocytes (10, 11). The specific features of this cell type may underlie the effective immune response of these species.

A novel cell type, the spherical large plasmatocyte with characteristic features of both the plasmatocytes and the giant cells (including MGHs and nematocytes) as well as the anucleated cytoplasmic fragments, could be one key component of the immune response of *Z. indianus*. Large plasmatocytes develop specifically after parasitoid wasp infection. Bacteria, fungi, or inert foreign particles do not cause differentiation of large plasmatocytes (Figure 3); hence, we hypothesize that components of the egg, the venom, and virus-like particles injected during oviposition may be recognized by the pattern recognition factors of the host and may serve as special triggers and promote differentiation of these cells. Large plasmatocytes could be key components of the anti-parasitoid response, producing substances targeted against the invaders, or they may serve as an intermediate cell subpopulation through MGH differentiation. Large plasmatocytes carry one, two, or more nuclei of different sizes and occasionally express the 4G7 antigen, a characteristic feature of giant hemocytes (Figure 4) (11), and their phagocytic capacity is lower than that of the normal-sized plasmatocytes (Figure 5). Video microscopy showed that large, spherical cells, most probably large plasmatocytes, rapidly change shape and become elongated, vigorously moving cells (Supplementary Movie 1), implying that they apparently differentiate into giant hemocytes. The elongated shape and high motility of the giant hemocytes could provide highly effective encapsulation capacity for this cell type.

Though the 4G7-positive, encapsulating cell fraction, including MGHs, nematocytes, and anucleated cytoplasmic fragments, increased in number and size after parasitoid infection, this subpopulation was also present in naïve *Z. indianus* larvae. Here, we provide evidence for a novel function of the giant hemocytes, as we found that in both naïve and wasp-infected larvae, they were present at wound sites and hence could be involved in the wound healing process. This finding is also supported by the ultrastructural similarities observed between the giant hemocytes of *Z. indianus* and the mammalian megakaryocytes. Both cell types have an elaborated open canalicular system communicating with the extracellular space, and both release a large number of anucleated cell fragments (11, 40). Anucleated cell fragments were also described in *D. falleni* and *D. phalerata*, where they carry mRNA to translate into proteins (39), which provides them remarkable autonomy, similar to mammalian platelets (41, 42).

D. melanogaster possesses the wound healing machinery, which involves hemolymph components secreted by the fat body, such as fondue and glutacin, and hemocyte-derived factors, such as hemolectin, hemomucin, transglutaminase, and phenoloxidases, which are all involved in the formation of a fibrous or gelatinous network at the epithelial breaches, thus sealing the damaged tissue (43–45). Interestingly, multinucleated epidermal cells were also

detected at the *Drosophila* wound sites, which helped to eliminate the intracellular spaces and restore tissue integrity (18). Transcriptomic analysis of *Z. indianus* blood cells, on the basis of the analysis of their *D. melanogaster* orthologs, revealed constitutive expression of several genes, which could be involved in wound healing and coagulation processes (Table 2). Furthermore, we identified several genes expressed in *Z. indianus* blood cells, which encoded orthologs of proteins involved in mammalian blood coagulation (Supplementary Table 3); hence, they may also be involved in wound healing in this insect species. Based on the involvement of *Z. indianus* anucleated fragments in wound healing processes, here, we present an example where, in phylogenetically distant species, small, anucleated cell fragments with special ultrastructure evolved through distinct evolutionary trajectories in insects and mammals to act in similar biological processes.

Transcriptomic analysis revealed further characteristic features of gene expression patterns in this species. Several differentially expressed genes in naïve and wasp-induced hemocyte samples could be involved in the immune response against parasitoid wasps (Supplementary Table 2). Based on previous studies (33–38), *D. melanogaster* genes, such as *atilla*, *itgbn*, *Treh*, Esyt2, and CG1208, were enriched in the lamellocytes and were also expressed at significantly higher levels in the MGHs of *D. ananassae* and the blood cells of parasitoid-infected *Z. indianus*; hence, they could be involved in the anti-parasitoid defense of each species (Supplementary Table 5, Supplementary Table 6). We have also shown rapidly evolving gene families to be expressed in the transcriptome of *Z. indianus* blood cells, including FREPs and C-type lectins, which have been described to act as pattern recognition factors in other insect species. Hence, in *Z. indianus*, blood cell differentiation may be induced through them.

The JAK–STAT signaling pathway has been highly conserved throughout evolution, as it is involved in the regulation of immune responses in mammals (46) and also controls different steps of hematopoiesis and the response to immune challenge in *D. melanogaster* (47). We previously found that gene orthologs encoding elements of this pathway were not enriched in MGHs of *D. ananassae* (12). Here, we have shown that, although some components of the JAK–STAT pathway were expressed constitutively, upd1 and upd3 genes, encoding the ligands of this pathway, had no or very low expression, while the upd2 ortholog is not encoded by the genome of *Z. indianus* (21). However, several components of the JNK pathway, including bsk and Cdc37 genes involved in the activation of the pathway (48, 49), were expressed at a higher level in blood cells isolated from wasp-infected *Z. indianus* samples (Supplementary Table 1), indicating that JNK signaling is likely involved in blood cell differentiation after parasitoid infection.

Finally, we conclude that the blood cells of *Z. indianus* generally represent an extremely plastic population of cells, which could contribute to the highly efficient immune response against parasitoids and may also participate in defense processes such as wound healing and cuticle remediation. Our research provides insights into the differentiation and function of blood cells, highlights the importance of different molecules involved in blood cell-mediated responses, and suggests possible model organisms for further investigations.

Data availability statement

The data presented in the study are deposited in the NCBI SRA repository, accession number PRJNA1041101.

Ethics statement

The manuscript presents research on animals that does not require ethical approval for their study.

Author contributions

GC: Conceptualization, Data curation, Funding acquisition, Investigation, Methodology, Project administration, Supervision, Validation, Visualization, Writing – original draft, Writing – review & editing. LM: Conceptualization, Data curation, Formal Analysis, Funding acquisition, Investigation, Methodology, Software, Validation, Visualization, Writing – original draft, Writing – review & editing. HK: Data curation, Methodology, Validation, Visualization, Writing – original draft. VV: Data curation, Validation, Visualization, Writing – original draft. LB: Data curation, Investigation, Resources, Software, Writing – original draft. NZ: Data curation, Investigation, Software, Writing – original draft. GN: Data curation, Software, Writing – original draft. ZH: Data curation, Software, Writing – original draft. DH: Conceptualization, Data curation, Formal Analysis, Funding acquisition, Software, Validation, Writing – original draft, Writing – review & editing. IA: Conceptualization, Funding acquisition, Investigation, Methodology, Project administration, Supervision, Validation, Visualization, Writing – original draft, Writing – review & editing.

Funding

The author(s) declare that financial support was received for the research, authorship, and/or publication of this article. This research was supported by the NKFI K135877 (IA) grant from the Hungarian National Science Foundation, the BO/00552/20/8 Bolyai János Research Scholarship (GC) from the Hungarian Academy of Sciences, the Doctoral School of Biology, University of Szeged (LBM), the National Research, Development and Innovation Office grant GINOP-2.3.2-15-2016-00032 (LB), and grant 2018-05114 from the Swedish Research Council (DH).

Acknowledgments

We are grateful to Olga Kovalcsik and Anita Balázs for the technical help. We thank Prof. Todd Schlenke for the parasitoid wasps, Dr. Bálint Z. Kacsoh for the *Z. indianus* strain, and Dr. Gábor Steinbach of the Laboratory of Cellular Imaging, BRC, for 3D confocal picture reconstruction.

Conflict of interest

The authors declare that the research was conducted in the absence of any commercial or financial relationships that could be construed as a potential conflict of interest.

Publisher's note

Supplementary material

The Supplementary Material for this article can be found online at: https://www.frontiersin.org/articles/10.3389/fimmu.2023.1322381/full#supplementary-material

SUPPLEMENTARY FIGURE 1
The wound site of an uninduced *Z. indianus* larva. The image corresponds to Supplementary Movie 2, and was captured using an Olympus FV1000 confocal LSM microscope, 2 h after sterile wounding.

SUPPLEMENTARY FIGURE 2
GO enrichment analysis in the "biological process" category for the differentially expressed genes between the induced and uninduced samples. Genes that were significantly upregulated in the induced samples are labeled in green and those that were significantly downregulated are labeled in red. GO terms are plotted according to the significance of their enrichment (-log10 p-value).

SUPPLEMENTARY FIGURE 3
GO enrichment analysis in the "cellular component" category for the differentially expressed genes between the induced and uninduced samples. Genes that were significantly upregulated in the induced samples are labeled in green and those that were significantly downregulated are labeled in red. GO terms are plotted according to the significance of their enrichment (-log10 p-value).

SUPPLEMENTARY TABLE 1
List of the *Z. indianus* genes expressed in the blood cells of uninduced and *L. victoriae*-infected larvae. FPKM values show gene expression levels for each sample. *D. melanogaster* and *D. ananassae* orthologs are listed.

SUPPLEMENTARY TABLE 2
Set of genes differentially expressed in uninduced and *L. victoriae*-induced *Z. indianus* blood cells. Positive and negative log2FoldChange values indicate higher and lower gene expression levels, respectively, in induced compared to uninduced samples. Genes expressed exclusively in uninduced samples are labeled with a light grey background and those expressed exclusively in induced samples are labeled with a dark grey background. *D. melanogaster* and *D. ananassae* orthologs are listed.

SUPPLEMENTARY TABLE 3
List of the mammalian coagulation-associated genes possessing constitutively expressed orthologs in *Z. indianus* blood cells. The corresponding *D. melanogaster* and *D. ananassae* orthologs are also shown.

SUPPLEMENTARY TABLE 4
Set of putative serine protease, FREPs, and C-type lectin genes expressed either differentially (grey) or constitutively in *Z. indianus* blood cells. *D. melanogaster* and *D. ananassae* orthologs are listed. Not applicable (NA).

SUPPLEMENTARY TABLE 5
D. melanogaster blood cell specific markers expressed differentially in *Z. indianus*. Data originating from single cell RNA sequencing of lamellocytes (LC), crystal cells (CC), and plasmatocytes (PC).

SUPPLEMENTARY TABLE 6
Common differentially expressed genes in the blood cells of *Z. indianus* and *D. ananassae*. Activated plamsatocytes (aPC), naïve hemocytes (nHC).

SUPPLEMENTARY MOVIE 1
A large plasmatocyte differentiating into an elongated giant hemocyte. Blood cells were isolated 48 h following *L. victoriae* parasitoid wasp infection. Shooting duration: 75 min.

SUPPLEMENTARY MOVIE 2
Three-dimensional confocal picture reconstruction of a 4G7- and DAPI-stained wound. Wounding was generated using a 100 µm diameter sterile minutien pin on an uninduced larva. Analysis was performed 2 h after wounding using an Olympus FV1000 confocal LSM microscope. The corresponding trans light image is presented in Supplementary Figure 1.

References

1. Evans CJ, Hartenstein V, Banerjee U. Thicker than blood: conserved mechanisms in *Drosophila* and vertebrate hematopoiesis. *Dev Cell* (2003) 5(5):673–90. doi: 10.1016/s1534-5807(03)00335-6

2. Gautam DK, Chimata AV, Gutti RK, Paddibhatla I. Comparative hematopoiesis and signal transduction in model organisms. *J Cell Physiol* (2021) 236(8):5592–619. doi: 10.1002/jcp.30287

3. Rizki TM, Rizki RM. Properties of the larval hemocytes of. *Drosophila melanogaster Experientia* (1980) 36(10):1223–6. doi: 10.1007/BF01976142

4. Meister M, Lagueux M. *Drosophila* blood cells. *Cell Microbiol* (2003) 5(9):573–80. doi: 10.1046/j.1462-5822.2003.00302.x

5. Honti V, Csordás G, Kurucz E, Márkus R, Andó I. The cell-mediated immunity of *Drosophila melanogaster*: hemocyte lineages, immune compartments, microanatomy and regulation. *Dev Comp Immunol* (2014) 42 (1):47–56. doi: 10.1016/j.dci.2013.06.005

6. Anderl I, Vesala L, Ihalainen TO, Vanha-Aho LM, Andó I, Rämet M, et al. Transdifferentiation and proliferation in two distinct hemocyte lineages in *Drosophila melanogaster* larvae after wasp infection. *PloS Pathog* (2016) 12(7):e1005746. doi: 10.1371/journal.ppat.1005746

7. Parsons B, Foley E. Cellular immune defenses of. *Drosophila melanogaster Dev Comp Immunol* (2016) 58:95–101. doi: 10.1016/j.dci.2015.12.019

8. Cattenoz PB, Monticelli S, Pavlidaki A, Giangrande A. Toward a consensus in the repertoire of hemocytes identified in Drosophila. *Front Cell Dev Biol* (2021) 9:643712. doi: 10.3389/fcell.2021.643712

9. Hultmark D, Andó I. Hematopoietic plasticity mapped in *Drosophila* and other insects. *Elife* (2022), 11:e78906. doi: 10.7554/eLife.78906

10. Márkus R, Lerner Z, Honti V, Csordás G, Zsámboki J, Cinege G, et al. Multinucleated giant hemocytes are effector cells in cell-mediated immune responses of. *Drosophila J Innate Immun* (2015) 7:340–53. doi: 10.1159/000369618

11. Cinege G, Lerner Z, Magyar LB, Soós B, Tóth R, Kristó I, et al. Cellular immune response involving multinucleated giant hemocytes with two-step genome amplification in the drosophilid Zaprionus Indianus. *J Innate Immun* (2020) 25:1–16. doi: 10.1159/000502646

12. Cinege G, Magyar LB, Kovács AL, Lerner Z, Juhász G, Lukacsovich D, et al. Broad ultrastructural and transcriptomic changes underlie the multinucleated giant hemocyte mediated innate immune response against parasitoids. *J Innate Immun* (2022) 14(4):335–54. doi: 10.1159/000520110

13. Miron RJ. Bosshardt DD Multinucleated giant cells: good guys or bad guys? *Tissue Eng Part B Rev* (2018) 24:1. doi: 10.1089/ten.TEB.2017.0242

14. Pagán AJ, Ramakrishnan L. Formation and function of granulomas. *Annu Rev Immunol* (2018) 36:639–65. doi: 10.1146/annurev-immunol-032712-100022

15. Anderson RS. Polykaryon formation by mercenaria hemocytes. *Biol Bull* (1987) 172:2. doi: 10.2307/1541796

16. Brodbeck WG, Anderson JM. Giant cell formation and function. *Curr Opin Hematol* (2009) 16(1):53–7. doi: 10.1097/MOH.0b013e32831ac52e

17. Sakai H, Okafuji I, Nishikomori R, Abe J, Izawa K, Kambe N, et al. The CD40-CD40L axis and IFN-γ play critical roles in Langhans giant cell formation. *Int Immunol* (2012) 24:5–15. doi: 10.1093/intimm/dxr088

18. Galko MJ. Krasnow MA Cellular and genetic analysis of wound healing in *Drosophila* larvae. *PloS Biol* (2004) 2(8):e239. doi: 10.1371/journal.pbio.0020239

19. Kacsoh BZ, Bozler J, Schlenke TA. A role for nematocytes in the cellular immune response of the Drosophilid. *Zaprionus Indianus Parasitol* (2014) 141:697–715. doi: 10.1017/S0031182013001431

20. Vilmos P, Nagy I, Kurucz E, Hultmark D, Gateff E, Andó I. A rapid rosetting method for separation of hemocyte sub-populations of. *Drosophila melanogaster Dev Comp Immunol* (2004) 28(6):555–63. doi: 10.1016/j.dci.2003.10.001

21. Comeault A, Wang J, Tittes S, Isbell K, Ingley S, Hurlbert A, et al. Genetic diversity and thermal performance in invasive and native populations of African fig flies. *Mol Biol Evol* (2020) 37(7):1893–906. doi: 10.1093/molbev/msaa050

22. Behnke O. An electron microscope study of the megacaryocyte of the rat bone marrow: I. The development of the demarcation membrane system and the platelet surface coat. *J Ultrastruct Res* (1968) 24:412–33. doi: 10.1016/S0022-5320(68)80046-2

23. Machlus KR, Italiano JE. The incredible journey: From megakaryocyte development to platelet formation. *J Cell Biol* (2013) 201(6):785–96. doi: 10.1083/jcb.201304054

24. Jang IH, Nam HJ, Lee WJ. CLIP-domain serine proteases in Drosophila innate immunity. *BMB Rep* (2008) 41(2):102–7. doi: 10.5483/bmbrep.2008.41.2.102

25. Veillard F, Troxler L, Reichhart JM. *Drosophila melanogaster* clip-domain serine proteases: Structure, function and regulation. *Biochimie* (2016) 122:255–69. doi: 10.1016/j.biochi.2015.10.007

26. Kumar K, Mhetre A, Ratnaparkhi GS, Kamat SS. A Superfamily-wide activity atlas of serine hydrolases in Drosophila melanogaster. *Biochemistry* (2021) 60 (16):1312–24. doi: 10.1021/acs.biochem.1c00171

27. Middha S, Wang X. Evolution and potential function of fibrinogen-like domains across twelve *Drosophila* species. *BMC Genomics* (2008) 30:9. doi: 10.1186/1471-2164-9-260

28. Dong Y, Dimopoulos G. Anopheles fibrinogen-related proteins provide expanded pattern recognition capacity against bacteria and malaria parasites. *J Biol Chem* (2009) 284(15):9835–44. doi: 10.1074/jbc.M807084200

29. Hanington PC, Zhang SM. The primary role of fibrinogen-related proteins in invertebrates is defense, not coagulation. *J Innate Immun* (2011) 3(1):17–27. doi: 10.1159/000321882

30. Cerenius L, Söderhäll K. Variable immune molecules in invertebrates. *J Exp Biol* (2013) 216:4313–9. doi: 10.1242/jeb.085191

31. Xia X, You M, Rao XJ, Yu XQ. Insect C-type lectins in innate immunity. *Dev Comp Immunol* (2018) 83:70–9. doi: 10.1016/j.dci.2017.11.020

32. Lu Y, Su F, Zhu K, Zhu M, Li Q, Hu Q, et al. Comparative genomic analysis of C-type lectin-domain genes in seven holometabolous insect species. *Insect Biochem Mol Biol* (2020) 126:103451. doi: 10.1016/j.ibmb.2020.103451

33. Cattenoz PB, Sakr R, Pavlidaki A, Delaporte C, Riba A, Molina N, et al. Temporal specificity and heterogeneity of *Drosophila* immune cells. *EMBO J* (2020) 39(12): e104486. doi: 10.15252/embj.2020104486

34. Cho B, Yoon SH, Lee D, Koranteng F, Tattikota SG, Cha N, et al. Single-cell transcriptome maps of myeloid blood cell lineages in. *Drosophila Nat Commun* (2020) 11(1):4483. doi: 10.1038/s41467-020-18135-y

35. Fu Y, Huang X, Zhang P, van de Leemput J, Han Z. Single-cell RNA sequencing identifies novel cell types in *Drosophila* blood. *J Genet Genomics* (2020) 47(4):175–86. doi: 10.1016/j.jgg.2020.02.004

36. Girard JR, Goins LM, Vuu DM, Sharpley MS, Spratford CM, Mantri SR, et al. Paths and pathways that generate cell-type heterogeneity and developmental progression in hematopoiesis. *Elife* (2021) 10:e67516. doi: 10.7554/eLife.67516

37. Leitao AB, Arunkumar R, Day JP, Geldman EM, Morin-Poulard I, Crozatier M, et al. Constitutive activation of cellular immunity underlies the evolution of resistance to infection in *Drosophila*. *eLife* (2020) 9:e59095. doi: 10.7554/eLife.59095

38. Tattikota SG, Cho B, Liu Y, Hu Y, Barrera V, Steinbaugh MJ, et al. A single-cell survey of drosophila blood. *eLife* (2020) 9:e54818. doi: 10.7554/eLife.54818

39. Bozler J, Kacsoh BZ, Bosco G. Nematocytes: discovery and characterization of a novel anculeate hemocyte in *Drosophila falleni* and *Drosophila phalerata*. *PloS One* (2017) 12(11):e0188133. doi: 10.1371/journal.pone.0188133

40. Cramer EM, Norol F, Guichard J, Breton-Gorius J, Vainchenker W, Masse JM, et al. Ultrastructure of platelet formation by human megakaryocytes cultured with the Mpl ligand. *Blood* (1997) 89(7):2336–46. doi: 10.1182/blood.V89.7.2336

41. Zimmerman GA, Weyrich AS. Signal-dependent protein synthesis by activated platelets new pathways to altered phenotype and function. *Arterioscler Thromb Vasc Biol* (2008) 28(3):17–24. doi: 10.1161/ATVBAHA.107.160218

42. Li JL, Zarbock A, Hidalgo A. Platelets as autonomous drones for hemostatic and immune surveillance. *J Exp Med* (2017) 214(8):2193–204. doi: 10.1084/jem.20170879

43. Scherfer C, Karlsson C, Loseva O, Bidla G, Goto A, Havemann J, et al. Isolation and characterization of hemolymph clotting factors in *Drosophila melanogaster* by a pullout method. *Curr Biol* (2004) 14:625–9. doi: 10.1016/j.cub.2004.03.030

44. Tsai CR, Wang Y. Galko MJ Crawling wounded:molecular genetic insights into wound healing from Drosophila larvae. *Int J Dev Biol* (2018) 62(6-7-8):479–89. doi: 10.1387/ijdb.180085mg

45. Dziedziech A, Shivankar S, Theopold U. *Drosophila melanogaster* responses against entomopathogenis nematodes: focus on hemolymph clots. *Insects* (2020) 11 (1):62. doi: 10.3390/insects11010062

46. Darnell JE, Kerr IM, Stark GR. Jak-STAT pathways and transcriptional activation in response to IFNs and other extracellular signaling proteins. *Science* (1994) 264:1415–21. doi: 10.1126/science.8197455

47. Morin-Poulard I, Vincent A, Crozatier M. The *Drosophila* JAK-STAT pathway in blood cell formation and immunity. *JAK-STAT* (2013) 2(3):e25700. doi: 10.4161/jkst.25700

48. Williams MJ, Wiklund ML, Wikman S, Hultmark D. Rac1 signalling in the *Drosophila* larval cellular immune response. *J Cell Sci* (2006) 119:2015–24. doi: 10.1242/jcs.02920

49. Lee CW, Kwon YC, Lee Y, Park MY, Choe KM. *cdc37* is essential for JNK pathway activation and wound closure in *Drosophila*. *Mol Biol Cell* (2019) 30(21):2651–8. doi: 10.1091/mbc.E18-12-0822

frontiers | Frontiers in Immunology

TYPE Original Research
PUBLISHED 12 January 2024
DOI 10.3389/fimmu.2023.1310117

OPEN ACCESS

EDITED BY
Susanna Valanne,
Tampere University, Finland

REVIEWED BY
Ryohei Furukawa,
Keio University, Japan
Pierre Cattenoz,
INSERM U964 Institut de Génétique et de Biologie Moléculaire et Cellulaire (IGBMC), France

*CORRESPONDENCE
Iwan R. Evans
i.r.evans@sheffield.ac.uk

RECEIVED 09 October 2023
ACCEPTED 13 December 2023
PUBLISHED 12 January 2024

CITATION
Brooks EC, Zeidler MP, Ong ACM and Evans IR (2024) Macrophage subpopulation identity in *Drosophila* is modulated by apoptotic cell clearance and related signalling pathways.
Front. Immunol. 14:1310117.
doi: 10.3389/fimmu.2023.1310117

Macrophage subpopulation identity in *Drosophila* is modulated by apoptotic cell clearance and related signalling pathways

Elliot C. Brooks[1], Martin P. Zeidler[2], Albert C. M. Ong[1] and Iwan R. Evans[1*]

[1]School of Medicine and Population Health and the Bateson Centre, University of Sheffield, Sheffield, United Kingdom, [2]School of Biosciences and the Bateson Centre, University of Sheffield, Sheffield, United Kingdom

In *Drosophila* blood, plasmatocytes of the haemocyte lineage represent the functional equivalent of vertebrate macrophages and have become an established *in vivo* model with which to study macrophage function and behaviour. However, the use of plasmatocytes as a macrophage model has been limited by a historical perspective that plasmatocytes represent a homogenous population of cells, in contrast to the high levels of heterogeneity of vertebrate macrophages. Recently, a number of groups have reported transcriptomic approaches which suggest the existence of plasmatocyte heterogeneity, while we identified enhancer elements that identify subpopulations of plasmatocytes which exhibit potentially pro-inflammatory behaviours, suggesting conservation of plasmatocyte heterogeneity in *Drosophila*. These plasmatocyte subpopulations exhibit enhanced responses to wounds and decreased rates of efferocytosis when compared to the overall plasmatocyte population. Interestingly, increasing the phagocytic requirement placed upon plasmatocytes is sufficient to decrease the size of these plasmatocyte subpopulations in the embryo. However, the mechanistic basis for this response was unclear. Here, we examine how plasmatocyte subpopulations are modulated by apoptotic cell clearance (efferocytosis) demands and associated signalling pathways. We show that loss of the phosphatidylserine receptor Simu prevents an increased phagocytic burden from modulating specific subpopulation cells, while blocking other apoptotic cell receptors revealed no such rescue. This suggests that Simu-dependent efferocytosis is specifically involved in determining fate of particular subpopulations. Supportive of our original finding, mutations in *amo* (the *Drosophila* homolog of *PKD2*), a calcium-permeable channel which operates downstream of Simu, phenocopy *simu* mutants. Furthermore, we show that Amo is involved in the acidification of the apoptotic cell-containing phagosomes, suggesting that this reduction in pH may be associated with macrophage reprogramming. Additionally, our results also identify Ecdysone receptor signalling, a pathway related to control of cell death during developmental transitions, as a controller of plasmatocyte subpopulation identity. Overall,

10.3389/fimmu.2023.1310117

these results identify fundamental pathways involved in the specification of plasmatocyte subpopulations and so further validate *Drosophila* plasmatocytes as a heterogeneous population of macrophage-like cells within this important developmental and immune model.

KEYWORDS

macrophage, Drosophila, apoptotic cell clearance, haemocyte, apoptosis, ecdysone

Introduction

Macrophages are highly phagocytic cells of the vertebrate innate immune system, which are responsible for tissue homeostasis, fighting infection and removing apoptotic cells (1). Heterogeneity of the vertebrate macrophage is a fundamental component of the immune system, allowing these cells to respond to a variety of stimuli in a wide range of environments through differentiation into a range of tissue resident cell types and an ability to adopt various activation states, termed macrophage polarisation (2, 3). These activation states range from pro-inflammatory (M1-like) states associated with microbicidal activities and initial recruitment to wounds, to anti-inflammatory states (M2-like) that are associated with apoptotic cell clearance and the later stages of wound healing (M2-like) (4), with this spectrum of activation states regulated in response to immediate environmental challenges (5). Aberrant macrophage polarisation has been implicated in numerous chronic inflammatory conditions, such as Chronic Obstructive Pulmonary Disease (COPD) and atherosclerosis, which are associated with increased M2-like polarisation and M1-like polarisation, respectively (6–8). Though numerous experimental models have been exploited to facilitate our understanding of these fundamental processes, these often rely on *ex vivo* approaches that do not fully reproduce the temporal and spatial dynamics of *in vivo* biological systems. As such, low complexity *in vivo* models to study macrophage heterogeneity *in situ* have the potential to provide unique biological insights.

The fruit fly *Drosophila melanogaster* possesses an innate immune system comprising three lineages of haemocytes, specified via Serpent (Srp), the fly orthologue of the GATA transcription factors involved in vertebrate haematopoiesis (9). The plasmatocyte lineage is the dominant blood cell throughout normal development and represents the functional equivalent of vertebrate macrophages. Plasmatocytes mediate the same essential functions as macrophages, responding to wounds, fighting infection and removing apoptotic cells (efferocytosis) (10). Efferocytosis, has been particularly well studied in the fly, and multiple apoptotic cell receptors are broadly expressed across the total plasmatocyte population: those characterised include Simu and Draper (both CED1 family members), and Croquemort, which is homologous to the CD36 scavenger receptor expressed on human macrophages (11–15). Mutations in these receptors prevent efficient identification of dying cells, resulting in a build-up of uncleared apoptotic corpses *in vivo*, the persistence of which disrupts other plasmatocyte functions, such as migration and wound responses (16, 17). However, despite the undoubted similarities between plasmatocytes and macrophages, until recently there was limited evidence to suggest that plasmatocytes were as functionally or molecularly diverse as their vertebrate counterparts.

Recent studies into plasmatocyte behaviour *in vivo* reveal that these cells do not behave in a uniform manner. Following their dispersal across the embryo, plasmatocytes surrounding the ventral nerve cord appear to move randomly as if they are no longer migrating towards chemotactic cues. Imaging this random movement in stage 15 embryos revealed a wide range in migration speeds, suggesting some plasmatocytes may be developmentally programmed to have enhanced motility capabilities. Similarly, imaging plasmatocyte movements in the vicinity of a sterile wound indicated that some plasmatocytes exhibit a rapid and robust migratory response, while others at similar distances from the wound site fail to respond (17, 18). There is also remarkable variability in the number of apoptotic corpses phagocytosed by plasmatocytes (17–19). These data hint that the overall plasmatocyte population is made up of subpopulations, each of which exhibit distinct innate immune behaviours. Consistent with this cellular diversity, transcriptional profiling studies using single cell RNA sequencing (scRNAseq) approaches confirm the existence of molecularly-defined plasmatocyte clusters in larvae (20–23), while reporter studies indicate heterogeneity across the *Drosophila* lifecourse (18).

In addition to a diversity of activities at any one developmental stage, the behaviour of *Drosophila* plasmatocytes also changes markedly throughout the life cycle of the fly. During embryogenesis, plasmatocytes are highly migratory as they disperse around the embryo, shaping tissues and organs via deposition of extracellular matrix (24) and phagocytosis of apoptotic cells (25). By contrast, plasmatocytes are largely sessile during larval stages, adhering to the body wall where they proliferate under the control of Activin-β released from nearby neurons (26, 27). At the onset of metamorphosis, plasmatocyte behaviour changes once more, as these cells are reprogrammed to become more highly phagocytic and migratory to deal with the high levels of cell death associated with the tissue remodelling during this developmental stage (28). These alterations in plasmatocyte behaviour are influenced by the action of the steroid hormone 20-hydroxyecdysone (hereafter referred to as ecdysone), itself

central to progression through these developmental stages which require significant tissue remodelling and apoptosis. Whether these changes in behaviour are linked to changes in subpopulation identity is unknown. Further examples of the importance of ecdysone in behavioural transition points is illustrated by the fact that embryonic plasmatocytes expressing a dominant-negative isoform of the ecdysone receptor (EcR) fail to mount effective responses to infection (29), while increasing ecdysone levels acting via the ecdysone receptor B1 stimulate plasmatocytes to become highly motile and phagocytic during pupation (30–32). Thus, plasmatocytes exhibit plasticity, with their behaviours changing across the lifecourse, according to the developmental stage, with the action of ecdysone implicated in contributing to these changes.

Following up *in vivo* evidence hinting at plasmatocyte heterogeneity and plasticity, we recently exploited the Vienna Tiling (VT) array library of non-coding enhancer elements (33) and identified enhancers active in a subset of plasmatocytes (18). This approach revealed the existence of functionally-distinct subpopulations that were associated with enhanced migratory responses to wounds and decreased rates of apoptotic cell clearance compared to the overall plasmatocyte population, behaviours which are typical of pro-inflammatory macrophages. These subpopulations are developmentally regulated, with relatively high numbers in embryonic stages preceding a drastic decrease in larval stages, before subpopulations ultimately re-emerge at the onset of metamorphosis and persist into adulthood (18), patterns consistent with the changes in plasmatocyte behaviour seen during development, including those regulated by ecdysone signalling.

The plasticity of *Drosophila* plasmatocytes can also be observed by increasing the apoptotic challenge they face *in vivo*. During embryogenesis, the other major cell-type involved in efferocytosis are glial cells, specified via the transcription factor *repo* (14, 34, 35). Loss of glial specification in *repo* null embryos results in increased levels of uncleared apoptotic cells – a change previously shown to impair plasmatocyte migration and wound responses (36). Interestingly, the plasmatocyte subpopulations studied to date exhibit a significant decrease in their relative numbers in a *repo* mutant background (18); this suggests that the high-apoptotic environment seen in *repo* mutants may either prevent plasmatocytes acquiring pro-inflammatory subpopulation identities or alternatively drive exit from those subpopulations.

The fact that putative pro-inflammatory macrophage subpopulations decrease in the presence of high levels of uncleared apoptotic cells suggests that signalling downstream of apoptotic cell receptors may influence subpopulation fate. Here, we show that Simu, a receptor for apoptotic cells, mediates decreases in the numbers of specific plasmatocyte subpopulation cells on exposure to enhanced levels of apoptosis. Furthermore, mutations affecting the calcium-permeable cation channel Amo, which regulates calcium homeostasis downstream of phagocytosis (37), phenocopy results seen in *simu* mutants. This is consistent with a model whereby Amo functions downstream of Simu to facilitate plasmatocyte reprograming to alternative fates. Finally, we demonstrate a requirement for ecdysone signalling in the establishment of subpopulation identity, both in the embryo and pupa. Overall, these findings further reinforce the utility of *Drosophila* plasmatocytes as a robust macrophage model – with cells clearly exhibiting heterogeneity, plasticity, and the apparent ability to switch activation states in response to different environmental challenges.

Methods

Fly genetics and reagents

Stocks of *Drosophila* were kept at 25°C on standard cornmeal/molasses agar. To collect embryos, at least 20 male and 20 female flies were placed in a 100mL beaker which was capped with a 5cm apple juice agar plate supplemented with a small amount of yeast paste (50% in dH_2O), secured with an elastic band and incubated at 22°C for embryo collections. For pupal experiments, crosses were kept at 25°C and white pre-pupae were collected during 30-minute windows and aged at 25°C. All transgenes and mutations were crossed into a w^{1118} background and *CyO dfd-nvYFP* and *TM6b dfd-nvYFP* were used as fluorescent balancers to enable genotyping of embryos (Supplementary Table 1).

The following *Drosophila* drivers and constructs were used: *crq-GAL4* (38), *srpHemo-GAL4* (39), *hml(Δ)-GAL4* (40), *VT17559-GAL4, VT32897-GAL4, VT57089-GAL4, VT62766-GAL4* (18, 33). When exploiting the split GAL4 system (41), the GAL4 activation domain (AD) was expressed via *srpHemo-AD*, while the GAL4 DNA binding domain (DBD) was expressed via *srpHemo-DBD*, *VT17559-DBD*, *VT32897-DBD, VT57089-DBD* and *VT62766-DBD* (18). The following UAS lines were used: *UAS-Stinger* (42), *UAS-eGFP* (Bloomington *Drosophila* Stock Centre), *UAS-drpr-II* (43), and *UAS-EcR.B1*$^{\Delta C655}$ (44). The following GAL4-independent reporter lines were used: *srpHemo-3x-mCherry*, *srpHemo-H2A-3x-mCherry* (45), *srpHemo-GMA* (James Bloor, University of Kent), *VT17559-RFP, VT32897-RFP, VT57089-RFP* and *VT62766-RFP* (18). The following *Drosophila* mutants were used: *amo*^{1} (46), *simu*^{2} (14), *repo*^{03702} (47) and *crq*^{ko92} (48). Supplementary Table 1 contains a full list of genotypes (including parental genotypes) used in this paper.

Imaging of *Drosophila* embryos

All embryos were dechorionated in bleach (49) prior to being mounted ventral-side-up on double-sided tape (Scotch) in a minimal volume of Voltalef oil (VWR). All imaging of embryos was carried out on an UltraView Spinning Disk System (Perkin Elmer) using a 40x UplanSApo oil immersion objective lens (NA 1.3). The ventral region (most medial body segments) of embryos was imaged from the embryonic surface to a depth of 20μm, with z-slices spaced every 1μm. For lysotracker experiments requiring staining of live embryos, stage 15 dechorionated embryos were selected and transferred to a 50:50 mixture of peroxide-free heptane (VWR) and 10μM lysotracker red (Thermofisher) in PBS (Oxoid) in a glass vial, which was shaken in the dark for 30 minutes. Embryos were then transferred into a Watchmaker's glass

containing Halocarbon oil 700 (Sigma), before being mounted as described above.

Embryos requiring fixation and immunostaining were fixed and stained as previously described (17). For Fascin staining, embryos were treated with a mouse anti-Fascin primary antibody (sn7c; Developmental Studies Hybridoma Bank; used at 1:500), with Alexa fluor 568 goat anti-mouse used as a secondary antibody (A11031, Life Technologies; 1:200).

Imaging of pupae

Pupae of the appropriate genotypes were selected and aged to 48h after puparium formation (APF) at 25°C and attached to slides via double-sided tape. Pupae were carefully removed from their pupal cases and covered in a small volume of Voltalef oil. Stacks of 5 coverslips (22 x 22mm, thickness 1) were glued together with nail varnish and then placed either side of pupae. A coverslip (22 x 32mm, thickness 1) was then placed over the top of the pupae, in contact with the oil, supported by the coverslip stacks to prevent damage to pupae. Z-stacks were then taken of the thoracic regions of pupae using a Nikon spinning disk system (Nikon Eclipse Ti2 microscope with a CSU-W1 Okagawa confocal scanner unit and Photometrics Prime 95B 22mm camera; 20X Plan Apo/0.75 objective lens, GFP and RFP filters, 2µm between slices).

Image and statistical analyses

All images were converted to a tiff format, despeckled to reduce background noise, and blinded prior to analysis, which was performed using Fiji/ImageJ (50). To work out the relative number of plasmatocytes within subpopulations in embryos, z-stacks were converted into a maximum intensity projection in Fiji. The total number of plasmatocytes, labelled with pan-plasmatocyte reporters (such as *srpHemo-3x-mCherry*, *crq-GAL4,UAS-GFP; srpHemo-GAL4,UAS-GFP* or anti-Fascin staining), was counted. Numbers of subpopulation plasmatocytes were quantified from images of cells labelled using *VT-GAL4* lines (33), or *srpHemo-AD* in concert with *VT-DBD* transgenes (18) to drive expression from UAS reporters, or via GAL4-independent *VT-RFP* lines (18). The proportion of plasmatocytes within a given subpopulation was then expressed as a percentage of the overall population.

To quantify phagosome acidification, the number of phagosomes of the 5 most-ventral plasmatocytes were selected using the multi-point selection tool (GFP channel; phagosomes exclude cytoplasmic GFP present in plasmatocytes) from z-stacks of the ventral surface imaged as described above. These most-superficial cells are typically, but not exclusively, on the ventral midline, and the number of these phagosomes that overlapped with lysotracker red staining was counted to work out a percentage of phagosome acidification (RFP channel of the z-stacks); again the multi-point selection tool was used to ensure accuracy of scoring. All images were blinded ahead of quantification.

For quantification of subpopulations within the pupal thorax (at 48h APF), maximum projections corresponding to 10 z-slices were assembled starting from the z-position in which the most superficial plasmatocytes were visible (labelled via *hml(Δ)-GAL4,UAS-GFP*), moving deeper into the pupa. All images in the dataset underwent identical contrast adjustment and were blinded ahead of analysis. Cells were then scored as *hml*-positive only or double-positive for *hml* and *VT62766* on the basis of the presence/absence of visible fluorescence in the GFP (*hml(Δ)-GAL4,UAS-GFP*) and RFP (*VT62766-RFP*) filter channels. Cells obscured by the bounding vitelline membrane ("rings" RFP channels of pupal images) were not assessed. The multi-point tool in Fiji was used to keep track of cells that had been assessed. To normalise total numbers of *hml*-positive cells within the thoracic region, the area bounded by the vitelline membrane was measured using the polygon selection tool in Fiji. As an additional means of quantification, the same maximum projections were cropped to the region of interest (demarcated by the vitelline membrane). The green channel was then manually thresholded to create a mask corresponding to plasmatocyte localisation. This was then used to measure total fluorescence (integrated density) within *hml*-positive plasmatocytes for GFP and RFP channels to quantify reporter activity.

Statistical analysis was conducted in GraphPad Prism. Mann-Whitney and Student's unpaired t-tests were used to compare non-parametric and parametric data, respectively. Where greater than two means were to be compared a one-way ANOVA with Dunnett's post-test was used (parametric data).

Results

Loss of Simu, an apoptotic cell receptor, drives expansion of specific plasmatocyte subpopulations

We previously described how numbers of haemocytes in subpopulations defined by the *VT17559*, *VT32897*, *VT57089* and *VT62766* enhancers are reduced in a genetic background containing excess apoptotic cells (*repo* mutants; 18, 36). To explore the mechanistic basis for this effect, we examined the effect of loss of *simu* upon macrophage subpopulations in stage 15 embryos (Figure 1). Subpopulation plasmatocytes were labelled via the split GAL4 system (41) driving *UAS-GFP* specifically in cells with overlapping expression of *serpent* (*srpHemo-AD*) and the subtype-specific VT enhancer (*VT-DBD*) activity (18), while the total plasmatocyte population was independently labelled via a GAL4-independent reporter (*srpHemo-3x-mCherry*; 45; labelled in magenta in Figure 1).

In contrast to *repo* mutants, where an increased apoptotic challenge correlates with a decrease in numbers of subpopulation plasmatocytes (18), no change was observed for the *VT17559*, *VT32897* and *VT62766* subpopulations in a *simu* mutant background (Figures 1A–E), while numbers of *VT57089*-labelled cells actually increased in *simu* mutants compared to controls (Figures 1C, E). This suggests that Simu normally antagonises acquisition or maintenance of the *VT57089* fate. These results suggest that the relative decreases in subpopulation cells seen in *repo* mutants (18) may depend upon the presence of Simu on the surface of plasmatocytes.

10.3389/fimmu.2023.1310117

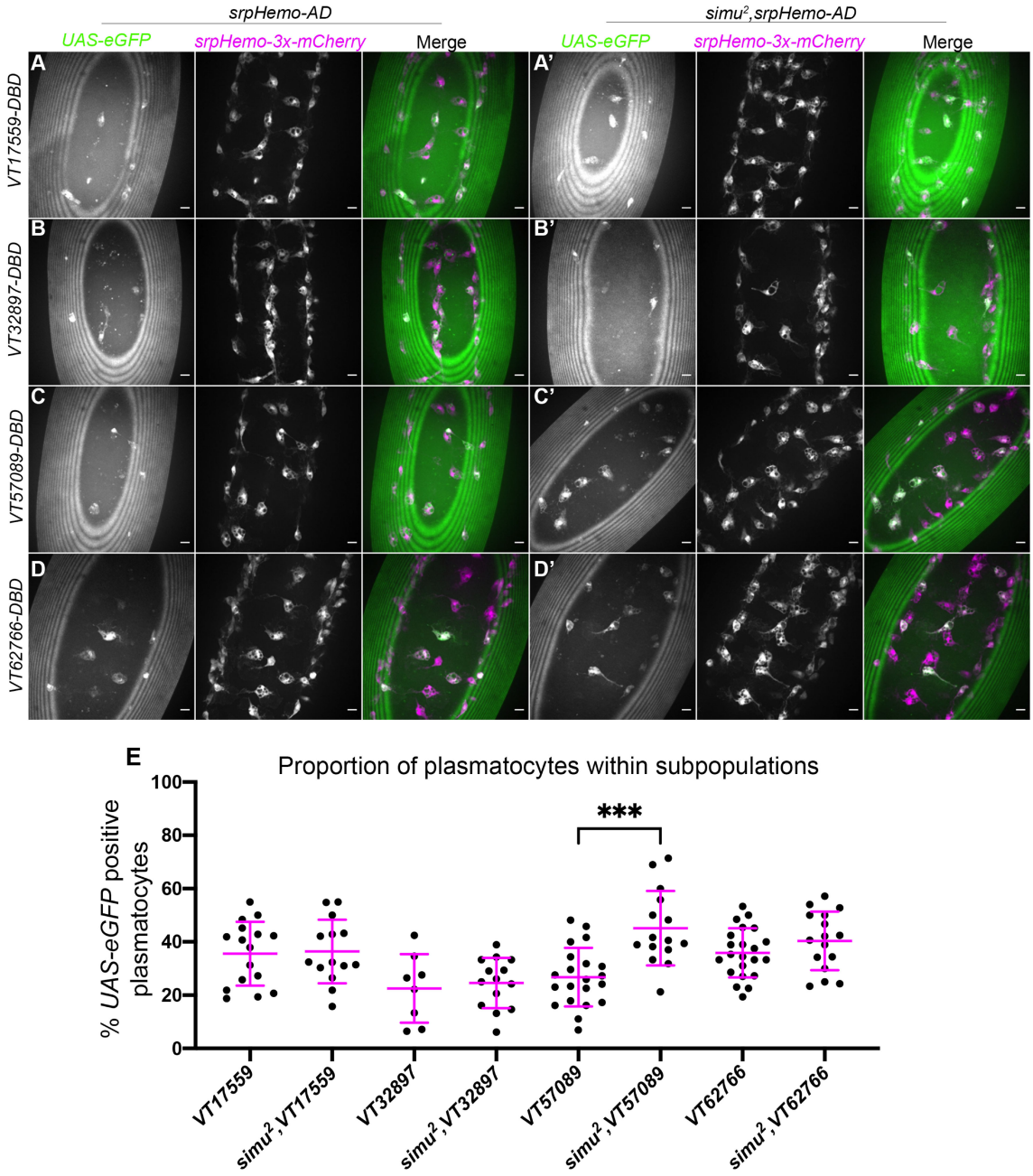

FIGURE 1
Overexposure of plasmatocytes to apoptotic cells via loss of *simu* is not sufficient to cause a decrease in plasmatocyte subpopulations. **(A-D')** representative images of the ventral midline of control **(A–D)** and *simu*^{2} **(A'-D')** embryos at stage 15. *UAS-eGFP* shows plasmatocytes labelled via split-*GAL4* (green in merge), while *srpHemo-3x-mCherry* labels every plasmatocytes (magenta in merge). Anterior is up in all images, scale bars denote 10μm. **(E)** scatterplot showing proportion of plasmatocytes within subpopulations in control and *simu*^{2} embryos. *n*=16, 14, 8,14, 21, 15, 22 and 16, respectively. Only significantly different results are shown on the graph (p=0.0003), all statistical comparisons were carried out via non-paired t-tests. *** Denotes p<0.001.

Simu mediates antagonism of specific subpopulation fates in the presence of large amounts of apoptosis

The contrasting results seen between *repo* and *simu* mutant embryos indicate that increased levels of uncleared apoptotic cells may not be sufficient to mediate decreases in subpopulation numbers – instead, specific interactions between apoptotic cells and plasmatocytes may be required for phenotypic switches. To test whether effective recognition and/or engulfment of apoptotic cells is responsible for mediating the reduction in subpopulation plasmatocytes observed in *repo* mutants, *simu;repo* double mutants were generated and compared to controls (as well as *simu* and *repo* single mutants). Due to the genetics involved in this experiment, subpopulation plasmatocytes were labelled via *VT-GAL4* (as opposed to split *VT-GAL4*) driving expression of *UAS-Stinger* (Figures 2A–D).

10.3389/fimmu.2023.1310117

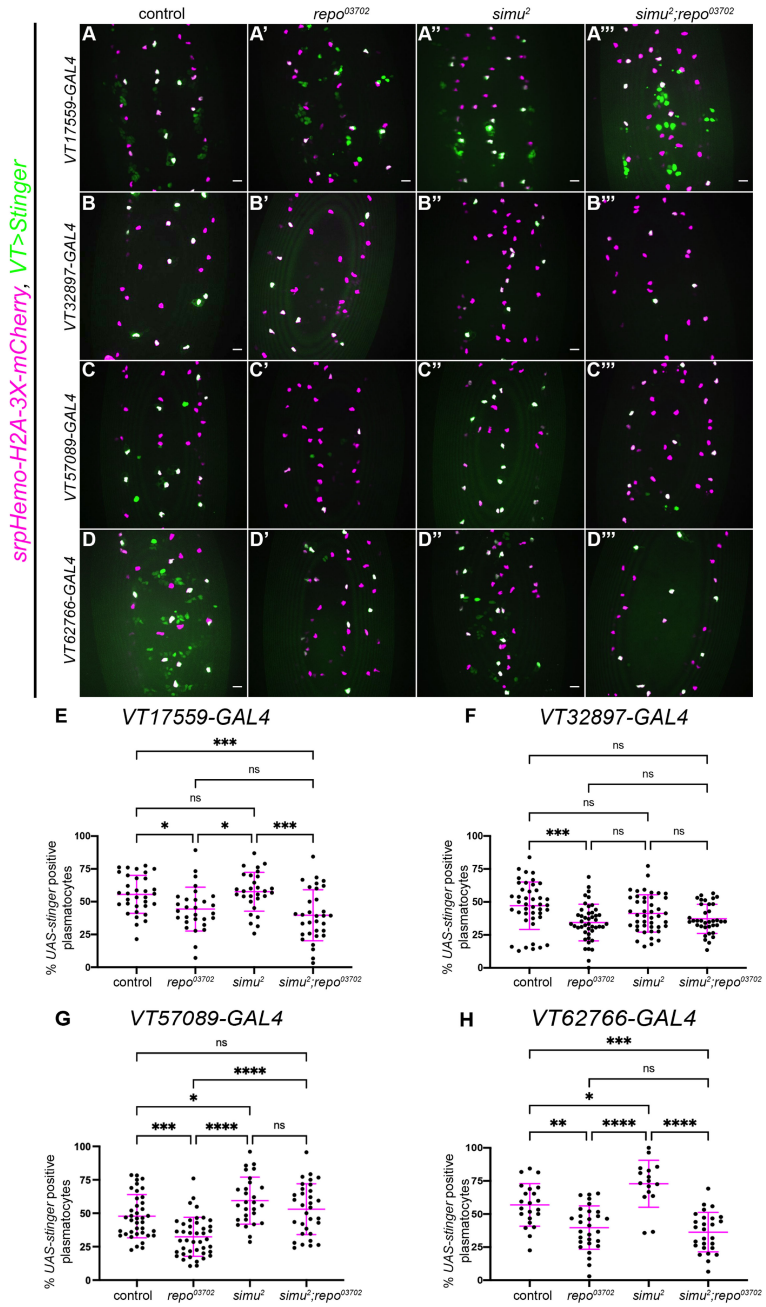

FIGURE 2
Simu-dependent efferocytosis is required for the decrease in the *VT57089* subpopulation seen in *repo* mutants. **(A-D''')** representative maximum projection images of the ventral midline of control **(A–D)**, *repo*^{03702} single mutants **(A'-D')**, *simu*^{2} single mutant **(A'''-D''')** and *simu*^{2};*repo*^{03702} double mutant **(A'''-D''')** embryos at stage 15. *UAS-Stinger* shows subpopulation plasmatocytes labelled via *VT-GAL4* (green in merge), while *srpHemo-H2A-3x-mCherry* labels every plasmatocytes (magenta in merge). Anterior is up in all images, scale bars denote 10μm. **(E)** scatterplot showing proportion of plasmatocytes within the *VT17559* subpopulation. *n*=33, 29, 29 and 32, respectively. **(F)** scatterplot showing proportion of plasmatocytes within the *VT32897* subpopulation. *n*=44, 45, 43 and 36, respectively. **(G)** scatterplot showing proportion of plasmatocytes within the *VT57089* subpopulation. *n*=39, 42, 28 and 32, respectively. **(H)** scatterplot showing proportion of plasmatocytes within the *VT62766* subpopulation. *n*=22, 29, 16 and 27, respectively. Statistical analyses carried out via one-way ANOVA with Dunnett's multiple comparison test. *, **, *** and **** represent p<0.05, p<0.01, p<0.001 and p<0.0001, respectively.

As we have previously shown (18), fewer plasmatocytes were present in all subpopulations examined in the presence of *repo* mutations alone (Figures 2E–H). The loss of *simu* in addition to *repo* (*simu;repo* double mutants) was unable to rescue relative plasmatocyte subpopulation numbers to control levels for the *VT17559* and *VT62766* reporters (Figures 2E, H); there is considerable variability in subpopulation numbers and results for the *VT32897* reporter were not statistically significant (Figure 2F), though the trends were consistent with those observed for *VT17559* and *VT62766* (Figures 2E, H). This variability potentially stems, in part, from the stochastic nature of contact between apoptotic corpses and plasmatocytes in the embryo. In contrast, numbers of

cells labelled via the *VT57089* reporter were completely rescued to control levels in *simu;repo* double mutants (Figure 2G). This implies that Simu-dependent efferocytosis, or an effector downstream of Simu-dependent recognition of apoptotic cells, may mediate the apparent shift out of the *VT57089* subpopulation seen in the presence of large numbers of apoptotic cells. Furthermore, this suggests distinct mechanisms may control plasmatocyte identity from subpopulation to subpopulation in response to the high apoptotic challenge presented to plasmatocytes (as assayed via *repo* loss-of-function).

Other apoptotic cell clearance receptors do not appear to contribute to subpopulation identity

Given the role of *simu*, we next examined the role of *crq* and *drpr* in regulation of subpopulation identity following challenge with large numbers of apoptotic cells (i.e., in a *repo* mutant background). A loss-of-function *crq* allele (crq^{ko}; 48) was used alongside *repo* mutations to investigate whether *crq* is required for the decreased numbers of subpopulation plasmatocytes seen in *repo* mutants. Subpopulation plasmatocytes were labelled via *VT-GAL4* transgenes driving *UAS-Stinger*, while all plasmatocytes were labelled via immunostaining for Fascin, an Actin-bundling protein highly enriched in *Drosophila* plasmatocytes (51; Figures 3A–D). This approach revealed no differences in the proportion of plasmatocytes found within each subpopulation when comparing *repo* single mutants to *crq;repo* double mutants (Figure 3E). This suggests that the decrease in subpopulation numbers seen in *repo* mutants is independent of Crq.

To investigate the involvement of *drpr* in modulating plasmatocyte subpopulations, an inhibitory isoform of *drpr* (*UAS-drpr-II*; 43) was expressed specifically in subpopulation plasmatocytes. This was driven using *VT-GAL4* transgenes, which simultaneously enabled expression of *UAS-Stinger* to label subpopulation cells; the overall plasmatocyte population was labelled via *srpHemo-H2A-3x-mCherry* (Figures 3F–I). Similar to the use of *crq* mutants, expression of *drpr*-II specifically in subpopulation cells in a *repo* mutant background did not impact subpopulation numbers when compared to *repo* mutants lacking *UAS-drpr-II* expression (Figures 3F–J). Consistently, expression of *drpr-II* in all plasmatocytes did not impact subpopulation numbers in the absence of increased apoptotic cell challenge (Supplementary Figures 1, 2). Taken together this suggests that neither Drpr nor Crq modulate subpopulation identity at embryonic stages, in contrast to Simu.

Amo functions downstream of Simu to control identity of specific subpopulations

Our results so far have shown that Simu appears to be involved in shifting plasmatocytes out of the *VT57089* subpopulation, both in control backgrounds (Figure 1E) and in response to the high apoptotic challenge presented by *repo* mutations (Figure 2G). The calcium-permeable cation channel Amo, homologous to human *PKD2*, which is causative of Autosomal Dominant Polycystic Kidney Disease (ADPKD), has previously been shown to maintain calcium homeostasis downstream of Simu during later stages of efferocytosis in *Drosophila* (37). We therefore used a loss-of-function *amo* allele (amo^{1}; 46) to investigate whether Amo-dependent calcium homeostasis is involved in modulating the identity of *VT57089* subpopulation plasmatocytes in stage 15 embryos. As per Figure 1C, *VT57089* subpopulation plasmatocytes were labelled using the split GAL4 system to drive expression of *UAS-eGFP*, while the overall plasmatocyte population was labelled via *srpHemo-3x-mCherry* (Figures 4A, B).

Unlike *simu* mutants, no differences in the proportion of plasmatocytes within the *VT57089* subpopulation were observed when comparing wild-type embryos to amo^{1} single mutants (Figure 4C). These experiments were initially conducted in embryos with 'normal' – i.e., developmental levels – of apoptosis. We therefore next introduced *repo* mutations to address how loss of Amo impacted the *VT57089* subpopulation in response to an increased apoptotic challenge. Subpopulation plasmatocytes were labelled using *VT-GAL4* transgenes to drive expression from *UAS-Stinger*, while anti-Fascin staining was again used to label the overall macrophage population to calculate the proportion of plasmatocytes within this subpopulation (Figures 4D–E). Interestingly, these results phenocopied *simu* mutants, with a significantly higher proportion of *VT57089* plasmatocytes found in *amo;repo* double mutants compared to *repo*-only controls (Figure 4F). This suggests that Amo-mediated calcium homeostasis is an important aspect of signalling downstream of Simu, which may prevent acquisition of *VT57089* identity, or mediate reprogramming of plasmatocytes away from this specific subpopulation.

To investigate the functional impact of *amo* mutations in the presence of elevated apoptotic challenge – i.e., in a *repo* mutant background – lysotracker staining was utilised to visualise defects in phagosome acidification. Phagosome acidification occurs during the later stages of efferocytosis, downstream of engulfment (52), and is a calcium-dependent process (53). Thus, this process was an attractive pathway to investigate with respect to *amo* mutations, due to the calcium permeability of the Amo cation channel. All plasmatocytes were labelled via *crq-GAL4* driving expression of *UAS-eGFP* (Figures 5A–C), and the number of acidified (lysotracker red positive) vacuoles per plasmatocyte was quantified. Lysotracker staining of *repo* single mutants and *amo;repo* double mutants revealed a significant reduction in the total number of acidified phagosomes present within in *amo;repo* double mutant plasmatocytes compared to *repo*-only controls (Figure 5D). Furthermore, the proportion of phagosomes that were acidified was also significantly lower in *amo;repo* double mutants (Figure 5E). These results suggest that Amo is either required for phagosomal acidification or plays an upstream role in that process during efferocytosis. Defects in acidification may interfere with specification of plasmatocytes as *VT57089* subpopulation cells. Alternatively, this process could lead to plasmatocytes exiting this

10.3389/fimmu.2023.1310117

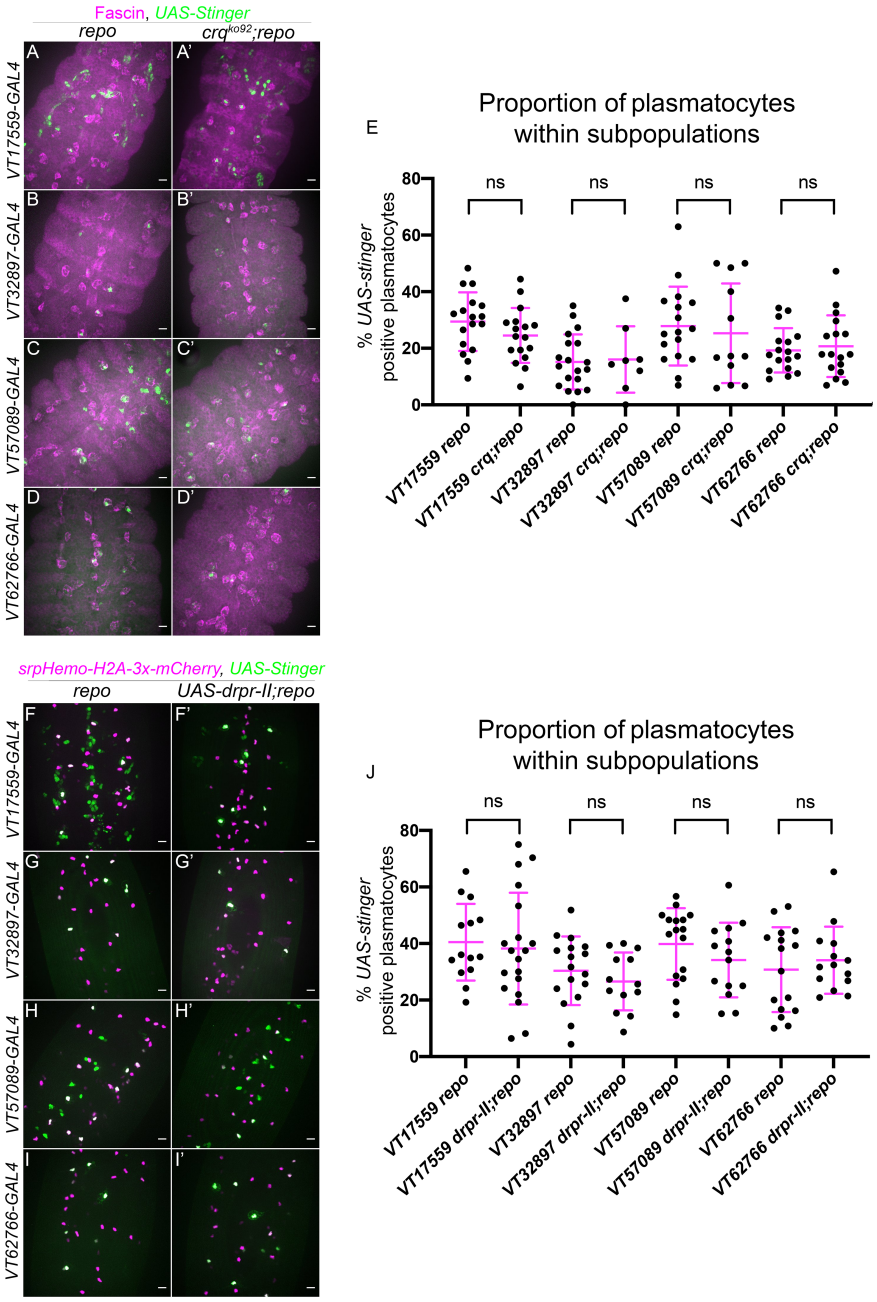

FIGURE 3
Croquemort and Draper do not affect plasmatocyte subpopulations. **(A-D')** representative maximum projection images of the ventral midline of *repo*-only single mutant embryos **(A–D)** and *crq;repo* double mutant embryos **(A'-D')** at stage 15. Plasmatocytes labelled via Fascin staining (magenta) while subpopulation plasmatocytes are labelled via *VT-GAL4* driving expression of *UAS-Stinger* (green). Anterior is up in all images, scale bars denote 10μm. **(E)** scatterplot showing proportion of plasmatocytes within subpopulations. *n*= 18, 17, 20, 8, 17, 12, 17 and 17, respectively. Statistical analyses carried out via unpaired *t*-tests. **(F-I')** representative maximum projection images of the ventral midline of *repo*-only single mutant embryos **(F–I)** and *repo* mutant embryos expressing *UAS-drpr-II* specifically in plasmatocytes **(F'-I')** at stage 15. All plasmatocytes labelled via srpHemo-H2A-3x-mCherry, while subpopulation plasmatocytes are labelled via VT-GAL4 lines driving expression from UAS-Stinger. Anterior is up in all images, scale bars denote 10μm. **(J)** scatterplot showing proportion of plasmatocytes within subpopulations. *n*=14, 19, 17, 13, 17, 14, 16 and 14, respectively. Statistical analyses in **(E, J)** carried out via unpaired *t*-tests.

subpopulation fate. Overall, we have shown that Simu negatively regulates *Drosophila* plasmatocyte subpopulation identity. *Amo* also appears required, with its role potentially linking effective phagosome acidification during the later stages of efferocytosis to regulation of cell identity.

Ecdysone signalling contributes to regulation of subpopulation identity

In the context of *Drosophila* development and metamorphosis, the levels of the steroid hormone ecdysone (20-hydroxyecdysone)

10.3389/fimmu.2023.1310117

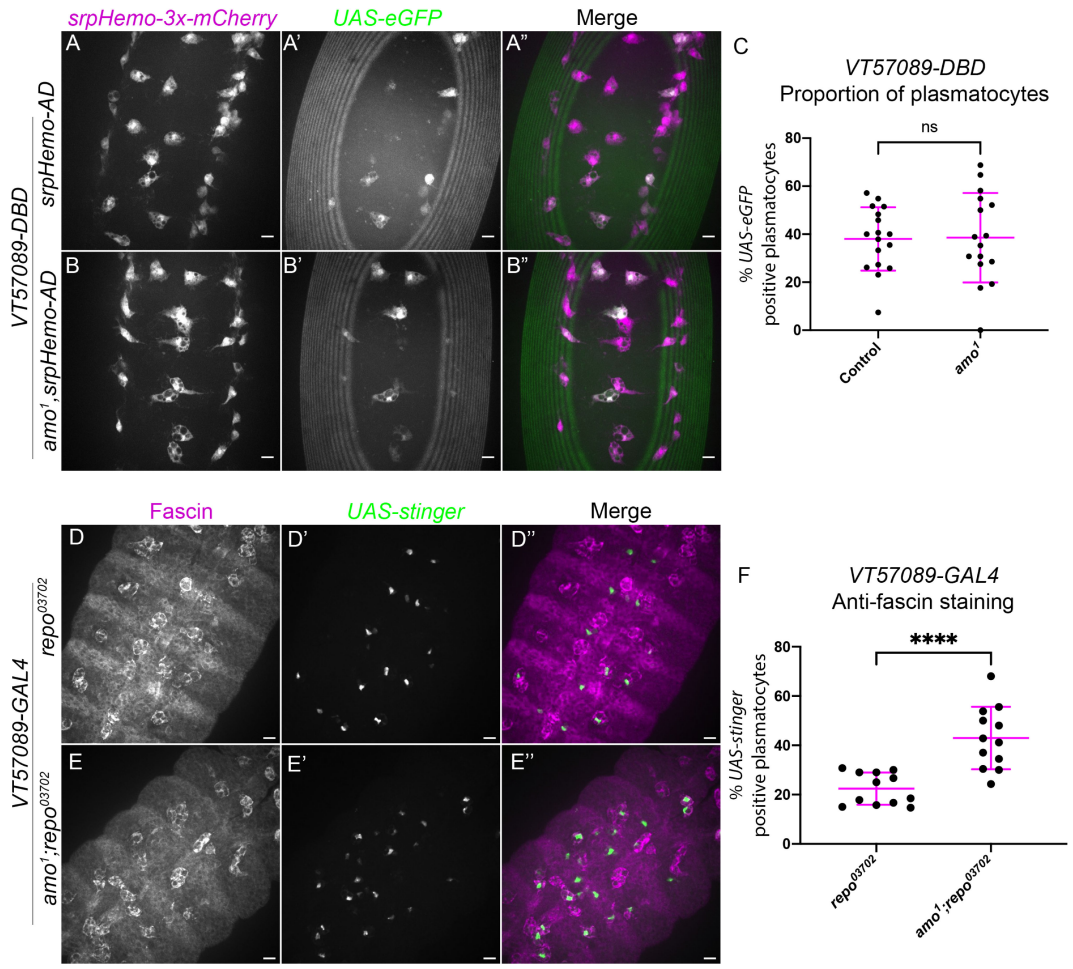

FIGURE 4
The calcium-permeable cation channel Amo is required for the shift out of the *VT57089* subpopulation seen in *repo* mutants. **(A-B")** representative images of the ventral midline of control **(A-A")** and *amo*^{1} **(B-B")** embryos at stage 15. *srpHemo-3x-mCherry* labels every plasmatocyte (magenta in merge), while *VT57089* subpopulation plasmatocytes labelled via split *GAL4* system to drive expression of *UAS-eGFP* (green in merge). Anterior is up in all images, scale bars denote 10µm. **(C)** scatterplot showing the proportion of plasmatocytes within the *VT57089* subpopulation in control and *amo*^{1} embryos. *n*=17 and 16, respectively. **(D-E")** representative maximum projection images of the ventral midline of *repo*^{03702} single mutant **(D-D")** and *amo*^{1};*repo*^{03702} double mutant **(E-E")** embryos at stage 15. Plasmatocytes have been labelled via Fascin staining (magenta in merge), with *VT57089* positive cells labelled via *UAS-Stinger* (green in merge). Anterior is up in all images, scale bars denote 10µm. **(F)** scatterplot showing proportion of plasmatocytes within the *VT57089* subpopulation between *repo*^{03702} single mutant and *amo*^{1};*repo*^{03702} double mutant embryos based on anti-Fascin staining. *n*=12 and 13, respectively. Statistical analyses in **(C, F)** carried out via unpaired *t*-tests. **** represents p<0.0001.

are absolutely central to a multitude of developmental events (54) – including the switching of plasmatocytes between different behavioural and transcriptional states (28, 31). Given these important roles in programming of *Drosophila* immune cells and association of ecdysone with developmental transitions during which there are significant changes in plasmatocyte subpopulation numbers, we sought to investigate whether this hormone also plays an instructive role in establishing subpopulation identity. A dominant-negative isoform of the nuclear ecdysone receptor (*UAS-EcR.B1*$^{\Delta C655}$; referred to hereafter as *EcR-DN*; 44) was therefore specifically expressed in all plasmatocytes via *srpHemo-GAL4* and *crq-GAL4*, with subpopulations labelled via GAL4-independent *VT-RFP* reporters, with the percentage of plasmatocytes within each subpopulation then determined (Figures 6A–D).

The proportion of plasmatocytes within the *VT17559* and *VT32897* subpopulations was unchanged on expression of EcR-DN, suggesting that ecdysone signalling is not responsible for establishing these subpopulations in the embryo (Figure 6E). Although the *VT57089* subpopulation exhibited a trend suggesting a modest decrease in numbers in the presence of EcR-DN, this was not statistically significant (Figure 6E). By contrast, the *VT62766* subpopulation exhibited a 30% decrease of subpopulation plasmatocytes in the presence of EcR-DN, suggesting ecdysone signalling is autonomously required in plasmatocytes for the differentiation and/or maintenance of this subpopulation in the embryo (Figure 6E).

VT62766-labelled cells appear absent during late larval stages but can once more be found in large numbers in pupae (18). Haemocytes are exposed to multiple waves of ecdysone during pupal development.

10.3389/fimmu.2023.1310117

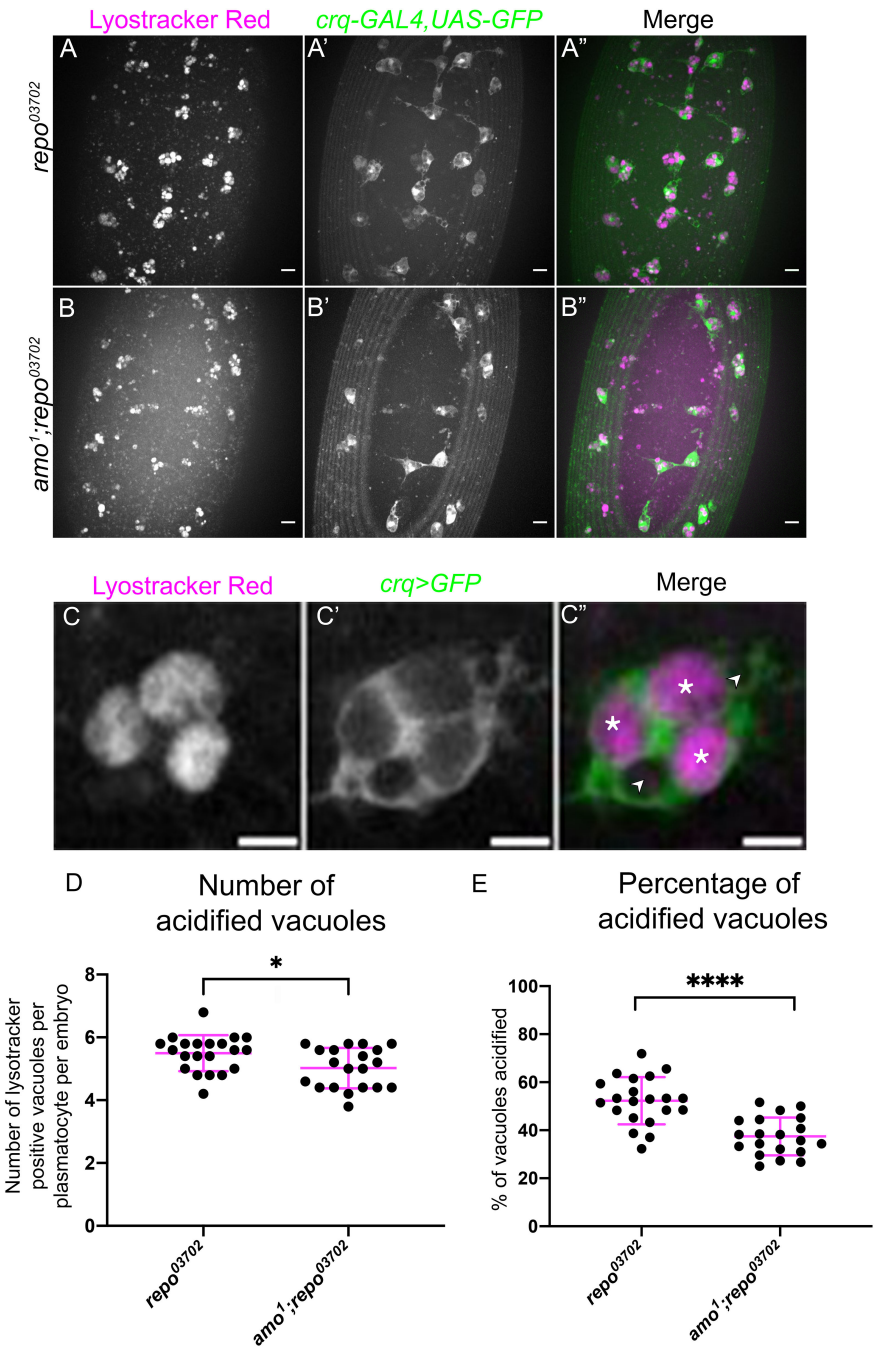

FIGURE 5
Amo is required for effective phagosome acidification. **(A-B")** representative maximum projection images of the ventral midline of *repo*^{03702} single mutant **(A-A")** and *amo*^{1};*repo*^{03702} double mutant **(B-B")** embryos at stage 15. Lysotracker red shows acidified phagosomes **(A, B)**, while all plasmatocytes are labelled via *crq-GAL4,UAS-eGFP* **(A'-B')**. Anterior is up in all images, scale bars denote 10μm. **(C-C")** zoom of a representative plasmatocyte showing both acidified (marked with an asterisk) and non-acidified (marked with an arrowhead) phagosomes. Scale bar denotes 5μm. **(D)** scatterplot showing average number of lysotracker red positive vacuoles per plasmatocyte. *n*=21 and 20, respectively. Statistical analysis carried out via Mann-Whitney test; * represents p<0.05. **(E)** scatterplot showing proportion of vacuoles counted which were lysotracker red positive (i.e., acidified). *n*=21 and 20, respectively. Statistical analyses carried out via unpaired *t*-tests; **** represents p<0.0001.

Therefore, to test whether ecdysone signalling contributed to re-emergence of this population of cells, we manipulated ecdysone signalling specifically within haemocytes in pupae. As in the embryo, blocking ecdysone signalling within the majority of plasmatocytes (using *hml(Δ)-GAL4* to drive expression from *UAS-GFP* and *UAS-EcR-DN*) decreased the numbers of cells that could be labelled via the *VT62766-RFP* reporter (Figure 7). Clear morphological differences were also obvious comparing plasmatocytes in the thorax in controls and upon overexpression of EcR-DN, whereby cells were less vacuolated and less spherical in the latter (Figures 7A–C).

Overall, our data provide further evidence that the immune system of *Drosophila* comprises of heterogeneous subpopulations of

10.3389/fimmu.2023.1310117

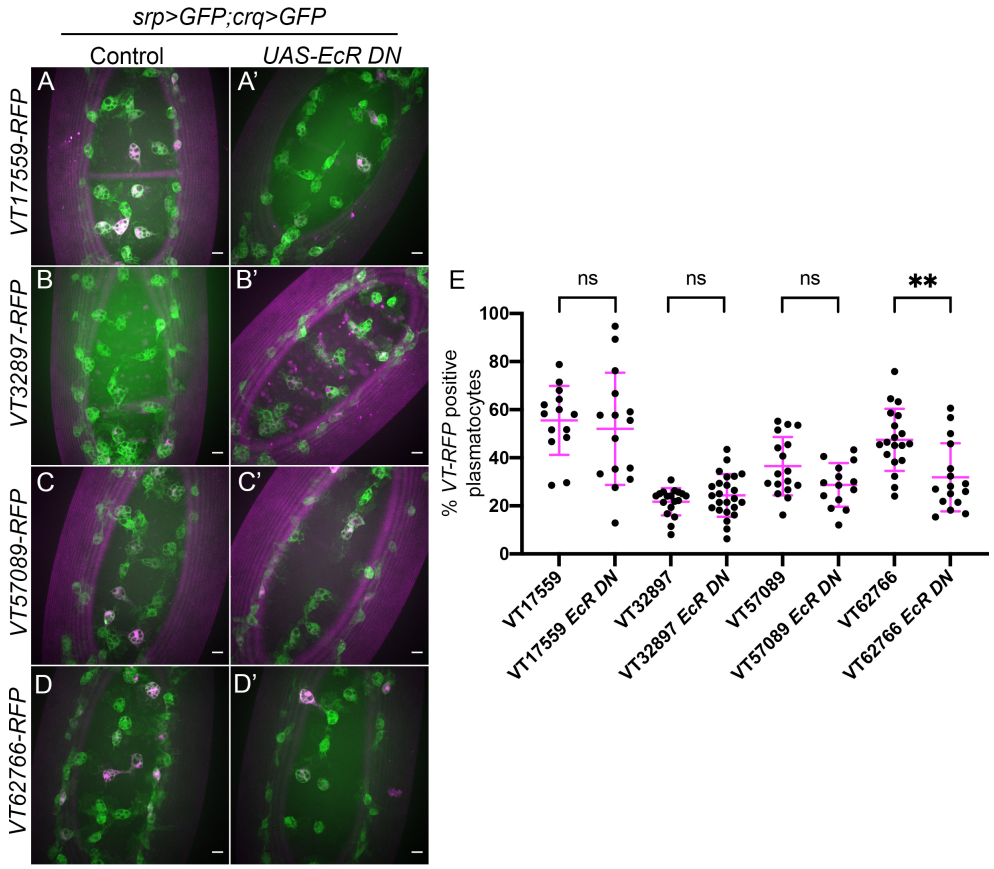

FIGURE 6
Ecdysone is required for establishing the *VT62766* subpopulation in the embryo. **(A-D')** representative maximum projection images of the ventral midline of control embryos **(A–D)** and embryos expressing *UAS-EcR*$^{\Delta C655}$ (*EcR DN*) specifically in plasmatocytes **(A'-D')** at stage 15. Plasmatocytes labelled via *srpHemo-GAL4,UAS-GFP* and *crq-GAL4,UAS-GFP* (green) while subpopulation plasmatocytes are labelled via *VT-RFP* transgenes (magenta). Anterior is up in all images, scale bars denote 10μm. **(E)** Scatterplot showing proportions of plasmatocytes within subpopulations in the presence and absence of pan- plasmatocyte *UAS-EcR*$^{\Delta C655}$ expression. *n*=14, 15, 18, 24, 17, 14, 19 and 16, respectively. Statistical analyses carried out via unpaired t-tests, ** represents p<.0.01.

plasmatocytes, akin to vertebrate macrophages. The identities of plasmatocyte subpopulations appear to be modulated by distinct processes, and we have identified signalling pathways (Simu and ecdysone signalling) involved in the establishment of specific subpopulations.

Discussion

We and others have previously demonstrated macrophage heterogeneity in *Drosophila* (18, 20–23). In this study we investigated mechanisms regulating *Drosophila* macrophage subpopulations *in vivo*, focusing on signalling pathways associated with ingestion of apoptotic cells and developmental transitions and using variations in subpopulation numbers induced by apoptotic cell challenge and developmental stage as experimental tools (18). We show that the phosphatidylserine receptor Simu antagonises *VT57089* subpopulation fate and is necessary for reprogramming events that reduce numbers of this subpopulation in the face of excess apoptotic cells. Consistent with a role downstream of Simu, the calcium-permeable cation channel Amo also regulated this subpopulation. Amo was implicated in mediating effective phagosome acidification, which may represent an important process in modulating numbers of cells within the *VT57089* subpopulation. Interestingly, Simu-dependent efferocytosis did not affect other subpopulation identities, while other apoptotic cell receptors (Crq and Drpr) did not seem to integrate apoptotic cell sensing and reprogramming of immune cells. Finally, we show that ecdysone signalling, itself associated with developmental timepoints featuring significant alternations in subpopulation numbers, also impacts identity of specific subpopulations. Taken together, individual plasmatocyte subpopulations are regulated by distinct processes at specific developmental stages. These results further reinforce the model that plasmatocytes exist as a heterogeneous population of cells that are programmed (and/or re-programmed) in response to the precise *in vivo* microenvironment.

Repo mutants have previously been used in genetic approaches to challenge plasmatocytes with large amounts of apoptosis (18, 19, 36). Loss of *repo* prevents the specification of glia, another important phagocyte lineage in the embryo (47). This results in increased numbers of uncleared apoptotic cells, as fewer phagocytes

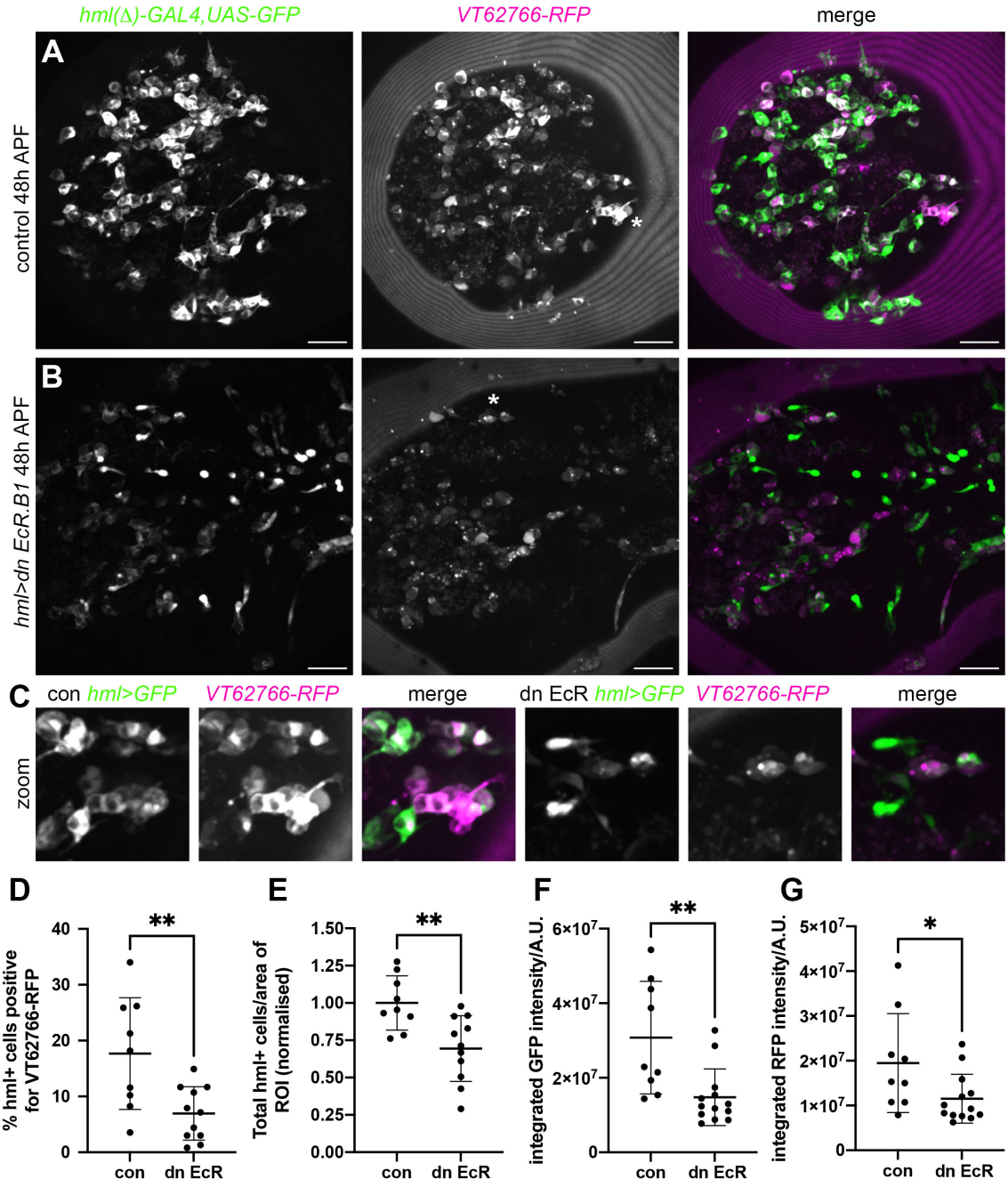

FIGURE 7
Ecdysone signalling regulates *VT62766* subpopulation cells in pupae. **(A, B)** Maximum projections of thoracic regions at 48h APF of a control pupa **(A)** and a pupa in which dominant negative EcR.B1 (*hml>dn EcR.B1*), **(B)** was expressed in haemocytes via *hml(Δ)-GAL4*. Pupae contain *hml(Δ)-GAL4, UAS-GFP* (*hml>GFP*, green in merge) and *VT62766-RFP* (magenta in merge) to label haemocytes and *VT62766*-expressing cells, respectively. **(C)** zooms of asterisked areas in **(A, B)**, which contain examples of haemocytes positive for both GFP and RFP. Scale bars denote 50μm **(A, B)**. **(D–G)** Scatterplots showing percentage of *hml*-positive cells that also express *VT62766-RFP* **(D)**, total number of *hml*-positive cells per area of the thorax analysed (normalised according to the control mean) **(E)**, and quantification of GFP and RFP levels within cells segmented as *hml*-positive (integrated GFP and RFP fluorescent intensities under a GFP mask; **F, G**). Lines and error bars represent mean and standard deviation; * and ** denote p<0.05 and p<0.01, respectively, following Student's t-tests **(D, E)** or Mann-Whitney test **(F, G)**.

remain to clear dying cells (15). The resulting challenge impairs effective migration and wound responses (36), and alters subpopulation numbers (18). Plasmatocytes within *repo* mutant embryos maintain expression of pan-plasmatocyte reporters (e.g., *srpHemo-GAL4*, *crq-GAL4, pxn-GAL4*) and are able to efficiently phagocytose apoptotic cells (36). Nonetheless, we cannot exclude the possibility that glia can also influence plasmatocyte specification independently of apoptosis.

Similarly, we cannot completely exclude that altered developmental dispersal accounts for differences in the number of subpopulation cells on the ventral midline (where we assay proportions of different subpopulations) upon manipulation of

apoptotic cell clearance signalling pathways. However, we regard this explanation as unlikely, since plasmatocyte responses to apoptotic cell death appear highly local in the *Drosophila* embryo (17, 55) and changes in the numbers of apoptotic cells should only occur proximally to Repo-positive glia, which are absent in other regions of the embryo (e.g., along their dorsal migration route). Furthermore, if specific subpopulation cells are re-routed elsewhere in *repo* mutant embryos, it might be expected that there are differences in the total number of plasmatocytes on the ventral surface of the embryo; we do not detect differences in the total number of cells across the genotypes analysed, nor is there an increase observed between *repo* and *simu;repo* mutants where loss of *simu* rescues *repo* phenotypes (*VT57089*-labelled cells; data not shown).

Here we demonstrate a role via which Simu can antagonise acquisition of specific subpopulation identities. In both *repo* and *simu* mutant embryos, plasmatocytes face elevated levels of apoptosis (17, 36). However, increasing the levels of apoptotic cells triggered by loss of *repo* has a broad effect on the expression of multiple subpopulation reporters, whereas loss of *simu* is more specific. This suggests that, in some circumstances, contact with apoptotic cells may not be sufficient for changes in subpopulation identity. That loss of *simu* function can block *repo*-induced changes in reporter expression suggests that signalling through this apoptotic cell clearance receptor is mediating these alterations in plasmatocyte identity. Consistent with a role for Simu-dependent signalling, a cation channel known to operate downstream of Simu, Amo (37), also impacts subpopulation numbers. However, the precise mechanisms remain to be determined, not least since Simu lacks an intracellular signalling domain (14). In comparison to *simu*, *amo* expression remains less well characterised; *simu* is broadly expressed but without correlation with subpopulation identity (18). Thus, we cannot rule out that varying levels of *amo* expression contribute to differences in how individual subpopulations are controlled.

The human homolog of *amo* is *PKD2*, which encodes Polycystin-2 (PC-2). Mutations in *PKD2* and *PKD1* cause autosomal dominant polycystic kidney disease (ADPKD), a relatively common genetic nephropathy, wherein tubular epithelial cells proliferate to form cysts, ultimately resulting in renal failure (56). Though the exact mechanisms involved in the pathogenesis of ADPKD remain poorly understood, there appears to be a role for immune cells in cyst expansion, with macrophage polarisation also implicated. Monocyte chemoattractant protein (MCP-1) and macrophage migration inhibitory factor (MIF) lead to an initial influx of pro-inflammatory macrophages, which then polarise towards a more anti-inflammatory, pro-proliferative activation state, driving cyst expansion and disease progression (57–59). Our data revealed decreased phagosome acidification in *amo;repo* mutant plasmatocytes compared to *repo*-only controls. The changes in the type of innate immune cells present in ADPKD and in the fly embryo on loss of *PKD2*/*amo* suggests manipulation of phagosome maturation may represent a novel pathway to target with respect to further understanding pathogenesis of the disease.

Amo is a cation channel and calcium signals have long been linked to phagocytic events, albeit the data has not always proven consistent (53). A recent paper beautifully delineates a requirement of calcium nanodomains for activation of dynamin during phagocytosis (60), though the key channels here were NAADP-regulated two-pore channels. Phagocytosis is also associated with more global elevations in cytoplasmic calcium and these authors speculate that these may regulate changes in mitochondrial energetics and gene expression. It is plausible that Amo might contribute to global Ca^{2+} signals under conditions of phagocytic stress. In turn, this may facilitate a contribution to changes in gene expression necessary to reprogramme macrophage subpopulations. Notably, calcium signalling is already known to be associated with changes in gene expression following apoptotic cell clearance in *Drosophila* (61).

The steroid hormone ecdysone is known to be involved in mediating large-scale phenotypic changes in the overall plasmatocyte population associated with different developmental stages (28–31). For example, larval plasmatocytes, which are typically sessile and proliferative, become highly migratory and phagocytic at the onset of metamorphosis in response to ecdysone (28). Similarly, embryonic plasmatocytes are unable to mount an effective immune response until being exposed to ecdysone at stage 12 (29). Expression of a dominant-negative ecdysone receptor isoform revealed a decreased proportion of plasmatocytes within the *VT62766* subpopulation in both embryos and pupae. It is therefore possible that ecdysone is required to help establish this plasmatocyte subpopulation. Other subpopulations were not affected by this approach, highlighting specificity in how subpopulation identity is established and controlled.

Ecdysone signalling has been shown to drive expression of phagocytic genes in pupae (28), stimulate motility and cytoplasmic rearrangements (31, 62), and help establish immune responses (29). The *VT62766* subpopulation exhibits enhanced wound responses, but reduced rates of phagocytosis (18), so while ecdysone could be argued to drive cells towards a more activated state, associated changes in behaviour do not completely align. However, it is important to note that earlier papers quantify behaviour across the total population of plasmatocytes so subpopulation-specific effects could be obscured.

Like steroid hormone signalling, apoptotic cell death is also associated with reprogramming of vertebrate macrophages (4). Pro-inflammatory cytokines are inhibited in macrophages following phagocytosis of apoptotic cells (63). Contact with large numbers of apoptotic cells reprograms plasmatocytes away from identities that exhibit less efficient apoptotic cell clearance (18), which potentially might signify a less pro-inflammatory state. Loss of an apoptotic cell clearance receptor blocks that effect for at least one discrete population of cells, reinforcing differences between the cells marked using our transgenic reporters.

In summary, we have identified new molecular players involved in determining the acquisition of specific plasmatocyte subpopulation identities in *Drosophila*: Simu and the downstream effector Amo regulate *VT57089* identity, with phagosome acidification a potential point of integration. Meanwhile, ecdysone appears important in establishing identity of *VT62766*-labelled cells in both the embryo and pupa. The role of steroid hormone signalling and apoptosis suggest that mechanisms controlling

innate immune cell behaviour in *Drosophila* and vertebrates may be more similar than previously thought. Finally, this further supports the existence of macrophage heterogeneity within this important immune model and will enable use of the fly to further dissect regulation of this important facet of biology *in vivo*.

Data availability statement

The original contributions presented in the study are included in the article/Supplementary Materials, further inquiries can be directed to the corresponding author/s.

Ethics statement

The manuscript presents research on animals that do not require ethical approval for their study.

Author contributions

EB: Conceptualization, Data curation, Formal analysis, Investigation, Methodology, Validation, Visualization, Writing – original draft, Writing – review & editing. MZ: Conceptualization, Formal analysis, Methodology, Resources, Supervision, Validation, Writing – review & editing. AO: Conceptualization, Funding acquisition, Methodology, Project administration, Supervision, Writing – review & editing. IE: Conceptualization, Data curation, Formal analysis, Funding acquisition, Investigation, Methodology, Project administration, Resources, Software, Supervision, Validation, Visualization, Writing – original draft, Writing – review & editing.

Funding

The author(s) declare financial support was received for the research, authorship, and/or publication of this article. This work was funded by an MRC Discovery Medicine North (DiMeN DTP) PhD studentship awarded to EB, AO, and IE (MR/N013840/1) and a Wellcome/Royal Society Sir Henry Dale Fellowship awarded to IE (102503/Z/13/Z). This work used a Perkin Elmer spinning disk system (MRC grant G0700091 and Wellcome grant 077544/Z/05/Z) and a Nikon W1 spinning disk system (BBSRC ALERT2021 award BB/V019368/1) housed in the Wolfson LMF at the University of Sheffield.

Acknowledgments

We thank Emma Bristow for her assistance in the preparation of *Drosophila* pupae for live imaging (Figure 7) and Juliette Howarth for help with the ecdysone signalling experiments in the embryo. We acknowledge Karen Plant and the University of Sheffield Fly Facility for support with fly husbandry. We are grateful for access to the microscopes of the University of Sheffield Wolfson Light Microscopy Facility and to Darren Robinson and Nicholas Van Hateren for assistance with imaging. This work would not be possible without reagents and resources obtained from or maintained by the Bloomington *Drosophila* Stock Centre (NIH P40OD018537) and Flybase (MRC grant MR/N030117/1). We thank Brian Stramer, Estee Kurant and Daria Siekhaus for providing additional fly lines.

Conflict of interest

The authors declare that the research was conducted in the absence of any commercial or financial relationships that could be construed as a potential conflict of interest.

Publisher's note

Supplementary material

The Supplementary Material for this article can be found online at: https://www.frontiersin.org/articles/10.3389/fimmu.2023.1310117/full#supplementary-material

SUPPLEMENTARY FIGURE 1
Pan-macrophage expression of Draper-II causes no effect on the *VT17559* or *VT32897* subpopulations. **(A-B", D-E")** representative maximum projection images of the ventral midline of wild-type control embryos **(A-A", D-D")** and embryos expressing *UAS-drpr-II* specifically in plasmatocytes **(B-B", E-E")** at stage 15. Plasmatocytes labelled via *srp-GAL4,UAS-GFP;crq-GAL4,UAS-GFP* **(A, B, D, E)** while subpopulation macrophages labelled via *VT17559-RFP* **(A', B')** or *VT32897-RFP* **(D', E')**. Anterior is up in all images; scale bars denote 10μm. **(C, F)** scatterplots showing proportion of plasmatocytes within the *VT17559* **(C)** and *VT32897* **(F)** subpopulations. **(C)** *n*= 20 and 22, respectively; **(F)** *n*= 19 and 17, respectively. Statistical analyses carried out via unpaired *t*-tests; ns denotes not significant; lines and error bars represent mean and standard deviation, respectively.

SUPPLEMENTARY FIGURE 2
Pan-macrophage expression of Draper-II causes no effect on the *VT57089* or *VT62766* subpopulations. **(A-B", D-E")** representative maximum projection images of the ventral midline of wild-type control embryos **(A-A", D-D")** and embryos expressing *UAS-drpr-II* specifically in plasmatocytes **(B-B", E-E")** at stage 15. Plasmatocytes labelled via *srp-GAL4,UAS-GFP;crq-GAL4,UAS-GFP* **(A, B, D, E)** while subpopulation macrophages labelled via *VT57089-RFP* **(A', B')** or *VT62766-RFP* **(D', E')**. Anterior is up in all images; scale bars denote 10μm. **(C, F)** scatterplots showing proportion of plasmatocytes within the *VT57089* **(C)** and *VT62766* **(F)** subpopulations. **(C)** *n*= 18 and 18, respectively; **(F)** *n*= 15 and 22, respectively. Statistical analyses carried out via unpaired *t*-tests; ns denotes not significant; lines and error bars represent mean and standard deviation, respectively.

SUPPLEMENTARY TABLE 1
Table showing genotypes of *Drosophila* lines used in this study.

References

1. Gordon S, Plüddemann A. Tissue macrophages: heterogeneity and functions. *BMC Biol* (2017) 15(1):53. doi: 10.1186/s12915-017-0392-4

2. Murray PJ. Macrophage polarization. *Annu Rev Physiol* (2017) 79(1):541–66. doi: 10.1146/annurev-physiol-022516-034339

3. Orecchioni M, Ghosheh Y, Pramod AB, Ley K. Macrophage Polarization: Different Gene Signatures in M1(LPS+) vs. Classically and M2(LPS–) vs. Alternatively Activated Macrophages. *Front Immunol* (2019) 0:1084(MAY). doi: 10.3389/FIMMU.2019.01084

4. Serhan CN, Savill J. Resolution of inflammation: the beginning programs the end. *Nat Immunol* (2005) 6(12):1191–7. doi: 10.1038/ni1276

5. Hume DA. The many alternative faces of macrophage activation. *Front Immunol* (2015) 6:370/BIBTEX(JUL). doi: 10.3389/FIMMU.2015.00370/BIBTEX

6. Shaykhiev R, Krause A, Salit J, Strulovici-Barel Y, Harvey B-G, O'Connor TP, et al. Smoking-dependent reprogramming of alveolar macrophage polarization: implication for pathogenesis of chronic obstructive pulmonary disease. *J Immunol* (2009) 183(4):2867–83. doi: 10.4049/JIMMUNOL.0900473

7. de Gaetano M, Crean D, Barry M, Belton O. M1- and M2-type macrophage responses are predictive of adverse outcomes in human atherosclerosis. *Front Immunol* (2016) 7:275/BIBTEX(JUL). doi: 10.3389/FIMMU.2016.00275/BIBTEX

8. Cornwell WD, Kim V, Fan X, Vega ME, Ramsey FV, Criner GJ, et al. Activation and polarization of circulating monocytes in severe chronic obstructive pulmonary disease. *BMC Pulmonary Med* (2018) 18(1):101. doi: 10.1186/S12890-018-0664-Y

9. Lebestky T, Chang T, Hartenstein V, Banerjee U. Specification of *Drosophila* hematopoietic lineage by conserved transcription factors. *Science* (2000) 288 (5463):146–9. doi: 10.1126/science.288.5463.146

10. Wood W, Martin P. Macrophage functions in tissue patterning and disease: new insights from the fly. *Dev Cell* (2017) 40(3):221–33. doi: 10.1016/j.devcel.2017.01.001

11. Franc NC, Dimarcq J-L, Lagueux M, Hoffmann J, Ezekowitz RAB. Croquemort, A novel *Drosophila* hemocyte/macrophage receptor that recognizes apoptotic cells. *Immunity* (1996) 4(5):431–43. doi: 10.1016/S1074-7613(00)80410-0

12. Freeman MR, Delrow J, Kim J, Johnson E, Doe CQ. Unwrapping Glial Biology: Gcm Target Genes Regulating Glial Development, Diversification, and Function brain barrier that isolates and protects neural tissue. Glia mediate many brain responses to injury and neuro-degenerative diseases. *Neuron* (2003) 38(4):567-80. doi: 10.1016/s0896-6273(03)00289-7

13. Manaka J, Kuraishi T, Shiratsuchi A, Nakai Y, Higashida H, Henson P, et al. Draper-mediated and phosphatidylserine-independent phagocytosis of apoptotic cells by *Drosophila* hemocytes/macrophages. *J Biol Chem* (2004) 279(46):48466–76. doi: 10.1074/jbc.M408597200

14. Kurant E, Axelrod S, Leaman D, Gaul U. Six-microns-under acts upstream of draper in the glial phagocytosis of apoptotic neurons. *Cell* (2008) 133(3):498–509. doi: 10.1016/j.cell.2008.02.052

15. Shklyar B, Sellman Y, Shklover J, Mishnaevski K, Levy-Adam F, Kurant E. Developmental regulation of glial cell phagocytic function during *Drosophila* embryogenesis. *Dev Biol* (2014) 393(2):255–69. doi: 10.1016/j.ydbio.2014.07.005

16. Evans IR, Rodrigues FSLM, Armitage EL, Wood W. Draper/CED-1 mediates an ancient damage response to control inflammatory blood cell migration *in vivo*. *Curr Biol* (2015) 25(12):1606–12. doi: 10.1016/j.cub.2015.04.037

17. Roddie HG, Armitage EL, Coates JA, Johnston SA, Evans IR. Simu-dependent clearance of dying cells regulates macrophage function and inflammation resolution. *PloS Biol* (2019) 17(5):e2006741. doi: 10.1371/journal.pbio.2006741

18. Coates JA, Brooks E, Brittle AL, Armitage EL, Zeidler MP, Evans IR. Identification of functionally distinct macrophage subpopulations in *Drosophila*. *ELife* (2021) 10:e58686. doi: 10.7554/ELIFE.58686

19. Raymond MH, Davidson AJ, Shen Y, Tudor DR, Lucas CD, Morioka S, et al. Live cell tracking of macrophage efferocytosis during *Drosophila* embryo development in *vivo*. *Science* (2022) 375(6585):1182–7. doi: 10.1126/SCIENCE.ABL4430

20. Cattenoz PB, Sakr R, Pavlidaki A, Delaporte C, Riba A, Molina N, et al. Temporal specificity and heterogeneity of *Drosophila* immune cells. *EMBO J* (2020) 39(12):1–25. doi: 10.15252/embj.2020104486

21. Cho B, Yoon SH, Lee D, Koranteng F, Tattikota SG, Cha N, et al. Single-cell transcriptome maps of myeloid blood cell lineages in *Drosophila*. *Nat Commun* (2020) 11(1):4483. doi: 10.1038/s41467-020-18135-y

22. Fu Y, Huang X, Zhang P, van de Leemput J, Han Z. Single-cell RNA sequencing identifies novel cell types in *Drosophila* blood. *J Genet Genomics* (2020) 47(4):175–86. doi: 10.1016/j.jgg.2020.02.004

23. Tattikota SG, Cho B, Liu Y, Hu Y, Barrera V, Steinbaugh MJ, et al. A single-cell survey of *Drosophila* blood. *ELife* (2020) 9:1–35. doi: 10.7554/eLife.54818

24. Matsubayashi Y, Louani A, Dragu A, Sánchez-Sánchez BJ, Serna-Morales E, Yolland L, et al. A moving source of matrix components is essential for *de novo* basement membrane formation. *Curr Biol* (2017) 27(22):3526–3534.e4. doi: 10.1016/j.cub.2017.10.001

25. Page DT, Olofsson B. Multiple roles for apoptosis facilitating condensation of the *Drosophila* ventral nerve cord. *Genesis* (2008) 46(2):61–8. doi: 10.1002/dvg.20365

26. Leitão AB, Sucena É. *Drosophila* sessile hemocyte clusters are true hematopoietic tissues that regulate larval blood cell differentiation. *ELife* (2015) 4:1–38. doi: 10.7554/eLife.06166

27. Makhijani K, Alexander B, Rao D, Petraki S, Herboso L, Kukar K, et al. Regulation of *Drosophila* hematopoietic sites by Activin-β from active sensory neurons. *Nat Commun* (2017) 8(1):1–12. doi: 10.1038/ncomms15990

28. Regan JC, Brandão AS, Leitão AB, Mantas Dias ÂR, Sucena É, Jacinto A, et al. Steroid hormone signaling is essential to regulate innate immune cells and fight bacterial infection in *Drosophila*. *PloS Pathog* (2013) 9(10):e1003720. doi: 10.1371/journal.ppat.1003720

29. Tan KL, Vlisidou I, Wood W. Ecdysone mediates the development of immunity in the *Drosophila* embryo. *Curr Biol* (2014) 24(10):1145–52. doi: 10.1016/j.cub.2014.03.062

30. Jiang C, Baehrecke EH, Thummel CS. Steroid regulated programmed cell death during *Drosophila* metamorphosis. *Development* (1997) 124(22):4673–83. doi: 10.1242/DEV.124.22.4673

31. Sampson CJ, Amin U, Couso JP. Activation of *Drosophila* hemocyte motility by the ecdysone hormone. *Biol Open* (2013) 2(12):1412–20. doi: 10.1242/bio.20136619

32. Zirin J, Cheng D, Dhanyasi N, Cho J, Dura JM, VijayRaghavan K, et al. Ecdysone signaling at metamorphosis triggers apoptosis of *Drosophila* abdominal muscles. *Dev Biol* (2013) 383(2):275–84. doi: 10.1016/J.YDBIO.2013.08.029

33. Kvon EZ, Kazmar T, Stampfel G, Yáñez-Cuna JO, Pagani M, Schernhuber K, et al. Genome-scale functional characterization of *Drosophila* developmental enhancers in *vivo*. *Nature* (2014) 512(7512):91-5. doi: 10.1038/nature13395

34. Halter D, Urban J, Rickert C, Ner SS, Ito K, Travers AA, et al. The homeobox gene repo is required for the differentiation and maintenance of glia function in the embryonic nervous system of *Drosophila melanogaster*. *Development* (1995) 121 (2):317–32. doi: 10.1242/dev.121.2.317

35. Sonnenfeld MJ, Jacobs JR. Macrophages and glia participate in the removal of apoptotic neurons from the *Drosophila* embryonic nervous system. *J Comp Neurol* (1995) 359(4):644–52. doi: 10.1002/cne.903590410

36. Armitage EL, Roddie HG, Evans IR. Overexposure to apoptosis via disrupted glial specification perturbs *Drosophila* macrophage function and reveals roles of the CNS during injury. *Cell Death Dis* (2020) 11(8):627. doi: 10.1038/s41419-020-02875-2

37. Van Goethem E, Silva EA, Xiao H, Franc NC. The *Drosophila* TRPP cation channel, PKD2 and Dmel/Ced-12 act in genetically distinct pathways during apoptotic cell clearance. *PloS One* (2012) 7(2):e31488. doi: 10.1371/journal.pone.0031488

38. Stramer B, Wood W, Galko MJ, Redd MJ, Jacinto A, Parkhurst SM, et al. Live imaging of wound inflammation in *Drosophila* embryos reveals key roles for small GTPases during in *vivo* cell migration. *J Cell Biol* (2005) 168(4):567–73. doi: 10.1083/jcb.200405120

39. Brückner K, Kockel L, Duchek P, Luque CM, Rørth P, Perrimon N. The PDGF/VEGF receptor controls blood cell survival in *Drosophila*. *Dev Cell* (2004) 7(1):73–84. doi: 10.1016/j.devcel.2004.06.007

40. Sinenko SA, Mathey-Prevot B. Increased expression of *Drosophila* tetraspanin, Tsp68C, suppresses the abnormal proliferation of ytr-deficient and Ras/Raf-activated hemocytes. *Oncogene* (2004) 23(56):9120–8. doi: 10.1038/sj.onc.1208156

41. Pfeiffer BD, Ngo TTB, Hibbard KL, Murphy C, Jenett A, Truman JW, et al. Refinement of tools for targeted gene expression in *Drosophila*. *Genetics* (2010) 186 (2):735-55. doi: 10.1534/genetics.110.119917

42. Barolo S, Carver LA, Posakony JW. GFP and β-galactosidase transformation vectors for promoter/enhancer analysis in *Drosophila*. *BioTechniques* (2000) 29(4):726–732). doi: 10.2144/00294bm10

43. Logan MA, Hackett R, Doherty J, Sheehan A, Speese SD, Freeman MR. Negative regulation of glial engulfment activity by Draper terminates glial responses to axon injury. *Nat Neurosci* (2012) 15(5):722–30. doi: 10.1038/nn.3066

44. Cherbas L, Hu X, Zhimulev I, Belyaeva E, Cherbas P. EcR isoforms in *Drosophila*: testing tissue-specific requirements by targeted blockade and rescue. *Development* (2003) 130(2):271–84. doi: 10.1242/DEV.00205

45. Gyoergy A, Roblek M, Ratheesh A, Valoskova K, Belyaeva V, Wachner S, et al. Tools allowing independent visualization and genetic manipulation of *Drosophila melanogaster* macrophages and surrounding tissues. *G3 Genes|Genomes|Genetics* (2018) 8(3):845–57. doi: 10.1534/g3.117.300452

46. Watnick TJ, Jin Y, Matunis E, Kernan MJ, Montell C. A flagellar polycystin-2 homolog required for male fertility in *Drosophila*. *Curr Biol* (2003) 13(24):2179–84. doi: 10.1016/J.CUB.2003.12.002

47. Xiong WC, Okano H, Patel NH, Blendy JA, Montell C. repo encodes a glial-specific homeo domain protein required in the *Drosophila* nervous system. *Genes Dev* (1994) 8(8):981-94. doi: 10.1101/gad.8.8.981

48. Guillou A, Troha K, Wang H, Franc NC, Buchon N. The *Drosophila* CD36 homologue croquemort is required to maintain immune and gut homeostasis during

development and aging. *PloS Pathog* (2016) 12(10):e1005961. doi: 10.1371/journal.ppat.1005961

49. Evans IR, Hu N, Skaer H, Wood W. Interdependence of macrophage migration and ventral nerve cord development in *Drosophila* embryos. *Development* (2010) 137 (10):1625–33. doi: 10.1242/dev.046797

50. Schindelin J, Arganda-Carreras I, Frise E, Kaynig V, Longair M, Pietzsch T, et al. Fiji: An open-source platform for biological-image analysis. *Nat Methods* (2012) 9 (7):676–82. doi: 10.1038/nmeth.2019

51. Zanet J, Stramer B, Millard T, Martin P, Payre F, Plaza S. Fascin is required for blood cell migration during *Drosophila* embryogenesis. *Development* (2009) 136 (15):2557–65. doi: 10.1242/dev.036517

52. Kinchen JM, Ravichandran KS. Phagosome maturation: going through the acid test. *Nat Rev Mol Cell Biol* (2008) 9(10):781–95. doi: 10.1038/nrm2515

53. Westman J, Grinstein S, Maxson ME. Revisiting the role of calcium in phagosome formation and maturation. *J Leukocyte Biol* (2019) 106(4):837–51. doi: 10.1002/JLB.MR1118-444R

54. Nicolson S, Denton D, Kumar S. Ecdysone-mediated programmed cell death in *Drosophila*. *Int J Dev Biol* (2015) 59(1-2–3):23–32. doi: 10.1387/ijdb.150055sk

55. Moreira S, Stramer B, Evans I, Wood W. Prioritization of competing damage and developmental signals by migrating macrophages in the *Drosophila* embryo. *Curr Biol* (2010) 20:464–70.

56. Ong ACM, Harris PC. A polycystin-centric view of cyst formation and disease: the polycystins revisited. *Kidney Int* (2015) 88(4):699–710. doi: 10.1038/ki.2015.207

57. Karihaloo A, Koraishy F, Huen SC, Lee Y, Merrick D, Caplan MJ, et al. Macrophages promote cyst growth in polycystic kidney disease. *J Am Soc Nephrology* (2011) 22(10):1809–14. doi: 10.1681/ASN.2011010084

58. Chen L, Zhou X, Fan LX, Yao Y, Swenson-Fields KI, Gadjeva M, et al. Macrophage migration inhibitory factor promotes cyst growth in polycystic kidney disease. *J Clin Invest* (2015) 125(6):2399–412. doi: 10.1172/JCI80467

59. Cassini MF, Kakade VR, Kurtz E, Sulkowski P, Glazer P, Torres R, et al. Mcp1 promotes macrophage-dependent cyst expansion in autosomal dominant polycystic kidney disease. *J Am Soc Nephrol* (2018) 29(10):2471–81. doi: 10.1681/ASN.2018050518

60. Davis LC, Morgan AJ, Galione A. NAADP -regulated two-pore channels drive phagocytosis through endo-lysosomal Ca 2+ nanodomains, calcineurin and dynamin. *EMBO J* (2020) 39(14):e104058. doi: 10.15252/embj.2019104058

61. Weavers H, Evans IR, Martin P, Wood W. Corpse engulfment generates a molecular memory that primes the macrophage inflammatory response. *Cell* (2016) 165(7):1658–71. doi: 10.1016/j.cell.2016.04.049

62. Edwards SS, Delgado MG, Nader GP, de F, Piel M, Bellaïche Y, et al. An in *vitro* method for studying subcellular rearrangements during cell polarization in *Drosophila melanogaster* hemocytes. *Mech Dev* (2018) 154:277–86. doi: 10.1016/j.mod.2018.08.003

63. Fadok VA, Bratton DL, Konowal A, Freed PW, Westcott JY, Henson PM. Macrophages that have ingested apoptotic cells *in vitro* inhibit proinflammatory cytokine production through autocrine/paracrine mechanisms involving TGF-beta, PGE2, and PAF. *J Clin Invest* (1998) 101(4):890–8. doi: 10.1172/JCI1112

frontiers | Frontiers in Immunology

TYPE Mini Review
PUBLISHED 14 March 2024
DOI 10.3389/fimmu.2024.1349027

OPEN ACCESS

EDITED BY
Susanna Valanne,
Tampere University, Finland

REVIEWED BY
Yeon Soo Han,
Chonnam National University,
Republic of Korea
Ioannis Eleftherianos,
George Washington University, United States

*CORRESPONDENCE
Ilias Kounatidis
ilias.kounatidis@open.ac.uk

RECEIVED 04 December 2023
ACCEPTED 27 February 2024
PUBLISHED 14 March 2024

CITATION
Mpamhanga CD and Kounatidis I (2024) The utility of *Drosophila melanogaster* as a fungal infection model.
Front. Immunol. 15:1349027.
doi: 10.3389/fimmu.2024.1349027

The utility of *Drosophila melanogaster* as a fungal infection model

Chengetai D. Mpamhanga and Ilias Kounatidis*

School of Life Health and Chemical Sciences, The Open University, Milton Keynes, United Kingdom

Invasive fungal diseases have profound effects upon human health and are on increase globally. The World Health Organization (WHO) in 2022 published the fungal priority list calling for improved public health interventions and advance research. *Drosophila melanogaster* presents an excellent model system to dissect host-pathogen interactions and has been proved valuable to study immunopathogenesis of fungal diseases. In this review we highlight the recent advances in fungal-*Drosophila* interplay with an emphasis on the recently published WHO's fungal priority list and we focus on available tools and technologies.

KEYWORDS

***Drosophila*, model organisms, fungal diseases, WHO, FFPL, infection models**

Introduction

Fungal infections

The global impact of opportunistic fungal infections has gone underrecognized for a long time (1). However, with the increase in chronic and immunosuppressive health conditions including HIV/AIDS, cancer, cystic fibrosis and diabetes, antimicrobial therapies and invasive procedures that leave individuals vulnerable to opportunistic infections, the impact of these infections are becoming more apparent (1, 2). Fungi cause disease through direct infection of the host or through their secondary metabolites, mycotoxins, pigments that can contaminate the environment, food products and air (3). The disease burden ranges from superficial to invasive fungal infections and is estimated to be in the 100s of millions of patients per year, resulting in >1.5 million deaths/year (2, 4). These infections are caused by long recognised pathogens such as *Aspergillus fumigatus* and *Candida albicans* (5–7), neglected tropical diseases like eumycetoma (8, 9), and newly emerged pathogens, such as *Candida auris* (10, 11).

With the development of advanced molecular and cellular biology technologies, fungal pathogenicity and virulence factors are being studied in greater detail (12–14). However, the fungal threat continues to grow while the development of novel effective antifungal therapies remains inadequate (15, 16). As a result, in 2022 the WHO published the WHO

fungal priority pathogens list, classifying 18 medically relevant fungal species as "Critical", "High" or "Medium" priority, according to the perceived public health burden (2, 17).

Model organisms

The use of model organisms is one of the technologies that has been developing over time and has become indispensable to investigating the nuances of host-pathogen interactions (18, 19). A cursory search of PubMed using the keywords "*Drosophila*" AND "fungi" yielded 8,617 results (1948 – 2023), with over a third (36.2%) of the publications having been released in the last decade alone. Seminal proof of concept studies in the 1990s and early 2000s, utilising wild-type and mutant *Drosophila* strains and fungi, provided a comprehensive framework for employing *Drosophila* in fungal research (20–25). Over the last decade, more extensive *Drosophila*-fungi work has taken place, leading to a better understanding of virulence, pathogenicity, and host immune responses (26–30).

Purpose of review

This review sets out to provide a brief update on tools currently being applied to host-fungal interaction studies in *Drosophila* and highlight examples of research in the last 5 years with a focus on the WHO's fungal priority pathogens list (17).

Drosophila as the model organism

Drosophila, affectionately dubbed the biology "work horse", has been used in fundamental biology, inbreeding and heredity studies since the early 1900s (27, 31) and has led to substantial contributions to our understanding of genetics, cellular biology, neurobiology and immunology (31, 32). Of note, the discovery of *Drosophila* Toll receptor nearly 3 decades ago elucidated the function of the analogous mammalian Toll-like receptor (TLR) pathway, which is indispensable to innate immunity (20; Lemaitre, 21, 26). *Drosophila* genome can be genetically manipulated, and genome-wide studies performed to determine genes crucial for survival and infection (27, 33). 75% of the genes responsible for human diseases have a homologue identified in Drosophila genome, an observation that highlights Drosophila's suitability as a model for the study of mammalian disease conditions (34, 35).

Drosophila immunity relies on the innate immune system, made up of cellular and acellular components and regulatory pathways (Figure 1) (36, 37).These have been traditionally siloed into the humoral and cellular responses, though recent studies have shown that there is considerable crosstalk between the two branches (38, 39). *Drosophila* shares the following conserved innate immune pathways with vertebrates: the Toll and IMD NF-κB signalling pathways, the JNK pathway and the JAK/STAT pathway (40, 41). The Toll pathway responds to fungi and Gram-positive bacteria, while IMD responds to Gram-negative bacteria (40, 42). These pathways are activated by the recognition of pathogen antigens and host cell damage, and result in the production of effector molecules

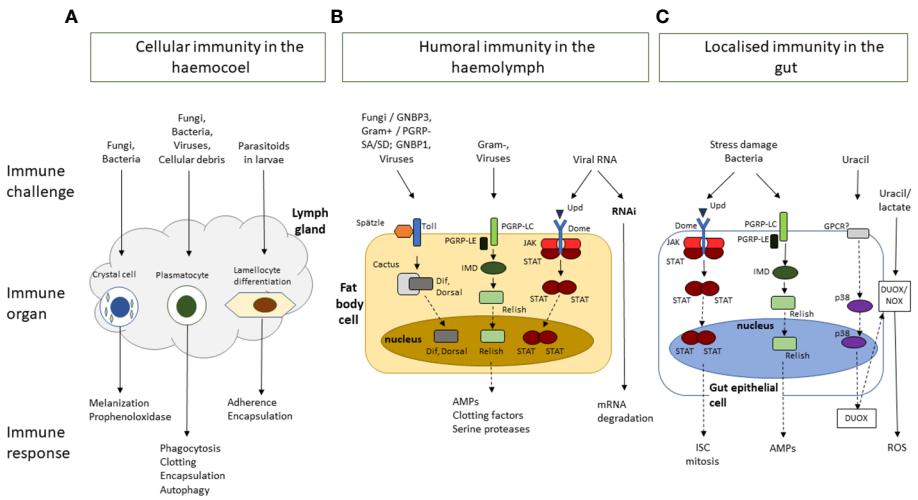

FIGURE 1
A simplified schematic overview of *Drosophila* melanogaster innate immune response to challenges by bacteria, viruses, fungi, or parasites, and to damage induced by stress or wounding. The immune responses are clustered by response type and location. **(A)** Cellular immunity in the hemocoel is mediated by crystal cells, plasmatocytes and lamellocytes, which are involved in, melanisation, phagocytosis, and encapsulation, respectively. **(B)** Humoral immunity in the haemolymph is mediated by the activation of signalling cascades in the Toll, Immune deficient (IMD) and JNK, JAK/STAT and mRNA degradation pathways following the recognition of pathogens and their virulence factors. It results in the production of a range of effector molecules including antimicrobial peptides (AMPs), clotting factors, and serine proteases. **(C)** The gut epithelium functions as an immune organ in response to pathogens and stress damage though the following responses: The JAK/STAT pathway responds to damage to increased proliferation of intestinal stem cells (ISC). The IMD pathway in response to bacteria presence in the gut leads to the production of AMPs. Finally bacterial-derived uracil induces the generation of reactive oxygen species (ROS) through the dual-oxidase (DUOX) and the NADPH oxidase (NOX). Dashed arrows represent additional steps involved in the signalling cascade, transcription, and translation, involved in the immune response.

necessary for eliminating pathogens, autophagy and cellular repair, and immunomodulation as well as other *Drosophila*-induced Immune Molecules (DIMs) yet to be characterized fully (43, 44). These effectors have not yet been fully identified, but include antimicrobial peptides (AMPs), Boms (encoded by *Bomanins*), Daisho peptides (39, 45). AMPs are small, positively charged peptides that interact with hydrophobic regions of microbial cells walls and cause cell wall degradation and microbial death and are secreted into the haemolymph by the fat body (45, 46). In addition to AMPs, reactive oxygen species (ROS) are produced by Dual Oxidase (DUOX) and NADPH (Nox) at the epithelial cells (26, 32). The humoral response also provides protection against viral attack through RNAi and autophagy processes (36, 47).

Drosophila cellular immunity is mediated by the blood cell system which comprises of three differentiated populations. The major class of hemocytes are plasmatocytes which are considered equivalent to vertebrate macrophages. More than 90% of all hemocytes are plasmatocytes in every developmental stage of Drosophila (aside from the early-stage embryo) and they are responsible for the disposal of both microorganism and apoptotic cells. Another class are the crystal cells which are responsible for the melanisation in larvae. They contain the enzyme prophenoloxidase a key enzyme in melanin biosynthesis which is released upon rupture of the crystal cells. The third class refers to the lamellocytes, they are rare, but their number increases following oviposition by parasitoid wasps 48, 49). Haematopoiesis occurs at two different stages of ontogenesis: a first population derives from the head mesoderm during the stage of early embryogenesis, and a following second population that arises from the mesodermal lymph gland at a later stage of development (50).

Drosophila antifungal immune responses rely heavily on the Toll pathway (37, 51). Toll signalling is activated by the binding of the surface antigen β-glucan to *Drosophila* recognition receptor Gram-negative binding protein 3 (GNBP3) and activates Toll through the activity of the Spätzle ligand and subsequent signalling cascade (51, 52). The Toll signalling cascade is also activated by the cleavage of the haemolymph serine protease Persephone by fungal enzymes contributing to the subsequent downstream activity of the Toll pathway (22, 53). The signalling cascade results in the production of specific AMPs, including Drosomycin, Daisho, Defensin and Metchnikowin, circulated in the hemolymph and the activation of the melanisation cascade to help resist the infection (42, 43, 45, 53).

Application of *Drosophila* to human fungal pathogens

Tools available for *Drosophila*-fungal studies

Drosophila is currently being utilised to investigate how medically relevant fungi interact with host immunity, and how they transition from colonization to infection (26–30). Wild-type and genetic mutant strains (e.g., Toll-deficient) are commercially available for distribution across the world from stock centres, such as the Bloomington Drosophila Stock Centre and Kyoto Stock Centre (54, 55). Table 1 summarises *Drosophila* strains used in fungal research studies included in the current review. The Drosophila Genomics Resource Centre and ATCC are some of the suppliers who distribute Drosophila cell lines, like Schneider's Drosophila Line 2 (S2) cell line, GFP-tagged cells, and cells from various organs for *ex vivo* studies (67, 68). These fly strains and cell lines are relatively inexpensive to purchase and maintain, increasing accessibility of the model (68). The model systems are infected or exposed to fungi, fungal secondary metabolites, and antifungal compounds to investigate these interactions (26, 55) via feeding, rolling over, or co-culture and in a standardised manner via needle pricking or microinjection, allowing for rapid inoculation of experimental groups (57, 58). Infection progression can be measured through survival, microbial load, mRNA quantification, melanisation and microscopy assays (55, 64). The efficacy and toxicity of antimicrobial compound screens can be measured in similar ways to determine their efficacy and toxicity (69, 70). Examples of microscopy techniques include confocal microscopy for visualising phagocytosis in fungi-stimulated plasmatocytes (71), electron microscopy for imaging effects of treatment on host cell

TABLE 1 List of *Drosophila* strains used in fungal infection studies.

Drosophila strain	Description	References
Wild type		
w^{A5001}	White-eyed, wild-type immune system.	55
w^{1118}	White-eyed, wild-type immune system.	43, 56;
Canton-S	Wild-type.	55
y^1w^1	Yellow body, white eyed.	55
$w^{1,118}$; y^1	Yellow body, white-eyed.	57
$Oregon^R$	Red-eyed.	58, 59
Mutant		
$MyD88^{c03881}$	Toll deficient.	55, 58
MyD88-/-	Toll deficient.	60, 61
$MyD88^{kra1}$	Toll deficient.	51
imd^{shadok}	Imd deficient.	51
$Bom^{\Delta 55C}$	Bomanin deficient (elimination of 10 out of 12 Bom genes in the genome)	42, 43, 55, 62
Tl^{r632}/Tl^{1-RXA}	Toll-deficient transheterozygote.	11, 63
Tl[r3]/+)	Heterozygous Toll deficiency.	64
Rel^{E20}	White-eyed, Imd mutant.	56
spz^6	Red-eyed, Toll mutant.	56
w^{1118}; *np1-GAL4; DuoxRNAi*	GAL4 reporter system and dual oxidase (dDuox) knockout, wild type w^{1118} background.	65
$FucTA^{f03774}$	a piggyBac insertional mutant for the fucTA gene	66

morphology (35) and fungal burden (72). Immunofluorescence staining and bioluminescence allow visualisation of individual cell types in tissue, larvae or adult flies, and can be done through RNA *in situ* hybridization (30, 73, 74), intravital 2-d photon microscopy and reporter systems (GFP, lacZ) (62).

The development of molecular techniques including DNA and RNA sequencing, RNAi gene silencing and CRISPR/Cas9 has advanced the field in leaps and bounds. Molecular techniques have made it possible to sequence the *Drosophila* genome (75); sequence coding and non-coding RNA and determine functionality through RNAi-based screening assays and gene silencing or overexpression (66, 76, 77). They facilitate quantification of messenger RNA (mRNA) or transfer RNA (tRNA) through quantitative PCR, reverse transcriptase PCR and modified-induced misincorporation tRNA sequencing (mim-tRNASeq) (78, 79). The gene editing tool CRISPR/Cas9 utilises guide RNA which matches with target gene (CRISPR) and CRISPR-associated protein 9 (Cas9), an endonuclease which helps to break the dsDNA and facilitate editing of the target gene (80) and it can be used for loss-of-function studies (12, 45, 81). Bioinformatics tools have been developed and adapted for genomic studies across microbial, *Drosophila* and human genomes and these allow for rapid screening of genomes and vast publicly available pathogen and fly data for potential targets for further study (79, 82). These software tools coupled with publicly accessible databases such as *Drosophila* Evolution over Space and Time (DEST), FlyRNAi (Drosophila RNAi Screening Center and Transgenic RNAi Project (DRSC/TRiP)) and FlyBase form a powerful computational component of the *Drosophila* tool kit (67, 82, 83).

With a focus on the WHO priority pathogens, we will highlight some examples of how *Drosophila* has been used to address key questions around host-fungal pathogen interactions, immunology and drug interactions with a focus on developments in the last five years.

Critical priority group

The WHO classified *Cryptococcus neoformans*, *A. fumigatus*, *C. albicans*, and the recently emerged *C. auris* as "Critical" pathogens. *A. fumigatus* is a filamentous, airborne pathogen that causes invasive aspergillosis, in vulnerable populations, like cystic fibrosis patients (32, 84). *Drosophila* has been used to study *A. fumigatus* pathogenesis since as far back as 2005 (85, 86). In 2010, Chamilos and colleagues showed that pathogenicity of *A. fumigatus* strains in a Toll-deficient fly model was comparable to that in a mice model (25). Since then, the fly model has been used to study the virulence of *A. fumigatus* mating types, effects of fungal volatile organic compounds on larval development and comparative pathogenicity of *Aspergillus* strains collected from diverse sources (environmental, clinical, airborne) (29, 57, 87).

Fungi produce volatile organic compounds (VOCs) which are easily vapourised, carbon-based compounds made up of "alcohols, aldehydes, acids, ethers, esters, ketones, terpenes, thiols and their derivatives" (56, 57, 88). A study of the effects of *A. fumigatus* VOCs in *Drosophila* was carried out over a 15-day period, by co-culturing the fungi and fly model. Quantitative measurements of VOCs production showed that greater volumes of VOCs were secreted when *A. fumigatus* was cultivated at 37°C, than at the fly's preferred incubation temperature of 25°C (57, 89). In addition, exposure to VOCs resulted in varying levels of toxicity, ranging from mild to severe, including reduced speed and success rate of metamorphosis or death of 3rd instar larvae (57, 90). Gas-chromatography mass spectrometry analysis of *A. fumigatus* VOCs detected isopentyl alcohol 1-octen-3-ol at the highest volume (57). A *Drosophila* infection model was subsequently used to show that 1-octen-3-ol caused greater sensitivity in male than female flies, resulting in reduced dehydrogenase activity and nitric oxide production, and increased ROS production (35). The connection to sex may explain the similar sensitivity distribution witnessed in humans postexposure to mould (35, 91). The *Drosophila* models used to investigate the immune response to mycotoxins and studies have shown that the Toll pathway and secreted Bomanins, specifically neuronal BomS6, mitigate the symptoms of *Aspergillus* mycotoxin exposure, namely restrictocin and verruculogen (55). This could contribute to our understanding of how mammalian immunity interacts with mycotoxins.

The study by Almaliki (57) investigated the effect of VOCs produced by a single *C. neoformans* strain and found that the VOCs of this severe pathogen caused more severe morphological effects and higher death rates than all the *A. fumigatus* strains that were tested (57). *C. neoformans* is a pathogenic yeast able to establish invasive infections in immunocompromised patients. It has been frequently associated with HIV/AIDS and accounts for as much as 15% of HIV-related deaths (17). A *Drosophila* S2 protein expression system has been used to produce and purify a recombinant cryptococcal protease, May1. This protease was used for further investigation as a target to identify compounds that could simultaneously inhibit the fungal protease and HIV-1 protease, which would provide dual protection and lower toxicity for HIV/AIDS patients (92). In the study by Almaliki and colleagues (57) regarding the toxicity of VOCs in *Drosophila, C. neoformans* VOCs cause significant delays in metamorphosis with eclosion rates of 44% compared to 80% for controls.

Contemporaneously with the growing number of studies in *Aspergillus*, *Drosophila* has been used to study *C. albicans*, one of the most common causes of candidiasis and blood stream infections (7, 93). In 2004, Alarco and colleagues published a Toll-deficient *Drosophila* model through which they demonstrated concordant *C. albicans* pathogenicity findings with mouse models, giving validity to the use of fly models (94). This was further corroborated by similar study in *Candida glabrata* mutant libraries (65, 95). Drosophila studies have been used to investigate host adaptation by *C. albicans*. Liu et al. (59) demonstrated the necessity of phosphate transporter, Pho48, in establishing candidiasis in the wild type *Oregon*^{R} fly via infection with wild type *C. albicans* and *Pho48* null mutants (59). Null mutants were 3.5 times less likely to cause fly death than wild type strains 5 days post-infection (59). Glittenberg and colleagues (66) via a targeted genetic screening of 5698 RNAi lines described the protective impact of fucosylation in immune defence against *C. albicans*. A recent study in a *Bom*$^{\Delta 55C}$ fly model, (lacking the ability to produce the full range

of Bomanin peptides) highlighted the ability of *Candida* sp. (including *C. albicans* and *C. auris*) to break down proline for energy, which may promote virulence. Moreover *C. albicans* mutants lacking the Proline UTilization genes *put1, put3* or *put1/put2* genes) showed reduced virulence compared to control fungal strain in the same fly infection model (62).

Drosophila infection models have been used to investigate the efficacy and toxicity of potential antifungal compounds. These include a Toll heterozygous Drosophila, *Tl[r3]/+*, used to test the naturally occurring compound, acid ellagic acid, against *C. albicans* where researchers showed statistically significant survival rates, and no toxicity at the proposed effective doses (64). Raj et al. (96) demonstrated a >70% survival rate of wild-type *Drosophila* infected with *C. albicans* when treated with *Syzygium samarangense* leaf extracted in methanol and dissolved in dimethyl sulfoxide. While the dosage applied to the *Drosophila* infection model was not specified, 50 mg of the *Syzygium samarangense* leaf extract was effective at clearing colonisation in an *ex vivo* porcine tongue and skin model, suggesting it could have utility as part of a topical treatment (96). *Drosophila* infection models can also be applied to antifungal studies for known compounds with the goal of reintroducing or repurposing old therapies. Clioquinol was administered orally to treat parasitic infections in the mid-1900s, however its use was discouraged due to perceived side effects (63, 97). Researchers investigated the antifungal efficacy and toxicity of Clioquinol in a Toll-deficient Drosophila model infected with *C. albicans* (63).

Drosophila has been utilised to investigate the novel pathogen *C. auris*. Wurster et al. (11) used a Toll-deficient mutant, *Tlr632/Tll-RXA* (which shows reduced AMP production and reduced phagocytic ability) to investigate the pathogenicity of *C. auris* clades identified at the time (Clade I-IV), and to determine the efficacy of azole to treatment (11). Their findings suggested that there was variability among the strains' pathogenicity, though all strains were more pathogenic than *C. albicans* (11, 98).

High priority group

Species of non-*C. albicans* (NCA) have been investigated using *Drosophila* models. While NCAs have typically accounted for a smaller fraction of candidiasis infections, their prevalence and resistance to azoles and echinocandins is on the rise (17, 53, 99). NCAs in the high priority group include *Nakaseomyces glabrata* (*C. glabrata*), *Candida tropicalis* and *Candida parapsilosis*.

In 2018, researchers harnessed CRISPR/Cas9 for the targeted deletion of individual *Drosophila Bomanin* genes to determine their immunoprotective role against *C. glabrata* (43). Using *in vivo* and *ex vivo* infection models, they demonstrated that *Bomanin* genes do not act in tandem and the short-form Bom peptide was immunoprotective against *C. glabrata* on its own (43). They showed that flies lacking 10 out of the 12 *Bomanin* genes (42) were as susceptible to infection as Toll-deficient flies, highlighting the importance of Boms in host immunity (43). Studies in *Drosophila* cell lines have been used to identify mechanisms by which *C. glabrata* evades innate immunity strategies, like AMPs and ROS, and potential drug targets. A study by Kounatidis and colleagues showed that *C. glabrata ADA2* gene is essential for the pathogen to resist oxidative stress as the *ADA2* knockout yeast could only grow in flies with suppressed ROS, while overexpressing *ADA2* promoted *C. glabrata* growth and resulted in lower host survival rates (65). The role of the potassium transporter *C. glabrata* TRK1 was elucidated through infection of *MyD88* and $Bom^{\Delta 55C}$ *Drosophila* strains with wild type and *C. glabrata trk1* knockout (60). Loss of *TRK1* gene resulted in cell wall modifications and reduced virulence within the host environment, in a potassium concentration dependent manner (60).

C. parapsilosis is associated with neonatal infections in addition to candidemia and candidiasis in immunosuppressed patients (17, 53). The Toll pathway has been shown to be crucial for *Drosophila* survival when infected by *C. parapsilosis* (which was not the case for *Persephone* protease), by comparing the susceptibility of wild type and mutant *MyD88−/−* flies to *C. parapsilosis* (53).

In addition, the high group includes Mucorales, *Fusarium* sp. *Histoplasma* sp. and eumycetoma causative agents (17). Mucorales are a large group of ubiquitous, filamentous fungi, frequently found in soil, which can cause infections ranging from mild to invasive (100, 101). The Order includes genera like *Rhizopus*, *Mucor* and *Lichthiemia* (101). Building on previous preexposure studies that showed the utility of *Drosophila* in Mucorales studies, Wurster and colleagues showed that exposing three Mucorales, *Rhizopus arrhizus, R, pusillus*, and *Mucor circinelloides*, to the triazoles isavuconazole and voriconazole, triggered hypervirulence in the fungi, resulting in lower survival rates in a Toll-deficient model (Tlr^{632}/Tll^{-RXA}). This was a significant finding as it could explain infections arising in patients undergoing prophylaxis or treatment with isavuconazole (102). While the number of Mucorales tested was small, this gives some insight into this treatment challenge. This is in contrast with *A. fumigatus*, which often occupies the same niche and is managed in a similar way, but does not develop isavuconazole-induced hypervirulence (102).

The *Fusarium solani* species complex, includes *F. solani sensu stricto*, *F. falciforme* and *F. keratoplasticum*, and they are major opportunistic fungal pathogen, capable of causing keratitis (58). A screen of 42 environmental and clinical isolates from South India revealed that all isolates were intrinsically resistant to first-generation azoles and susceptible to imidazole, which contributes to treatment challenges (58). Survival assays comparing Oregon-R wild type and *Myd88* mutant flies, infected with 6 Fusarium sp. found that MyD88 is required to mount an effective Toll defence against all *Fusarium* strains (58). Homa et al. (58) also showed that *Fusarium* virulence was distinct at strain level (58). Subsequently, Cohen et al. found that survival rates following Daisho peptide knockout also varied among *Fusarium* species (51).

Medium priority group

The lower priority category has the highest number of pathogens including *Scedosporium* sp, *Lomentospora prolificans*, *Coccidioides* sp, *Pichia kudriavzeveii* (*Candida krusei*), *Cryptococcus gattii*, *Talaromyces marneffei*, *Pneumocystis jirovecii* and *Paracoccidioides* sp (17). These pathogens have the lowest relative global incidence and

mortality rates, but still have substantial impacts (2). One of these pathogens, *T. marneffei* is a thermally dimorphic fungal pathogen localised to South and Southeast Asia (61, 103). It is found in the environment and Bamboo rats and can be inhaled and establish severe invasive infections in humans and animals (61). Its prevalence is not fully known due to limited surveillance and diagnostics and though mortality rates can be as high as 30%, few host-pathogen interaction studies have been performed (103, 104). Qu et al. (61) used the *MyD88 −/−* fly model to investigate the significance of the *T. marneffei* mating type on virulence in 107 clinical, Bamboo rat and environmental samples. They demonstrated that the mating type (MAT1-1 or MAT1-2) did not have an impact on flies survival upon infection, despite the fact that MAT1-2 isolates were overabundant across the entire sample population (61).

Perspective and future opportunities

The utility of *Drosophila* infection models in fungal research has been substantiated through the development of a good range of infection models and relevant findings. In spite of challenges and limitations around selecting the most suitable animal model, the extensive research work carried out in *Drosophila* over the last decade shows that this model is suitable. Fitting this extensive work within the boundaries of a Mini review article was a key challenge in setting up this review, therefore the WHO fungi prioritisation proved valuable into narrowing down the relevant content. While *Drosophila* presents a useful and relatively simple tool, subsequent investigations in other animal models are often required and should be considered to further corroborate findings, prior to reaching any general conclusions. Future work could focus on further characterisation of effector molecules (many of them have yet unknown function), on the role of innate immune mechanisms on immune memory adaptions, and on the use of *Drosophila* as a preclinical model on screening for antimicrobial efficacy against the fungal pathogens highlighted by WHO (17).

Author contributions

CM: Writing – review & editing, Investigation, Writing – original draft. IK: Writing – review & editing, Conceptualization, Supervision, Validation.

Funding

The author(s) declare that no financial support was received for the research, authorship, and/or publication of this article.

Conflict of interest

The authors declare that the research was conducted in the absence of any commercial or financial relationships that could be construed as a potential conflict of interest.

Publisher's note

References

1. Almeida F, Rodrigues ML, Coelho C. 'The still underestimated problem of fungal diseases worldwide'. *Front Microbiol*. (2019) 10:214. doi: 10.3389/fmicb.2019.00214

2. Rodrigues ML, Nosanchuk JD. Recognition of fungal priority pathogens: What next? *PloS Negl Trop Diseases*. (2023) 17:e0011136. doi: 10.1371/journal.pntd.0011136

3. Esheli M, Thissera B, El-Seedi HR, Rateb EM. Fungal metabolites in human health and diseases—An overview. *Encyclopedia*. (2022) 2:1590–601. doi: 10.3390/encyclopedia2030108

4. Xu J. Assessing global fungal threats to humans. *mLife*. (2022) 1:223–40. doi: 10.1002/mlf2.12036

5. Glittenberg MT, Kounatidis I, Christensen D, Kostov M, Kimber S, Roberts I, et al. Pathogen and host factors are needed to provoke a systemic host response to gastrointestinal infection of Drosophila larvae by Candida albicans. *DMM Dis Models Mech*. (2011) 4:515–25. doi: 10.1242/dmm.006627

6. Arastehfar A, et al. Aspergillus fumigatus and aspergillosis: From basics to clinics. *Stud Mycol*. (2021) 100:100115. doi: 10.1016/j.simyco.2021.100115

7. Lopes JP, Lionakis MS. Pathogenesis and virulence of *Candida albicans*. *Virulence*. (2022) 13:89–121. doi: 10.1080/21505594.2021.2019950

8. Zijlstra EE, van de Sande WWJ, Welsh O, Mahgoub ES, Goodfellow M, Fahal AH. Mycetoma: a unique neglected tropical disease. *Lancet Infect Dis*. (2016) 16:100–12. doi: 10.1016/S1473-3099(15)00359-X

9. Emmanuel P, Dumre SP, John S, Karbwang J, Hirayama K. Mycetoma: A clinical dilemma in resource limited settings. *Ann Clin Microbiol Antimicrobials*. (2018) 17:35. doi: 10.1186/s12941-018-0287-4

10. Lockhart SR, Etienne KA, Vallabhaneni S, Farooqi J, Chowdhary A, Govender NP, et al. Simultaneous emergence of multidrug-resistant candida auris on 3 continents confirmed by whole-genome sequencing and epidemiological analyses. *Clin Infect Dis*. (2017) 64:134–40. doi: 10.1093/cid/ciw691

11. Wurster S, Bandi A, Beyda ND, Albert ND, Raman NM, Raad II, et al. Drosophila melanogaster as a model to study virulence and azole treatment of the emerging pathogen Candida auris. *J Antimicrobial Chemother*. (2019) 74:1904–10. doi: 10.1093/jac/dkz100

12. Song R, Zhai Q, Sun L, Huang E, Zhang Y, Zhu Y, et al. CRISPR/Cas9 genome editing technology in filamentous fungi: progress and perspective. *Appl Microbiol Biotechnol*. (2019) 103:6919–32. doi: 10.1007/s00253-019-10007-w

13. Malavia D, Gow NAR, Usher J. Advances in molecular tools and *in vivo* models for the study of human fungal pathogenesis. *Microorganisms*. (2020) 8:803. doi: 10.3390/microorganisms8060803

14. Lorenz A, Papon N. New tools for the new bug Candida auris. *Trends Microbiol*. (2022) 30:203–5. doi: 10.1016/j.tim.2022.01.010

15. Peyclit L, Yousfi H, Rolain JM, Bittar F. Drug repurposing in medical mycology: identification of compounds as potential antifungals to overcome the emergence of multidrug-resistant fungi. *Pharmaceuticals*. (2021) 14:488. doi: 10.3390/ph14050488

16. Velazhahan V, McCann BL, Bignell E, Tate CG. Developing novel antifungals: lessons from G protein-coupled receptors. *Trends Pharmacol Sci*. (2023) 44:162–74. doi: 10.1016/j.tips.2022.12.002

17. World Health Organization. WHO fungal priority pathogens list to guide research, development and public health action(2022). Available online at: https://www.who.int/publications/i/item/9789240060241 (Accessed 29 September 2023).

18. Hedges SB. The origin and evolution of model organisms. *Nat Rev Genet*. (2002) 3:838–49. doi: 10.1038/nrg929

19. Baldridge D, Wangler MF, Bowman AN, Yamamoto SUndiagnosed Diseases Network, , Schedl T, et al. Model organisms contribute to diagnosis and discovery in the undiagnosed diseases network: Current state and a future vision. *Orphanet J Rare Dis*. (2021) 16:206. doi: 10.1186/s13023-021-01839-9

20. Belvin MP, Anderson KV. A CONSERVED SIGNALING PATHWAY: the *Drosophila* toll-dorsal pathway. *Annu Rev Cell Dev Biol*. (1996) 12:393–416. doi: 10.1146/annurev.cellbio.12.1.393

21. Lemaitre B, Nicolas E, Michaut L, Reichhart JM, Hoffmann JA. The Dorsoventral Regulatory Gene Cassette spä tzle/Toll/cactus Controls the Potent Antifungal Response in Drosophila Adults. *Cell*. (1996) 86:973–83. doi: 10.1016/s0092-8674(00)80172-5

22. Ligoxygakis P, Pelte N, Hoffmann JA, Reichhart JM. Activation of *Drosophila* toll during fungal infection by a blood serine protease. *Science*. (2002) 297:114–6. doi: 10.1126/science.1072391

23. Lamaris GA, Chamilos G, Lewis RE, Kontoyiannis DP. Virulence studies of Scedosporium and Fusarium species in Drosophila melanogaster. *J Infect Dis*. (2007) 196:1860–4. doi: 10.1086/523765

24. Levitin A, Marcil A, Tettweiler G, Laforest MJ, Oberholzer U, Alarco AM, et al. Drosophila melanogaster Thor and response to Candida albicans infection. *Eukaryotic Cell*. (2007) 6:658–63. doi: 10.1128/EC.00346-06

25. Chamilos G, Bignell EM, Schrettl M, Lewis RE, Leventakos K, May GS, et al. Exploring the concordance of aspergillus fumigatus pathogenicity in mice and Toll-deficient flies. *Med Mycol*. (2010) 48:506–10. doi: 10.3109/13693780903225813

26. Buchon N, Silverman N, Cherry S. Immunity in Drosophila melanogaster — from microbial recognition to whole-organism physiology. *Nat Rev Immunol*. (2014) 14:796–810. doi: 10.1038/nri3763

27. Harnish JM, Link N, Yamamoto S. Drosophila as a model for infectious diseases. *Int J Mol Sci*. (2021) 22. doi: 10.3390/ijms22052724

28. Liegeois S, Ferrandon D. Sensing microbial infections in the Drosophila melanogaster genetic model organism. *Immunogenetics*. (2022) 74:35–62. doi: 10.1007/s00251-021-01239-0

29. Ramírez-Camejo LA, Bayman P, Mejía LC. Drosophila melanogaster as an emerging model host for entomopathogenic fungi. *Fungal Biol Rev*. (2022) 42:85–97. doi: 10.1016/j.fbr.2022.09.001

30. White JS, Lafever KS, Page-McCaw A. Dissecting, fixing, and visualizing the Drosophila pupal notum. *J Visualized Experiments*. (2022) 2022. doi: 10.3791/63682

31. Jennings BH. Drosophila – a versatile model in biology and medicine. *Mater Today*. (2011) 14:190–5. doi: 10.1016/S1369-7021(11)70113-4

32. Touré H, Herrmann J-L, Szuplewski S, Girard-Misguich F. '*Drosophila melanogaster* as an organism model for studying cystic fibrosis and its major associated microbial infections'. *Infect Immun*. (2023) 91:e0024023. doi: 10.1128/iai.00240-23

33. Hamilos G, Samonis G, Kontoyiannis DP. Recent advances in the use of Drosophila melanogaster as a model to study immunopathogenesis of medically important filamentous fungi. *Int J Microbiol*. (2012) 2012:1–10:583792. doi: 10.1155/2012/583792

34. Cheng L, Baonza A, Grifoni D. *Drosophila* models of human disease. *BioMed Res Int*. (2018), 7214974. doi: 10.1155/2018/7214974

35. Macedo GE, Vieira PB, Rodrigues NR, Gomes KK, Rodrigues JF, Franco JL, et al. Effect of fungal indoor air pollutant 1-octen-3-ol on levels of reactive oxygen species and nitric oxide as well as dehydrogenases activities in drosophila melanogaster males. *J Toxicol Environ Health - Part A: Curr Issues*. (2022) 85:573–85. doi: 10.1080/15287394.2022.2054887

36. Yu S, Luo F, Xu Y, Zhang Y, Jin LH. 'Drosophila innate immunity involves multiple signaling pathways and coordinated communication between different tissues'. *Front Immunol*. (2022) 13:905370. doi: 10.3389/fimmu.2022.905370

37. Qin B, Yu S, Chen Q, Jin LH. Atg2 regulates cellular and humoral immunity in Drosophila. *Insects*. (2023) 14:706. doi: 10.3390/insects14080706

38. Tafesh-Edwards G, Eleftherianos I. Drosophila immunity against natural and nonnatural viral pathogens. *Virology*. (2020) 540:165–71. doi: 10.1016/j.virol.2019.12.001

39. Arch M, Vidal M, Koiffman R, Melkie ST, Cardona PJ. Drosophila melanogaster as a model to study innate immune memory. *Front Microbiol*. (2022) 10:991678. doi: 10.3389/fmicb.2022.991678

40. Kounatidis I, Ligoxygakis P. Drosophila as a model system to unravel the layers of innate immunity to infection. *Open Biol*. (2012) 2:120075. doi: 10.1098/rsob.120075

41. Tafesh-Edwards G, Eleftherianos I. JNK signaling in Drosophila immunity and homeostasis. *Immunol Lett*. (2020) 226:7–11. doi: 10.1016/j.imlet.2020.06.017

42. Clemmons AW, Lindsay SA, Wasserman SA. An effector peptide family required for Drosophila toll-mediated immunity. *PloS Pathog*. (2015) 11:e1004876. doi: 10.1371/journal.ppat.1004876

43. Lindsay SA, Lin SJH, Wasserman SA. Short-form bomanins mediate humoral immunity in Drosophila. *J Innate Immun*. (2018) 10:306–14. doi: 10.1159/000489831

44. Huang C, Xu R, Liégeois S, Chen D, Li Z, Ferrandon D. Differential requirements for mediator complex subunits in Drosophila melanogaster host defense against fungal and bacterial pathogens. *Front Immunol*. (2021) 11:478958. doi: 10.3389/fimmu.2020.478958

45. Lin SJH, Cohen LB, Wasserman SA. Effector specificity and function in Drosophila innate immunity: Getting AMPed and dropping Boms. *PloS Pathog*. (2020) 16:e1008480. doi: 10.1371/journal.ppat.1008480

46. Huang J, Lou Y, Liu J, Bulet P, Cai C, Ma K, et al. A Toll pathway effector protects Drosophila specifically from distinct toxins secreted by a fungus or a bacterium. *Proc Natl Acad Sci United States America*. (2023) 120:e2205140120. doi: 10.1073/pnas.2205140120

47. Hanson MA, Lemaitre B. New insights on Drosophila antimicrobial peptide function in host defense and beyond. *Curr Opin Immunol*. (2020) 62:22–30. doi: 10.1016/j.coi.2019.11.008

48. Meister M, Laguex M. *Drosophila* blood cells. *Cell Microbiol*. (2003) 5:573–80. doi: 10.1046/j.1462-5822.2003.00302.x

49. Vlisidou I, Wood W. Drosophila blood cells and their role in immune responses. *FEBS J*. (2015) 282:1368–82. doi: 10.1111/febs.13235

50. Williams MJ. Drosophila hemopoiesis and cellular immunity. *J Immunol*. (2007) 178:4711–6. doi: 10.4049/jimmunol.178.8.4711

51. Cohen LB, Lindsay SA, Xu Y, Lin SJH, Wasserman SA. The daisho peptides mediate Drosophila defense against a subset of filamentous fungi. *Front Immunol*. (2020) 11:9. doi: 10.3389/fimmu.2020.00009

52. Mishima Y, Quintin J, Aimanianda V, Kellenberger C, Coste F, Clavaud C, et al. The N-terminal domain of Drosophila gram-negative binding protein 3 (GNBP3) defines a novel family of fungal pattern recognition receptors. *J Biol Chem*. (2009) 284:28687–97. doi: 10.1074/jbc.M109.034587

53. Csonka K, Tasi Z, Vedelek V, Vágvölgyi C, Sinka R, Gácser A. Deciphering of Candida parapsilosis induced immune response in Drosophila melanogaster. *Virulence*. (2021) 12:2571–82. doi: 10.1080/21505594.2021.1980989

54. Troha K, Buchon N. Methods for the study of innate immunity in *Drosophila melanogaster*. *WIREs Dev Biol*. (2019) 8:e344. doi: 10.1002/wdev.344

55. Xu R, Lou Y, Tidu A, Bulet P, Heinekamp T, Martin F, et al. The Toll pathway mediates Drosophila resilience to Aspergillus mycotoxins through specific Bomanins. *EMBO Rep*. (2023) 24:e56036. doi: 10.15252/embr.202256036

56. Almaliki HS, Drazanin E, Sadovnik R, Yin G, Bennett WJ. Eight-carbon volatiles are more toxic to wild-type Drosophila melanogaster than to flies with blocked immune system mutations. *Entomologia Experimentalis Applicata*. (2021) 169:1092–102. doi: 10.1111/eea.13108

57. Almaliki HS, Angela A, Goraya NJ, Yin G, Bennett JW. Volatile organic compounds produced by human pathogenic fungi are toxic to Drosophila melanogaster. *Front Fungal Biol*. (2020) 1:629510. doi: 10.3389/ffunb.2020.629510

58. Homa M, Galgóczy L, Manikandan P, Narendran V, Sinka R, Csernetics Á, et al. South Indian Isolates of the *Fusarium solani* species complex from clinical and environmental samples: Identification, antifungal susceptibilities, and virulence. *Front Microbiol*. (2018) 9:1052. doi: 10.3389/fmicb.2018.01052

59. Liu NN, Uppuluri P, Broggi A, Besold A, Ryman K, Kambara H, et al. Intersection of phosphate transport, oxidative stress and TOR signalling in Candida albicans virulence. *PloS Pathog*. (2018) 14:e1007076. doi: 10.1371/journal.ppat.1007076

60. Llopis-Torregrosa V, Vaz C, Monteoliva L, Ryman K, Engstrom Y, Gacser A, et al. Trk1-mediated potassium uptake contributes to cell-surface properties and virulence of Candida glabrata. *Sci Rep*. (2019) 9:7529. doi: 10.1038/s41598-019-43912-1

61. Qu Q, Lu S, Li Z, Zhang J, Wang X, Zheng H, et al. The relationship between the preference of mating type (MAT) and source in the opportunistic pathogen Talaromyces marneffei. *Med Mycol*. (2023) 61:myad027. doi: 10.1093/mmy/myad027

62. Silao FGS, Jiang T, Bereczky-Veress B, Kühbacher A, Ryman K, Uwamohoro N, et al. Proline catabolism is a key factor facilitating Candida albicans pathogenicity. *PloS Pathog*. (2023) 19:e1011677. doi: 10.1371/journal.ppat.1011677

63. Pippi B, Merkel S, Staudt KJ, Teixeira ML, de Araújo BV, Zanette RA, et al. Oral clioquinol is effective in the treatment of a fly model of Candida systemic infection. *Mycoses*. (2019) 62:475–81. doi: 10.1111/myc.12888

64. Sampaio ADG, Gontijo AVL, Araujo HM, Koga-Ito CY. *In vivo* efficacy of ellagic acid against Candida albicans in a drosophila melanogaster infection model. *Antimicrobial Agents Chemother*. (2018) 62:e01716-18. doi: 10.1128/AAC.01716-18

65. Kounatidis I, Ames L, Mistry R, Ho HL, Haynes K, Ligoxygakis P. A host-pathogen interaction screen identifies ada2 as a mediator of candida glabrata defenses against reactive oxygen species. *G3: Genes Genomes Genet*. (2018) 8:1637–47. doi: 10.1534/g3.118.200182

66. Glittenberg MT, Kounatidis I, Atilano M, Ligoxygakis P. A genetic screen in Drosophila reveals the role of fucosylation in host susceptibility to Candida infection. *DMM Dis Models Mech*. (2022) 15:dmm049218. doi: 10.1242/dmm.049218

67. Cherbas L, Gong L. Cell lines. *Methods*. (2014) 68:74–81. doi: 10.1016/j.ymeth.2014.01.006

68. Kúthy-Sutus E, Kharrat B, Gábor E, Csordás G, Sinka R, Honti V. A novel method for primary blood cell culturing and selection in Drosophila melanogaster. *Cells*. (2023) 12:24. doi: 10.3390/cells12010024

69. Pippi B, Joaquim AR, Merkel S, Zanette RA, Nunes MEM, da Costa Silva DG, et al. Antifungal activity and toxicological parameters of 8-hydroxyquinoline-5-sulfonamides using alternative animal models. *J Appl Microbiol*. (2021) 130:1925–34. doi: 10.1111/jam.14915

70. Lorenz A. *Candida auris*. In: Lorenz A, editor. *Methods in Molecular Biology*. Springer US, New York, NY (2022). doi: 10.1007/978-1-0716-2417-3

71. Weaver CM, Makdissi S, Di Cara F. Modified protocol for culturing Drosophila S2 R+ cells and adult plasmatocytes to study actin cytoskeleton dynamics. *STAR Protoc*. (2022) 3:101588. doi: 10.1016/j.xpro.2022.101588

72. Flores Dalla Lana D, Neiva Lavorato S, Minussi Giuliani L, Cruz L, Lopes W, Henning Vainstein M. Discovery of a novel and selective fungicide that targets fungal cell wall to treat dermatomycoses: 1,3-bis(3,4-dichlorophenoxy)propan-2-aminium chloride. *Mycoses*. (2020) 63:197–211. doi: 10.1111/myc.13027

73. Chen J, Johnston DS. Dissection, fixation, and immunostaining of the Drosophila midgut. In: Chang C, Wang J, editors. *Cell Polarity Signalling, Methods and Protocols*. Humana Press, Springer Protocols, New York, NY (2022). p. 309–21. doi: 10.1007/978-1-0716-2035-9_20

74. Amin S, Basu M, Buzinova V, Delgado A, Mahadevan T, Mishra S. Glyoxal-based fixation of Drosophila embryos for immunofluorescence staining and RNA in *situ* hybridization. *STAR Protoc*. (2023) 4:102385. doi: 10.1016/j.xpro.2023.102385

75. Adams MD, Celniker SE, Holt RA, Evans CA, Gocayne JD, Amanatides PG, et al. The genome sequence of *Drosophila melanogaster*. *Science*. (2000) 287:2185–95. doi: 10.1126/science.287.5461.2185

76. Kanoh H, Kato H, Suda Y, Hori A, Kurata S, Kuraishi T. Dual comprehensive approach to decipher the Drosophila Toll pathway, ex vivo RNAi screenings and immunoprecipitation-mass spectrometry. *Biochem Biophys Res Commun*. (2019) 508:332–7. doi: 10.1016/j.bbrc.2018.11.007

77. Kim ES, Rajan A, Chang K, Govindarajan S, Gulick C, English E, et al. Generation of LexA enhancer-trap lines in Drosophila by an international scholastic network. *G3: Genes Genomes Genet*. (2023) 13:jkad124. doi: 10.1093/g3journal/jkad124

78. Behrens A, Rodschinka G, Nedialkova DD. High-resolution quantitative profiling of tRNA abundance and modification status in eukaryotes by mim-tRNAseq. *Mol Cell*. (2021) 81:1802–1815.e7. doi: 10.1016/j.molcel.2021.01.028

79. Zhou H, Li S, Pan W, Wu S, Ma F, Jin P. Interaction of lncRNA-CR33942 with dif/dorsal facilitates antimicrobial peptide transcriptions and enhances Drosophila toll immune responses. *J Immunol*. (2022) 208:1978–88. doi: 10.4049/jimmunol.2100658

80. Redman M, King A, Watson C, King D. What is CRISPR/cas9? *Arch Dis Childhood - Educ Pract Ed*. (2016) 101:213–5. doi: 10.1136/archdischild-2016-310459

81. Szebenyi C, Gu Y, Gebremariam T, Kocsubé S, Kiss-Vetráb S, Jáger O, et al. cotH genes are necessary for normal spore formation and virulence in mucor lusitanicus. *mBio*. (2023) 14:e0338622. doi: 10.1128/mbio.03386-22

82. Kapun M, Nunez JCB, Bogaerts-Márquez M, Murga-Moreno J, Paris M, Outten J, et al. *Drosophila* evolution over space and time (DEST): A new population genomics resource. *Mol Biol Evol*. (2021) 38:5782–805. doi: 10.1093/molbev/msab259

83. Hu Y, Comjean A, Rodiger J, Liu Y, Gao Y, Chung V, et al. FlyRNAi.org—the database of the Drosophila RNAi screening center and transgenic RNAi project: 2021 update. *Nucleic Acids Res*. (2021) 49:D908–15. doi: 10.1093/nar/gkaa936

84. Van De Veerdonk FL, Gresnigt MS, Romani L, Netea MG, Latgé JP. Aspergillus fumigatus morphology and dynamic host interactions. *Nat Rev Microbiol*. (2017) 15:661–74. doi: 10.1038/nrmicro.2017.90

85. Lionakis MS, Kontoyiannis DP. Fruit flies as a minihost model for studying drug activity and virulence in Aspergillus. *Med Mycol*. (2005) 43:S111–4. doi: 10.1080/13693780400020030

86. Spikes S, Xu R, Nguyen CK, Chamilos G, Kontoyiannis DP, Jacobson RH, et al. Gliotoxin production in Aspergillus fumigatus contributes to host-specific differences in virulence. *J Infect Dis*. (2008) 197:479–86. doi: 10.1086/525044

87. Nafis MMH, Quach ZM, Al-Shaarani AAQA, Muafa MHM, Pecoraro L. Pathogenicity of aspergillus airborne fungal species collected from indoor and outdoor public areas in Tianjin, China. *Pathogens*. (2023) 12:1154. doi: 10.3390/pathogens12091154

88. Bennett JW, Inamdar AA. Are some fungal volatile organic compounds (VOCs) mycotoxins? *Toxins*. (2015) 7:3785–804. doi: 10.3390/toxins7093785

89. Dillon ME, Wang G, Garrity PA, Huey RB. Thermal preference in Drosophila. *J Thermal Biol*. (2009) 34:109–19. doi: 10.1016/j.jtherbio.2008.11.007

90. Almaliki HS, Niu M, Keller NP, Yin G, Bennett JW. Mutational analysis of Aspergillus fumigatus volatile oxylipins in a Drosophila eclosion assay. *J Fungi*. (2023) 9:402. doi: 10.3390/jof9040402

91. Belmonte RL, Corbally MK, Duneau DF, Regan JC. Sexual dimorphisms in innate immunity and responses to infection in Drosophila melanogaster. *Front Immunol*. (2020) 10:3075. doi: 10.3389/fimmu.2019.03075

92. Kryštůfek R, Šácha P, Starková J, Brynda J, Hradilek M, Tloušťová E, et al. Re-emerging aspartic protease targets: examining cryptococcus neoformans major aspartyl peptidase 1 as a target for antifungal drug discovery. *J Medicinal Chem*. (2021) 64:6706–19. doi: 10.1021/acs.jmedchem.0c02177

93. Mroczyńska M, Brillowska-Dabrowska A. Virulence of clinical candida isolates. *Pathogens*. (2021) 10:466. doi: 10.3390/pathogens10040466

94. Alarco A-M, et al. *Immune-Deficient Drosophila melanogaster: A Model for the Innate Immune Response to Human Fungal Pathogens 1,2*, *The Journal of Immunology* (2004). Available online at: http://journals.aai.org/jimmunol/article-pdf/172/9/5622/1186248/5622.pdf.

95. Brunke S, Quintin J, Kasper L, Jacobsen ID, Richter ME, Hiller E, et al. Of mice, flies - and men? Comparing fungal infection models for large-scale screening efforts. *DMM Dis Models Mech*. (2015) 8:473–86. doi: 10.1242/dmm.019901

96. Raj S, Vinod V, Jayakumar J, Suresh P, Kumar A, Biswas R, et al. Antifungal activity of Syzygium samarangense leaf extracts against Candida. *Lett Appl Microbiol*. (2021) 73:31–8. doi: 10.1111/lam.13471

97. Perez DR, Sklar LA, Chigaev A. Clioquinol: To harm or heal. *Pharmacol Ther*. (2019) 199:155–63. doi: 10.1016/j.pharmthera.2019.03.009

98. Wurster S, Albert ND, Kontoyiannis DP. Drosophila melanogaster as a Rapid and Reliable *In Vivo* Infection Model to Study the Emerging Yeast Pathogen Candida auris. In: Lorenz A, editor. *Candida auris, Methods and Protocols*. Springer Press, New York, NY (2022). p. 375–405. doi: 10.1007/978-1-0716-2417-3_24

99. Pristov KE, Ghannoum MA. Resistance of Candida to azoles and echinocandins worldwide. *Clin Microbiol Infect*. (2019) 25:792–8. doi: 10.1016/j.cmi.2019.03.028

100. Lecointe K, Cornu M, Leroy J, Coulon P, Sendid B. Polysaccharides cell wall architecture of mucorales. *Front Microbiol*. (2019) 10:469. doi: 10.3389/fmicb.2019.00469

101. Tahiri G, Lax C, Cánovas-Márquez JT, Carrillo-Marín P, Sanchis M, Navarro E, et al. Mucorales and mucormycosis: recent insights and future prospects. *J Fungi*. (2023) 9:335. doi: 10.3390/jof9030335

102. Wurster S, Lewis RE, Albert ND, Kontoyiannis DP. Preexposure to Isavuconazole Increases the Virulence of Mucorales but Not Aspergillus fumigatus in a Drosophila melanogaster Infection Model. *Antimicrobial Agents Chemother*. (2019) 63:e01896-18. doi: 10.1128/AAC.01896-18

103. Singulani JL, Scorzoni L, de Oliveira HC, Marcos CM, Assato PA, Fusco-Almeida AM, et al. Applications of invertebrate animal models to dimorphic fungal infections. *J Fungi*. (2018) 4:118. doi: 10.3390/jof4040118

104. Sephton-Clark P, Nguyen T, Hoa NT, Ashton P, van Doorn HR, Ly VT, et al. Impact of pathogen genetics on clinical phenotypes in a population of *Talaromyces marneffei* from Vietnam. *Genetics*. (2023) 224:iyad100. doi: 10.1093/genetics/iyad100

Frontiers in Immunology

Explores novel approaches and diagnoses to treat immune disorders.

The official journal of the International Union of Immunological Societies (IUIS) and the most cited in its field, leading the way for research across basic, translational and clinical immunology.

Discover the latest Research Topics

See more →

Frontiers

Avenue du Tribunal-Fédéral 34
1005 Lausanne, Switzerland
frontiersin.org

Contact us

+41 (0)21 510 17 00
frontiersin.org/about/contact